

Investigation of Morphological Changes along the South West Texel Coastline and the Initial Response of a Mega Nourishment

Final report

Delft University of Technology

Felix Francken

4577256

19-08-2023

Investigation of Morphological Changes along the South West Texel Coastline and the Initial Response of a Mega Nourishment

Author

Felix Francken, 4577256

Track & specialisation

Hydraulic Engineering - Coastal Engineering

Supervisors:

Dr. ir. M.A. de Schipper

Chair assessor, TU Delft

Dr. W. Ridderinkhof

Daily supervisor, Witteveen + Bos

Dr. J.A. Arriaga Garcia

Daily supervisor, TU Delft

Dr. M.F.S. Tissier

Third assessor, TU Delft



Saturday 19th August, 2023

Faculty of Civil Engineering and Geosciences, Delft University of Technology, and
Witteveen + Bos Utrecht - Delta's, Kusten en Rivieren

Preface

This is the final report of the master thesis of Felix Francken. It presents the analysis of the development of the SW Texel coastline, its relation to the lawfully protected coastline, and it shows a preliminary design of a mega nourishment in the project area using a model.

This project is executed in the interest of Witteveen+Bos in cooperation with TU Delft.

I would like to thank Wim Ridderinkhof for his guidance throughout the whole project, his ability to critically think about the results I showed, and for offering me the opportunity to temporarily join the Witteveen+Bos organization and make use of its resources. Furthermore I would like to thank Jaime Arriaga Garcia, who was very helpful thinking about solutions when I got stuck during modeling and helped me to see the bigger picture of the project. Finally, I want to thank Matthieu de Schipper and Marion Tissier for their accurate remarks during progress meetings. I want to thank all supervisors for taking the time and energy to supervise me in order to obtain the diploma of MSc Civil Engineering - TU Delft.

Felix Francken (4577256)

Abstract

In 1990 the Dutch government passed legislation that dictates the South West Texel coast must be maintained with regard to the 1990 coastline. The coast is currently maintained by applying shoreface and beach nourishments with an interval of approximately 3 years, because it experiences erosion. The problems with this approach are that the mobilization of the dredging vessels is expensive, dredging vessels cause nuisance in the ecological system and moreover, the dredging vessels emit carbon dioxide and therefore contribute to climate change. The first goal of this study was to investigate if an alternative coastal protection strategy is able to mitigate the drawbacks of the current scheme. Consequently, the application of a mega nourishment was chosen over a cross-shore dam or an outer delta nourishment. To optimally design a mega nourishment, a morphological analysis was executed that focused on elements in the sediment balance of the system. Using Vaklodingen and JARKUS data, volume changes of each transect were identified for 4 parts of the transect: the dune, the beach, the shallow part of the foreshore and the Molengat channel. It was found that dune and beach growth started growing from the moment that the nourishments were structurally applied. When nourishments are aborted, it is expected that the shrinking of the dunes will resume, just like the pre-1990 situation. The Molengat in the transects was found to be moving towards shore before the nourishment program started, and its landward movement was not influenced by the implementation of the nourishment program. The Molengat filling rate was projected into the future, leading to a fill date in transects 880-930 by 2035, and in transects 930-1013 by 2055. In transects 1013-1108 and 1108-1210 the Molengat has already been filled. The late projection filling date of transects 930-1013 is a reason to put the mega nourishment at that location, combined with the largest natural erosion occurring at the same location. The application of a mega nourishment is done by putting 20 years worth of sediment at transect range 945-1053 in one construction project. Simultaneously, the mega nourishment aims to diffuse sediment alongshore in the shallow part of the transects, providing sediment to adjacent transects. The sediment supply to other transects could be able to limit the shrinking of the adjacent dunes, or even let them grow. However, this requires further investigation. Delft3D Model results showed that sediment transport in this area is mainly caused by waves on the NUN-shoal, and by the current in the Molengat ebb-tidal channel. The model resolution was not fine enough to accurately describe the accretion and erosion patterns alongshore. Yet, by the use of results of morphological updates it could be determined that the mega nourishment will likely cause accretion south of the nourishment area. This research can be used as a stepping stone for future design steps of a mega nourishment, and also for acquiring knowledge about future behaviour of different parts of the bottom profiles in the South West Texel area.

Contents

	Page
1 Introduction	1
1.1 Problem statement and objective	1
1.2 Research questions	2
2 Description of SW Texel	4
2.1 Background nourishment program and Dynamic Preservation Act	4
2.2 Stakeholders overview	7
2.3 Characteristics of SW Texel	8
2.3.1 Morphological characteristics	8
2.3.2 Hydrodynamic characteristics - Tide	8
2.3.3 Hydrodynamic characteristics - Waves	9
2.3.4 Wind	14
3 Conceptualization of solutions	15
3.1 Design alternatives and choice	15
4 Morphological analysis of SW Texel	19
4.1 Overview sediment balance for SW Texel	19
4.1.1 Methods and definitions	19
4.1.2 Sediment balance	22
4.2 Nourishment volume ($V_{nourish,tot}$)	24
4.3 Volume difference in 1991-2021 (ΔV_{tot})	26
4.4 Natural transport term ($V_{Nat,transect}$)	28
4.5 Molengat infilling volume ($\Delta V_{Molengat\ infilling,transect}$)	29
4.5.1 Calculation of $V_{Molengat\ infilling,transect}$	30
4.5.2 Molengat fill date projection	31
4.6 Dune and beach volume ($\Delta V_{Dune,transect}$ and $\Delta V_{Beach,transect}$)	34
4.6.1 Calculation of $\Delta V_{Dune,transect}$ and $\Delta V_{Beach,transect}$	34
4.6.2 Dune development through time	37
4.7 Shallow volume ($\Delta V_{Shallow}$)	39
5 Delft3D model set-up	42
5.1 Model research questions	42
5.2 Principles of Delft3D	43
5.3 Model domain	45
5.3.1 Design of mega nourishment	46
5.4 Flow input	48
5.4.1 Simulation time	48

5.4.2	Initial conditions	49
5.4.3	Boundary conditions	49
5.4.4	Physical parameters	50
5.5	Numerical stability	51
5.6	Wave input	51
5.6.1	Wave conditions	52
5.6.2	Physical and numerical parameters	52
5.7	Model sensitivity	53
6	Delft3D model results	55
6.1	Overview sediment transport results of simulations	55
6.2	Storm-calm-ratios	58
6.3	NW and SW waves	60
6.4	2021 bathymetry and mega nourishment	61
6.5	Gradients in sediment transport/ Erosion-accretion patterns AS	63
7	Discussion	65
7.1	Transition from current nourishment scheme to mega nourishment	65
7.2	Research compared to literature	68
7.3	Limitations morphological analysis	70
7.4	Limitations model setup and results	71
8	Conclusion and recommendations	73
8.1	Conclusions about system behavior	73
8.2	Recommendations for future research	75
	References	76
	Appendices	80
A	Additional photos SW Texel coastline	80
B	Bathymetry maps from Vaklodingen at SW Texel	83
C	Transects of depth profiles along coast (JARKUS)	90
C.1	Post-1990 transects	90
C.2	Pre-1990 transects	110
D	List of all nourishments and transect widths at SW Texel	116
E	Molengat filling projections transect 703-1210	117
F	Total volume change of transects (Vaklodingen)	133
G	Volume tables	143

1 | Introduction

1.1 Problem statement and objective

The majority of the Dutch population is living below sea level. If all coastal protection structures would be breached, at least 9 million people would be significantly impacted from the consequences of flooding (Ministerie van Infrastructuur en Milieu, 2015). This threat of flooding requires flood protection along the entire Dutch coastline. The Dynamic Preservation policy has determined that the entire Dutch coast must be protected for different service levels. The service levels are maintained by the governmental organization Rijkswaterstaat (RWS) through construction and management of coastal protection structures. One example of coastal maintenance by Rijkswaterstaat is periodic nourishments to supply the Dutch coast with sediment to keep the coastline in place and avoid landward coastline retreat.

Since the start of the coastal nourishment program in 1990, the Texel coast has required nourishments to keep its position in place. This study focuses on the South West (SW) area of Texel. Keeping the coastline in place is achieved by application of nourishments on the foreshore and on the beach with a frequency of once every 3 years on average. Nourishments are still necessary for the future, as the cancellation of the current nourishment program would lead to coastal retreat, known as structural erosion (Rijkswaterstaat, 2021). It is a political decision to keep the coastline in place, and the reasons that this coastline is maintained are the diverse functions of South-West Texel:

- **Economical:** beach pavilions and camp grounds are located on and near the beach.
- **Ecological:** behind the first dune at SW Texel there are protected Natura2000 areas.
- **Recreational:** the beach is home to beach guests, surfers and walkers.
- **Flood protection:** The beach is part of the flood protection line to keep Texel safe from floods.

These functions will be jeopardized if the current nourishment scheme is aborted and the land retreats freely. However, the current every-3-year nourishment scheme includes multiple disadvantages which form the main problem of this study:

- The beach is vastly reduced in length at the end of each maintenance cycle (De Sonnaville and Van der Spek, 2012).
- The frequent mobilization of dredging vessels to the South West Texel is expensive.
- The dredging vessels cause disturbances in the ecosystem, such as noise disturbances and temporal turbidity increase (Barbanti et al., 2005).
- Dredging vessels emit carbon dioxide through fuel consumption and therefore contribute to climate change.

The nourishment program until 2027 has already been prepared by Rijkswaterstaat, meaning that the above mentioned disadvantages continue on the short term. In the long term of around 20 years, alternative coastal protection methods may mitigate the drawbacks of the current scheme. This study formulates alternative interventions to protect the coastline of SW Texel, while continuing to protect the current values of the beach and hinter-lying area. Then, a potential first order design is given of a mega nourishment. Before the design of a mega nourishment, a deeper understanding of the morphology changes through the last decades is required. Understanding of sediment volume changes in the tidal channel, the beach and the dune helps to define a location for the mega nourishment. Subsequently, a model is created to gain understanding in the initial response of the system to a mega nourishment, which is one of the potential interventions. It is investigated what processes have the most impact on sediment transport in this system and how areas of accretion and erosion change after the intervention. This thesis focuses on 3 aspects: characterize the morphological evolution of the SW Texel area since 1990, identify which processes are the main drivers of sediment transport, and identify the effect on shoreline changes if the current nourishment strategy is replaced by a mega nourishment.

This study focuses on the beach of SW Texel and the shore directly in front of it. However, the system interacts with features evolving at different time and spatial scales. Therefore, it is important to broaden the scope to beyond the SW Texel area, but only for relevant processes.

1.2 Research questions

The effects of hydrodynamic processes on sediment transport in the area of South West Texel have been investigated by Elias et al. (2021), and Cleveringa (2001). However, there is currently limited knowledge available on the impact of new nourishment proposals or the construction of new structures to locally fix the coastline of SW Texel. Therefore, the main research questions in this study are:

1. *What alternatives exist to protect the coastline of SW Texel in the future, while maintaining its current values?*
2. *How has the morphology developed since 1990, including the nourishment program?*
3. *How could the morphology change by a replacement of the nourishment program by a mega nourishment?*
4. *What is the optimal location of a mega nourishment and what is the effect of the nourishment on shoreline changes in the system?*

This study consists of 3 main parts, as shown in Figure 1.1. The first part is the definition of the system and its characteristics. The second part is a data analysis of morphological characteristics and a model setup of the application of a mega nourishment. The third part is the overarching relation of the morphological analysis and the model and the accompanying conclusions. For clarity, some sections start with the sub research question that they answer.

To answer the research questions, first the features of the system of interest are described in detail in Chapter 2. It gives the background on why nourishments are applied and contains information on what tide and wave climates are present. The next step (Chapter 3) is the description of potential coastal protection alternatives. From the different alternatives one alternative is worked out in detail: the application of a mega nourishment. Other alternatives can still be viable options for coastal protection, but they are not the main focus of this study. In Chapter 4, the relevance of periodic nourish-

ments is explored in a morphological analysis, as they comprise Rijkswaterstaat’s coastal maintenance scheme at SW Texel. Subsequently it is investigated what sediment flows are important, where they are coming from, where they are heading and how they developed through time. This gives insight in the behaviour of the current nourishment scheme. Understanding of coastal behaviour without nourishments is important when it would be replaced by another type of coastal protection. Subsequently, topographic measurements are used to identify alongshore areas that experience erosion and accretion, which allows to indicate a location for system interventions.

To finalize the study, it is investigated how a mega nourishment could be applied in the system, how large it needs to be, and what initial impact it has on the system in terms of sediment transport. Chapter 5 explains the setup of a Delft3D model, followed by the presentation of results in Chapter 6.

Both the data analysis and the model results are combined in an overarching description in Chapter 7, together with the limitations from both the data analysis and the model. Chapter 8 wraps up the most important conclusions and presents recommendations for future research on this study.

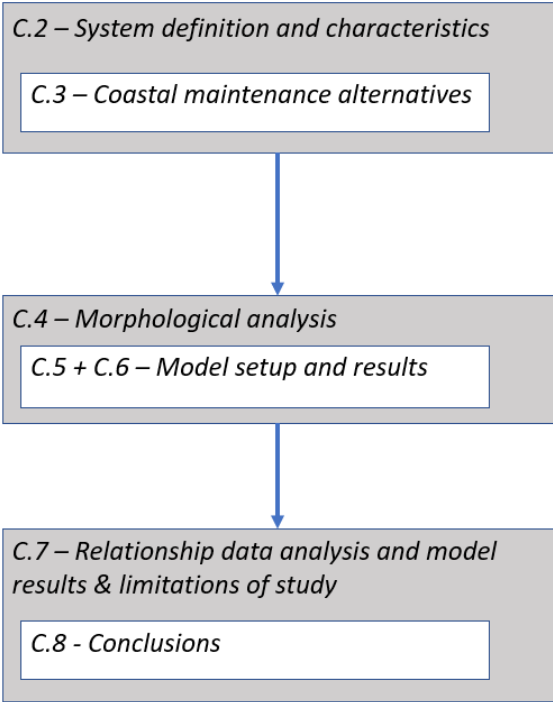


Figure 1.1: Overview research steps.

2 | Description of SW Texel

The research first focuses on system analysis, as shown in Figure 1.1. This chapter describes why are nourishments needed. This is done by an explanation of Rijkswaterstaat's nourishment program (Section 2.1) and how this relates to the Dynamic Preservation Act at SW Texel. A short overview of stakeholders follows then in Section 2.2. Thereafter, an overview is given of the morpho-, hydrodynamic and wind characteristics of the area (Section 2.3).

2.1 Background nourishment program and Dynamic Preservation Act

As mentioned in Section 1.1, the coast of SW Texel comprises multiple values for society. These values are preserved for the future because of the Dynamic Preservation Act. The Dynamic Preservation Act is legislation that states the coastline has to be maintained to a reference coastline from 1990. The reference coastline is called Basis Kustlijn (Base CoastLine, or BKL) and the coast is allowed to exceed this coastline seaward, but not landward. The cross-shore position of the BKL at 1 location is mathematically defined based on the cross-shore position of the mean low water level, the dune foot and the sand volume in between. Rijkswaterstaat annually compares the actual coastline - the Momentary CoastLine (Momentane KustLijn, MKL) - to the BKL and is then able to conclude what alongshore areas do satisfy the BKL and what areas do not. The BKL is the MKL of 1990.

Generally, when the MKL is closer to shore than the BKL the coast must be nourished, see Figure 2.1. Rijkswaterstaat both monitors the MKL and plans the nourishment program. Since the start of this coastal preservation, the entire Dutch shoreline in 1990 has been nourished with an average volume of 12 million m^3 of sediment per year, of which 33.8% is used for the Wadden Sea islands (Brand et al., 2022). Within the Wadden coastline 50.2% of the volume is dedicated to the protection of Texel. Since this is a significant portion of the total nourished volume, Texel is an interesting location for an attempt to optimize the nourishment strategy. The main reason that Texel requires a large portion of nourishment volume is that it experiences large structural erosion and therefore requires more sediment than other areas to keep up with the BKL of 1990 (Rijkswaterstaat, 2021).

The coast of Texel facing the North Sea can be divided into 3 parts: North Texel, Middle Texel and South West (SW) Texel, see Figure 2.1. This research looks at South West Texel only. The area of interest is limited to a Dutch coastal reference system called JARKUS, and the SW Texel area ranges from transects 416-1210. Within this range the BKL is only defined for transects 880-1210, meaning that the coast in other transects is allowed to retreat. Structural erosion occurs at SW Texel as sediment is transported from both the ebb-tidal delta (ETD) and the coastline of Texel towards the Texel basin, which forms part of the Wadden Sea basin (Rijkswaterstaat, 2021). This can be observed by landward migra-

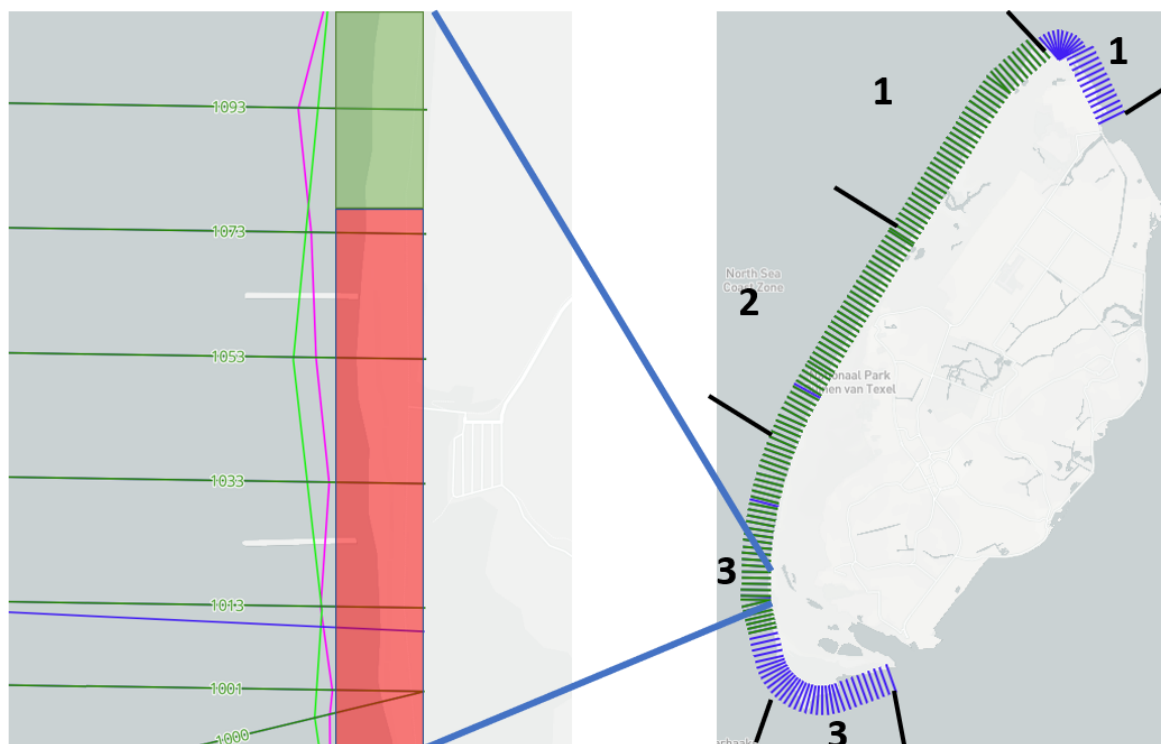


Figure 2.1: Right: Overview of North Sea facing Texel coastline. The numbers indicate: 1) North Texel (transects 2580-3432), 2) Middle Texel (transects 1210-2580), 3) South Texel (transects 416-1210). The green transects indicate the coast that needs to satisfy the BKL, the blue transects do not have to satisfy the BKL. Left: The BKL satisfaction in transect range 1000-1093 is shown in detail: the green vertical line indicates the BKL, the pink line indicates the 2021 MKL. The MKL is further offshore than the BKL in transect 1075-1100, so this area satisfies the BKL and is indicated with a green rectangle on the coast. In transect 1000-1075 the MKL is closer to shore, meaning the BKL is not satisfied and this is indicated with a red rectangle on the coast.

tion of the ebb tidal channel called Molengat in front of the Texel coast. However, not all sediment is transported to the Wadden Sea, as particles can also end up in the dune section of Texel, or alongshore at the northern island coasts (Elias, 2021). Rijkswaterstaat applies nourishments at this coast to compensate the lost sediment volume and make the MKL satisfy the BKL.

The observation of SW Texel losing sediment is evident when looking at the sediment budgets at Wadden Sea scale, as investigated by Elias and Wang (2020). Figure 2.2 shows a negative sediment budget for the coast of Texel, indicating there is net sediment transport from the coast towards the Texel basin. The Texel and Den Helder coast are eroding with a rate of $4.05 \text{ Mm}^3/\text{yr}$. Elias and Wang constructed this figure with data from 1997 - 2015, taking into account the nourishment program. Therefore it is likely that the sediment loss would have been even larger without nourishments, which confirms the need for nourishments by Rijkswaterstaat. As a result, the coastline retreats and the coastline does not satisfy the BKL anymore. This information is on basin-scale, but there is no research available on the distribution of volume changes on the detail level of JARKUS transects. This research fills that knowledge gap in Chapter 4. Together, landward migration and the satisfaction of the BKL highlight the need for the nourishment program of Rijkswaterstaat.

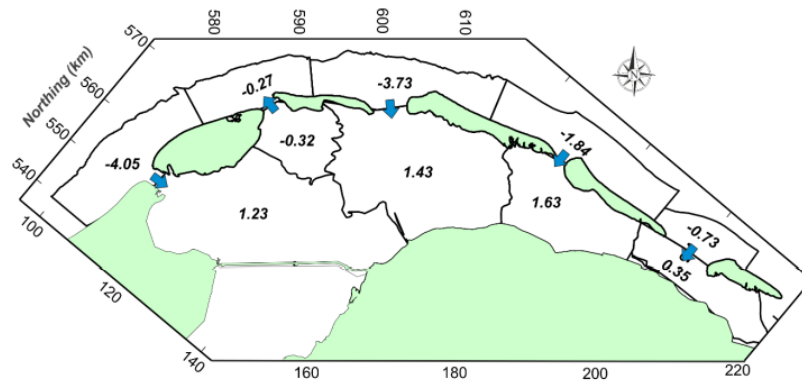


Figure 2.2: Sediment balance of entire Wadden Sea. Elias and Wang (2020) concluded that the sediment budget is negative at SW Texel and Den Helder. Figure from Elias and Wang (2020).

Satisfaction of the BKL on the timescale of decades

Rijkswaterstaat is responsible for the position of the MKL with respect to the BKL. Their current goal on scale of the Wadden Sea is to nourish the North Sea coast with such a volume that it increases in height proportional to the North Sea level rise (Lodder, Interview, 2022). Figure 2.3 shows the conceptual idea Rijkswaterstaat is aiming to achieve: a nourishment during sea level rise can be applied such that the dune does not retreat. The Kustgenese 2.0 research found that the required nourishment volume for all Wadden Sea islands is $5.7 \text{ Mm}^3/\text{yr}$ for the coastline to keep up with sea level rise (Rijkswaterstaat, 2020). Kustgenese 2.0 did not state where the nourishments along the Wadden Sea islands must be applied. Yet, the nourishment volume of $5.7 \text{ Mm}^3/\text{yr}$ is set as a quota by Rijkswaterstaat to achieve every year. Some locations along the Texel coast always have to be nourished to satisfy the BKL, and therefore experience structural erosion. The sum of the required volume by these locations is less than the quota of $5.7 \text{ Mm}^3/\text{yr}$. This leaves Rijkswaterstaat with creative freedom to nourish at locations that do not necessarily require it.

Figure 2.3 is the concept that is followed, yet there are differences with the SW Texel coast. Firstly, the concept is based on alongshore uniform beaches, while SW Texel is not alongshore uniform. Secondly, the presence of the Texel basin impacts currents and sediment transport. Thirdly, there is an ebb-tidal channel called Molengat in front of SW Texel, making prediction of future coastal development more complex than the concept.

Currently, there is a financial disadvantage regarding the nourishment of the South West Texel coast. 67% of the nourishment volume at South West Texel has been applied at the beach, while only 33% has been applied at the shoreface (Brand et al., 2022). Beach nourishments ($\pm 5\text{€}/\text{m}^3$) are more expensive than shoreface nourishments ($\pm 3\text{€}/\text{m}^3$), because they require more fuel to pump the dredged sediment to the correct location on the beach (Rijksbegroting, 2013). In contrast, during shoreface nourishments dredging vessels can just dump their sediment at the bottom. Nourishments at SW Texel mainly use the expensive option. This is mainly caused by the fact the area is shallow, making it difficult for dredging vessels to get to the location and apply shoreface nourishments.

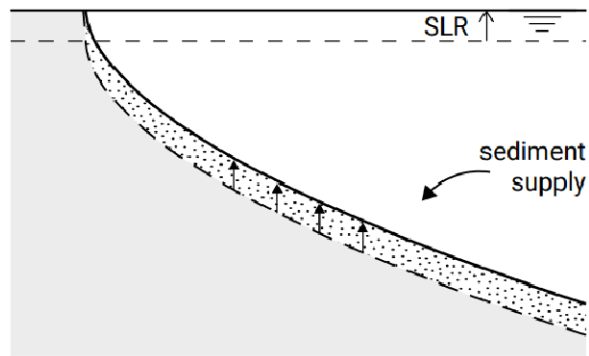


Figure 2.3: When a sufficiently large and well-distributed nourishment is applied during sea level rise, the dune profile does not retreat landward. Simultaneously, the entire profile grows. This conceptual model is followed by Rijkswaterstaat to nourish the Texel coast. Figure from Bosboom and Stive (2021).

2.2 Stakeholders overview

This section shows an overview of stakeholders that are concerned with the future of SW Texel's coastline. This description of power dynamics has been confirmed by the Technical Manager of Coastlines E. Brand, who has a central role within the organization of Rijkswaterstaat (Brand, Interview, 2022).

Stakeholders can be categorized into 4 groups:

- **Beach businesses:** pavilion owners and camp ground owners represent the economic activity near the beach. Their interest is to have wide beaches, so that there is more accommodation space for visitors and therefore a higher capacity for economic activity.
- **Environmental organizations:** these parties have the interest to let the sea, beach and hinter lying dune area develop as freely as possible, with minimum human interference. One example of these organizations is Stichting Noordzee, that is concerned with sustainable use of the North Sea by preferring shoreface nourishments over beach nourishments. Also there are Natura 2000 areas, in which it is aimed to contribute to biodiversity as much as possible by allocating land to nature. These areas are designated by the Ministry of Agriculture, Nature and Food quality, and being maintained by Staatsbosbeheer (State Forestry). These organizations try to enforce among others the Bird Policy and Habitat Policy (Natura2000, n.d.).
- **Recreational stakeholders:** beach visitors that go to the beach for leisure. Their interests are to enjoy the beach and nature. Typical groups in this category are beach goers, people exercising sports, bird spotters and sports fishermen. Nourishment works are paused in July-August to accommodate to this group's interests.
- **Governmental organizations:** they represent the interests of local population to defend the area against flood risk, and also aim to facilitate smooth cooperation between stakeholders to create new legislation. One example is Hoogheemraadschap Hollands Noorderkwartier, which maintains the land side of dikes and dunes with emphasis on flood safety. Next, Rijkswaterstaat is responsible to manage the sandy coast and the dunes. Staatsbosbeheer manages the natural areas in dunes and areas designated for recreation.

2.3 Characteristics of SW Texel

This section answers the question: *What are the characteristics of the area of interest?* The section is divided into morphological features, hydrodynamic features and characteristics of the wind.

2.3.1 Morphological characteristics

The structural erosion that occurs at South West Texel is related to the complex morphodynamics in the area (Elias and Van der Spek, 2012). The left part of Figure 2.4 is taken from Elias (2021) and shows multiple morphological elements in front of the beach of South West Texel. Just south of the South West beach there is the Texel inlet. The Texel Inlet consists of a tidal channel (Marsdiep) that connects the Texel basin to the North Sea. During ebb the water flows out of the inlet into the Schulpengat and the Nieuwe Schulpengat (Elias et al., 2006). The Noorderhaaks is a shallow sandy shoal right in front of the Texel inlet that divides the water outflow. A small fraction of the tidal prism flows through the Molengat, which is a tidal channel located closely to the beach of South West Texel (Elias et al., 2017). At the beach of SW Texel there are submerged cross-shore groynes with a length of $O(80m)$ and spaced by $400m$ in alongshore direction. Their goal is to keep the beach near the waterline from too much erosion. The location of the Molengat has slowly moved towards Texel's shoreline during the past decades, and therefore it has impacted the morphological behaviour of the beach at South West Texel (Elias, 2021). The Noorderhaaks is related to the long term beach evolution, and is also important in the development of the South West Texel beach (Elias, 2021).

The Noordelijke Uitlopers of the Noorderhaaks (the NUN) is a shallow submerged area that is connected north of the Noorderhaaks and almost attaches to the coast of Texel at a chart datum of $-5 m NAP$ (Rijkswaterstaat, 2020). Furthermore, there is the Helderse Zeewering at the tip of the North-Holland coast: this is a stone seawall that keeps the shore of North-Holland fixed in place. Finally, the southern tip of the Texel island is a large beach called De Hors, see Figure 2.6 . This beach has not been nourished as it does not adhere to the managed BKL. Figure 2.5 shows a bird perspective of the actual coastline looking over transects 915-1000.

2.3.2 Hydrodynamic characteristics - Tide

The area of SW Texel is influenced by both tidal flow and individual waves (Van der Moolen, 2002). Ebb-tidal delta systems can be classified based on tidal wave and individual wave characteristics, as proposed by Davis and Hayes (1984). Figure 2.7 shows the general classification of ebb-tidal deltas. Rijkswaterstaat (2023) has measured tidal wave data and individual wave data for multiple decades, and from these data it can be concluded that the mean wave height is $1.27m$. From literature it can be found that the mean tidal range is $1.40m$ (Elias et al., 2022). This classifies the ebb-tidal delta as a mixed-energy wave-dominated system, based on the classification system proposed by Davis and Hayes (1984). Its position in the graph is indicated by a red dot. This mixed-energy system indicates

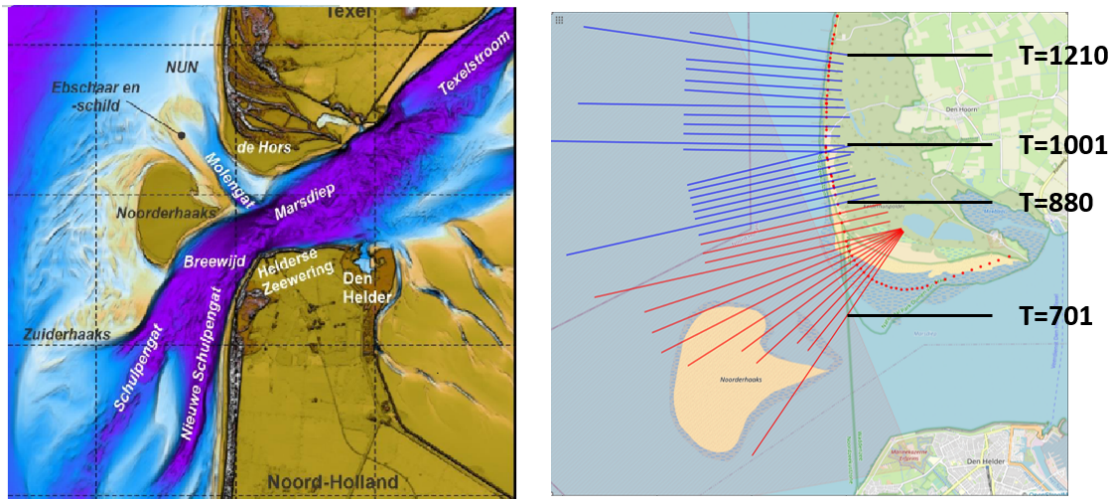


Figure 2.4: Left: overview of the morphology at the South West Texel coastline. The color indicates the depth of the map, or the extrusion of the island. Purple indicates the deepest part (-30m NAP), brown indicates 0m NAP. Figure from Elias (2021). Right: overview of transects at SW Texel. Some of the transects are indicated in the map. The blue transects adhere to the BKL and have been nourished multiple times since 1990. The red transects are outside the BKL zone, but are used in the analysis of the Molengat in Section 4.5. The red dots indicate the 0-coordinates of all transects.

that both tidal flow and individual waves are likely to have significant impact on changes in the morphology, and must therefore be taken into account in a model.

Tidal flow at Texel is semidiurnal. Rijkswaterstaat has tidal data available for a time range of 1 month with time steps of 10 minutes. These data are available at multiple locations in the North Sea, and are used to set up the model in Chapter 5. Figure 2.8 shows this tide at 1 location (west of the Noorderhaaks) and the spring-neap range varies between 1.0 – 2.2m. Research from Elias et al. (2006) and Elias and Van der Spek (2017) mention a spring, neap and average tidal range of respectively 2.0, 1.0, and 1.4m, which is in line with the data presented here. Therefore, the time series is used as a representative tide. The tidal wave through the system propagates from the south-west alongshore to the north-east.

2.3.3 Hydrodynamic characteristics - Waves

Since this coast has a mixed-energy system, both tidal current and wave conditions are important in morphological analysis. It is relevant to have information about different wave classes in order to accurately model the impact of waves, which is done in Chapter 5. Multiple researches have been conducted to determine the average significant wave height H_s , accompanying wave period T_s (Elias and Van der Spek, 2017. Elias et al., 2006) and typical storm wave conditions (Elias and Van der Spek, 2017. Elias et al., 2022). Yet, the available data lack the incoming direction of these waves and their directional spread, or they consider a too small fraction of waves, which the required information for wave modelling incomplete. Therefore, a more extensive wave analysis using raw data from Rijkswaterstaat is presented below.



Figure 2.5: Bird perspective of the South West Texel coastline. In the middle of the photo there are a few horizontal lines in the water, which indicate submerged cross-shore groynes that get exposed only during low tides. The photo is taken at approximately JARKUS transect 900 and the coast bend starts at around transect 1000. The white single line of white-capping waves indicates that during these conditions the waves break only at 1 breaker bank.

The wave analysis is based on Rijkswaterstaat on hourly averaged significant wave height measurements from the period 1995-2021 (Rijkswaterstaat, 2023). This data has been measured at the wave buoy Eierlandse Gat (Figure 2.9), where the bottom is located at a depth of 26m. This is the closest location to SW Texel that has measured sea wave data and it is therefore assumed that these wave data are most reliable for SW Texel. There are wave measurement locations near Den Helder too, but they are not useful as the wave heights in the Wadden Sea are severely impacted by the diffraction in the basin and the geometry of the basin.

Figure 2.10 (left) shows the wave rose based on the wave data from this wave buoy. The colours indicate the value of the wave height, and the thickness of each color layer indicates the percentage of waves that occurs for each wave height. Waves predominantly come from the North West (NW) or South West (SW). The right graph shows the occurring wave height for each hourly measurement, distributed over the direction. Waves from the NW are bounded between $270^\circ - 360^\circ$ and SW waves between $180^\circ - 270^\circ$. This graph shows that the highest waves originate from these 2 directions. The lower bound of 180° is not important for the analysis, because the number of waves from that direction is low, shown by the small bracket in the left figure. Moreover, the highest waves from this direction are 2m, which has significantly less impact than NW and SW waves of 5 – 7m (see Equation 2.1 and 2.2).

To answer research question 5B - what processes cause most sediment - it is important to split the wave data into wave classes. This research distinguishes both wave conditions from SW ($180^\circ - 270^\circ$) and NW ($270^\circ - 360^\circ$), and also distinguishes storm and calm wave conditions. NW waves occurred



Figure 2.6: Overview of the southern tip of Texel: De Hors, an area that does not have a BKL to satisfy. The land in the distance is Den Helder, and the island on the right is the Noorderhaaks. The narrow white line just in front of the Noorderhaaks indicates a separation of the flow into 2 channels: the big channel is the Molengat, and the small one is a developing tidal channel (Elias, 2021). This photo is taken at JARKUS transect 900. More photos of the coast can be found in Appendix A.

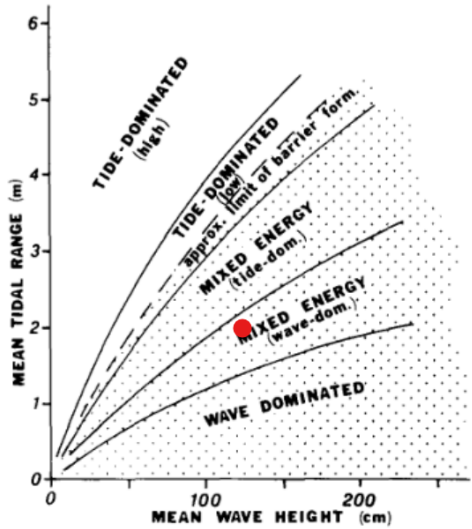


Figure 2.7: Classification of ebb-tidal delta system based on average wave height and average tidal range. Figure from Davis and Hayes (1984).

45% of the time, whereas this was 33% for SW waves. Storm conditions are defined based on time: a storm exists 5% of the time, while calm conditions occur 95% of the time. From the number of wave height recordings it can be concluded that the highest 5% of the waves are larger than 2.80m and therefore is the threshold value of storm waves. This time-based storm approach is based on Elias and Van der Spek (2017).

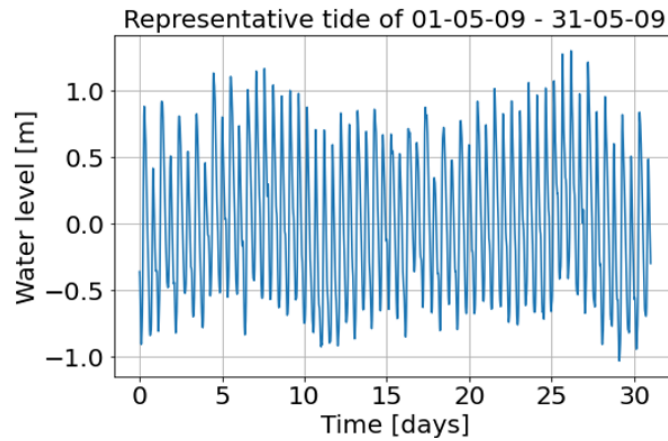


Figure 2.8: Overview of observed tidal water levels west of the Noorderhaaks in the period 01-05-2009 to 31-05-2009. The tidal range varies throughout each tidal cycle.

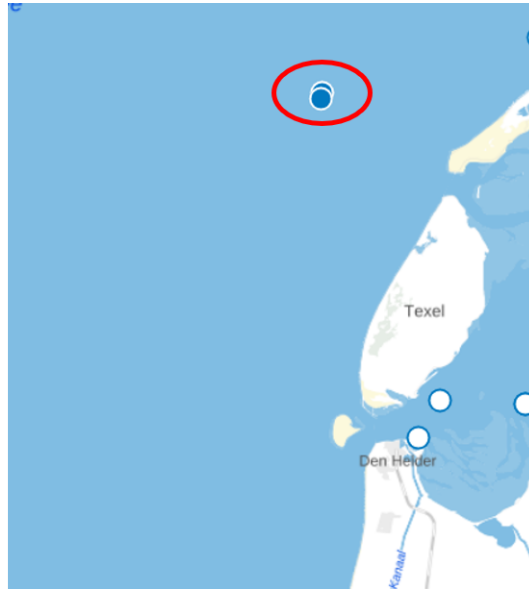


Figure 2.9: Location of wave buoy near Eierlandse Gat that measured the wave data used for SW Texel.

The waves are separated in 4 classes. Given a wave is from NW, storm conditions occur 5% of the time. The probability of a wave from the NW is 45%, so the probability of a NW storm is $0.45 * 0.05 = 0.025$. The probability of NW calm conditions is $0.45 * 0.95 = 0.4275$. The probability of each wave class is used in the model results in Chapter 6. The significant wave height for NW calm conditions is then calculated using all NW wave data points below the storm wave height, indicated by 1 in Figure 2.10. Wave classes 2,3 and 4 are also indicated in the figure and their characteristics are shown in Table 2.1.

Waves drive alongshore sediment transport S and this transport is proportional to the cubed significant wave height H_s (Komar and Inman, 1970):

$$S \propto H_s^3 \quad (2.1)$$

This proportionality indicates that higher waves contribute more to the total sediment transport at

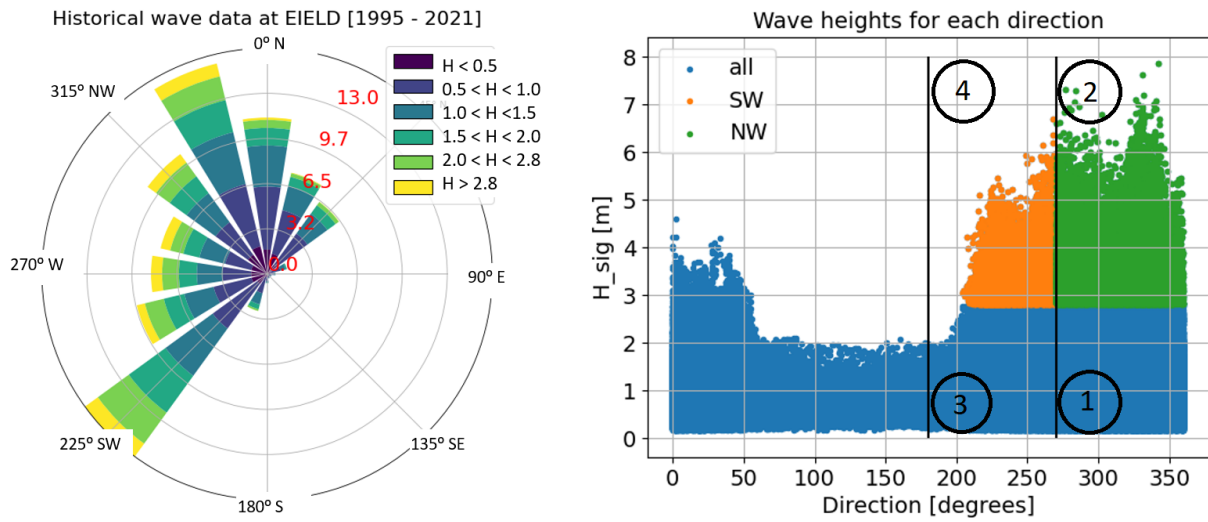


Figure 2.10: Left: wave rose at Eierlandse Gat based on data from 1995-2021. The values on the circle axis indicate the percentage of the waves that occurs in each directional bracket. Right: this graph shows all hourly measured wave heights plotted over the direction. The orange part indicates SW storm waves ($H_s > 2.80m$) and the green indicates NW storm waves.

each location, and therefore this needs to be taken into account to find the average sediment transport wave. This is done by giving the higher waves a larger weight factor, which is a methodology based on Kaergaard and Fredsoe (2012):

$$H_s = \sqrt[3]{\frac{\sum_{i=1}^n H_{s,i}^3}{n}} \quad (2.2)$$

The average wave period T_m and average wave direction θ_m are calculated using the wave height as a weight factor:

$$T_m = \frac{\sum_{i=1}^n (H_{s,i}^3 * T_{p,i})}{\sum_{i=1}^n (H_{s,i}^3)} \quad (2.3)$$

$$\theta_m = \frac{\sum_{i=1}^n (H_{s,i}^3 * \theta_i)}{\sum_{i=1}^n (H_{s,i}^3)} \quad (2.4)$$

For calm conditions the 95% lowest wave data are used in this calculation and for storm conditions the 5% highest waves are used. The threshold of the storm wave height is $H_s = 2.80m$. In Figure 2.10 the storm values are indicated with orange and green color for SW and NW waves respectively. Using the above equations the characteristic values of each wave condition is determined and summarized in Table 2.1

The average waves are in the same order of magnitude as those of Elias et al. (2006): $H_s = 1.3m$, $T_s = 5s$, Elias and Van der Spek (2017): $H_s = 1.44m$, $T_s = 5s$, and Ridderinkhof et al. (2015): $H_s = 1.37m$, $T_s = 6.0s$. The used significant wave height for the storm waves cannot be compared with this literature, because the storm definition is different. Differences with literature can be explained by the

#	Wave direction [°]	Conditions	H_s [m]	T [s]	θ [°]	Directional spread [°]	Wind speed [m/s]
1	NW [270-360]	Calm	1.39	6.8	319		7.8
2	NW [270-360]	Storm	3.65	8.6	312	21	15.4
3	SW [180-270]	Calm	1.49	6.1	235		8.7
4	SW [180-270]	Storm	3.37	7.5	239		15.2

Table 2.1: Characteristics of average waves and storm waves as input for wave-modelling, as described in Chapter 5.

different approach of using weight factors, but the order of magnitude serves as a reference of this estimation.

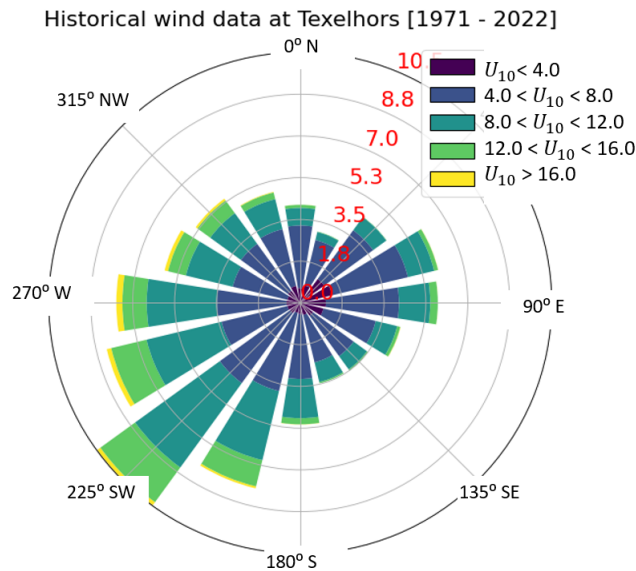


Figure 2.11: Wind rose from wind data at Texelhors from KNMI (2022). The dominant wave direction is from the south-west.

2.3.4 Wind

A wind rose is plotted in Figure 2.11 using daily averaged wind speed U_{10} and direction data from KNMI - the Dutch meteorological institute (KNMI, 2022). The data is taken from the period 1971-2022. The dominant wind direction is from the SW. The wave rose in Figure 2.10 shows a dominant wave direction in the same range. Simultaneously, the wave rose also contains a dominant wave direction from the North West, whereas the wind rose does not. Elias and Van der Spek (2017) explained this difference by the geometry of the North Sea basin: NW waves have a long fetch and SW waves a much shorter fetch. Using the same approach as the previous section, the wind speeds per wave characteristic are estimated and summarized in Table 2.1.

3 | Conceptualization of solutions

This chapter focuses on the question what interventions can be applied to maintain the coast landward of the BKL in the future. In Section 3.1 multiple alternatives are discussed, followed by an argumentation for the considered solution in this research.

3.1 Design alternatives and choice

Multiple future protection schemes are possible for the area of SW Texel. They are listed first and subsequently discussed in more detail. It is emphasized that this research only focuses on the results of 1 solution, and does not focus on the comparison of multiple alternatives, as the design of the alternatives is not done in detail. As a result, other alternatives can still be a viable option for the future of coastal maintenance at SW Texel. The alternatives are shown in Figure 3.1.

1. Continue the current nourishment program.
2. Apply a localized mega nourishment at the coast of SW Texel to protect and feed adjacent beaches in the long term.
3. Construct a cross-shore dam to catch sediment in front of the BKL-maintained beach at SW Texel.
4. Apply an outer delta nourishment to nourish the coastal foundation for the long term.

1. Continuation of current nourishment program

The current nourishment program has been able to keep the BKL largely satisfied since 1990. Small adjustments of the BKL have been made, and at some locations the MKL has retreated so far landward that the BKL was not satisfied anymore on the time scale between 2 nourishments (3 years). Yet, over the decade time scale this maintenance program has been successful.

The main research question is to find more sustainable measures to protect the coastline of SW Texel compared to the current scheme. Limiting the research to only this solution would not answer the question. It is stressed that this research looks at alternatives for coastal protection, but it does not mean the current scheme has to be cancelled. It is still an option for the foreseeable future. The disadvantages are listed in Section 1.1, and the advantages (+) below:

- + The coast can be locally strengthened by location-specific nourishments.
- + The coast remains sandy, which is attractive for beach goers and beach businesses.
- + This method has proven to work, by satisfying the BKL since the implementation of the BKL requirement.

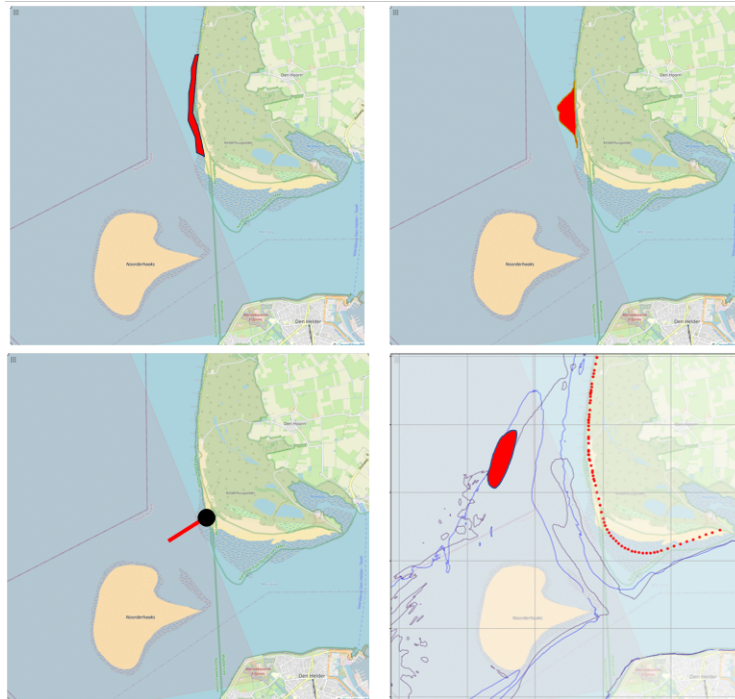


Figure 3.1: Potential future coastal maintenance options. Upper left: continuation of current nourishment program. Upper right: mega nourishment at coast. Bottom left: construction of cross-shore dam. Bottom right: outer delta nourishment.

2. Mega nourishment at coast

The application of a mega nourishment (upper right panel in Figure 3.1) at the coast has the goal of nourishing the adjacent coastline by alongshore diffusion of sediment. This modification could change the bottom and the beach such that the erosion and accretion patterns alongshore change. When waves break at different alongshore locations - in this case because of the bottom change of the mega nourishment - there is a change of wave energy flux that could cause a shift in alongshore sediment transport gradients (Grady et al., 2013). As a result, the erosion and accretion patterns could potentially change. Grady et al. explain that the degree to which alongshore sediment transport gradients are altered depends on the alongshore non-uniformity of the bottom. Computing future sediment transport gradients in a model includes more uncertainty in this area than alongshore uniform coasts, because the bottom at SW Texel consists of the Molengat and the mega nourishment.

The volume of the mega nourishment must be an order of magnitude larger than the regular nourishments at SW Texel. It could be regarded as multiple nourishments that are combined in one nourishment acting as a buffer. As a result, dredging ships only have to be mobilized once, which reduces total costs and the frequency of nuisance compared to multi-annual smaller nourishment activities. This reduces the disadvantages of the current nourishment scheme, as mentioned in Section 1.1.

- + Dredging happens only at the beginning of the project, which is cheaper.
- + Dredging vessels only have to be mobilized once, which limits nuisance and turbidity increase in the ecosystem.
- + It feeds the shoreline for the long term by alongshore diffusion.
- + The coast remains sandy, which is attractive for beach goers and beach businesses.

- The total investment costs must be paid at the start of the project instead of an annual payment procedure.
- Uncertainties of BKL satisfaction far from the mega nourishment on the long term may increase.

3. Construction of cross-shore dam

The construction of a cross-shore dam (bottom left panel in Figure 3.1) aims to locally catch sediment from the tidally averaged mean transport direction. The goal of such a dam on the shoreline morphology is that the littoral drift is blocked completely or partially (Kristensen et al., 2016). Kristensen et al. claim that as a result, the bed contours updrift of the dam tip tend to turn against the predominant waves. As a result, the downdrift side of a dam at SW Texel is likely to experience erosion. This means that the coast would be locally fixed in place, but it shifts the erosion problem to downdrift. Erosion is allowed south of transect 880 because there is no BKL to be satisfied there, so transect 880 would be an interesting location to investigate the effects of the construction of this dam. In regard of this project, lessons could be learned from the effects the Eierlandse Dam has had on the coast of North Texel at transect 3051.

The construction of a dam means that no sediment is added to the system. A cross-shore dam is a hard solution (structure), as opposed to a mega nourishment (soft solution). While the transects close to the dam may benefit from the sediment catchment, the transects further north may experience erosion, and therefore require additional interventions. These are unknowns that could be researched more extensively, and may be solvable by investigating the optimal location and length of the dam extending into sea.

- + In transects close north of the dam the BKL is satisfied for long term due to the catchment of sediment by the dam.
 - + The structure does not need periodic construction works as the current nourishment program does. It requires maintenance at most.
 - + The Eierlandse Dam on North-Texel is similar to this dam, which can serve as a good learning tool for considerations in this project.
- It is a hard solution.
 - Depending on location and structure size, transects far from the structure may require additional interventions on the long term.
 - Lack of sediment nourishment may affect the functionality during sea level rise.

4. Outer delta nourishment

A very new alternative is the application of an outer delta nourishment (bottom right panel in Figure 3.1). This type of nourishment is placed in the tidal channel(s) of the outer delta and aims to nourish the coastal foundation on the long term in the order of T 20 years (Ministerie van Infrastructuur en Waterstaat, 2022). The same research claims that outer delta nourishments could merge into the existing sediment transport flows towards the downdrift island - in this case being from the NUN to Texel. The research claims that such a nourishment could also be altering existing sediment transport patterns and thus erosion and accretion spots, but this topic requires more research.

The amount of available knowledge about outer delta nourishments is limited due to its novelty. The impact of the outer delta nourishment on the direction of currents and subsequent sediment transport

is one example that remains unpredictable.

- + Application of the nourishment is farther from the coast, meaning nuisance and turbidity disturbance is further from the protected system.
- + The nourishment may nourish the coast on the long term.
- + Dredging happens only at the beginning of the project, which is cheaper.

- The intervention is not applied directly at the coast, which imposes a risk of BKL dissatisfaction on the short term.
- It is unknown what percentage of the nourishment ends up in the wanted coastal area.
- The impact on sediment transport is unknown.

Alternative choice and argumentation

Each solution has its own advantages and disadvantages. There are many unknowns regarding each project, making it impossible to argue which alternative is better than the other. Each solution could be viable. Nonetheless, one intervention is chosen for this study, and that is the mega nourishment.

The mega nourishment is a soft solution, and soft solutions have a higher priority of realisation for Rijkswaterstaat than hard solutions. Therefore, the construction of a cross-shore dam is not chosen. Rijkswaterstaat has recently started looking into the opportunities of the application of a cross-shore dam, but because of their soft-hard-solutions-prioritization the research of a mega nourishment is more relevant (Brand, interview, 2022). Since Rijkswaterstaat is the manager of the coastline, their valuation is deemed to be leading. Furthermore, the application of an outer delta nourishment currently has many unknowns. The mega nourishment is applied directly at the coast and thus contributes to the satisfaction of the BKL on the short term too, whereas the outer delta nourishment does not.

In the current advantages and disadvantages the amount of emitted CO₂ is not considered, as first order approximations are difficult to make and not the goal of this research. However, in Section 1.1 CO₂-emissions are indicated as a disadvantage, but the comparison of this value requires an analysis on higher project scale than this study. Considering all alternatives, the application of a mega nourishment has the best arguments from the perspective of Rijkswaterstaat to investigate first and is therefore analysed in the model in Chapter 5 and 6.

4 | Morphological analysis of SW Texel

Chapter 4 zooms in on specific locations along the SW Texel coastline, which was illustrated in Figure 1.1. The research question is: *How has the morphology developed since 1990, including the nourishment program?* This is examined on scale of the system, and also more detailed in 4 transect parts. The goal is to identify at what locations nourishments have been applied, and how the dunes and the Molengat channel have changed in the coastal profile. In Section 4.1 an overview is given of the important factors in the sediment balance of SW Texel. In Section 4.2 till Section 4.4 the 3 factors of the sediment balance are discussed in order to show the volume changes of the area between 1991 and 2021. In Section 4.5 till Section 4.7 each of the sub-factors that contribute to each transect are discussed.

4.1 Overview sediment balance for SW Texel

The SW Texel coast is defined as transect numbers below 1210, see Figure 2.4. The area of interest in this research is transect range limited in the south by transect 880 and in the north by transect 1210.

4.1.1 Methods and definitions

Method datasets

This research uses data from 2 data sets: JARKUS and Vaklodingen. Both datasets are used to calculate volume differences between 1991-2021 for each transect. Gradients in alongshore volume differences help to identify at which locations alongshore erosion and accretion have occurred.

Definition of datasets

JARKUS contains bathymetrical data in transect lines orthogonal to the shoreline and these data are collected annually by Rijkswaterstaat. The bathymetry points are spaced every 5m nearshore and every 10m starting at 500m. In alongshore direction the transects are spaced by the difference in transect number times 10. This means the distance between transects 900-1000 is 1km. The JARKUS transects have a maximum cross-shore distance of 3km. An example of a JARKUS transect measurement is shown in Figure 4.1. On the horizontal axis the cross-shore distance is shown to the beach pole lane ('Rijksstrandpalenlijn' in Dutch, or RSP) onshore. The RSP indicates the 0-coordinate of the JARKUS data in cross-shore direction. Positive values are seaward, negative values are landward. On the vertical axis the bottom level with relative to NAP is shown. The other definitions are explained later.

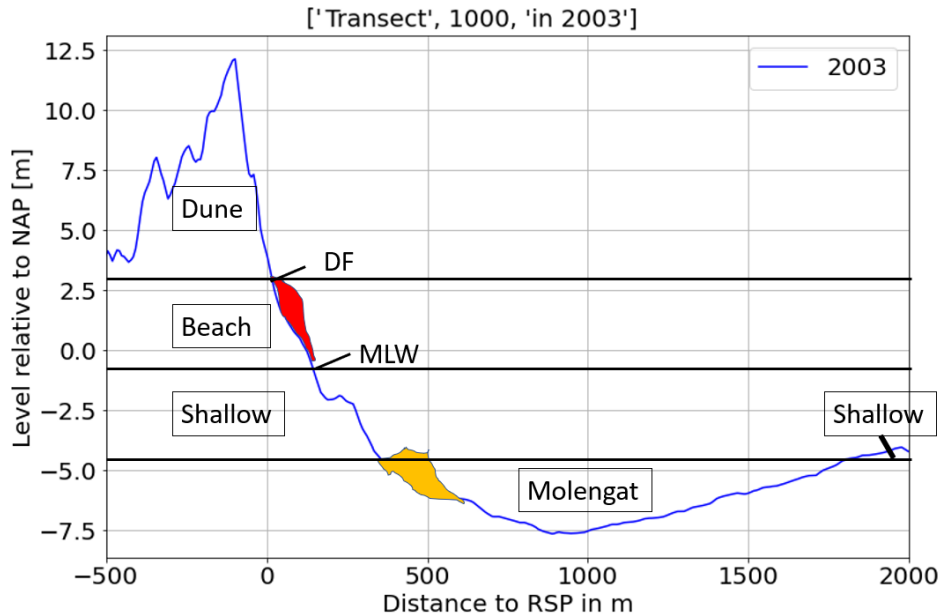


Figure 4.1: Example of JARKUS transect. The red shape indicated the location of a beach nourishment, the orange shape indicated the location of a shoreface nourishment.

Vaklodingen also contains bottom values, but measured on a 2D-grid. The bathymetrical values are divided in cells of $20 * 20m$ and they are measured approximately every 3 years. The Vaklodingen data are measured over a much larger area than JARKUS data. The Vaklodingen maps 'KB121_2120' and 'KB122_2120' from the period 1971-2021 are shown in Appendix B. Vaklodingen data are used in the analysis where the JARKUS data are not far enough offshore. In Section 7.3 a calculation is shown that in terms of accuracy, both datasets can be used interchangeably. Using Vaklodingen data allows to plot contour lines of the bottom (see Figure 4.2) and differences in bottom level between years on maps. Using an interpolation function in Python, it is possible to draw transect lines on a map and retrieve the accompanying bottom profile. This leads to a similar profile as a JARKUS transect (for example Figure 4.1), provided the transect is taken at the exact same coordinates as the specific JARKUS transect. The main differences between Vaklodingen and JARKUS are:

- Vaklodingen consists of $20 * 20m$ cells, whereas JARKUS is measured along a transect in 1D.
- JARKUS data are measured further onshore, yielding better data on dune volume. However, Vaklodingen data reach further offshore.
- JARKUS data are mostly available per year since 1990, whereas Vaklodingen has been measured every 3 years since 1991. The research comparison period is set as 1991-2021, because this allows easily interchangeable bottom values from either JARKUS or Vaklodingen.

Figure 4.2 shows depth contours in the background of years 2000 (blue) and 2021 (purple) on the left. These depth contours indicate -5m NAP depth. The -5m NAP line is in particular interesting, because the shoal seems to have a flat bed between -4m and -5m at almost every submerged location on the NUN. Between 2000 and 2021 the -5m contour has moved landward. Furthermore, the -5m contour was not attached to the coast in 2000, and in 2021 the land- and seaward contour have merged. On the right the bottom level difference between 1991-2021 is shown. The red areas indicate a higher bottom, and blue areas have deepened. In front of the Texel coast there is a distinct pattern of bottom increase on the dunes (Section 4.6), a narrow deepening strip around the water-sand interface, and bottom in-

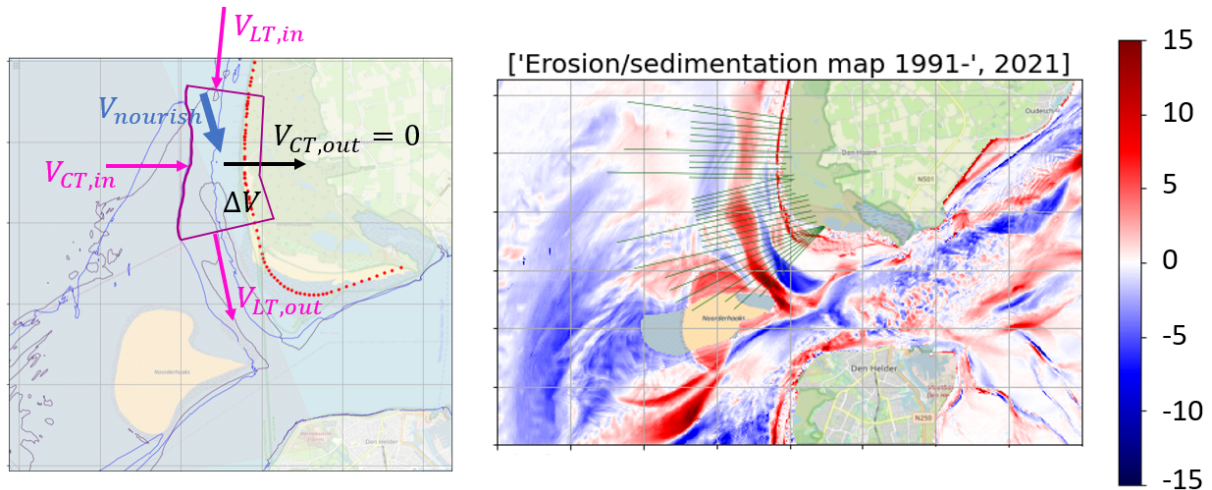


Figure 4.2: Left: the background shows a blue contour line, which represents the bottom from the year 2000. It also shows a purple contour, which represents the bottom in 2021. The Molengat has moved towards shore. Furthermore the sediment flows in and out of the system and the volume change are displayed. The purple box encloses transect range 880-1210, which must satisfy the BKL. The $V_{CT,in}$ -term is coming from the south west, as it mostly originates from the NUN entering the system. Right: Sedimentation-erosion map between 1991-2021. The map shows in red the areas that have become higher, the blue areas have experienced deepening. The scale on the right is height difference in meters.

crease further from shore. This bottom increase is a submerged bank slowly moving towards shore, and the Molengat channel in between moved towards shore. This effect is better visible between the Noorderhaaks and Texel, as the Molengat is deeper there. In the middle of the JARKUS transect area this effect is limited, because the Molengat has slowly filled up.

Method transect profiles

A sediment balance helps gaining understanding of the behaviour of the system. The sediment balance consists of nourishments applied by humans, natural sediment transport and the net difference of volume on each transect profile. The volume of nourishments is removed from the observed changes to gain insight on the behaviour of the system without nourishments, which is the case if the maintenance policy is replaced by a mega nourishment. Subsequently, each transect is divided into 4 parts, and the volume change in each part is calculated to show where in the profile the changes have been the largest. This information helps to plan a mega nourishment strategy.

Definition transect profile

A schematic representation of a transect profile is shown in Figure 4.1. The transect consists of 4 parts: the dune, the beach, the shallow area and the Molengat. The dune is defined as the volume of the first dune above the +3m NAP line, also known as the dune foot line (DF-line). In this example the DF is coincidentally located at the RSP-line. The beach exists between the DF and the mean low waterline (MLW), which has a value of -0.85m NAP at SW Texel. The shallow area has an upper bound at the MLW and a lower bound at -4.4m NAP. This area consists of a part onshore and for some transects an offshore part too. The lower bound is explained in Section 4.5. The Molengat is defined as the cross-sectional area between the -4.4m NAP line and the bed.

Transect	880	900	915	930	945	960	976	1000
$B_{Transect}$	100	175	150	150	150	155	200	125

Table 4.1: Width of transects 880-1000.

Rijkswaterstaat applies both beach and shoreface nourishments in their program. Beach nourishments are applied starting at the DF-level and going toward shore as far as possible (Brand, Interview, 2022). This is indicated by the red shape in Figure 4.1. There are no exact coordinates available for the cross-shore extent of beach nourishments. Shoreface nourishments - indicated in orange - are applied starting at $-5mNAP$.

Definition width of transects

The width of each transect is defined by half the distance to both adjacent transects. At transect 900 the adjacent transects are 880 and 915: half the distance to 880 is 100m and half the distance to 915 is 75m, totaling 175m, which is shown in Figure 4.4. All transects except the transects at the edges of the system have the width calculated the same way. Both transects at the edges of the area only have 1 adjacent transect, so transect 880 has a width of 100m. The width-values of transect range 880-1000 are shown in Table 4.1. The entire table including the entire transect range is shown in Appendix D.

4.1.2 Sediment balance

This section explains which sediment flows go in and out of the system. The magnitude of each of the sediment flows is determined in Section 4.4 to 4.7. A sediment balance helps understanding what would have happened without human intervention in the area. The in-, outflow and storage of sediment are shown on the left of Figure 4.2. The equation of a sediment balance in the SW Texel area is:

$$\Delta V_{tot} = V_{nourish,tot} + V_{CT,in} + V_{LT,in} - V_{LT,out} - V_{CT,out} \quad (4.1)$$

Where:

- ΔV_{tot} is the volume difference of the bathymetry between 1991 and 2021 of all transects. This term can be calculated from the JARKUS measurements.
- $V_{nourish,tot}$ is the sediment nourished into the system by dredging vessels. This term is known from RWS data.
- $V_{CT,out}$ is the sediment volume that moves behind the first dune of the coast. In Section 4.3 it is explained that this volume is negligibly small and is set to 0.
- $V_{CT,in}$, $V_{LT,in}$ and $V_{LT,out}$ represent the incoming cross-shore transport, incoming longshore transport and outgoing longshore transport respectively. The size of these individual terms is unknown.

The sum of the unknown individual terms can be combined into a term that describes the natural volume change of all transects without interference of the nourishment program $V_{Nat,tot}$. It can be taken

as the only unknown in Equation 4.1:

$$V_{nat,tot} = V_{CT,in} + V_{LT,in} - V_{LT,out} \quad (4.2)$$

$$\Delta V_{tot} = V_{nourish,tot} + V_{Nat,tot} \quad (4.3)$$

The control volume is bounded by the first dune on the coast and the location of the offshore Molengat bank in 1991 which is submerged at around -4.4m NAP. The volume change is calculated per transect, and the summation of all transects equals the total volume change. The total area alongshore is between transect 880-1210, as these transects must adhere to the BKL.

Equation 4.3 merely shows the volume change of the control volume between 2 moments in time. To better understand what happened in the area through time, in the next sections $\Delta V_{transect}$ of each transect part in the control volume is determined, then the changes of the volume per year are indicated, and also the spatial distribution of the volume along each transect is analysed in detail. Figure 4.3 shows $\Delta V_{transect\ 880}$ of transect 880 between 1991-2021, where nourishments have been added to the transect, and $V_{nat,transect\ 880}$ in this case is indicated offshore. Since it is a 2D-figure, it does not show the possibility of a net sediment flow in alongshore direction, orthogonal to the screen of the transect. The green area indicates erosion since 1991, and the purple area shows accretion since 1991. The green area corresponds to the blue part between the landward migrating bank as mentioned in Figure 4.2. Behind the first dune on the left cross-shore transport is indicated as 0. On the right the $\Delta V_{transect\ 880}$ of transect 880 is subdivided into the 4 transect parts:

$$\Delta V_{transect\ 880} = \Delta V_{Dune,transect\ 880} + \Delta V_{Beach,transect\ 880} + \Delta V_{Molengat\ infilling,transect\ 880} + \Delta V_{shallow,transect\ 880} \quad (4.4)$$

Where:

- $\Delta V_{Dune,transect\ 880}$ is the volume of sediment that went into the first dune above +3m NAP, as defined in Figure 4.1.
- $\Delta V_{Beach,transect\ 880}$ is the volume of sediment that went into the beach.
- $\Delta V_{Molengat\ infilling,transect\ 880}$ is the volume that has been deposited into the Molengat channel below -4.4m NAP. This term consists partly of erosion (green part) and partly of accretion (purple) and its value represents the net change.
- $\Delta V_{shallow,transect\ 880}$ is the remaining term between MLW and the Molengat (-4.4m) that represents the volume changes on the transect that are not incorporated by the other terms. In this example there is partial accretion on the beach ($x = 250m - 300m$), partial erosion too ($x = 300m - 500m$), and accretion above the -4.4m NAP-line in the offshore part of the transect ($x = 1000m - 2000m$). This last part needs to be considered because the offshore boundary was set at the 1991-cross-shore Molengat bank location.

In the next sections each term in Equation 4.3 is discussed in detail.

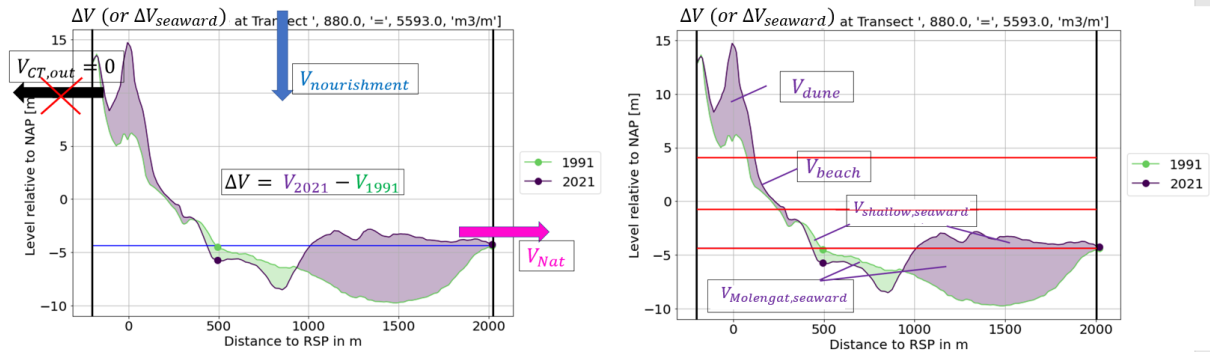


Figure 4.3: Left: overview of the sediment balance in a transect. The direction of $V_{nat,transect\ 880}$ in this example is pointed towards offshore, while it can also be partly directed orthogonal to the screen in alongshore direction. This depends on the values of the $V_{LT,out}$, $V_{LT,in}$ and $V_{CT,in}$, yet these are unknown. Right: subfactors of $\Delta V_{transect\ 880}$. Two $V_{Molengat\ infilling,transect\ 880}$ and $V_{shallow,transect\ 880}$ terms are illustrated, as they have a part that consists of erosion (green) and accretion (purple). The red lines indicate the separation between dune volume, beach volume, shallow volume and Molengat volume from up to down respectively.

4.2 Nourishment volume ($V_{nourish,tot}$)

The main question in this section is: *What has been the history of nourishment volumes at Texel and how have they been distributed?* Rijkswaterstaat has applied 2 types of nourishments in the SW Texel area: beach nourishments and shoreface nourishments. The cross-shore locations of both types is shown in Figure 4.1. It would be useful to know what percentage of nourishments end up at each location of the profile, so it could be checked whether the nourishment program contributes to its goal to maintain the BKL or not. However, it is difficult to observe changes between before- and after-nourishment bottom profiles in 2 successive years. This is caused by a combination of reasons:

1. The timescale of processes that cause changes at the location of nourishments seems to be in an order of smaller than a year. Brand et al. (2022) mention that beach nourishments on average disappear after 2.9 years, supporting the idea that profile changes are significant within 1 year.
2. Measurements of transects are not taken as frequently as the changes occur, which can cause large differences between 2 successive years.
3. The exact measurement date of the transects is unknown, as Rijkswaterstaat's dataset has set them at 1 July artificially.
4. Cross-shore coordinates of the applied nourishments are not logged by Rijkswaterstaat.

It is important to know where nourishments have been applied, and how much has been supplied at every transect along the SW Texel coast. This helps in understanding how much erosion of the area has occurred in 1991-2021 because of human intervention and how much could have occurred naturally ($\Delta V_{Nat,tot}$). Though, this is based on the assumption that the nourishment scheme does not significantly change the natural behaviour of the system, so that the nourishments come on top of that. The Rijkswaterstaat (2022b) Nourishment data set gives the information at what JARKUS transect and how many nourishments have been applied. The nourished volume is divided into beach and shoreface nourishments and are shown in Figure 4.4. The left part of the figure shows the overview of the area, where the transects are indicated by number. The blue shape shows the cross-shore location where

shoreface nourishments have been applied, and the yellow shape indicates the location of beach nourishments. Table 4.2 shows the used information of the shoreface nourishment in 2003 on the second line.

#	Transect Start	Transect End	Year	Volume [Mm ³]	Volume over beach width [m ³ /m]	Type of nourishment
1	880	1063	2005	0.301384	164.6907	Beach
2	900	1148	2003	0.972486	392.1315	Shoreface
3	900	1392	2007	2.00097	406.7012	Shoreface
4	900	1070	2009	0.4	235.2941	Beach
5	900	1210	2012	0.751589	242.4481	Beach
6	900	1190	2017	0.895	308.6207	Beach
7	900	1298	2021*	1	251.2563	Beach
8	930	1210	1994	0.761204	271.8586	Beach
9	1001	1190	2000	0.35702	188.8995	Beach
10	1038	1143	1997	0.340038	323.8457	Beach
11	1200	1312	2012	0.5	446.4286	Shoreface

Table 4.2: Nourishment data at SW Texel from Rijkswaterstaat (2022b). With the total volume known, spread out over a transect range, the volume per meter beach width can be calculated. *This beach nourishment has not been included in the analysis of Chapter 4, because its impact is not noticeable in the transects of 2021. The nourishment was applied after the measurements were finished.

The total volume of the 2003 shoreface nourishment in Table 4.2 is $V_{nourish,2003,tot} = 972,000 \text{ m}^3$ and is smeared out over an alongshore range from transect 900 to transect 1148. As a result the nourished volume of the 2003 nourishment is about $V_{nourish,2003,transect} = \frac{972,000}{2480} = 392.1 \text{ m}^3/\text{m}$ per alongshore meter. This is an approximation, because the coast is curved at transect 1000-1001 and not all transects are parallel. Further from shore the distance between transect 1000 and 1001 increases, meaning that the nourished volume on the foreshore is spread over a larger distance, leading to a slight overestimation of the calculated shoreface nourishment volume. When the total nourished volume per meter beach width alongshore is summed for all nourishments that have ever been applied in the project area, the result is $V_{nourish,transect}$ shown the right graph of Figure 4.4. The graph shows how much cumulative volume has been nourished from transect 880 to 1210 since 1991. The data also shows that no nourishments have ever been applied in this area before 1994. The cumulative nourished beach volume $V_{nourish,transect,beach}$ is largest around transect 1033-1053, which is the location where the NUN also attached to the coast of Texel.

Using both the width of each transect from Table 4.2 and the volume difference per meter beach width $V_{nourish,transect}$, the total nourished volume at SW Texel $V_{nourish,tot}$ can be calculated. From Rijkswaterstaat (2022b) Nourishment data, the total nourished beach volume $V_{nourish,tot,beach}$ in the area was calculated to be $V_{nourish,tot,beach} = 3.813 \cdot 10^6 \text{ m}^3$, the nourished shoreface volume is $V_{nourish,tot,shore} = 2.318 \cdot 10^6 \text{ m}^3$, amounting to a total nourished volume of $V_{nourish,tot} = 6.131 \cdot 10^6 \text{ m}^3$.

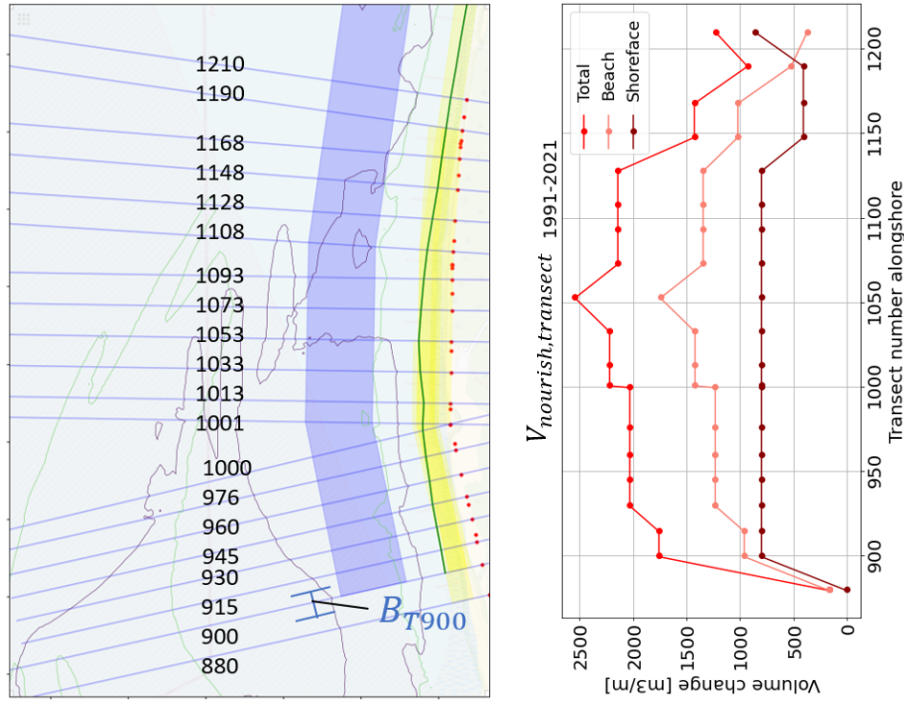


Figure 4.4: The left figure shows the location of the applied nourishments at SW Texel and the numbered transects. The width of transect 900 is illustrated in the figure. The right graph shows the cumulative nourished volume of the same transect area per m alongshore beach width $V_{nourish,transect}$.

4.3 Volume difference in 1991-2021 (ΔV_{tot})

The volume difference for each transect $\Delta V_{transect\ i}$ was already shown in Figure 4.3. For transect 880 it is calculated by:

$$\Delta V_{transect\ 880} = V_{2021,transect\ 880} - V_{1991,transect\ 880} \quad (4.5)$$

The definition of the cross-shore boundaries of $V_{2021,transect\ i}$ and $V_{1991,transect\ i}$ is important, as the location significantly impacts the size of the volume changes, see Figure 4.5 and 4.6. The boundary must be defined for all transects and also be far enough offshore to incorporate the effect of the landward migrating Molengat banks. The cross-shore boundaries are set on:

- A cut-off point behind the first dune. Appendix C.1 shows all transect developments through time, and they all show that the volume increase behind the first dune is negligible. One example is Figure C.9. As a result, on this boundary the outgoing cross-shore transport $V_{CT,out} = 0$.
- The offshore boundary is set at the 1991 location where the Molengat intersects the $-4.4m$ NAP line, as explained in Section 4.5. This is the seaward bank of the Molengat.

Next, the total volume difference between 1991-2021 for each transect $\Delta V_{transect}$ can be calculated. The volume difference shown in Figure 4.6 is positive everywhere (accretion), but it depends on where the offshore boundary of the system is chosen. The current offshore boundary is located at the Molengat seaward bank, and the corresponding volume difference is called $\Delta V_{seaward,transect}$. It is also possible to choose the offshore boundary at the landward bank of the Molengat, as shown in Figure 4.5. As a re-

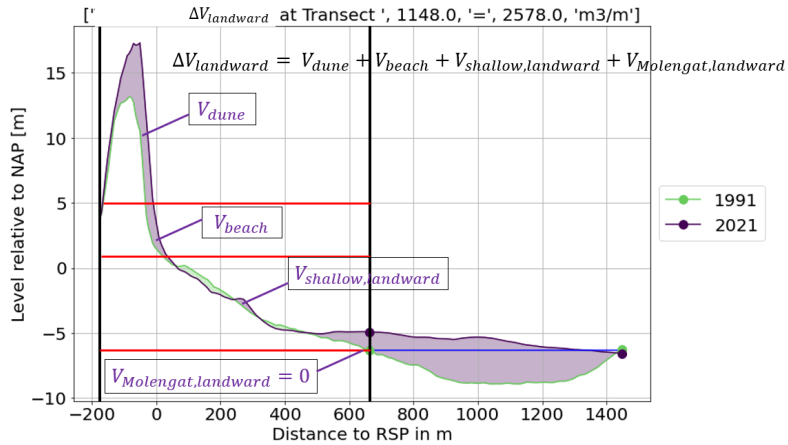


Figure 4.5: The offshore boundary is at the Molengat landward boundary instead of the seaward boundary. As a result, the volume changes in Figure 4.6 are much smaller. Boundaries are indicated by the vertical black lines. Erosion is indicated in green, and accretion in purple. The red lines indicate the separation between dune volume, beach volume, shallow volume and Molengat volume from up to down respectively.

sult, less volume enters the system - mainly due to the Molengat infilling being excluded. The volume difference resulting from the landward bank boundary - $\Delta V_{landward,transect}$ - is shown on the right of Figure 4.6. As a result, the area between the dune and the landward Molengat bank eroded in transect range 945-976 and 1013-1043. Both graphs are important, as the right graph shows where erosion has happened close to the coast where the BKL must be maintained. The left graph is important to show where large quantities of sediment are slowly migrating towards the Texel coastline. Knowing where large quantities are moving towards shore helps to prevent unnecessary selection of a location for future interventions if the coast will be nourished naturally on the long term without human intervention. In transect range 945-1053 the onshore volume changes are most disadvantageous (right graph), and the lowest volume of sediment is moving towards shore (left graph). The values of the left graph are shown in Table G.1 and G.2. The total volume change ΔV_{tot} is the sum of the volume change of all transects $\Delta V_{tot} = 8.22 \text{ Mm}^3$ between 1991-2021.

The remainder of this research uses the seaward boundary of the Molengat in volume calculations, and $\Delta V_{seaward,transect}$ is therefore also mentioned as $\Delta V_{transect}$. Next to just volume differences it is important to look at the other sub factors of $\Delta V_{transect}$ to see how the changes happened spatially in each transect.

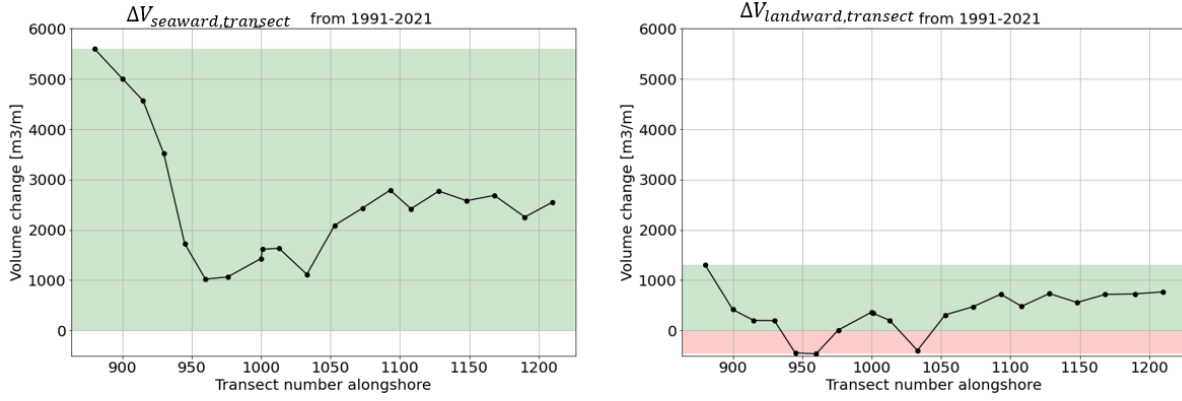


Figure 4.6: Left: $\Delta V_{seaward,transect}$ if the offshore boundary is chosen at the sea bank of the Molengat channel with the -4.4m line (right graph Figure 4.3). Right: $\Delta V_{landward,transect}$ if the boundary is chosen at the landward intersection point between the Molengat channel and the -4.4m line (Figure 4.5). Both graphs include the effect of applied nourishments.

4.4 Natural transport term ($V_{Nat,transect}$)

ΔV_{tot} and $V_{nourish,tot}$ are known, meaning that $V_{Nat,tot}$ can be calculated using Equation 4.3. In the preceding sections the volume changes include the applied nourishments in the area. $V_{Nat,tot}$ represents how much would have likely been accreted if the nourishment program was not applied. This is relevant when the current nourishment scheme is replaced with a mega nourishment. It is not possible to determine how the coast would have changed without nourishments to an exact degree, since the addition of nourishments could also change sediment transport gradients alongshore. According to Coelho et al. (2020) nourishments generally cause a smaller shoreline retreat and an increase of the cross-shore profile volumes during a limited period of time. This supports the assumption that the applied nourishments did not change the behaviour of sediment transport significantly. Figure 4.7 shows on the left the $V_{Nat,transect}$ in pink when the offshore boundary is chosen at the seaward bank of the Molengat. When $V_{Nat,transect} > 0$ and the nourishment scheme is aborted, there is accretion, and for $V_{Nat,transect} < 0$ without a nourishment scheme, there is erosion. The right graph shows the same, but for when the boundary is chosen at the landward bank of the Molengat. In this case there is only small accretion at transect 880 when looking at $V_{Nat,transect}$ 880, and there is erosion for all other transects. The actual volume changes including the nourishments are indicated by the black lines, which are the same as in Figure 4.6.

The erosion and accretion pattern without the nourishment scheme $V_{Nat,transect}$ depends on the location of the chosen boundary, because of the landward migrating shoal - the NUN - in front of the coast. The movement of the shoal is important to determine what the optimal location of an intervention in the area would be. The right graph shows there is erosion in the nearshore area of all transects when the nourishment scheme is aborted and the erosion is maximum between transect 945-1053. Since this range cannot expect natural nourishment by landward movement of the Molengat, it is reasonable to choose this location for a system intervention. The left graph shows that when looking at the movement of the shoal towards shore, the area of 945-1053 would still have experienced erosion without the nourishment program. Additionally, the observation of Figure 2.1 that the BKL is not satisfied between transect 940-1080 provides extra support to apply an intervention in transect range 945-1053. The dis-

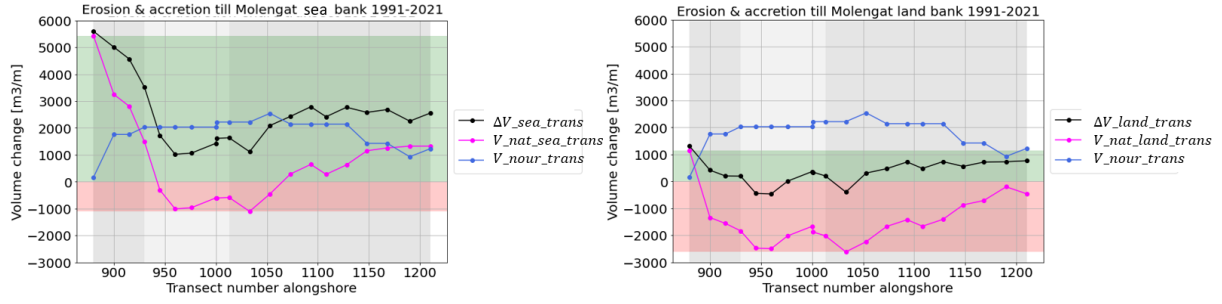


Figure 4.7: If the nourishment program at each transect $V_{nourish,transect}$ is subtracted from the volume changes at each transect $\Delta V_{transect}$, it shows in what transects erosion would have occurred naturally $V_{nat,transect}$. Left: the cross-shore boundary is chosen at the seaward Molengat bank (subscript sea), and without the nourishment scheme there is erosion between transect 945-1053. Right: the cross-shore boundary is set at the landward Molengat bank (subscript land), leading to a nearshore erosion profile almost everywhere without the nourishment scheme.

satisfaction of the BKL is instantaneous, and is generally alternating between satisfied and dissatisfied within the short term ($O(5yr)$), yet it still highlights short term need for a mega nourishment at this location.

The next sections discuss the sub-factors $\Delta V_{Dune,transect}$, $\Delta V_{Beach,transect}$, $\Delta V_{Molengat\ infilling,transect}$ and $\Delta V_{Shallow,transect}$ to gain understanding in how the volume changes for each transect $\Delta V_{transect}$ are spatially distributed.

4.5 Molengat infilling volume ($\Delta V_{Molengat\ infilling,transect}$)

The previous sections focused on the sediment flows, and the next sections highlight the volume changes in 4 parts of the profile of each transect. As a result, alongshore variability in volume changes can be identified. The first factor is the the Molengat infilling. Figure 4.5 shows that the infilling of the Molengat consists of landward bank erosion and seaward bank infilling. The sum of these 2 is the infilling of the Molengat. This volume change per meter beach width $\Delta V_{Molengat\ infilling,transect}$ is calculated by:

$$\Delta V_{Molengat\ infilling,transect} = V_{Molengat\ infilling,2021,transect} - V_{Molengat\ infilling,1991,transect} \quad (4.6)$$

Calculating the infilling rate is better than calculating the migration rate of the offshore seaward bank, because the bank becomes steeper and the infilling rate is about the entire cross-section. The cross-section of the Molengat $V_{Molengat\ infilling,transect}$ is defined as the area between $z = -4.4m$ NAP and the bottom underneath, see Figure 4.8. The value of z has been chosen because of 2 reasons:

1. To determine a correlation between time and $V_{Molengat\ infilling,transect}$ there must be enough data points, so the level must be chosen as low as possible to find an offshore boundary point.
2. The value must be as high in the profile as possible, because otherwise the $V_{Molengat\ infilling,transect}$ value becomes too low to show a correlation with time. The Molengat closure seems to be at a constant pace.

The landward intersection point is located onshore at approximately 450m from the RSP, the offshore intersection point is located offshore starting at 2000m and slowly migrating towards shore. In transect range 1128-1210 the Molengat offshore bank is deeper than $-4.4m$, so the offshore bank was determined manually by looking at the transect profiles. In these transects the Molengat has already been filled (see Appendix C.1), so they can be used to explain how the Molengat closes.

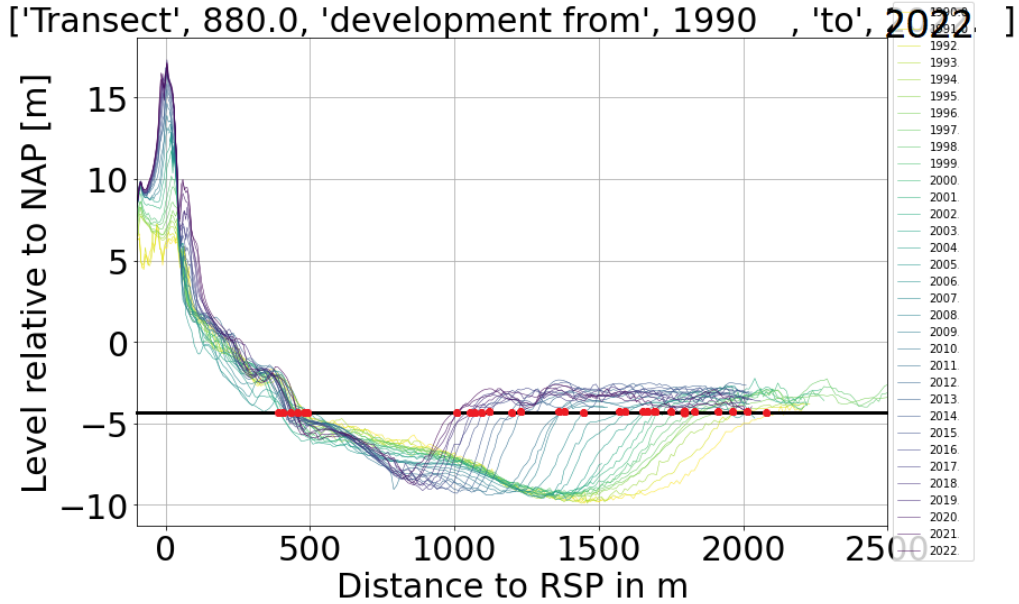


Figure 4.8: In the early 1990s the landward intersection of transect 880 moved towards shore. Starting around 2006 the intersection started moving seaward slightly offshore. Meanwhile, the offshore intersection point moved landward and simultaneously made the Molengat shallower.

4.5.1 Calculation of $V_{Molengat\ infilling,transect}$

The Molengat infilling volume for each transect $V_{Molengat\ infilling,transect}$ is relevant to know how large the influence is on $\Delta V_{transect}$ for each transect. Together with the other sub factors, the $V_{Molengat\ infilling,transect}$ is shown in Figure 4.18. This value is calculated using Equation 4.6.

For all transects that do not have a $V_{Molengat\ infilling\ 2021,transect}$ - or $V_{Molengat\ infilling\ 1991,transect}$ -value in JARKUS data, the Vakloedingen data is used to determine the value. The total volume infilling of the entire Molengat within this project range $\Delta V_{Molengat\ infilling,tot}$ can be calculated by multiplying each individual transect volume with the transect width $B_{transect}$ from Table D.2 and then summing all values, see Equation 4.7:

$$\Delta V_{Molengat\ infilling,tot} = \sum_{i=1}^n (\Delta V_{Molengat\ infilling,transect,i} * B_{transect,i}) \quad (4.7)$$

In transect range 880-1210 the $\Delta V_{Molengat\ infilling,tot} = 6.21Mm^3$. The volume values per transect are plotted in Figure 4.18 and can be found in Appendix G.

4.5.2 Molengat fill date projection

When the Molengat cross-section $V_{Molengat\ in\ filling,\ year,\ transect}$ is calculated for each year of the JARKUS transect at 1 location, it can be plotted over time. This is shown in the upper left of Figure 4.9 for transect 880. Subsequently, a linear line is fit through all data points and extrapolated for future years. The R^2 -value of the fitted line is 0.985. An R^2 -value of 1 means the a direct correlation between time and volume, and with a value of 0.985 the line can be concluded to be accurate. Therefore, if the data for this transect is extrapolated to the future, the trend forecasts that $V_{Molengat\ in\ filling\ transect\ 880}$ will be 0 in 2029, meaning that the Molengat is completely filled.

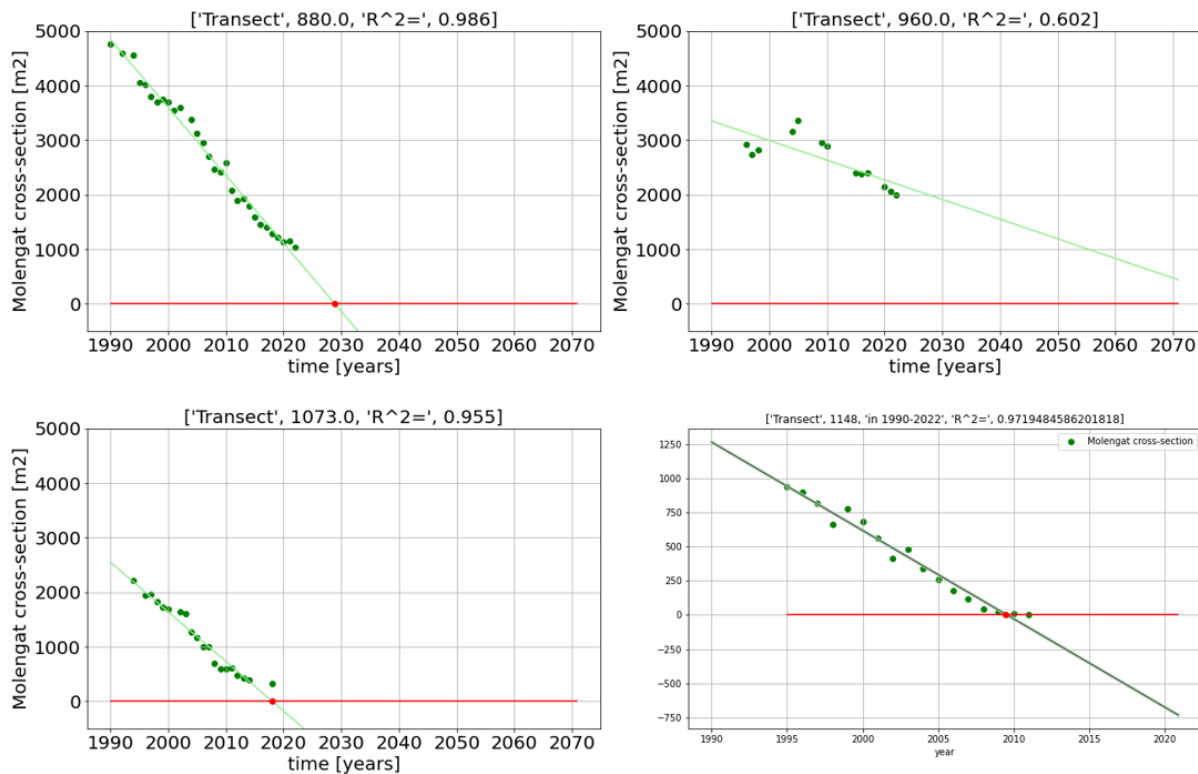


Figure 4.9: Linear fit and prediction of Molengat infilling at an example transect for each sub area in T1-T4. In transect 880 in T1 the Molengat will be closed at this location in 2029.

The Molengat fill date projection can be repeated for all transects, and these results are collected in Appendix E. For each alongshore location it is determined when the Molengat is likely to be filled. This is shown in the graph of Figure 4.10. On the left transect area 880-1210 is shown in blue, and transect 703-880 in red. The latter range is included to show the changes behind the Noorderhaaks in the Molengat. The reason is that in the past another shoal at the coast migrated towards shore, so the Noorderhaaks might affect Molengat development too (Elias, 2006).

Based on the fill date projection of Figure 4.10 transect range 880-1210 can be subdivided into 4 characteristic ranges T1-T4. Additionally, TE1-TE3 are formulated only for Molengat projected in transect range 703-880. Since these transects are on a curved part of the coast, only the volume differences of the transects $V_{Molengat\ in\ filling,\ transect}$ are considered. The ranges are defined in Table 4.3, and they show that a transect in T1 will likely be filled on the short term by the mid-2030s, T2 on the long term

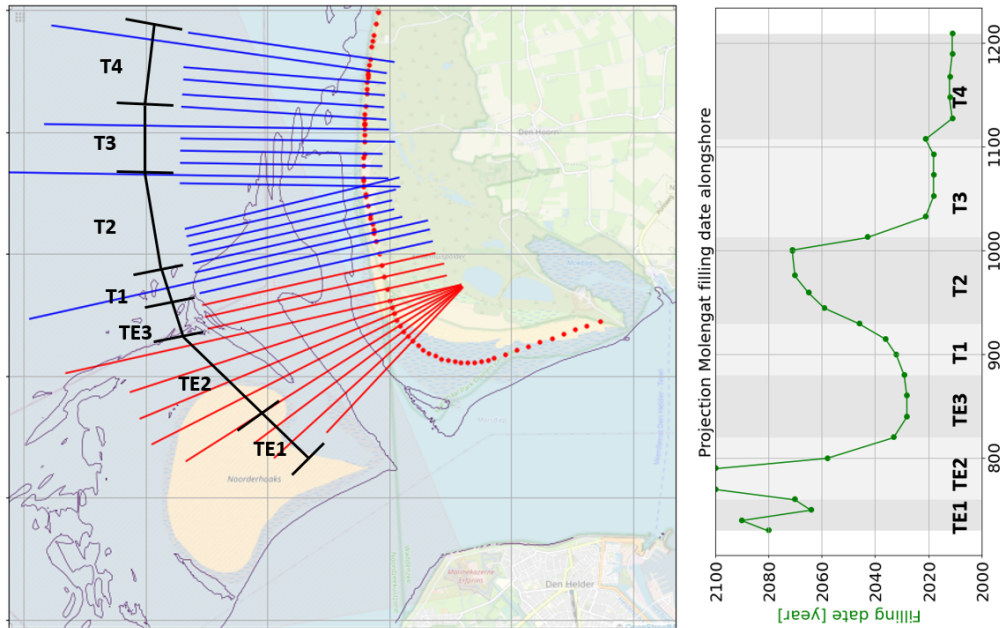


Figure 4.10: Overview transect areas TE1 to T4. On the right the alongshore graph is shown of the Molengat projection fill date. This filling date is the criterion that separates TE1-T4.

in the 2050s, T3 has been filled recently around 2020, and T4 has been filled around 2010. For T1 the R^2 -value is high, making it highly likely the Molengat will close by 2035 at this location.

In transects 703-880 the Molengat is much deeper than transect range 880-1210. This is one reason why it takes multiple decades more than transect 880-1210 to be completely filled. Within this range it is questionable if TE2 is going to close, because the cross-section has remained constant since approximately 2010. The reason is that around 2003 a new ebb-tidal channel started to develop on the NUN, causing the offshore Molengat bank to move offshore and increase the cross-section, as shown in Figure 4.12. Additionally, TE1 has a slightly lower R^2 -value than the other ranges. This is because transect 703 and 704 did experience less Molengat filling around 1990.

Just like TE2, T2 is a remarkable transect range. The R^2 -value is also much lower and the linear ap-

Sub area	Transect Range	BKL requirement	Molengat filling date	Average R^2 -value
TE1	703-707	No	2070	0.872
TE2	707-820	No	2080	0.659
TE3	820-880	No	2032	0.985
T1	880-930	Yes	2035	0.942
T2	930-1013	Yes	2055	0.638
T3	1013-1108	Yes	2023	0.924
T4	1108-1210	Yes	2010	0.924

Table 4.3: Transect ranges based on projection fill date of the Molengat channel.

proach does not fit as well to the data as other ranges. This is because the Molengat offshore boundary moved offshore in T2 around 2003-2005, see for example Figure 4.11, and as a result the future projection at this location is likely overestimated. Figure 4.12 shows the location and development of this ebb-tidal channel. The graph on the right shows the volume increase because of the offshore bank movement, and as a result the linear fit has a lower R^2 -value. The reason for this offshore movement could have been that a pre-existing small ebb-tidal channel just north of the Noorderhaaks was closed around that time, meaning that the entire ebb-current then started to flow out in T2. This could have halted the onshore migration of the offshore Molengat bank and caused a short back-and-forth movement. Since the closure of the small ebb tidal channel the new ebb-tidal channel described in the previous paragraph has started to grow on the same location on the NUN and the landward migration of the Molengat bank has restarted migrating towards shore in T2. However, since 2005 the $V_{Molengat\ infilling}$ linearly dropped in these transects, making it seem that the linear relation would hold after this trend break.

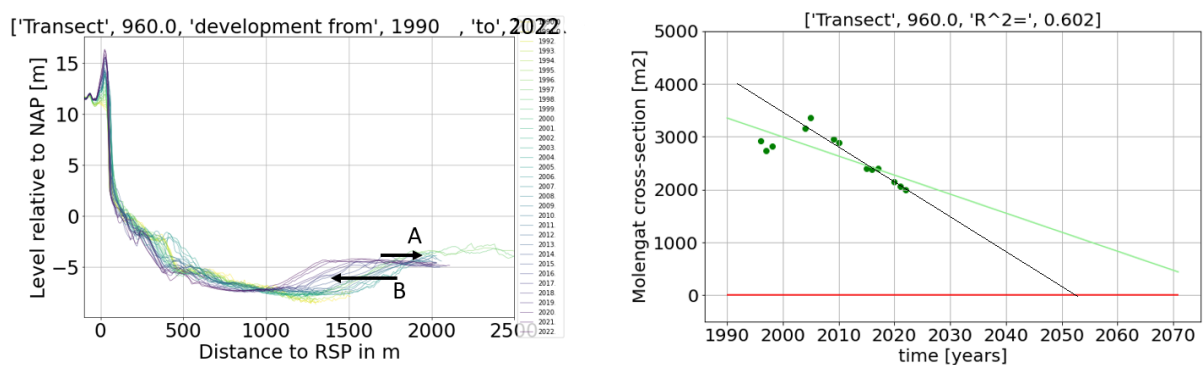


Figure 4.11: Left: Transect 960 from T2. In 2000-2005 the offshore boundary moved seaward (A), and thereafter it restarted migrating towards shore (B). Right: The offshore movement increased the Molengat cross-section and therefore disturbed the linear fit through data points. A second fit (black line) that only uses data after this event would estimate a Molengat closure around 2055.

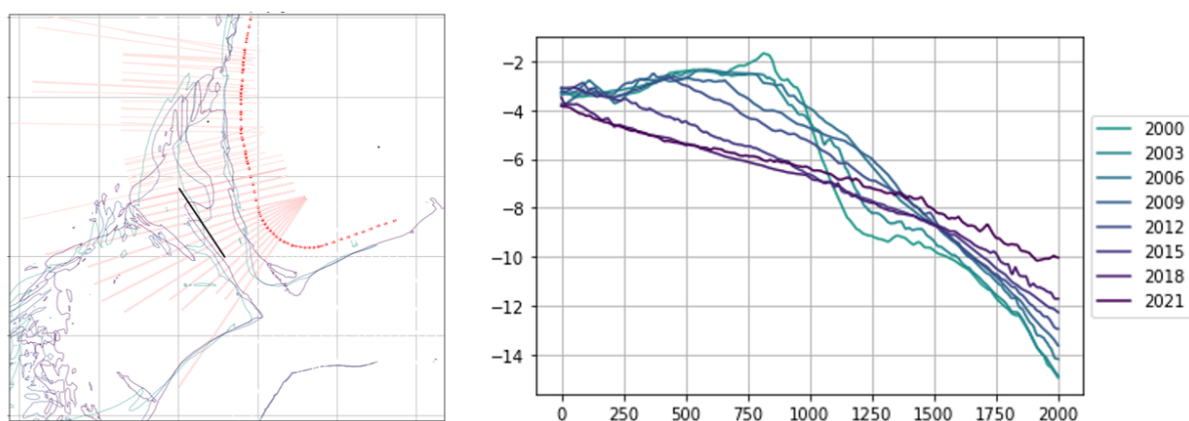


Figure 4.12: Left: Overview of location of ebb-tidal channel. Right: Development of ebb-tidal channel based on Vaklodingen data. The x-axis is the distance in meters from the cross section starting point (upper left). The y-axis shows the bottom level with respect to NAP. The ebb-tidal channel has flattened the initially steep Molengat bank connection with the NUN

The development of the new ebb-tidal channel has caused the R^2 -value of the infilling-graphs to be lower in TE2. Since the new tidal channel is cutting the Molengat bank, its sediment supply to fill the Molengat channel could be interrupted in the future. Currently, no effect is noticeable in the Molengat cross section values in Appendix E, but this development might delay the attachment of the NUN to the Texel coast by 2035 in TE3 and T1.

From the JARKUS data it is impossible to conclude what processes have caused these changes. To answer which processes are responsible, sediment transport is simulated in a model, which is explained in Chapter 6. Furthermore, few data points in transects from before 1990 are available (see Appendix E), implying that the Molengat migration has started before the application of the Dynamic Preservation Act and was unaffected by the nourishment program by Rijkswaterstaat. This means the processes were ongoing before human intervention.

In existing literature there are not many predictions about the attachment of the NUN to the Texel coast. Elias (2021) gave the prediction of under water attachment of the NUN to the Texel coast in 2030. Graphs in this research confirm that in TE3 and T1 the Noorderhaaks would attach by 2035, but attachment in T2 takes much longer. This means that T2 will experience the current erosion for the foreseeable future, which emphasizes the need for an intervention in this area.

4.6 Dune and beach volume ($\Delta V_{Dune,transect}$ and $\Delta V_{Beach,transect}$)

4.6.1 Calculation of $\Delta V_{Dune,transect}$ and $\Delta V_{Beach,transect}$

The 2 terms at the top of the transect profile are $\Delta V_{Dune,transect}$ and $\Delta V_{Beach,transect}$. The dune is defined landward of the dune foot level, and the beach is defined between the dune foot and the MLW-line, as shown in Figure 4.1. The change in dune volume is displayed in the left graph of Figure 4.13. It is the area between 2021 (green line), 1991 (red line), between the landward boundary (vertical black line) and the most offshore dot of the dune foot (horizontal blue line).

The landward boundary of the dune and its position is selected manually for each transect by selecting the point where the transects of 1991 and 2021 start overlapping in landward direction. Behind the overlapping point the dune profile has remained more or less constant. This is illustrated by the transect on the right: landward of the $-150m$ -coordinate the dune has not changed in profile height, so it can be assumed that there has been no cross-shore transportation of sediment behind this point. This explains the assumption in Figure 4.2 that $V_{CT,out} = 0$ and applies to all transects. All transects' developments in Appendix C.1 show that the overlapping point is behind the first dune. This point is chosen manually, because not all transects have data that extend far enough onshore to set the overlapping point at the same location.

Next, the volume difference $\Delta V_{dune,transect}$ is calculated using the following equation:

$$\Delta V_{dune,transect} = V_{dune,transect,2021} - V_{dune,transect,1991} \quad (4.8)$$

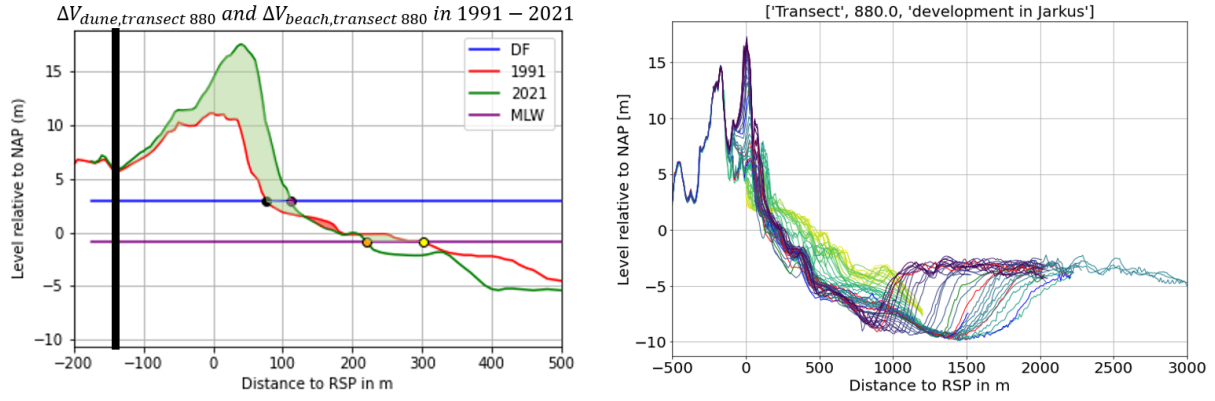


Figure 4.13: Left: beach volume growth is defined by the MHW-line and MLW-line, which are indicated in blue and purple. Beach volume increase is positive when the dune grows into seaward direction. Dune volume increase is indicated by the green shape above the DF-line and seaward of the overlapping point of the 1991 and 2021 transect, which is the landward boundary. Right: overview development of transect 880. At $-150m$ from the RSP the second dune starts, and through time it has shown no volume changes behind this point. This point is the overlapping point.

Where:

- $V_{dune,transect,1991} [\frac{m^3}{m}]$ is bounded by the manually selected landward boundary and the intersection point of the DF-level $z = +3m$ NAP. In Figure 4.13 these are $x = -150m$ RSP and $x = 75m$ RSP.
- $\Delta V_{dune,transect,2021} [m^3/m]$ is bounded likewise, but the seaward boundary is here $x = 110m$ RSP.
- The dune in this example has moved seaward and thus increased in volume, so $\Delta V_{dune,transect}$ is positive. Its value $\Delta V_{dune,transect 880} = 899[\frac{m^3}{m}]$.

Next, the beach volume $\Delta V_{beach,transect}$ is calculated. This is done similarly to the dune volume:

$$\Delta V_{beach,transect} = V_{beach,transect,2021} - V_{beach,transect,1991} \quad (4.9)$$

$\Delta V_{beach,transect}$ is the value between the 1991- and 2021- DF- and MLW-line, as shown in Figure 4.13. Since JARKUS-measurements have a spacing of 5m in cross-shore direction, the measured z -values are never exactly on DF- or MLW-level, so the values are interpolated linearly. Between 1991-2021 transect 900 has partly accreted and eroded, and the total $V_{beach,transect 900} = 84.7 \frac{m^3}{m}$.

The process of calculating $\Delta V_{dune,transect}$ and $\Delta V_{beach,transect}$ is repeated for each transect in the transect range of 880-1210. The volume change for each transect is shown in Figure 4.14. The dune growth is in the order of $500 \frac{m^3}{m}$ in all transects except transect 945 and 1033. The beach growth is an order of magnitude smaller: it is slightly eroding in transects 930-1033 and slightly accreting in transects 880 and 1093-1210. This sub factor is also shown in Figure 4.18.

It is remarkable that the dune growth at transect 945 and 1033 is limited, because the total amount of nourished volume has been equally much as the surrounding transects (see Figure 4.4). The limited dune growth can be explained by 2 things:

1. The initial steepness of the dune in transect 945 (1:2) was larger than the steepness of surrounding dunes ($O(1:4)$), see Figure C.5. Aeolian sediment transport capacity is lower when the slope is

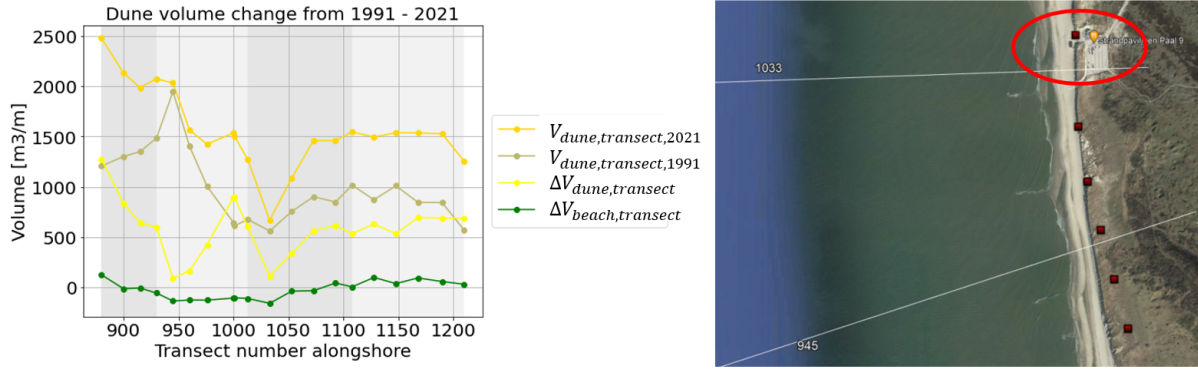


Figure 4.14: Left: Alongshore overview of the calculated volume changes of both the dune and the beach. Right: location of parking lot at transect 1033 (photo on the right, adapted from Google Maps).

steeper (De Vries, 2013). Thus, it can be argued that in the same time, under the same wind conditions the volume change is smaller in this transect.

2. There is a sediment sink present that reduces the volume of the transect. This is true for transect 1033 (Figure C.11), because the entrance to the beach is kept open. The deposited sediment gets removed by bulldozers from the entrance and from the parking lot. The width of the parking lot is however limited: it does not represent the entire transect, even though the measurement of the transect would imply so. Therefore, the volume change per meter beach width for this transect $\Delta V_{dune,transect\ 1033}$ in Figure 4.7 is underestimated. The underestimation can be estimated based on the ratio $\frac{width\ parking\ lot}{width\ transect}$ to be the order of $O(100 \frac{m^3}{m})$.

In Section 4.5.2 the area was divided into transect ranges T1-T4. Figure 4.15 shows both the dune and beach development in the period 1991-2021 for 1 representative transect of each sub area. In T1, T3 and T4 the dunes have increased in steepness and moved seaward, while the T2-dune moved landward. All dunes increased in height.

The total accreted $\Delta V_{Dune,tot}$ and $\Delta V_{Beach,tot}$ can be used for the sediment balance and are calculated using the same method as the Molengat infilling:

$$\Delta V_{Dune,tot} = \sum_{i=1}^n (\Delta V_{Dune,transect,i} * B_{transect,i}) \quad (4.10)$$

$$\Delta V_{Beach,tot} = \sum_{i=1}^n (\Delta V_{Beach,transect,i} * B_{transect,i}) \quad (4.11)$$

Where:

- $B_{transect,i}$ is width of each transect i in [m], given by Table D.2.

The total dune volume change of the system $\Delta V_{dune,tot} = 1.81 \text{ Mm}^3$, meaning the dunes have grown. The transect values that contribute to this number are shown in Appendix G. In a similar manner the total beach volume of the system $\Delta V_{beach,tot}$ amounts to -0.093 Mm^3 , meaning the beach volume has reduced. This supports the explanation of increasing steepness in the profiles. Figure 4.15 shows that the beach profile has lowered and simultaneously moved towards sea between MLW and DF-level.

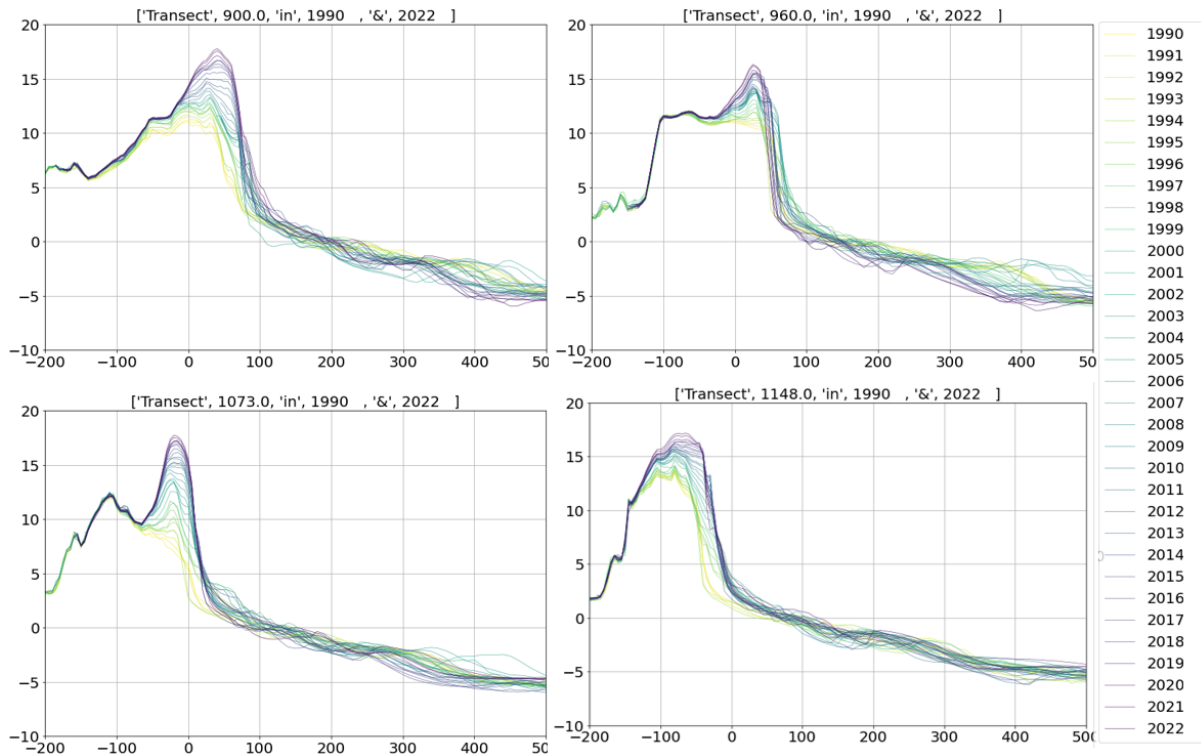


Figure 4.15: Dune development from 1990-2022 in T1 (900), T2 (960), T3 (1073) and T4 (1148).

Since the total beach volume is an order of magnitude lower than the beach, its development through time is not considered in the next section.

4.6.2 Dune development through time

Like the development of the Molengat volume, the development of dune volume changes through time gives insight in the behaviour of dune development. Pre-1990 JARKUS data was only sufficient for the Molengat infilling calculations to confirm that the Molengat closure was an ongoing process before the nourishment program started. Similar behaviour is described by comparing dune volumes before the start of the nourishment program with changes after the start of the program.

Dune volume pre-1990

The pre-1990 JARKUS data consists of other transect numbers than the post-1990 data. Therefore, the pre-1990 data of the already-considered transects are not adequate for a pre-1990 comparison. All pre-1990 transects are shown in Appendix C.2, of which a representative example is plotted in Figure 4.16: transect 1003.

Transect 1003 is shown for period 1965-1980. It shows the retreat of the front dune, its slope became milder and the dune top reduced. Since no overlapping point can be determined between the profiles of all years, the exact volume reduction cannot be determined. If the assumption of no volume loss behind the first dune ($V_{CT,out} = 0$) holds true in these years, then the general trend was a reducing

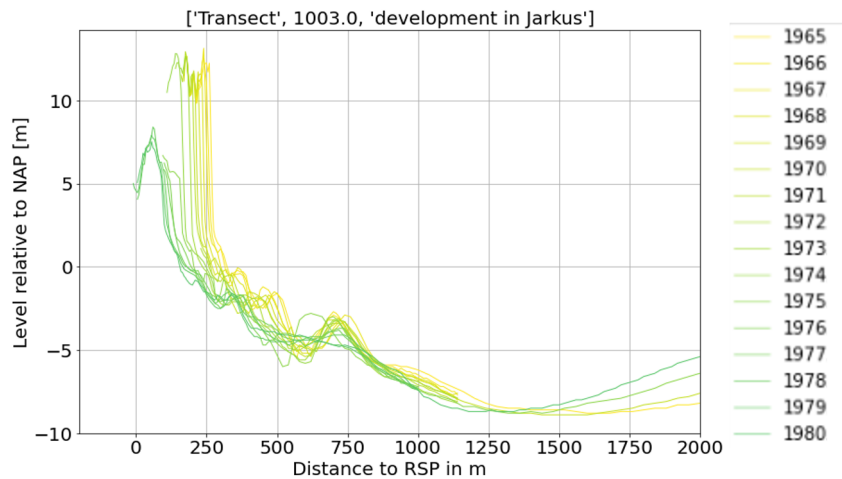


Figure 4.16: Pre-1990 JARKUS data at transect 1003. It shows the retreat of the dune in the period before the BKL started to be managed. The coast shows a diminishing trend in volume, steepness and height.

dune volume. This trend flipped to dune volume increase after the start of the nourishment program.

Dune volume in 1991 - 2021 and future

Since the start of the nourishments and the Dynamic Preservation of the BKL in 1990 the dunes increased in volume, which is shown in Figure 4.15 and 4.17. This change in transect profiles is likely caused by the application of beach and shoreface nourishments, since the dune volume started to increase after the application of the first nourishments in 1994, see Figure 4.17. The possibility of aeolian sediment transport from the beach to the dune is supported by the main wind direction being onshore, see Figure 2.11. It is unknown to what extent the shoreface nourishments cause sediment transport towards the dune. Since beach nourishments are closer to the dune than shoreface nourishments, it is likely the largest part of dune volume increase originates from beach nourishments, and less from shoreface nourishments. This is however a hypothesis that requires more research. Nonetheless, based on the overlapping starting date of dune volume increase and the start of the nourishment program, it can be calculated that the dunes have grown by a volume that is equal to 29.9% of the nourished volume: $\frac{\Delta V_{Dune,tot}}{V_{nourish,tot}} = \frac{1.836}{6.131} = 29.9\%$.

Dune volume growth can only be calculated for data post 1990. When these developments are plotted over time in Figure 4.17, it therefore includes the effect of the nourishment program. Transects 900 (T1), 1073 (T3) and 1148 (T4) show an almost linear increase in dune volume. Transect 960 (T2) started in a linear trend too, but the dune volume has remained constant since 2000. A possible explanation is that the current profiles in T2 have steepened so much that the aeolian sediment transport capacity reduced, similar to transect 945 (De Vries, 2013). Simultaneously, the dune started to retreat landward, meaning the front lost volume, while the volume growth at the top reduced. This combination could explain the constant volume of the dune. The steepness in T2 has not yet been reached in T1, T3 and T4. Transects in T2, T3 and T4 started increasing in volume in 1995, which coincides with the application of the first beach nourishment at those locations (see Appendix D).

The future projection of dune growth and dune stability requires further investigation. From this study it can be concluded that the dunes are likely to start losing sediment if they do not receive any future nourishments anymore. This is relevant when the current nourishment program is replaced by a mega

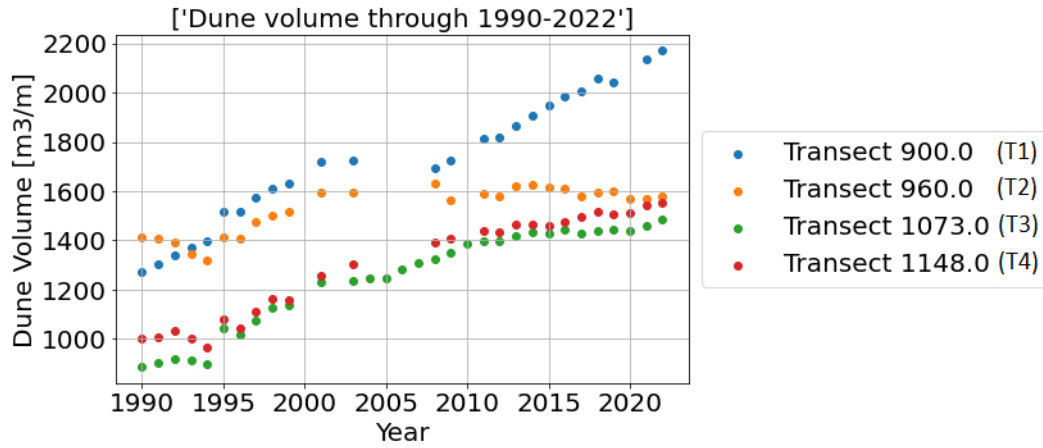


Figure 4.17: Dune volume development for representative transects in T1 (900), T2 (960), T3 (1073) and T4 (1148). Dune volumes started increasing after the application of the first beach nourishment in T2-T4. In T1 the increase could be explained by alongshore sediment transport.

nourishment. However, the mega nourishment aims to supply sediment to adjacent transects that did not directly receive part of the nourishment on their transect. This could result in long term sediment supply and therefore limited dune volume loss in the area. Furthermore, it can therefore be expected that transects that are within the mega nourishment range will continue dune growth till the maximum steepness is reached.

4.7 Shallow volume ($\Delta V_{Shallow}$)

From Equation 4.4 all terms have been discussed, except the volume per transect between the MLW-level and the limit of the Molengat at $-4.4m$ NAP: $V_{Shallow,transect}$. This term is calculated by:

$$\Delta V_{Shallow,transect} = \Delta V_{transect} - \Delta V_{dune,transect} - \Delta V_{beach,transect} - \Delta V_{molengat\ in\ filling,transect} \quad (4.12)$$

As explained in Figure 4.3, $\Delta V_{Shallow}$ consists of 2 parts: the accretion in the Molengat above $-4.4m$ near the sea bank boundary, and the onshore erosion or accretion. Since this term is split, its value depends on the location of the offshore boundary, as mentioned in Figure 4.7. Figure 4.18 shows the value of $\Delta V_{Shallow,seaward,transect}$ in the purple line for both the whole profile (boundary at Molengat sea bank) and $\Delta V_{Shallow,landward,transect}$ small profile (boundary at Molengat land bank). Additionally, it summarizes the alongshore volume changes of $\Delta V_{transect}$, $\Delta V_{Molengat\ in\ filling,transect}$, $\Delta V_{Beach,transect}$ and $\Delta V_{Dune,transect}$.

Similar to $\Delta V_{Molengat\ in\ filling,tot}$, $\Delta V_{dune,tot}$ and $\Delta V_{beach,tot}$, the value of the total volume change in the system of the shallow area $\Delta V_{Shallow,tot}$ is calculated by the sum of the product of the transect-value $\Delta V_{Shallow,transect}$ and the transect width:

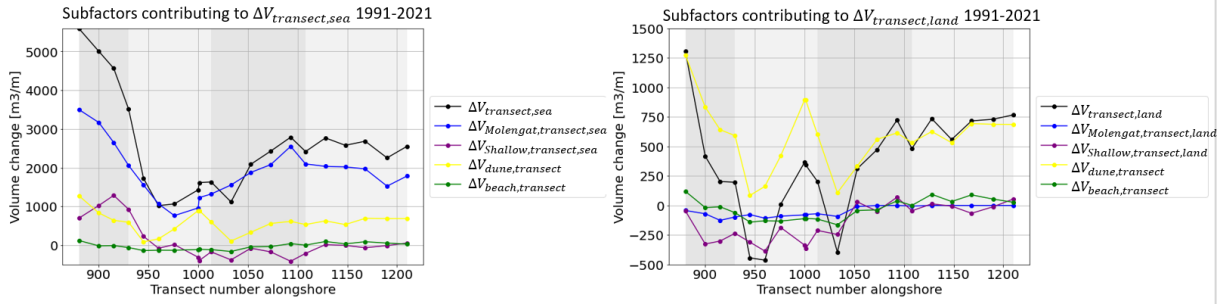


Figure 4.18: Left: all sub factors that contribute to $\Delta V_{transect,seaward}$. The sub factor values for each transect have been calculated using Equation 4.5, 4.6, 4.8, 4.9 and 4.12. Right: all sub factors that contribute to $\Delta V_{transect,landward}$. In this calculation the offshore boundary is at the landward bank of the Molengat.

$$\Delta V_{Shallow,tot} = \sum_{i=1}^n (\Delta V_{Shallow,transect,i} * B_{transect,i}) \quad (4.13)$$

The value of $\Delta V_{Shallow,tot} = 0.26 Mm^3$ when the sea bank of the Molengat is used as offshore boundary. The values of each subfactor of each transects are shown in Appendix G.

The offshore part of $\Delta V_{Shallow,transect,seaward}$ only exists in transects in transect range 880-945, see T1 in Figure 4.19. This accretion volume is significantly larger than the onshore part, and explains why $\Delta V_{Shallow,transect,seaward}$ in the left graph of Figure 4.18 is much larger in this range. In the right graph it is shown that the nearshore $\Delta V_{Shallow,transect,landward}$ -part is negative, meaning the nearshore area has eroded.

Figure 4.19 shows an overview of $\Delta V_{Shallow,transect}$ in all transects ranges T1-T4, based on Vaklodin-gen data. All transects can be found in Appendix F. In T1 and T2 the erosion values $\Delta V_{Shallow,transect}$ in Figure 4.18 are larger than in T3 and T4. In T3 and T4 the Molengat is close to complete filling and has finished closing already. The Molengat closure might therefore be a preceding indicator that future nearshore erosion will reduce. This observation is based on a small area, and would require more extensive research to support the same assumption for T1 and T2. In T3 and T4 the bottom in $\Delta V_{Shallow,transect}$ was approximately 0, while beach and shoreface nourishments were applied too. When the current nourishment scheme is replaced by a mega nourishment, the goal is to have the mega nourishment diffuse sediment alongshore in the shallow range such, that it compensates the erosion that would occur when no nourishments are applied.

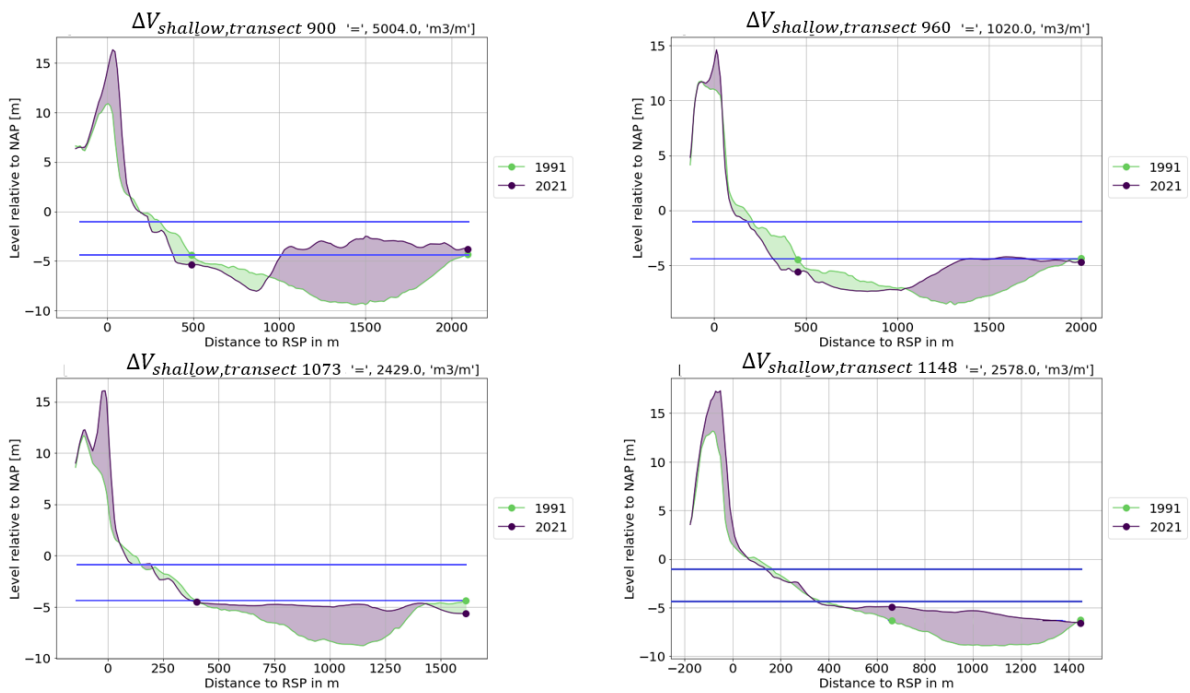


Figure 4.19: Overview of $\Delta V_{Shallow,transect}$ in each transect area in T1-T4 between the 2 blue lines. In T1-T2 the Molengat is still closing, and there is significant erosion on the Molengat land bank. In T3-T4 the Molengat has already closed and the erosion is much more limited.

5 | Delft3D model set-up

This chapter focuses on how the current system and the mega nourishment can be setup in a model, as shown in Figure 1.1. The mega nourishment at the coast has the goal to nourish the adjacent coastline through alongshore diffusion of sediment. The impacts of the nourishment are determined by building a process-based model in Delft3D-software. In order to accurately setup the model, first the research questions regarding the model are stated in Section 5.1, followed by an explanation of the basics behind Delft3D (D3D) in Section 5.2. Section 5.3, 5.4 and 5.6 discuss the input in the model and Section 5.5 checks the numerical stability of the model.

5.1 Model research questions

To accurately define the contents and detail of the model, the main question needs to be answered:

How would a mega nourishment at the coast change erosion and accretion patterns alongshore?

In Section 2.3.2 the hydrodynamic classification according to Davis and Hayes (1984) was determined to be dominated by mixed energy from tide and waves. Therefore, the model needs to consider both waves and tidal flow. Furthermore, there are multiple aspects regarding the boundaries of the model. The main modelling question can be subdivided into multiple sub-questions:

1. What is the modelling domain? [C5.3]
2. What processes are considered in the model? [C2.3.2]
3. How is each process modelled? [C5.4, C5.6]
4. What processes cause most sediment transport? [C6.2 - C6.3]
 - (a) How do waves and currents affect sediment transport? [C6.1, C6.3]
 - (b) Taking into account the frequency of storms, what is the difference in effect of calm wave conditions compared to storm wave conditions? [C6.2]
 - (c) How is sediment transport affected by waves coming from the NW or SW? [C6.3]
5. How does sediment transport change after the application of a mega nourishment? [C6.4]

The next sections answer questions 1-3 and Chapter 6 answers questions 4-6 with an analysis of the model results.

5.2 Principles of Delft3D

Delft3D is a process-based model that follows the processes as shown in Figure 5.1. First, the model requires a grid with at each cell a defined depth. Next, boundary conditions are imposed to simulate waves and a tidal flow. The waves and tidal flow interact with each other, so they are coupled. Together, they provide the information to calculate the sediment transport magnitude and direction at each grid cell. This is the final step of this model. Other modules in D3D have the option to add a final step that calculates the bottom change resulting from sediment transport. This step of calculations with bottom updates in this area is prone to severe uncertainties depending on the use of simplifying physical assumptions (Bertin et al., 2007). Since this project area is geometrically very complex due to the presence of the ebb tidal delta, tidal channels and the inlet system, the bottom updates could yield unreliable results. Therefore, this research looks at the sediment transport changes alongshore to assess the impact of the mega nourishment. This approach is also known as Initial Sedimentation Erosion Simulation or ISE.

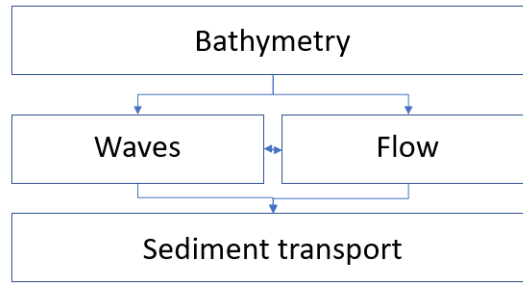


Figure 5.1: Processes in the Delft3D model are calculated in the indicated order.

Due to time limitations in the research the level of detail in the model is limited. As a result, it is opted to let D3D-FLOW+WAVE simulate a two dimensional model. D3D-WAVE uses a SWAN model to compute the wave field from a characteristic wave condition that is applied at the boundaries of the model. D3D-Flow simulates 2DH (depth-averaged) unsteady flow and transport by solving the shallow water equations using an Alternating-Direction Implicit numerical scheme. The shallow water equations are applicable because the tide in the North Sea has a wave length $L = O(450 \text{ km})$ and the depth is limited $h = O(50 \text{ m})$. Shallow water is defined as $\frac{h}{L} < 0.05$, which is a satisfied condition in the North Sea. The shallow water equations consist of the continuity equation and the momentum equation in 2 directions. The equations are taken from the Delft3D-Flow Manual and adapted to this 2DH-specific case (Deltares, 2022).

The D3D Continuity equation reads:

$$\frac{\partial \zeta}{\partial t} + \frac{1}{\sqrt{G_{\xi\xi}}\sqrt{G_{\eta\eta}}} \frac{\partial((d + \zeta)U\sqrt{G_{\eta\eta}})}{\partial \xi} + \frac{1}{\sqrt{G_{\xi\xi}}} \frac{\partial((d + \zeta)V\sqrt{G_{\xi\xi}})}{\partial \eta} = (d + \zeta)Q \quad (5.1)$$

In this model there are no external sources or sinks of the water quantity Q , meaning that term equals 0. Finally, since the grid is rectangular, no grid correction is needed, leading to a correction factor $G_{\eta\eta} = 1$ and $G_{\xi\xi} = 1$. In this case ξ and η represent the x - and y -directions. The simplified equation reads:

$$\frac{\partial \zeta}{\partial t} + \frac{\partial(d + \zeta)U}{\partial x} + \frac{\partial(d + \zeta)V}{\partial y} = 0 \quad (5.2)$$

Where:

- ζ = Water level with respect to NAP and positive above NAP [m].
- t = Time [s].
- d = Depth from bottom to NAP [m]. Deeper bottom means a more positive d .
- $h = \zeta + d$ = Total depth [m].
- U, V = Depth averaged velocity in respectfully x - and y -direction [m/s].

For the momentum equation 4 assumptions are made. First, a constant water density is assumed, so that no spatial temperature and spatial salinity differentials cause density-flows. Second, a constant Coriolis force is assumed. Third, the shear stress in a 2D depth-averaged flow is assumed to be a quadratic bed friction term. Finally it is assumed that there are no external forces of momentum by for instance the application of discharge as a source in the model area. The D3D momentum equation in 2D reads:

$$\frac{\partial U}{\partial t} + U \frac{\partial U}{\partial x} + V \frac{\partial U}{\partial y} = -g \frac{\partial \zeta}{\partial x} + fV - \frac{gU\sqrt{U^2 + V^2}}{(d + \zeta)C^2} + \nu_H \left(\frac{\partial^2 U}{\partial x^2} + \frac{\partial^2 U}{\partial y^2} \right) = 0 \quad (5.3)$$

$$\frac{\partial V}{\partial t} + U \frac{\partial V}{\partial x} + V \frac{\partial V}{\partial y} = -g \frac{\partial \zeta}{\partial y} + fU - \frac{gV\sqrt{U^2 + V^2}}{(d + \zeta)C^2} + \nu_H \left(\frac{\partial^2 V}{\partial x^2} + \frac{\partial^2 V}{\partial y^2} \right) = 0 \quad (5.4)$$

Where:

- g = Gravitational constant [m/s^2].
- f = Coriolis parameter [-]. This depends on the latitude and Earth's rotation and is constant in this research.
- C = Chézy coefficient [$\frac{\sqrt{m}}{s}$]
- ν = Horizontal eddy viscosity [m^2/s]. The term $\nu_H \left(\frac{\partial^2 V}{\partial x \partial x} + \frac{\partial^2 V}{\partial y \partial y} \right)$ includes turbulence.

The D3D-WAVE model transforms a wave condition at the boundaries of the model towards shore and calculates the evolution of the wave spectrum. This is done using the 2D wave action density spectrum (Deltares, 2023). This equation reads:

$$\frac{\partial}{\partial t} N + \frac{\partial}{\partial x} c_x N + \frac{\partial}{\partial y} c_y N + \frac{\partial}{\partial \sigma} c_\sigma N + \frac{\partial}{\partial \theta} c_\theta N = \frac{S}{\sigma} \quad (5.5)$$

Where:

- N = action density: this is the energy density divided by the relative frequency.
- $c_x, c_y, c_\sigma, c_\theta$ = propagation velocity in x -, y -, σ - and θ -space.
- σ = relative frequency: a frame of reference moving with the particle.
- θ = wave direction.
- S = source term that represents generation and dissipation of energy and non-linear wave-wave interactions.

Within the source term S there are processes that can be enabled, such as whitecapping and wind growth. These are discussed in Section 5.5.

The D3D-Flow and D3D-WAVE models are coupled, where in the first time step the FLOW computations are executed, and the results are used as input for the WAVE-calculation. The results of the WAVE computation are subsequently used to compute the next 60 time steps of the FLOW model. This process is repeated for the entire simulation time. In Section 5.5 it is explained that the time step is 1 minute, meaning the FLOW and WAVE module communicate once every hour.

5.3 Model domain

To identify the effects of the application of a mega nourishment, 2 model situations are tested: a model without additional nourishments, and a model including a mega nourishment. Within both cases it is investigated what processes cause most sediment transport. The model domains of both models are identical, except for the increased bottom at the mega nourishment.

Due to time constraints of the research, an already available model grid and accompanying depth values in each grid corner point created by Rijkswaterstaat is being used: the model schematization Delft3D-FLOW_Waddenzee-PACE_j09_v06. This model contains a grid of the entire Wadden Sea, as shown in Figure 5.2. The depth profile for each grid cell is taken from the 2021 Vaklodgingen data. The red box indicates the SW Texel area that is shown in Figure 5.4: only a small part of the entire grid is part of the area of interest. This model originally contained bathymetry from 2009, but this has been updated with the most recent Vaklodgingen data of 2021 (Rijkswaterstaat, 2022).

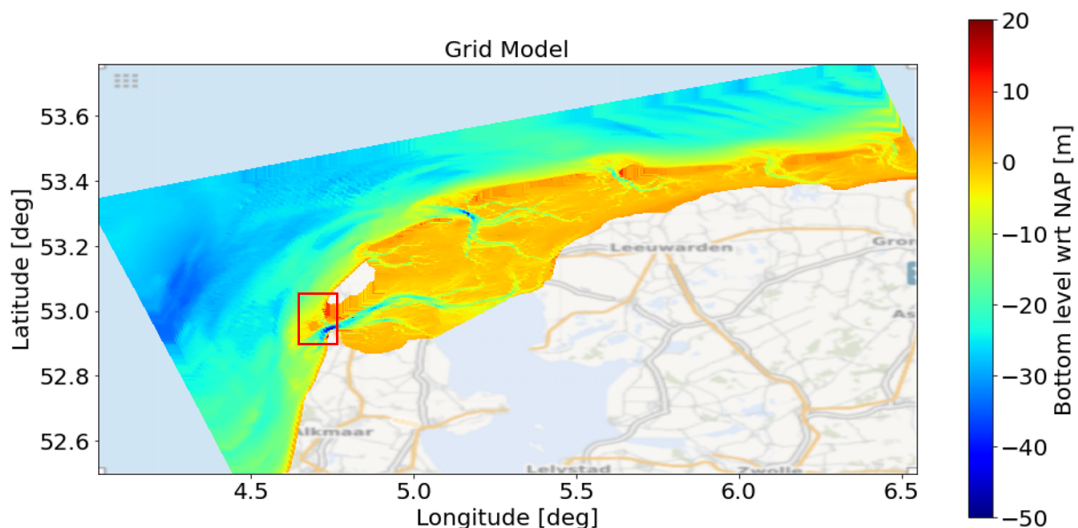


Figure 5.2: Entire model grid of the Wadden Sea with a spatial resolution of 200m. Depth is indicated in m and taken from Vaklodgingen data in 2021 (Rijkswaterstaat, 2022)

The grid cells of the model are slightly rotated. The model makes use of a rectangular grid. Each grid cell has a resolution of $200 * 200m$. Furthermore, the grid is 2D, meaning there are no multiple vertical layers in the water or soil.

5.3.1 Design of mega nourishment

This section answers how a mega nourishment could be applied in the system. Firstly, a location is required, then the volume is determined and spread over the location. From Figure 4.7 it was concluded that transect area 945 – 1053 is the area with most erosion without the application of nourishments (V_{nat}) and therefore the most interesting location to investigate the application of a mega nourishment. In this area the BKL is not satisfied, because the MKL is closer to shore than the BKL. The dissatisfaction is an additional short term reason to put the mega nourishment at this location. At the attachment point of the NUN to Texel in transect range 1093-1210 the BKL currently suffices. This emphasizes the need for a mega nourishment at transect range 945 – 1053. In order to define the characteristics of the mega nourishment 4 design choices are made:

- The mega nourishment must consist of the volume that would be used for 20 years of nourishments in this area. This volume is determined by taking the average annual nourishment volume at SW Texel since the start of the Dynamic Preservation Act and multiplying it by 20 years. The total nourished volume was determined in Section 4.2 and the total volume then results in $4.09 Mm^3$. The annual nourished volume in the Wadden Sea is $5.7 Mm^3$ and since this is a nourishment for the long term, the required volume is reasonable (Rijkswaterstaat, 2020).
- The volume is distributed between transect range 945-1053.
- The sediment is filled up above the MHW-line, so the beach remains dry during MHW-conditions. This prevents additional sediment runoff during high water conditions.
- The shape of the nourishment is triangular to allow diffusion of the nourishment to happen in north and south directions.

The left of Figure 5.3 shows the 2021-bathymetry of the project area where the mega nourishment would be applied between transects 945 – 1053. This location is far enough north so that the nourishment does not cut off the flow through the Molengat. The middle part shows the same area schematized in the grid of the model. The red area encloses the transect range 945 – 1053 from the dune towards the seaward Molengat bank. Within the area a dark green triangular shape is drawn that represents the shape of the to-be-applied mega nourishment. However, since the model only takes as input bottom values at the corner points of each grid cell, the real nourishment area does not entirely fit the nourishment area.

On the right of Figure 5.3 3 grid cells are colored black, which means the grid cell has a bathymetry with a bottom level above the MHW- line. The landward edges of these cells indicate the dune area. Since their average bed level is above MHW, the required nourished volume in these cells can be neglected. The remaining 21 green cells do receive sediment from the mega nourishment. The mega nourishment follows a rigid-lid approach, meaning sand is filled up to an equal level in all indicated cells. This rigid-lid-level - or the nourishment height level - is referred to with $z_{nour,level}$.

Each cell has a different average bottom level before the nourishment is applied. In Equation 5.6 the known total volume $V_{Mega\ nour}$ is distributed over all grid cells with area $A_{grid\ cell}$. Since the initial bottom level of each cell $z_{cell,av,i}$ is known (indicated in m below NAP on the right in Figure 5.3), the only unknown is $z_{nour,level}$ which can be calculated by isolating it from the following equation:

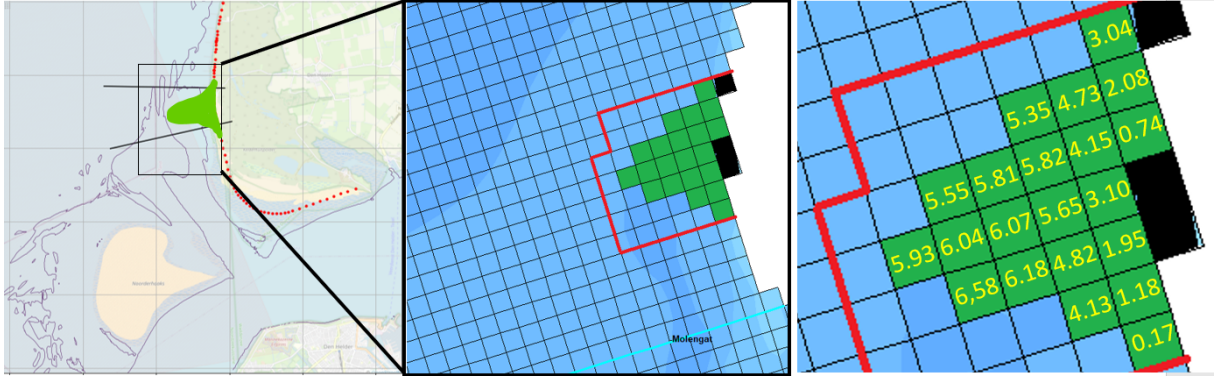


Figure 5.3: Left: schematic representation of mega nourishment between transects 945-1053 with the current - 5m depth contours. Middle: translation from schematic representation to bathymetry in the model. Right: Average depth values in m below NAP of all grid cells within nourishment.

$$\frac{V_{Mega\ nour}}{A_{grid\ cell}} = \sum_{i=i}^n (z_{cell,av,i} - z_{nour,level}) \quad (5.6)$$

Where:

- $V_{Mega\ nour} = 4.09 * 10^6 m^3$ is the total mega nourishment volume.
- $A_{grid\ cell} = 40,000 m^2$ is the area of 1 grid cell.
- $z_{cell,av,i}$ is taken from the depth map of the model, which is based on Vaklodingen data (Rijkswaterstaat, 2022).

The elevation of the bottom in the mega nourishment is the same in all green grid cells. The bathymetry gradients are largest between the grid cells with the highest elevation change. This is a maximum of 7m over a grid cell of 200m, meaning the maximum bathymetry gradient is 0.035, or 2 degrees, which is a reasonable value for under water slopes. The value of $z_{nour,level} = 1.12 m$, meaning if all indicated grid cells are filled until the mega nourishment is satisfied, the bottom will exceed the water level by 1.12m above NAP. The adapted bottom after mega nourishment is shown on the right in Figure 5.4.

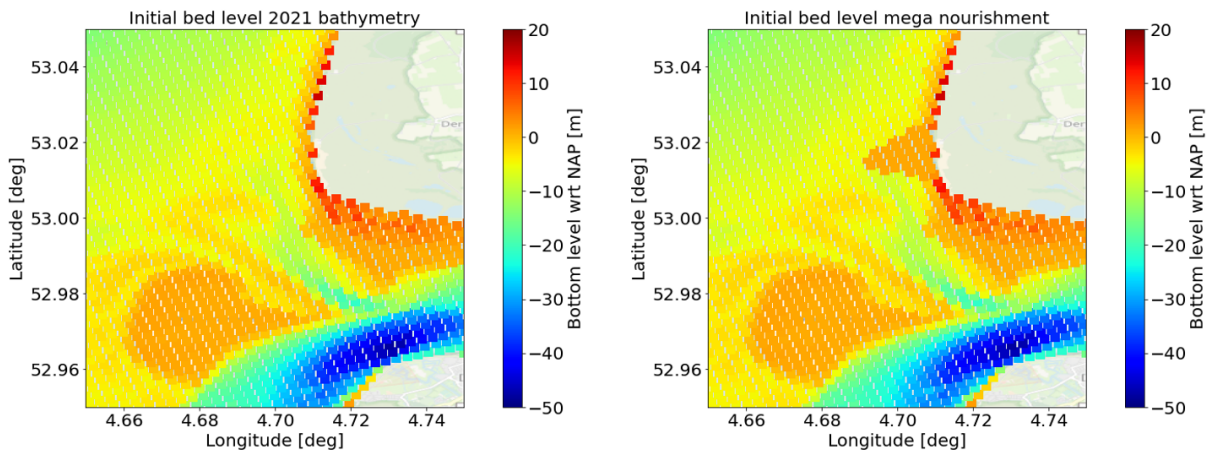


Figure 5.4: Left: The initial bed level in the area of interest. Right: Adapted 2021 bathymetry after the application of the mega nourishment. The rest of the bathymetry is identical.

5.4 Flow input

To set-up a model properly, many inputs need to be defined. The original model of Rijkswaterstaat used different processes as input than the adapted model in this research. Salinity and heat flux were included in the original model, but are not considered in the calculation of tidal flow in this model. Sensitivity of sediment transport to temperature was found to be limited by Barkdoll et al. (2019). Small temperature differences would lead to limited density fluxes, a limited change in flow velocity and hence a limited effect on sediment transport. The same holds for salinity. Barkdoll et al. based their research on rivers, yet these claims are assumed to be similar for this research. The original model of Rijkswaterstaat contained salinity and heat flux, but these inputs are neglected to save on computation time. The negligence can be observed in Figure 5.5: at the observation location Den Helder the water level development is almost the same in both cases after 6 hours of running time. This is the same at other observation locations. Therefore, heat flux and salinity are not considered in this model. In the next subsections the input of used variables is explained.

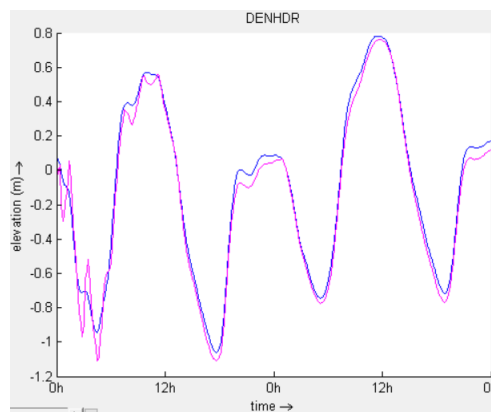


Figure 5.5: Water level development through over at observation location Den Helder. The blue line indicates the original model which includes heat flux and salinity and the purple line indicates the model without them.

5.4.1 Simulation time

The simulation time of morphology can vary from days (storm impact) to multiple years (large scale evolution). However, the goal of this model is to investigate how sediment transport flows change after the application of a mega nourishment. This is done without updating the bathymetry, because the uncertainties in this area could be large, especially because of the complex area that includes a tidal channel, an inlet and ebb tidal delta. Therefore, the model is used to look at the differences in mean sediment transport on a spring-neap tidal time scale. The spring-neap cycle is long enough to average out the effects of random low and high waters, and consequently offers a useful value for mean sediment transport. The cycle is also short enough to keep model computation time manageable. For clarity, in this research *computation time* means the real life duration a simulation takes to run, whereas *simulation time* means the artificial time range that is being modeled. The spring-neap tidal cycle in the North Sea depends mainly on the M_2 - and S_2 -constituents, which amount to a time of 14.7 days (Stive and Bosboom, 2021). This is confirmed by the tidal data shown in Figure 2.8.

5.4.2 Initial conditions

The initial conditions of the model are set as a so-called hotstart: at $t = 0$ the model uses a spatially varying field of wave-heights in all grid cells. The application of a hotstart allows the mean total sediment transport to be calculated without spin-up errors starting from the first time steps. The spin-up time in this model is approximately 5 hours, which can be concluded from multiple graphs that converge to oscillating signals, see Figure 5.6. At the start of the graph the peak consists of 2 peaks, which smooths out after the first wave. The spin-up time can influence the mean sediment transport value over the simulation time of 2 weeks. Therefore, a separate full simulation is applied using a hotstart.

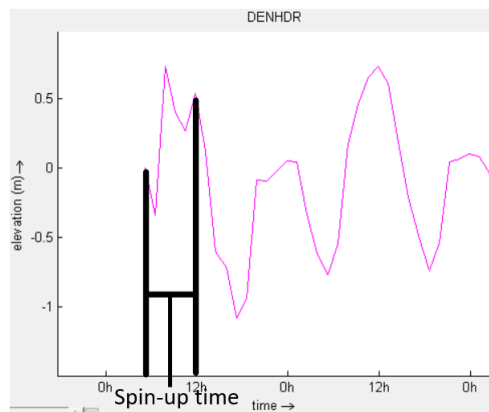


Figure 5.6: The spin-up time is the time it takes for the model to have no large random spikes in data anymore. In this graph the spikes stop after approximately 5 hours, meaning this is the spin-up time. The spin-up time has been determined by comparing the water levels and depth averaged velocities at different observation points.

This hotstart is different for each simulation. The hotstart is created by running test simulations that start with a uniform flat water level in the entire grid. The test simulations simulate 12 hours, during which a spin-up time occurs of approximately 5 hours. Next, the wave field at $t = 12h$ is exported as a hotstart file, and this is used as input in the full simulation. The full simulation is restarted using the end time of the cold start simulation.

5.4.3 Boundary conditions

The grid in Figure 5.2 contains four wet boundaries which are all open: south-west, west, north and east. The barrier islands of the Wadden Sea, the land and the Afsluitdijk are all closed boundaries with a reflection parameter of 0, meaning the wave energy is dissipated. The wet boundaries are forced by the original model water level time-series given by Rijkswaterstaat.

Each of the wet open boundaries is subdivided in groups of 4 or 5 cells, see Figure 5.7. Together these 4 cells share the same water level time-series. The next four cells on the boundary have a slightly different water level time-series, because the tidal wave has a different amplitude depending on the depth at those grid cells, and a different phase depending on the alongshore location. As a result, there is a small spatial variation of the tidal wave along all boundaries. The water level is defined at many

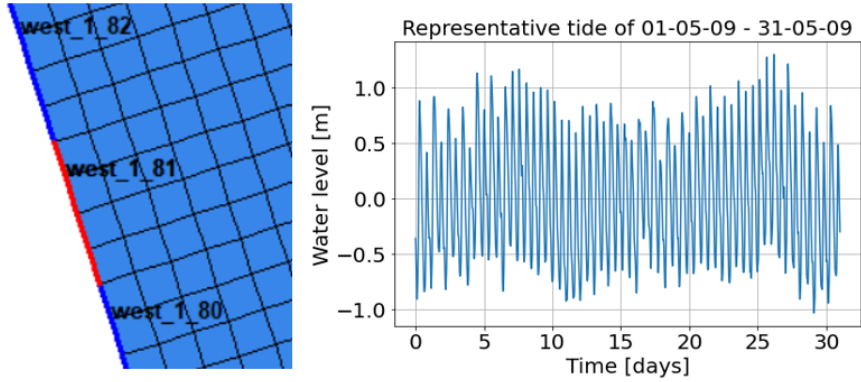


Figure 5.7: Left: overview of how the western boundary is subdivided into brackets of 4 cells. Right: each of these brackets has their own water level time-series, and therefore the phase and amplitude along the boundaries is more realistically represented in the model compared to imposing 1 boundary condition along the entire western boundary.

groups of grid cells, instead of using the same water level everywhere along the entire western boundary. This collection of water level time-series is based on measured water level data from 2009. The model simulation uses bathymetry from 2021, yet since the tidal wave characteristics at the open boundaries have not changed much in that period, it is still considered acceptable to use these same boundary conditions (Jacob et al., 2016).

Next to the water level the model requires a boundary condition for sediment concentration at each location. This has been set as the equilibrium concentration, so that there are no sources discharging sediment into the system at any boundary.

5.4.4 Physical parameters

The model requires multiple physical parameters to be defined. The gravitational constant $g = 9.81m/s^2$ and the density of the sea water $\rho_{sw} = 1025kg/m^3$. Then there are model dependent parameters:

- **Bottom roughness:** as input for bottom roughness the formula of Chézy is used with a value of $C = 61.5 \frac{m^{0.5}}{s}$. This value is based on the model of Elias et al. (2006): as they modeled the same Texel area, it is assumed this uniform Chézy-value is also applicable in this model. Just like Elias et al., the same enlargement of the bed shear stress due to waves is included using the formulation of Fredsoe (1984).
- **Background horizontal viscosity:** the horizontal eddy viscosity and diffusivity have both been set as $\nu = 5m^2/s$, based on the model of Lenstra et al., (2019). Their model is applied at Ameland, which is close to Texel, and therefore it is deemed reasonable that this value is representative for the model in this research as well.
- **Sediment characteristics:** the bed at SW Texel consists of sand. General values for this sediment are used, based on default input from the D3D-FLOW manual (Deltares, 2022). The specific density $\rho_s = 2650 kg/m^3$, the dry soil density $\rho_{s,dry} = 1600 kg/m^3$. The median sediment diameter amounts to $0.200mm$ and is taken from grain size studies in the Texel area by Elias and Van der Spek (2017) and McLaren et al. (1998). Furthermore, Van Rijn's sediment transport formulations

are used to compute sediment transport (2000). This is the default sediment transport setting in D3D and it distinguishes both bed load and suspended load transport.

- **Morphological characteristics:** to calculate the mean total sediment transport the morphological scale factor has been set to 1. Sediment transport parameters and multiplication factors have been set to default values in D3D (Deltares, 2022). No bathymetrical updates have been applied.

5.5 Numerical stability

The numerical model needs to converge to a stable solution over time. This requires the tidal wave to propagate through each grid cell during each time step. This can be calculated with the Courant number. The Courant number is defined as:

$$C = \frac{u\Delta t}{\Delta x} = \frac{\sqrt{gh}\Delta t}{\Delta x} \quad (5.7)$$

Where:

- Δt = time step [s].
- Δx = grid cell length [m].

The depth at each location is different, meaning the Courant number is different for each grid cell. The original Rijkswaterstaat model uses a time step of 60s, which results in the maximum Courant number in the grid being 18, which is only applicable on Marsdiep in the Texel Inlet. This is not in the area of interest at SW Texel. In the area of interest this Courant number still leads to stable results in the order of 5-6. A time step of 30s would mean a maximum Courant number of 9, leading to a stable solution at each location in the model. However, for a timestep of 60s the Courant number is only exceeded in the Marsdiep, which is not in the area of interest. The rest of the model still leads to stable results. The time step of 60s is accepted with the goal to save computation time of the model. The rest of the numerical parameters have been set to default values in D3D.

5.6 Wave input

The model from Rijkswaterstaat did not contain any information on waves, so this part of the model has been setup separately. The WAVE module executes a SWAN calculation and uses the water level from the FLOW calculations as input. As explained in Section 5.2, WAVE is coupled with FLOW every 60 minutes. The input variables are the wave conditions at the boundaries and the used physical parameters and models.

5.6.1 Wave conditions

To answer the research questions 5B in Chapter 1 or 4ABC - what wave directions cause the most impact on sediment transport, and the question whether the annual effect of storm conditions is bigger than calm conditions - multiple wave conditions have been defined. They are shown in Table 2.1. In general, the waves are distinguished in waves from the NW and SW and both calm and storm conditions from each direction.

This research focuses on the qualitative effect of waves from one direction for 2 weeks of simulation time. This means that the goal is not to model a representative wave climate for the 2 weeks of simulation time, but the goal is to gain insight in the effect of calm/storm waves from the NW/SW on sediment transport. This is different from studies that aim to formulate a representative wave climate as wave input to calculate morphological changes on the long term. The reason this study looks at a simulation time of 2 weeks is to limit the computation time of the model, and to avoid the high uncertainty in erosion and accretion in this complex area if the simulation time would be extended to 1 year.

Creating a representative wave class for a simulation of only 2 weeks is not realistic. In order to have a representative wave class, the wave rose of the 2 weeks should be almost equal to the wave rose of the measurements at Eierlandse Gat (Figure 2.10). If 2 random weeks of wave data was taken and used as input for the model, the probability of the wave rose resembling the measured data is low. The 2 weeks of data could be useful if this experiment was repeated 100x, but doing this many runs is outside of the available time limit of this research.

The same argumentation holds for the application of wind in the model: there are many possible configurations of different wave and wind fields, which would require many model simulations to approach an average value for the effect on mean sediment transport. This is avoided by assuming that wind is coming from the same direction as the waves. In Figure 2.11 the wind rose shows this holds true for waves from the SW, but not for the NW. The effects of NW waves may therefore be overestimated in the results of the model simulations.

In Section 2.3.3 it was mentioned the directional spread of the wave conditions is 21° on either side of the mean wave direction. The directional spread is entered by a cosine power MS in D3D, and according to the WAVE-manual from Deltares (2023) a directional spread of 21° translates to $MS = 6$.

The location of the model is within the North Sea, meaning that the shape of the wave spectrum is required to be JONSWAP. The peak enhancement factor was kept as a default at 3.3, just like Elias et al. did in their Texel model (2006).

5.6.2 Physical and numerical parameters

In the WAVE-module the same constants as the FLOW module were applied. An additional uniform wind was applied over the grid. The wind speed for each simulation was determined in Section 2.3.3 and the wind direction was assumed to be aligned with the waves, as explained in the previous section. Furthermore, there are processes that need to be defined for the waves specifically:

- **Depth-induced breaking:** this is applied using the Battjes and Janssen model. This model takes into account the coefficient to determine the rate of dissipation α and according to Battjes and Janssen (1978) the value $\alpha = 1$ applies to this model. The breaker parameter $\gamma = \frac{H_m}{d} = 0.73$ according to Battjes and Janssen.
- **Non-linear triad interactions (LTA):** this process is activated, because in very shallow water triad wave-wave interactions transfer energy from lower to higher frequencies, which often result in higher harmonics (Beji and Battjes, 1993). Non-linearity matters more in shallow conditions, especially during high energetic events, such as storms. At the NUN and at the shoreface the water is very shallow: the ratio of $\frac{\text{Storm wave height}}{\text{depth}} \approx 1.5 [-]$, and therefore this process is taken into account. The default inputs for this process are used, as was done in the Texel model of Elias et al. (2006).
- **Bottom friction:** this process is included by the JONSWAP bottom friction, as introduced by Hasseleman et al (1973). This model is applicable for fully developed wind-sea conditions in shallow water. This approach requires one variable, being a JONSWAP coefficient of $0.067 \frac{m^2}{s^3}$ for wind-sea conditions.
- **Whitcapping:** The model of Komen et al. (1984) is used, because that is applicable to fully developed wind-sea conditions and growing wind-seas, which is also the case in this project area (Deltares, 2023).
- **Refraction** is included, as the shallow bathymetry around the Noorderhaaks affects the direction of the waves. Frequency shift is also taken into account.

Finally, the numerical parameters have been set to default values in D3D. The only exception is the accuracy criterion of the percentage of wet grid points, which by default is 98%. This value is set as 90% to allow larger accuracy errors in the wave height of the model. This is done to avoid numerical errors at irrelevant locations in the grid. The wave height accuracy is still over 95% in the grid points near SW Texel, which is considered acceptably high. An example is shown in Figure 5.8 of simulation 3. The colored axis indicates a maximum of 5% (of $H_{sig} = 1.39m$) of accuracy error, which is not present in the project area. The same holds for all other simulations. For an overview of the characteristics of each simulation, see Table 6.1.

5.7 Model sensitivity

Regular modelling practise includes the application of a sensitivity analysis to investigate how much the results fluctuate because of deviations in specific input values. In this research no sensitivity analysis is applied because of time constraints. The model can still be useful, because the inputs that would be analysed in a sensitivity analysis are taken from other models, as mentioned in Section 5.4 and 5.6. These models include the same area near Texel or a relatively close location to Texel, meaning their values are likely to have the same application range as this model. Moreover, the used values in this model have been confirmed by scientific literature to be within the application ranges of said literature. This literature is referred to in the subsections that define the input-values of the model (Section 5.4.4 and 5.6.2).

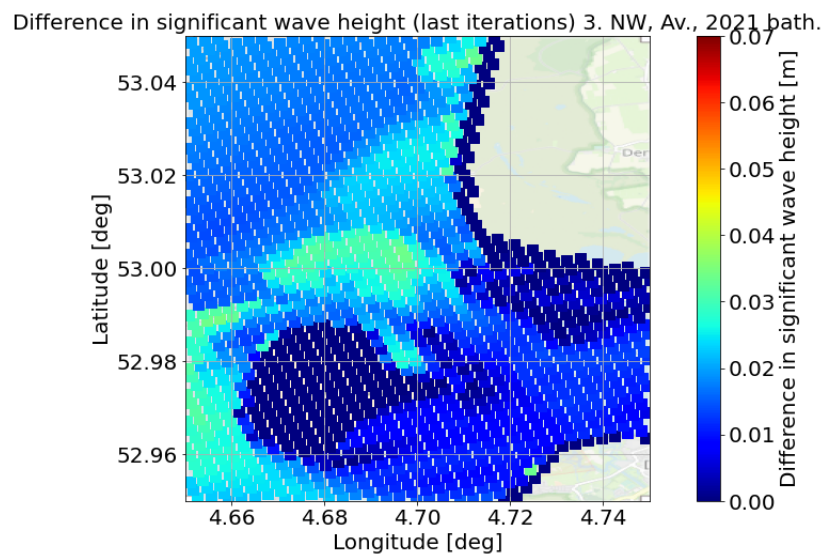


Figure 5.8: Example of wave height accuracy in simulation 3. The accuracy of 5% (0.07m) in this simulation does not get exceeded and therefore it can be concluded that the wave height error is accurate enough to consider the output results.

6 | Delft3D model results

This chapter presents the results from the model. A simulation results overview is given in Section 6.1. Sections 6.2, 6.3 and 6.4 present differences between the variables that are being tested with the simulations.

6.1 Overview sediment transport results of simulations

The model that has been set up in Chapter 5 is used for 10 simulations that are shown in Table 6.1. The simulations distinguish the following variables:

1. **Bathymetry:** the current bathymetry of 2021 and the adapted bathymetry including the mega nourishment are applied.
2. **Wave and wind direction:** wave conditions coming from either the NW or SW are used. These conditions are representative for respectively 45% and 33% of the time of the raw wave data provided by Rijkswaterstaat.
3. **Conditions:** wave conditions have been divided into calm and storm conditions with a probability of occurrence of respectively 95% and 5%.

Simulation	Type of model	Bathymetry	Wave and wind direction	Conditions
1	FLOW	2021	-	-
2	FLOW	Mega nourishment	-	-
3	FLOW + WAVE	2021	NW	Calm
4	FLOW + WAVE	2021	NW	Storm
5	FLOW + WAVE	2021	SW	Calm
6	FLOW + WAVE	2021	SW	Storm
7	FLOW + WAVE	Mega nourishment	NW	Calm
8	FLOW + WAVE	Mega nourishment	NW	Storm
9	FLOW + WAVE	Mega nourishment	SW	Calm
10	FLOW + WAVE	Mega nourishment	SW	Storm

Table 6.1: Overview of simulation characteristics.

Simulation #1 and #2 exist to show the mean total sediment transport if only the FLOW module of D3D is used and the WAVE module is neglected. Analysing the differences allow to investigate the effect of tidal currents in the area. To test differences between bathymetry, where all other model inputs are identical, simulation #3 must be compared to simulation #7, and so do simulations #4-8, #5-9 and #6-10. The effect of wave and wind direction can be distinguished by comparing simulation #3 and #5, #4-6, #7-9 and #8-10. Finally, the effect of calm and storm wave conditions is distinguished by comparing simulation #3-4, #5-6, #7-8 and #9-10.

Figure 6.2 shows the results of each simulation. At all coordinates at SW Texel the mean total sediment transport direction and magnitude $S \left[\frac{m^3}{m \cdot yr} \right]$ are shown. Differences between these runs are discussed in the next sections, but general remarks are stated below:

- The differences between simulation #1-2 and #3-10 indicate the effect of waves in the area. The current is present in the Molengat channel and the Marsdiep, but it has lower impact on sediment transport on the NUN and further from the coast.
- The color scale for storm simulations #4, #6, #8, and #10 is 6x higher than calm simulations, because it shows where mean total sediment transport is relatively high within those simulations.
- Sediment transport is always directed around the Noorderhaaks shoal.
- The simulations never show sediment transport values at Texelhors at the southern tip of Texel. This is because the depth in the model is above the MHW-line, so there is no sediment transport there. The background map is taken from Openstreetmap.org, but falsely shows the presence of water at this location. The scale at which the background has been downloaded did not have enough level of detail to show the Texelhors seaward extension. Figure 6.1 shows a more representative coast, so this island tip explains the absence of model data in the figures in this chapter.
- In all storm simulations there is significantly higher sediment transport on the NUN compared to sediment transport during calm conditions.

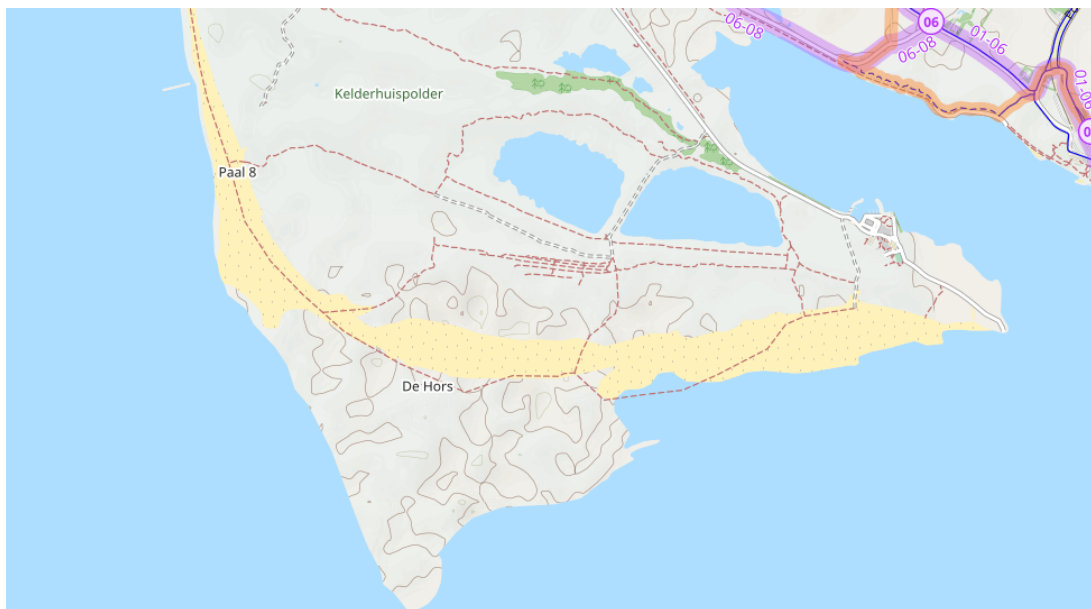


Figure 6.1: Coast at Texelhors showing the tip of SW Texel differently than the figures in this chapter. This tip is a better representation and must be kept in mind while viewing the other figures.

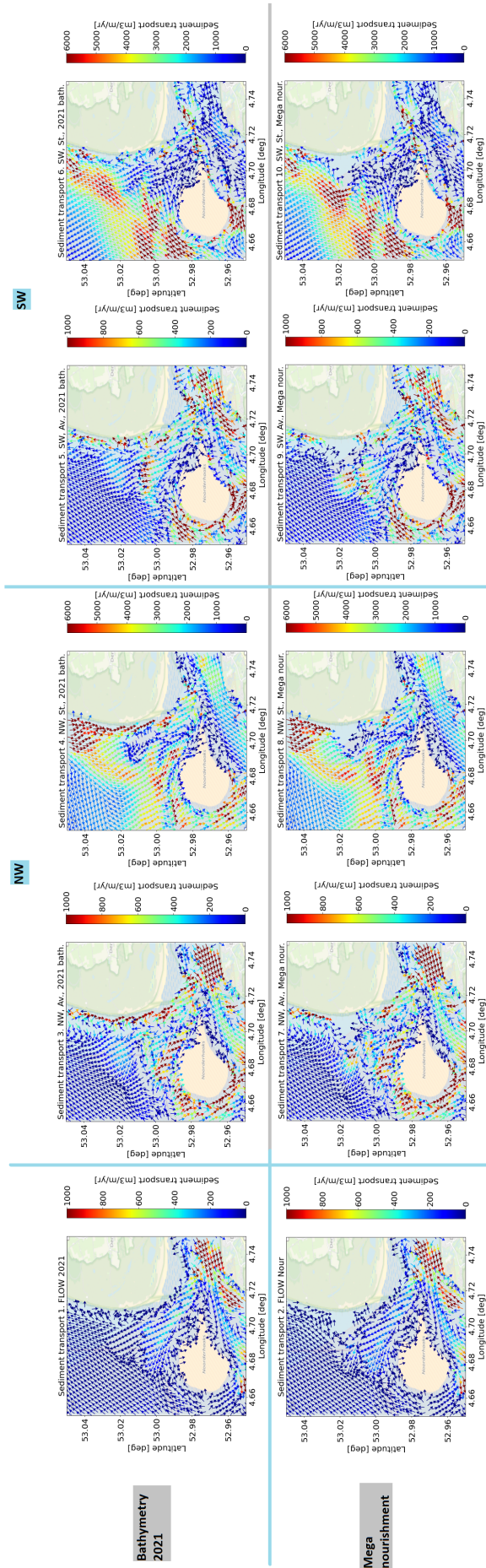


Figure 6.2: Overview of sediment transport directions and magnitudes for all simulations. Simulation #1-2 show the results from currents only. Sediment transport by currents is most dominant in the middle of the Molengat channel and outward directed. Simulation #3 till #10 include the effect of wave conditions, and simulations including storms (#4-6-8-10) experience the highest sediment transport rates.

6.2 Storm-calm-ratios

This section focuses on what processes cause the largest sediment transport. The simulations are compared in pairs: #4-3, #6-5, #8-7 and #10-9, as all other variables are identical. The necessity of knowing which conditions are dominant is important, because then it is known whether the most erosion happens gradually or in short energetic episodes. This could help future research in behaviour of the mega nourishment, or help design potential future interventions in unwanted erosion patterns alongshore to maintain the BKL. To fairly compare the effect of storm wave conditions and calm wave conditions the mean total transport values are time-weighted at each location. In Section 2.3.3 a storm was defined by occurrence of 5% of the time, so the storm results are multiplied by 0.05, and calm values by 0.95. Subsequently, the sediment transport values of the storm simulations are divided over the calm simulations, creating a $\frac{Storm}{Calm} - ratio$ and the result is shown in Figure 6.3.

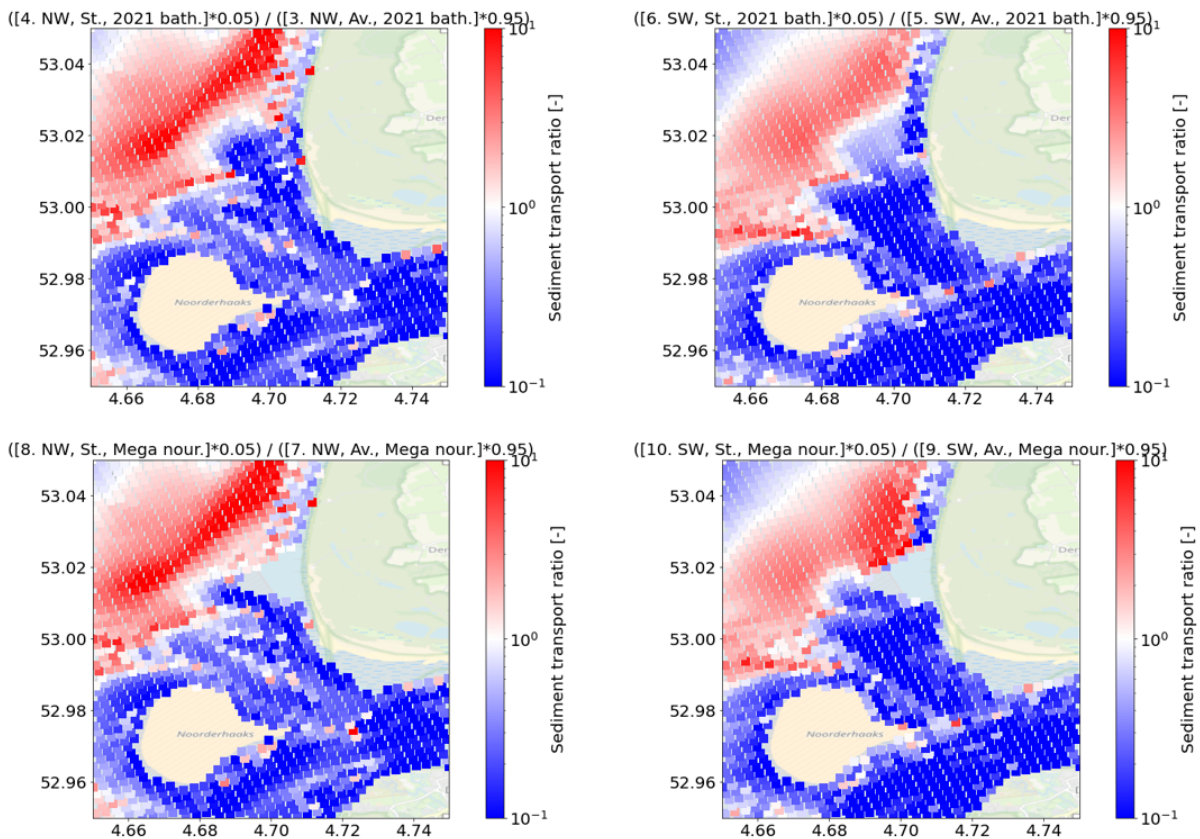


Figure 6.3: Storm-calm ratios where the time-weighted sediment transport values of storms are divided over its calm conditions counterpart. In all comparisons it shows a storm dominant effect on the NUN, and a calm dominant effect in the Molengat channel.

If the time-weighted $\frac{Storm}{Calm} - ratio$ is larger than 1, storm conditions cause more mean total sediment transport at that location. This area is red. When this value is smaller than 1, the calm conditions prevail and the value is blue. Since all 4 panels show a large red plain in the NUN-area and on the seaward side of the NUN, it can be concluded that on annual time scale this area is prone to the effects of storms. Next, the mega nourishment is located at the interface of both dominant storm conditions on the north and dominant calm conditions in the south. Therefore, the mega nourishment will likely have mixed response to sediment transport by storms and calm conditions. The Molengat channel is

dominated by calm conditions in all simulations. Furthermore, in NW-conditions the storm dominance on the NUN is higher than during SW conditions.

Sediment transport can be initiated by multiple causes:

- Bottom friction
- Depth-induced breaking
- Currents

Figure 6.4 shows the values of the orbital velocities near the bottom, which are a measure for the bottom friction. According to Bosboom and Stive the orbital motion under waves gives a time-varying shear stress at the bed, which can set sediment grains into motion (2021). In the left graph (#3 - calm conditions) the orbital velocities are 1.5-3x smaller than in the right graph (#4 - storm conditions). This means the orbital velocities contribute to sediment transport in this area. The graphs for the other simulation comparisons are not significantly different from these 2, and therefore are not shown.

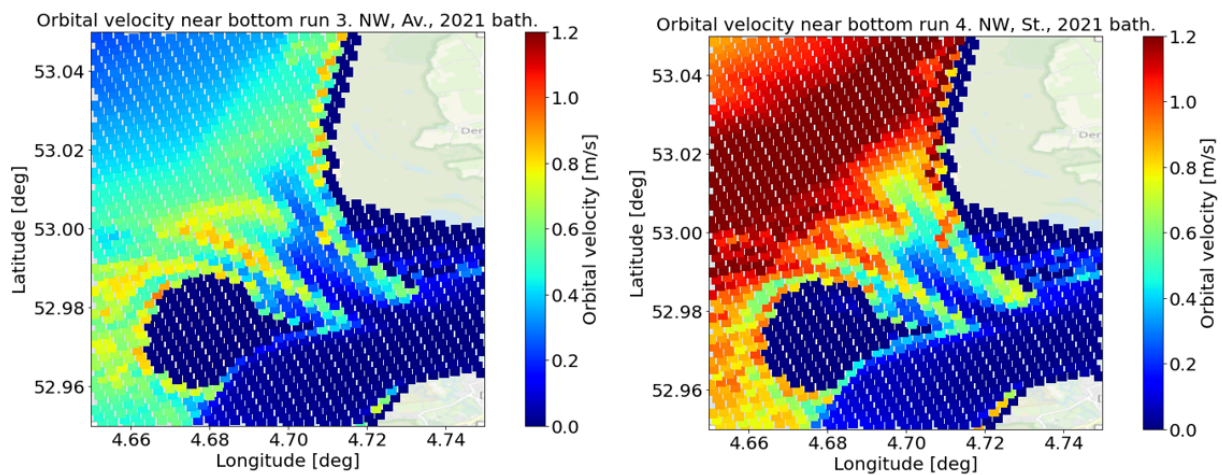


Figure 6.4: Orbital velocity for runs #3 and #4. During storm conditions the orbital velocity is 1.5-3x higher than during calm conditions, which indicates that bottom friction is a contributor to the sediment transport values in this area. These differences are the same for runs #5-6-7-8-9-10 and thus not shown.

Figure 6.5 shows for the same simulations the maps for depth-induced breaking. It is shown what fraction of the waves break at each location. When the patterns of both figures are compared, it can be concluded that depth-induced breaking does not contribute to sediment transport on the NUN, as the fraction of breaking waves is approximately 0. This pattern is the same for other simulations. Depth-induced breaking only plays a role at the beach in these simulations.

The third factor is sediment transport by currents. In Figure 6.6 the ratio between the simulations #3-1 and #4-1 and are shown. These 2 comparisons are representative for all simulations. This figure does not compare storm and calm conditions, but both storm conditions with just tide and average conditions with just tide. In the NUN area the ratios are higher than 1, which means the sediment transport is more heavily affected by waves. Therefore, the sediment transport on the NUN is not primarily caused by currents. In Figure 6.2 it was already shown that the current transport on the NUN is low, which supports this observation.

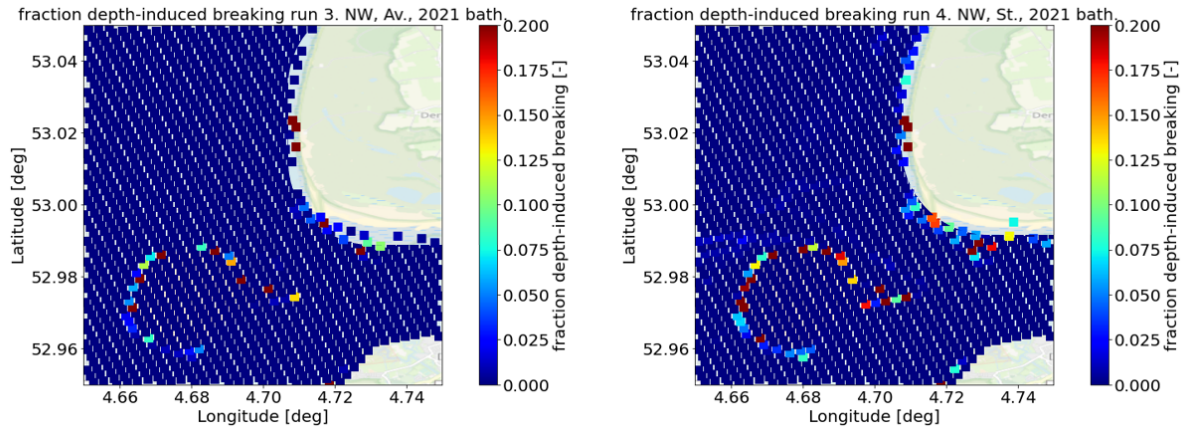


Figure 6.5: Fraction of depth-induced breaking waves for runs #3 and #4. The fraction of depth-induced breaking waves is almost 0 at the NUN.

Figure 6.6 shows ratio-values of ≤ 1 in the Molengat channel. This means that the tidal current causes as much sediment transport as the simulation including tidal current + waves. Consequently, sediment transport in the Molengat is mainly caused by the tidal current. In simulation #1 the flow velocity is significantly higher than outside the channel, which supports the statement that sediment transport is caused by the tidal current.

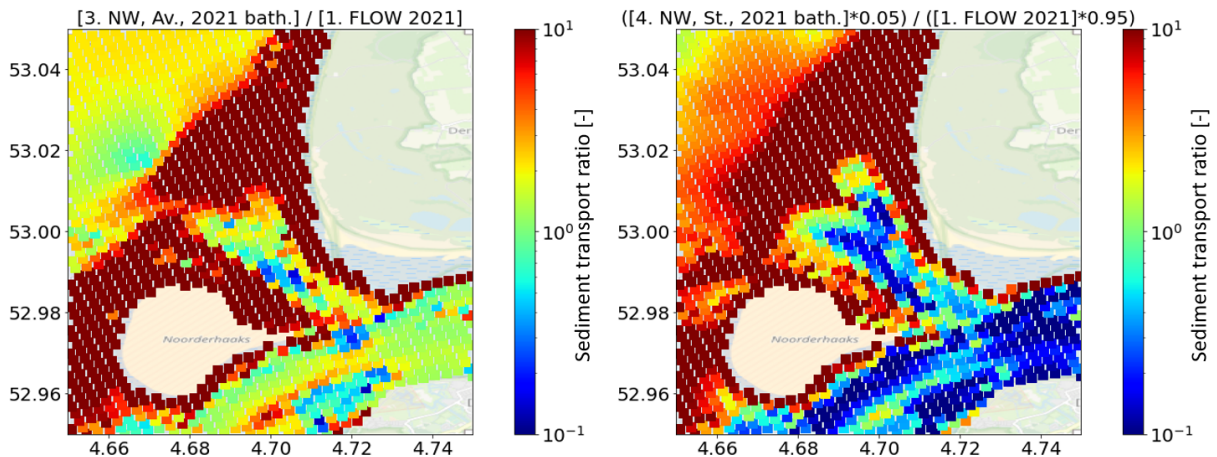


Figure 6.6: Sediment transport ratios of both $\frac{run3}{run1}$ and $\frac{run4}{run1}$. In both comparisons the sediment transport in the Molengat is equal or less than 1, meaning that the current causes most transport in this area. On the NUN this ratio is large, meaning the current does not contribute to transport here.

6.3 NW and SW waves

This section compares simulations with wave conditions from the NW (#3-4-7-8) and wave conditions from the SW (#5-6-9-10). The similarities are summarised in Figure 6.7. The sediment transport direction is the same for NW waves alongshore: in all simulations this is directed southward. Furthermore, in all NW simulations the sediment transport north of the Noorderhaaks is alongshore and pointed

towards the Texel basin.

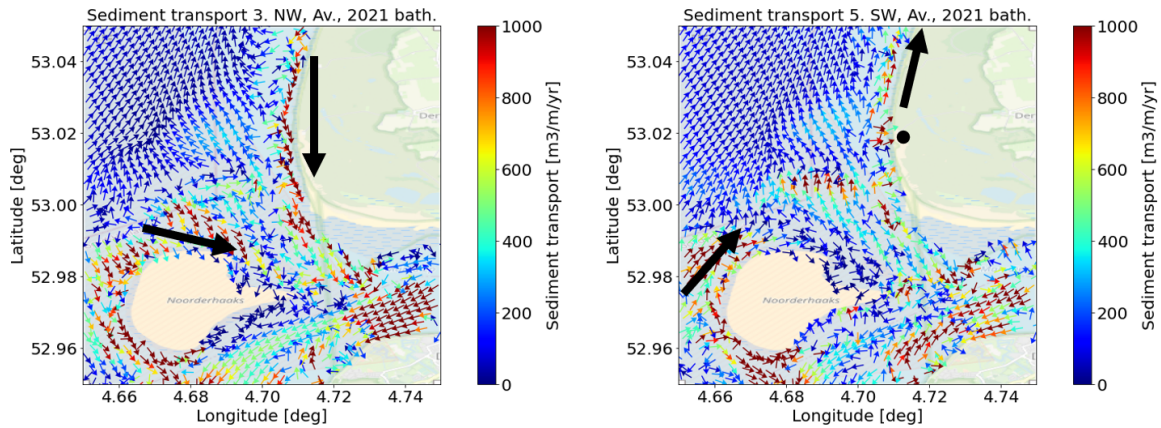


Figure 6.7: The black arrows in both figures indicate a sediment transport direction that is shared among all simulations with NW or SW wave conditions. NW waves all have alongshore sediment transport in southward direction, while this is mostly northward during SW wave conditions and landward during SW conditions.

Simulations with SW wave conditions show northward directed alongshore sediment transport. On the sea-facing side of the Noorderhaaks the sediment transport is directed northward. On the NUN the transport is always northward directed. At the location of the black dot the sediment is pointed on-shore. It is also pointed landward at the south-western tip of Texel. Sediment transport directions in the middle of the Molengat seem to be directed out of the tidal delta, at the Molengat banks the transport direction is pointed towards the Marsdiep.

6.4 2021 bathymetry and mega nourishment

Simulations #3-4-5-6 and #7-8-9-10 are used to compare the current bathymetry with the mega nourishment bathymetry, while all other variables are identical. Figure 6.8 shows the ratio of sediment transport when the nourishment is applied divided over the original bathymetry. Except the upper right panel the graphs show increased sediment transport at the tip of the mega nourishment. From Figure 6.2 it can be seen that the sediment transports at the tip of the nourishment for those simulations are pointed northwards, and for simulation #8-4 this is southward. Additionally, the mean sediment transport values are much lower on the sides of the nourishment, indicated by the blue plains in Figure 6.8. Also, the sediment transport directions have changed after the nourishment application: the transport in most runs was northward directed at the northern side of the nourishment. After nourishment application this changed to southward onto the nourishment, or west-/ eastward along the nourishment. The same holds for the southern side of the nourishment.

Higher sediment transport at the tip can be caused by higher flow velocities. Figure 6.9 shows the ratio of orbital velocity during the maximum outflow of the tidal cycle of simulation #6 and #10. Both depth-averaged flow velocities are taken at the same time and the values of simulation #10 are divided over #6. The other simulations are not significantly different and are therefore not shown. The flow velocities are higher at the nourishment tip in the simulation with the nourishment applied, and lower at

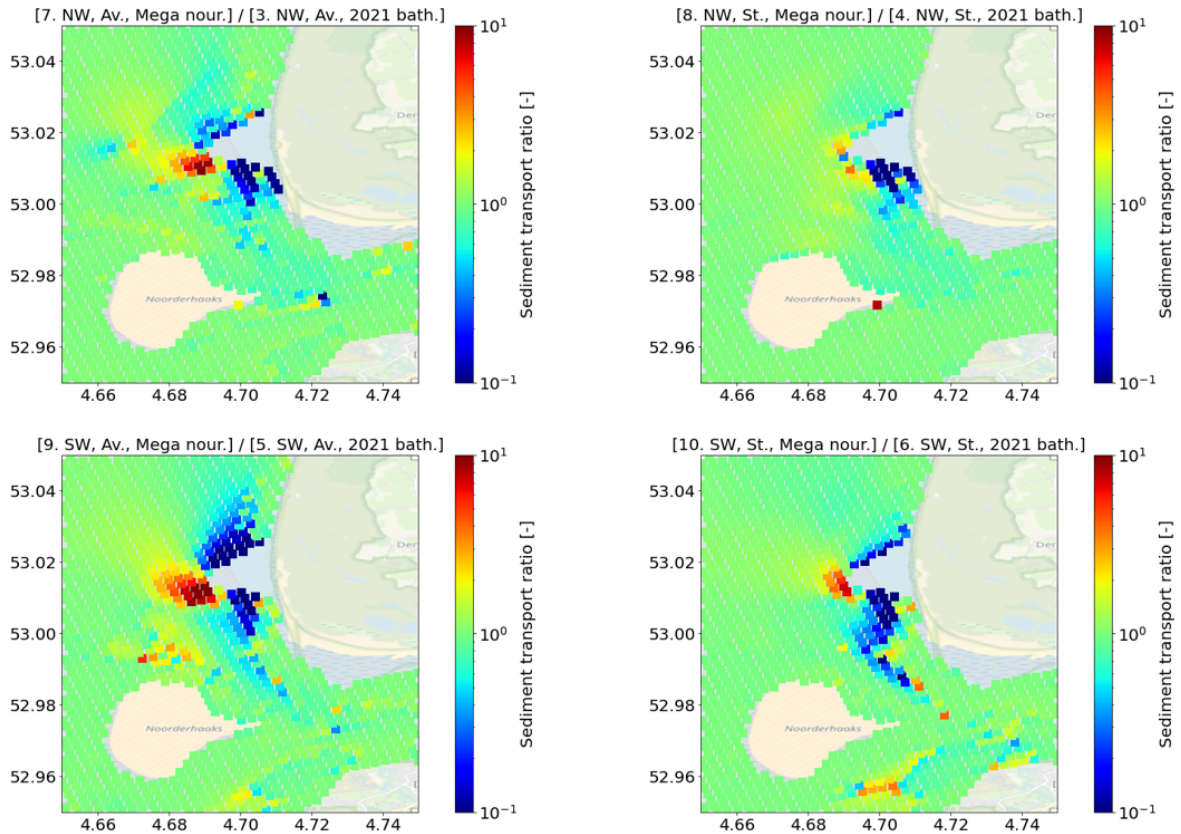


Figure 6.8: Sediment transport ratios of mega nourishment divided over initial bathymetry. At the tip of the nourishment the sediment transport has increased and at the sides it has reduced. This change is caused by higher flow velocities which are likely caused by the convergence of the flow.

both sides of the nourishment, just like the sediment transport in Figure 6.8. It could be hypothesized that since the tidal prism remained constant, and due to the cross-sectional reduction of the Molengat passage, the flow velocity has increased at the tip due to flow convergence, thus resulting in higher sediment transport rates at the tip of the nourishment. Simultaneously, the lee sides of the nourishment experience lower flow velocity and therefore lower sediment transport.

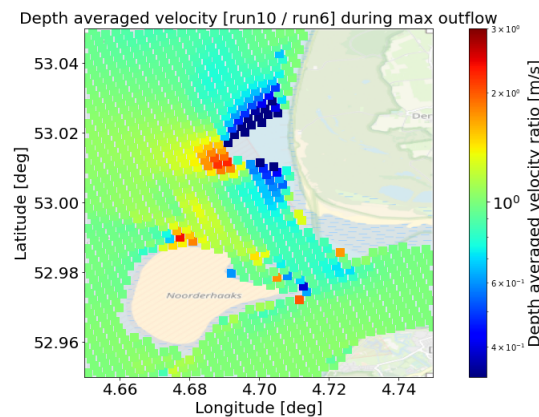


Figure 6.9: Flow velocity ratio of simulation #10 and #6 at the same time in the tidal cycle. The velocity map is similar to Figure 6.8. The scale of the map has been determined by taking the third root of the scale values of Figure 6.8, because flow velocity $u \propto H$ and $S \propto H^3$.

6.5 Gradients in sediment transport/ Erosion-accretion patterns AS

To answer research question 5B - how sediment transport gradients change after the application of the mega nourishment - the alongshore sediment transport gradients must be determined. Alongshore sediment transport is indicated by S_y , and the gradient determines an accretion or erosion pattern. To obtain sediment transport gradients, the following method is used:

1. Take the grid cells at the SW Texel coast and retrieve the sediment transport values in each cell.
2. Take $\frac{\partial S_y}{\partial y}$ of all alongshore cells at the same cross-shore location.
3. Erosion and accretion patterns are defined by:
 - $\frac{\partial S_y}{\partial y} > 0$: erosion
 - $\frac{\partial S_y}{\partial y} < 0$: accretion

Figure 6.10 shows 3 things: on the left the grid orientation is shown at SW Texel and the numbers 1-15 show the grid cells that experience significant sediment transport. These cells are highlighted in the middle, where a darker red color indicates more sediment transport ($O(1000m^3/m/yr)$) and blue ($O(10m^3/m/yr)$). The right shows the direction of the sediment transport in each cell, which is negative as the positive direction is upward as indicated.

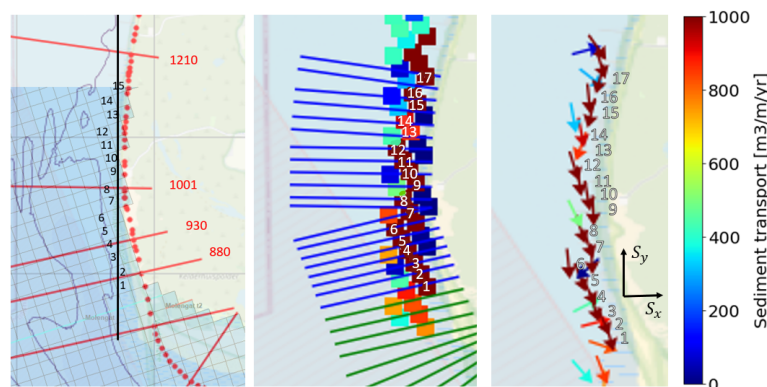


Figure 6.10: Overview of approach to determine sediment transport gradients alongshore. Left: Vertical line indicates the direction of the sediment transport S_y . Middle and right show the magnitude and direction of S_y .

Figure 6.11 shows the sediment transport volume S_y on the left, and the alongshore gradient $\frac{\partial S_y}{\partial y}$ of the same run on the right. Erosion is indicated in red, while accretion is green. The figure shows alternating erosion and accretion alongshore. This is unexpected, because there are no distinct alongshore characteristics that could cause the behaviour shift. This model can therefore not answer the last part of the research question 5B - where the sediment transport gradients change the most after the application of a mega nourishment. How this issue can be fixed is described in Section 7.1.

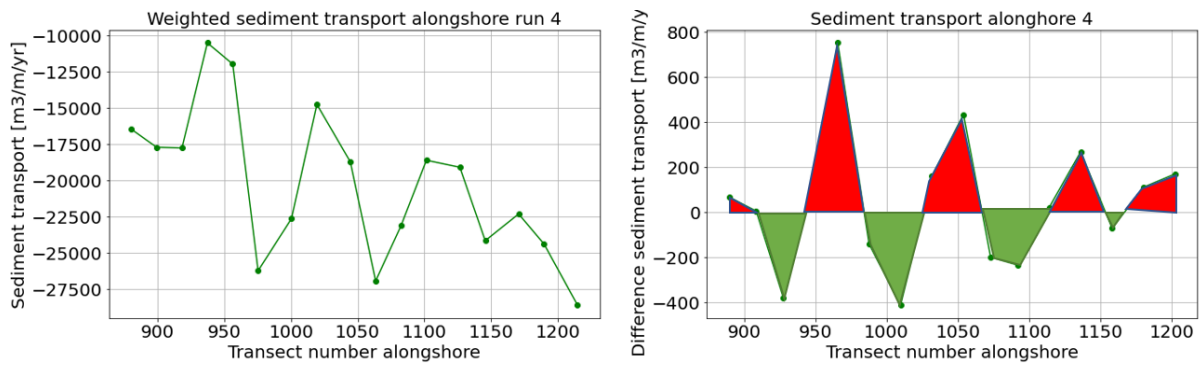


Figure 6.11: Left: Sediment transport from simulation 4 with storm conditions from the NW. Right: accompanying gradients $\frac{\partial S_y}{\partial y}$.

7 | Discussion

7.1 Transition from current nourishment scheme to mega nourishment

Section 4.5 and 4.6 investigated the behaviour of the transects and thus an expectation of future behaviour can be described if the nourishment scheme is continued. It was shown that the Molengat was being filled before the nourishment program started, and this rate did not change after the initiation of the program (see Appendix A and E). Therefore, it is likely the filling will continue in the unfilled transect sub areas T1 and T2. Furthermore, based on Figure 4.17 the dunes are likely to continue to grow, until they reach a maximum steepness, which reduces the landward aeolian sediment transport capacity (De Vries, 2013). This maximum steepness seems to be reached for the transects in T2, because the dune volume has remained constant since 2000. In T1, T3 and T4 the dune volume continues to linearly increase, and are therefore expected to grow till they reach their maximum steepness. The maximum steepness and dune volume change have not been researched further.

Another key finding is that the dune volume started increasing when the nourishment program started. Figure 4.16 and the figures in C.2 show the pre-1990 landward retreat and lowering of the first dune. Table 4.2 shows that the first nourishment was applied in 1994 in all transect ranges T1-T4, and Figure 4.17 shows that the start of dune volume increase happened in the same year in the same transect ranges. The total dune volume increase since the start of the nourishments is $1.936Mm^3$, which is 29.9% of the total nourished volume in the area. Beach nourishments are closer to the dune, and could therefore be contributing more to dune volume change than shoreface nourishments, but this hypothesis would require its own study.

If the nourishment program is aborted, it affects the 4 parts of each transect. It is expected that the Molengat will continue to fill. Furthermore, the dune and beach volume is likely to resume diminishing in the transects where nourishments are discontinued. One major difference compared to pre-1990 data is that in T3 and T4 the Molengat has been filled. In the shallow part ($V_{shallow}$) of the transect the landward bank erosion of the Molengat stopped after it was filled. This phenomenon occurred where nourishments were still applied, and it has not been investigated how this area would develop without nourishments. It could be hypothesized that the nourishments compensate the erosive process, which means that landward erosion could resume if the nourishment program is discontinued - albeit slower than pre-Molengat filling.

The mega nourishment has the goal to supply the adjacent coast with sediment such that erosive flows are compensated. Figure 4.19 showed that the unfilled Molengat transect areas T1 and T2 experience most nearshore erosion. T2 experiences most erosion so the mega nourishment is applied there to increase the buffer zone to satisfy the BKL the most. The purpose of the mega nourishment is to diffuse sediment alongshore such that it compensates the erosion in T1, T3 and T4, see Figure 7.1. The left

graph shows in orange the modeled nourishment and the goal sediment flows in purple. The right shows the erosion of the shallow area in green. Figure 6.3 showed that sediment transport is mainly directed southward, meaning the alongshore diffusion to the north is limited. In a further research a new shape could be investigated, where the nourishment is skewed more northward along the coast. De Vries et al. (2018) showed that in a reference project of the Sand Engine the nourishment shape could be made more asymmetrical by putting more volume in the part where waves are coming from. This could be applied at SW Texel too, and is indicated by the shape in black in Figure 7.1. One advantage of this new design is that the alongshore diffusion could end up in a larger shoreline that needs to satisfy the BKL, as a more northward nourishment means lower transport to transects south of transect 880. On the contrary, one risk is that the volume is placed in an area that already satisfies the BKL, and the alongshore diffusion needs to keep T2 in place.

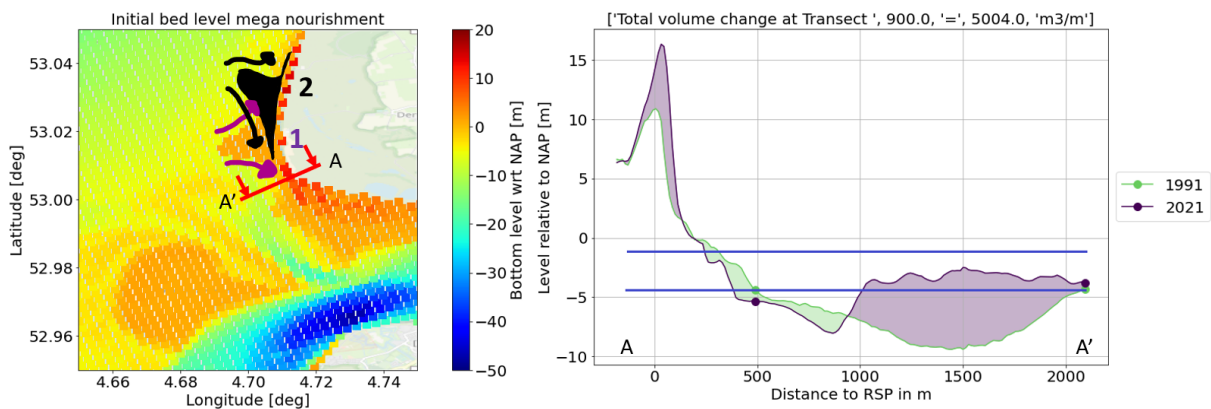


Figure 7.1: Left: applied mega nourishment and goal of sediment transport. The black shape indicates an option for future research to model. Right: transect 900 shows erosion on land, and this process needs to be compensated by the alongshore diffusion of the mega nourishment.

The model did not show sediment transport gradients accurately enough (see Section 6.5). First it is explained how this issue could be solved, and subsequently another method is described to qualitatively assess the effect, based on more uncertain results.

Potential improvement in next models

To compute $\frac{\partial S_y}{\partial y}$ more accurately, the model could be improved in multiple ways.

1. The current grid of $200 * 200m$ -cells is rotated and rectangular (see Figure 6.10, meaning the cross-shore location of the calculated sediment transport is different for each alongshore cell. The transport gradient must be taken at a constant distance cross-shore. A curvi-linear grid could be used instead of a rectangular grid to orthogonalize on the coast, which makes it possible to take S_y and $\frac{\partial S_y}{\partial y}$ at a constant cross-shore distance in the alongshore cells. The curvi-linear grid can have smaller cells onshore and larger cells in the deeper sea.
2. Apply time varying wave conditions in 1 run, so that the wave rose in the model corresponds to the wave rose from the RWS data. In the current model case only the effects of waves from 1 direction are applied to investigate the effects of specific wave directions, but the time-variation in 1 model run can improve the results.

Applying bottom updates to look at accretion and erosion patterns

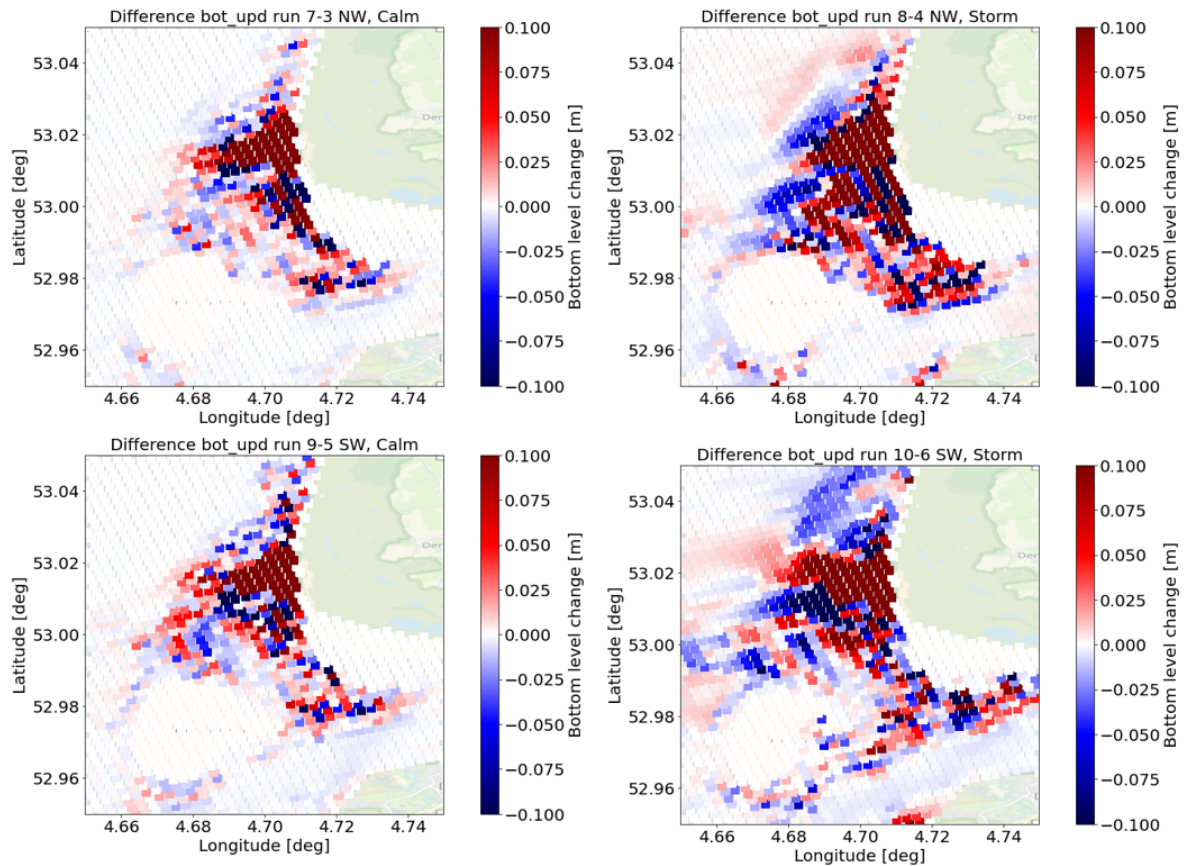


Figure 7.2: Overview of accretion (red) and erosion (blue) areas when bottom updates are included. Including bottom updates enhances uncertainty, as the area is morphologically complex.

Another method to look at sediment transport changes is to include the effect of bottom updates in the model, and subsequently investigate where the bottom erosion and accretion patterns are. In Section 5.2 it was mentioned that the inclusion of bottom updates has large uncertainty due to the ebb-tidal delta, the Texel basin, and the tidal channel. However, these simulations run for 1 tidal cycle, which is a much smaller time scale than large morphodynamic changes. Therefore, it could be argued that the initial response of the bottom during this cycle could still be indicative of sediment transport gradients alongshore. The effect of a mega nourishment compared to the current bathymetry can be assessed by applying the following method:

1. Run simulation #3-6 without nourishment and include bottom updates.
2. Run simulation #7-10 including the mega nourishment and bottom updates.
3. $Effect\ mega\ nourishment = z_{nourishment} - z_{current\ bathymetry}$
 - $Effect\ mega\ nourishment > 0$: accretion
 - $Effect\ mega\ nourishment < 0$: erosion

The results are shown in Figure 7.2. NW conditions cause accretion south of the nourishment and in the Molengat channel. Erosion occurs north of the nourishment. For SW conditions erosion occurs in the north as well. The total combined bottom change of all simulations can be calculated using the following equation:

$$z_{combined} = \sum_{i=1}^n (\Delta z_i * probability_i) \quad (7.1)$$

Where:

- Δz_i = the bottom difference between simulation 7 and 3 [m]
- $probability_i$ = probability of this simulation. The probabilities were defined in Section 2.3.3 and can be calculated using *occurrence direction * occurrence conditions*:
 - Run 7-3, NW calm waves: $0.45 * 0.95$
 - Run 8-4, NW storm waves: $0.45 * 0.05$
 - Run 9-5, NW calm waves: $0.35 * 0.95$
 - Run 10-6, NW storm waves: $0.35 * 0.05$

The total expected accretion and erosion pattern then is shown in Figure 7.3. In this combined result erosion occurs north of the nourishment, and accretion in the alongshore area south of the nourishment. Since the resolution of the grid cells was too low to compute transport gradients, the accuracy of these values can also be questionable. However, this could still be used as a first qualitative estimate of changes and this approach can also be used for future models.

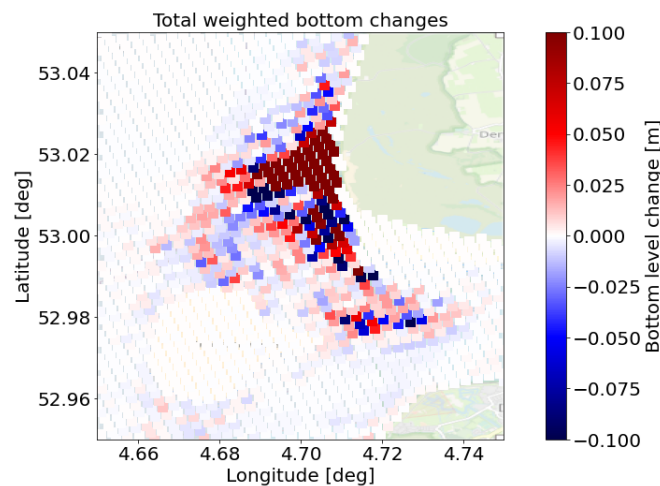


Figure 7.3: When the results of Figure 7.2 are weighted by occurrence in wave direction and conditions and then summed, the total result is slight erosion in the north of the nourishment. Northward alongshore there is slight accretion, and south of the nourishment there is accretion too.

7.2 Research compared to literature

Figure 7.4 shows representations of the tidal flow from Elias (2021) and Cleveringa (2001). The simulation of FLOW only is shown on the right. The model result is similar to the result of Elias: the 4 dashed lines are pointed in the same direction in both graphs. Sediment is transported alongside the NUN, there are 2 flows directed into the Marsdiep at both edges of the Molengat along the coast and the No-orderhaaks, while there is a seaward directed sediment flow in the middle of the Molengat in a new ebb tidal channel. This sediment transport is larger outward directed than to the Marsdiep. The effect

of the nourishment on the FLOW result in simulation 2 (see Figure 6.3) does not seem to significantly change the behaviour of the sediment transport by FLOW, as the directions largely remain the same. Though, the sediment transport magnitude slightly reduces in the middle of the channel. At the tip of the nourishment the transport increases. Elias does not mention anything about the magnitudes of the sediment transport. This FLOW results shows that the order of NUN-transport by just the tide is $O(10 \text{ m}^3/\text{m}/\text{yr})$, land bank Molengat = $O(150 \text{ m}^3/\text{m}/\text{yr})$, middle Molengat = $O(400 \text{ m}^3/\text{m}/\text{yr})$ and Noorderhaaks bank Molengat = $O(10 \text{ m}^3/\text{m}/\text{yr})$.

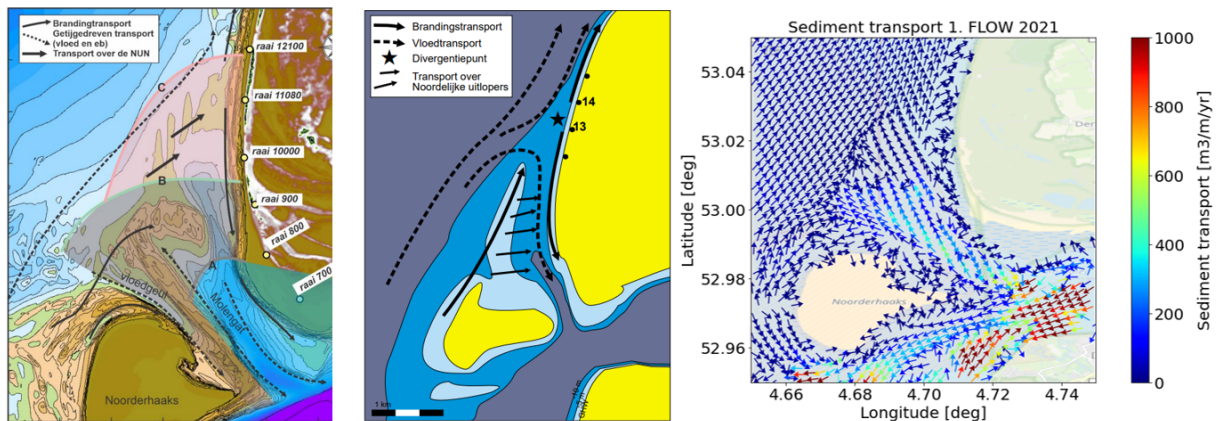


Figure 7.4: Left: Tidal sediment transport is indicated by dashed lines. Figure taken from Elias (2021). Middle: dashed lines indicate tidal sediment transport too. Figure taken from Cleveringa (2001). Right: model result FLOW only. The sediment transport directions are similar to those from literature.

Cleveringa (2001) depicted this location with a divergence point at transect 1300. This model and Vak-lodingen data (see Figure 4.4) show that the divergence point seems to be more south: between transect 1100-1200. The model results of the FLOW simulation are similar to the flow over the NUN and pointing southward when it arrives south of the divergence point. The tidal flow results of Cleveringa and Elias can therefore be confirmed in a qualitative sense.

Observations around the application can also be confirmed by literature. Figure 6.8 increased significant erosion at the tip of the nourishment, and less at the sides. Figure 6.9 confirmed the cause to be higher and lower flow velocities. Radermacher et al. (2017) described the effect of protruding nourishments on the surrounding flow velocity: the flow at the tip increases, while the lee side of the nourishment experiences lower flow velocities in a returning pattern. This is shown in Figure 7.5. The K_c -value represents the alongshore width of the nourishment, the α -value the protrusion into sea. The lee side is only on the north part of the nourishment in this figure, because there the outflow is sheltered. The right graph is a moment in time during outflow, while during inflow this pattern switches direction. Radermacher et al. show that the return current is behind the entire protrusion, which is not the case at Texel. This could be explained by the different hydrodynamic conditions at SW Texel. Radermacher et al. assumed alongshore uniform conditions, while at Texel the basin, the Noorderhaaks and the ebb-tidal channel could affect the size of the return current.

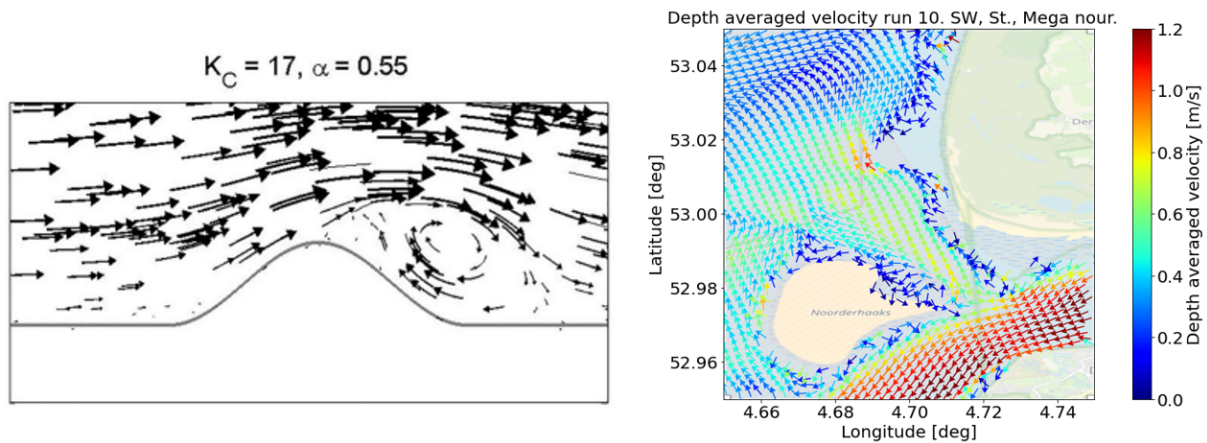


Figure 7.5: Left: Protrusion of mega nourishment at an alongshore uniform shoreline causes higher flow velocities at the tip, and a return current behind it. Figure from Radermacher et al. (2017). This can be observed on the right figure, north of the nourishment.

7.3 Limitations morphological analysis

The data analysis in Chapter 4 already explained multiple limitations of the used approaches. Below a list of the main limitations is given:

- In Chapter 4 it is assumed that all transects are parallel to each other to calculate volume changes, which is true for most transects. However, the transect orientation changes between transects 1000-1001, 1093-1108 and 1168-1190, see Figure 4.6. This rotation means that the volume changes are less accurate further from shore. Further from shore the area becomes larger so volume changes in reality are larger. It is assumed that these differences do not have such impact on the results of the data analysis that the described behaviour of the bottom lacks important information.
- The Molengat has not been filled linearly in sub area T2, as mentioned in Section 4.5.1. The back-and-forth movement of the Molengat seaward bank can be observed when the transects are compared in the plan view of the area, see Appendix A. It is hypothesized the closure of a small previous ebb-tidal channel could have caused higher flow velocities in the seaward bend of the Molengat, causing more erosion. Since the reopening of the ebb-tidal channel around 2000 (see Figure 4.12), the Molengat resumed linear landward migration.
- There seems to be a correlation between dune growth and beach nourishments: the dune volume increase is approximately 29.9% of the total nourished volume, where the dune profile has not yet reached an equilibrium profile in ranges T1, T3, and T4. The wind could have enabled this process, as the wind rose from Figure 2.11 shows a dominant landward direction from the SW, which is roughly orthogonal to the coast.

Interchangeability of JARKUS and Vaklodingen data

In Section 4.1 it was explained that Vaklodingen and JARKUS data are used interchangeably if JARKUS data did not extend far enough offshore, for example to define $V_{shallow}$. Figure 7.6 shows both the transect from Vaklodingen and JARKUS data at the same location in the year 1997, and the differences are mainly in the dune and at 2000m from the RSP. The cross-section difference is 24 m^2 over a length of 3400 m , meaning the average difference is $\frac{24 \text{ m}^2}{3400 \text{ m}} = 0.0071 \text{ m}$ between the 2 lines. The largest dif-

ferences occur behind the first dune, which is not used in morphological analysis, meaning this value could be lower in the positions of interest. If this process is repeated for all transects, the order of differences is small, and therefore it is justified to use Vaklodingen and JARKUS interchangeably.

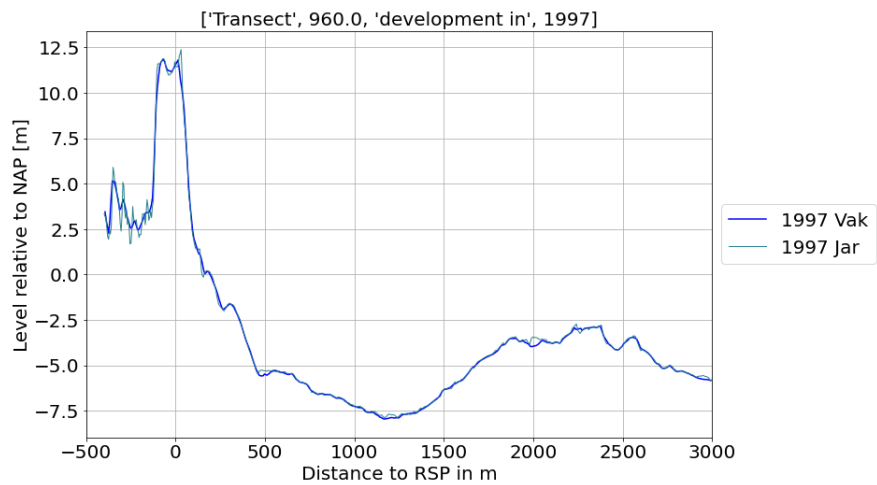


Figure 7.6: Comparison of Vaklodingen and JARKUS data for the same transect. JARKUS data does not always reach far enough offshore, meaning the the Vaklodingen data are required.

7.4 Limitations model setup and results

The model has multiple limitations. The main limitation was explained in Section 7.1: the grid cells did not have a satisfying resolution to determine the sediment transport gradients alongshore. By reducing the modeled area to SW Texel and refining the resolution, grid cells could likely be reduced to $50 * 50m$ without increasing the computation time. Additionally, a curvi-linear grid could be applied to improve the accuracy of smaller scale processes.

Furthermore, the following things could add better accuracy to the model:

- Perform a sensitivity analysis to investigate what parameters have relatively large impact on model results.
- The input of the waves was 1 tested wave class per simulation. A more realistic approach would be to distinguish more wave classes and their frequency of occurrence in the same simulation. Therefore, time varying wave characteristics could be applied. As a result, it is also required to increase the simulation time to 1 year, so the simulation time is long enough to have the wave characteristics resemble the wave rose of Figure 2.11. The different simulations of the current model would then be replaced by 1 large simulation, yielding a more accurate initial response of the mega nourishment.
- Wind was assumed to have a constant wind speed and direction. This input could be improved by making it time and spatially varying.
- Currently, the initial response of bottom changes is shown in Figure 7.2. Right after the start of a nourishment the bathymetry is furthest from morphological equilibrium, leading to an overestimation of the bottom changes (Arriaga et al., 2017). The focus should therefore not be on the bot-

tom change values, rather the locations experiencing erosion and accretion should be considered. Figure 7.7 from their research illustrates that the effect of bottom updates is larger during the first 6 months of a mega nourishment. This is illustrated by diffusivity ϵ , that decreases to a constant value. On the right part this diffusivity is shown in the bottom. This image illustrates why sediment transport at the tip of the nourishment increases as shown in Figure 6.8. After multiple days the bottom has updated and is diffused more than the initial conditions, which explains a smaller diffusivity.

- Create depth dependent Chézy-values for each grid cell instead of uniform values. The sensitivity analysis could indicate whether it is beneficial to the model results to create a spatially varying C-value-file. It could be hypothesized that in shallow areas the C-value will be lower, causing more dissipation of energy. As explained in Figure 6.4 bottom roughness plays a major role in the sediment transport calculation, meaning that lower C-values would likely result in higher transport rates and therefore this model could underestimate the actual sediment transport.
- The model only takes into account 1 type of sediment: grains with a $D_{50} = 200\mu m$, whereas this varies over the area, as described by Elias and Van der Spek (2017). A sensitivity analysis would give more understanding of the impact of this factor on the results.
- Adding the submerged cross-shore groynes in the refined grid, starting from transect 880 and spaced every 400m. Their length must extend approximately 80m into sea.

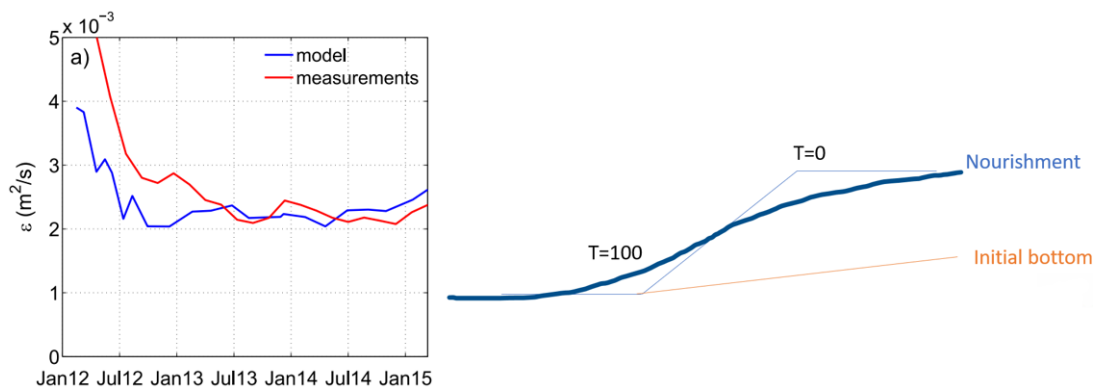


Figure 7.7: Left: diffusion coefficient development over time, taken from Arriaga et al., (2017). The graph shows that the initial phase of the model simulation yields larger sediment transport, because the bottom profile is furthest from equilibrium. As a result, the initial effect cannot be linearly extrapolated for the longer term, but the model results can still be used qualitatively.

8 | Conclusion and recommendations

8.1 Conclusions about system behavior

The Dynamic Preservation Act dictates that the current position of the coastline at SW Texel must be the same or seaward of the position in 1990. It is based on the valuation of the coast in economical, ecological, recreational and flood safety sense. The current coastal protection strategy consists of shoreface and beach nourishments with an interval of approximately 2-3 years, which requires frequent expensive dredging vessel mobilization that causes frequent nuisance in the system. Therefore, there were 4 research questions:

1. *What alternatives exist to protect the coastline of SW Texel in the future, while maintaining its current values?*
2. *How has the morphology developed since 1990, including the nourishment program?*
3. *How could the morphology change by a replacement of the nourishment program by a mega nourishment?*
4. *What is the optimal location of a mega nourishment and what is the effect of the nourishment on shoreline changes in the system?*

The first goal of this study was to formulate and design an alternative coastal protection strategy, where the application of a mega nourishment was chosen over a cross-shore dam or an outer delta nourishment based on 2 reasons. Firstly, the mega nourishment is a soft solution, which is in line with RWS policy. Secondly, the mega nourishment satisfies the BKL in the short term. The other alternatives may still be worth investigating in other studies. It has been investigated what the effect of a mega nourishment is on the erosion and accretion pattern alongshore. A mega nourishment requires roughly the same amount of CO₂-emissions by fuel consumption of sand displacement, but only requires a 1 time mobilization of dredging vessels to the project location, whereas the current program requires frequent mobilization. The values in fuel savings could be calculated in a more extensive study focused on CO₂-emissions in each solution.

The second question focused on a morphological analysis of the development of the SW Texel area in 1991-2021. This was done through a sediment balance of the SW Texel system, that consists of the nourishment volume, the natural sediment transport and the volume changes of the transect. Volume changes of each transect were identified for 4 parts of the transect: the dune, the beach, the shallow part and the Molengat channel.

The dune and the beach reduced in volume before 1990. Since the start of the nourishment program the volume started increasing in the entire area. Therefore, this strongly suggests that the dune growth is caused by the application of nourishments. 29.9% of the entire nourishment volume has ended up in the dunes. When nourishments are aborted, Figure 4.16 showed that it is expected that the shrinking

of the dunes will resume. This is because volumes started increasing after - and were decreasing before - the first nourishments. It was also found that transects in T2 reached a maximum dune volume, which can be explained by a maximum steepness of the dune front. As a result, the landward aeolian transport capacity reduces and limits further growth. This hypothesis needs further investigation. The transects in ranges T1, T3 and T4 have not yet reached this stage.

The Molengat in the transects was found to be moving towards shore before the nourishment program started (as shown in Appendix A), and its landward movement was not influenced by the implementation of the nourishment program. Therefore, the Molengat filling rate can be extrapolated into the future, projecting the future closing date of each transect range. The Molengat in T1 is projected to be filled by 2035, and in T2 by 2055. In T3 and T4 the Molengat has already been filled. Eventually, the landing of the NUN (the Molengat bank) on the coast could be able to nourish the coast. The data analysis showed that transect areas T3-T4 - where the Molengat has been filled already - have experienced limited shallow erosion, suggesting a correlation between Molengat closure and the amount of erosion at the shore. The late projection filling date of T2 is a reason to put the mega nourishment at that location. An additional short term reason for this location is that the BKL is not satisfied, but this is subordinate to the long term scale of this project.

The third question showed that the dunes would have reduced further if the nourishment program was not implemented. Furthermore, a point of attention that should be investigated is whether the dunes will resume shrinking if the nourishment program is replaced by a non-nourishment solution. The application of a mega nourishment is done by putting 20 years worth of sediment at transect range 945-1053 in one construction project. Transects in this range can expect a continuation of dune growth from the start, until their maximum steepness is reached. Simultaneously, the mega nourishment aims to diffuse sediment alongshore in the shallow part of the transects, providing sediment to adjacent transects. The sediment supply to other transects could be able to limit the shrinking of the adjacent dunes, or even let them grow. However, this requires further investigation.

Finally, a model simulation of the mega nourishment alongshore was created in Delft3D. The model setup was based on an existing model from Rijkswaterstaat: Delft3D-FLOW_Waddenzee-PACE_j09_v06. It incorporated tidal flow conditions and wave conditions, and multiple simulations that distinguished current bathymetry/mega nourishment, NW/SW wave directions and calm/storm conditions were executed. The model was able to show that storm conditions have the most time-averaged impact on sediment transport on the NUN, but in the Molengat this is dominated by calm conditions. In the Molengat, sediment transport is dominated by the tidal current. Furthermore, the application of a mega nourishment will increase sediment transport at the tip and decrease sediment transport on the sides compared to the situation without nourishment. The model did not have sufficient grid cell resolution to accurately show sediment transport gradients alongshore, which means the question about changes in accretion and erosion alongshore cannot be answered. When the model included a higher uncertainty bottom-updated calculation scheme, the total occurrence-and-direction-weighted effect indicated qualitatively that the bottom is likely to accrete south of the nourishment, while north of the nourishment erodes slightly. However, further research is required to support the robustness of this statement, since the combined simulated effect can be questionable and the grid cell resolution was too low to accurately incorporate the effect of smaller scale processes.

8.2 Recommendations for future research

1. The most important recommendation is to continue research with a more accurate model in the Texel area, by applying higher grid resolution and more wave characteristics for a longer simulation period to better show the accretion and erosion alongshore. Next, the nourishment shape can also be included in future research. Now it was taken as an initial design based on the erosion pattern and the BKL, but a more advanced model could test a skewed shape to the north on a more northward location that could (based on Figure 7.7) diffuse sediment more southward. That way the wave direction and alongshore sediment transport could be taken into account as well, which was not done in this research. The model could also be improved by implementing time-varying wave conditions. Yet, this research is still useful in determining the location of the nourishment and projecting when the Molengat could be closed, which led to the expectation of future reduced shallow shore erosion and therefore better manageable BKL. In further optimization a question could be how much sediment diffusion to the north and the south is preferred with respect to the nourishment program on Middle Texel and how adjust the shape of the nourishment accordingly.
2. The correlation between dune volume change and beach nourishment could be investigated by experiments. In the same research it could also be analysed what factors determine the maximum steepness in a dune profile so that it could be calculated how much sediment could be saved in future nourishments if the current nourishment scheme is continued indefinitely.
3. Create a study that analyses the effect of a cross-shore dam in the area. What would be the effect of the dam and what is the optimal length and location?
4. On a higher project scale level the current nourishment scheme could be compared with the proposed mega nourishment to calculate what the net savings would be of dredging costs and carbon dioxide emissions. This would be relevant in view of the responsibilities of Rijkswaterstaat regarding climate change.

References

- Arriaga, J., Rutten, J., Ribas, F., Falqués, A., Ruessink, G. (2017). *Modeling the long-term diffusion and feeding capability of a mega nourishment*. Coastal Engineering 121, 1-13. <http://dx.doi.org/10.1016/j.coastaleng.2016.11.011>
- Barbanti, A., Chiarlo, R., Fornasiero, P., Gabellini, M., La Valle, P., Nicoletti, L. (2005). *Innovative monitoring of turbidity due to dredging activities*. Volume 2, Pages 803 - 814 2005. 7th International Conference on the Mediterranean Coastal Environment. MEDCOAST 2005. Code 105144.
- Beji, S., Battjes J. (1993). *Experimental investigation of wave propagation over a bar*. Coastal Engineering 19: 151-162.
- Bertin, X., Fortunato, A., Oliveira, A. (2007). *Sensitivity analysis of a morphodynamic modeling system applied to a Portuguese tidal inlet*. River, Coastal and Estuarine Morphodynamics: RCEM 2007 - Proceedings of the 5th IAHR Symposium on River, Coastal and Estuarine Morphodynamics Volume 1, Pages 11 - 17. ISBN 978-041544167-4.
- Bosboom, J. and Stive, M. J. F. (2021). *Coastal Dynamics*. Delft University of Technology. Delft, The Netherlands. Revision no. 1269.
- Brand, E. (26-10-2022). *Huidig kustverdedigingsbeleid Nederland en Texel*. [Interview]. Technisch Manager Kustlijnzorg, Rijkswaterstaat.
- Brand, E., Ramaekers, G., Lodder, Q. (2022). *Dutch experience with sand nourishments for dynamic coast-line conservation – An operational overview*. Ocean and Coastal Management, 217, [106008]. <https://doi.org/10.1016/j.ocecoaman.2021.106008>
- Cleveringa, J. (2001). *Zand voor zuidwest Texel. Technisch advies RIKZ over vier mogelijke ingrepen in het Zeegat van Texel*. Rapport RIKZ/OS/2001/ 031. Rijkswaterstaat Rijksinstituut voor Kust en Zee / RIKZ.
- Davis, R.A., Hayes, M.O. (1984). *What is a wave-dominated coast?* Marine Geology, Volume 60, Issues 1-4. Pages 313–329. [https://doi.org/10.1016/0025-3227\(84\)90155-5](https://doi.org/10.1016/0025-3227(84)90155-5)
- De Schipper, M., De Vries, S., Ruessink, G., De Zeeuw, R., Rutten, J., Van Gelder-Maas, C., Stive, M. (2016). *Initial spreading of a mega feeder nourishment: Observations of the Sand Engine pilot project*. Coastal Engineering, Volume 111, Pages 23-38. ISSN 0378-3839. <https://doi.org/10.1016/j.coastaleng.2015.10.011>.
- De Vries, S. *Physics of blown sand and coastal dunes*. TU Delft - Civil Engineering and Geosciences. ISBN: 978-94-6191-878-9.

- De Vries, S., De Schipper, M., Roest, B., Luijendijk, A., Aarninkhof, S. (2018). *Diffusion of a mega feeder nourishment - assessing 5 years of sand engine spreading/*. ICCE.
- De Sonnevile, B., Van der Spek, A. (2012). *Sediment- and morphodynamics of shoreface nourishments along the North-Holland coast*. 33rd International Conference on Coastal Engineering 2012, ICCE 2012. ISBN 978-098966111-9
- Deltares. (2022). Delft3D-Flow User Manual. Version 4.05. SVN Revision: 75129. Delft, The Netherlands.
- Deltares. (2023). Delft3D-WAVE User Manual. Version 4.05. SVN Revision: 78281. Delft, The Netherlands.
- Elias, E. (2006). *Morphodynamics of Texel Inlet*. TU Delft. IOS Press. ISBN 1-58603-676-9
- Elias, E. (2021). *De morfologische ontwikkeling van de Noordelijke Uitlopers van de Noorderhaaks*. Deltares. 1206794-004-ZKS-0006
- Elias, E., Cleveringa, J., Buijsman, M.C., Roelvink, J.A., Stive, M.J.F. (2006). *Field and model data analysis of sand transport patterns in Texel Tidal inlet (the Netherlands)*. Coastal Engineering 53, p. 505-529. doi:10.1016/j.coastaleng.2005.11.006
- Elias, E., Van der Spek, A. J. F. (2017). *Dynamic preservation of Texel Inlet, the Netherlands: understanding the interaction of an ebb-tidal delta with its adjacent coast*. Netherlands Journal of Geosciences - Geologie en Mijnbouw. 96-4 P.293-317. <https://doi.org/10.1017/njg.2017.34>
- Elias, E., Van der Spek, A. J. F., Wang, Z. B., Ronde, J. d. (2012). *Morphodynamic development and sediment budget of the Dutch Wadden Sea over the last century*. Netherlands Journal of Geosciences, 91(3), 293–310. <https://doi.org/10.1017/S0016774600000457>
- Elias, E., Wang, Z. (2020). *Sedimentbalans Waddenzee - Synthese ten behoeve van Technisch Advies Kustgenese 2.0*. Deltares. 1220339-007-ZKS-0010
- Fredsoe, J. (1984). *Turbulent boundary layer in wave-current interaction*. Journal of Hydraulic Engineering 110, 1103–1120
- Grady, A.E., Moore, L.J., Storlazzi, C.D., Elias, E., Reidenbach, M.A. (2013). *The influence of sea level rise and changes in fringing reef morphology on gradients in alongshore sediment transport*. Geophysical research letters, VOL. 40, 3096–3101. <https://doi-org.tudelft.idm.oclc.org/10.1002/grl.50577>
- Jacob, B., Stanev, E.V., Zhang, Y.J. (2016). *Local and remote response of the North Sea dynamics to morphodynamic changes in the Wadden Sea*. Ocean Dynamics. Volume 66, Issue 5, Pages 671 - 690. DOI: 10.1007/s10236-016-0949-8
- Kaergaard, K., Fredsoe, J. (2012). *Numerical modeling of shoreline undulations part 2: Varying wave climate and comparison with observations*. Coastal Engineering Volume 75, 77-90. DOI: <http://dx.doi.org/10.1016/j.coastaleng.2012.11.003>
- KNMI. (2022). *Daggegevens van het weer in Texelhors*. [Data set CSV]. Retrieved at 14-10-2022 from: <https://>

www.knmi.nl/nederland-nu/klimatologie/daggegevens

- Komen, G., Hasselmann, S., Hasselmann, K. (1984). *On the existence of a fully developed wind-sea spectrum*. Journal of Physical Oceanography 14: 1271–1285.
- Komar, P.D., Inman, D.L. (1970). *Longshore sand transport on beaches*. Journal of Geophysical Research. Vol. 75. DOI: 10.1029/JC075i030p05914
- Kristensen, S.E., Drønen, N., Deigaard, R., Fredsoe, J. (2016). *Impact of groyne fields on the littoral drift: A hybrid morphological modelling study*. Coastal Engineering, Volume 111, Pages 13-22. ISSN 0378-3839. <https://doi.org/10.1016/j.coastaleng.2016.01.009>.
- Lenstra, K.J.H., Pluis, S.R.P.M., Ridderinkhof, W., Ruessink, G., Van der Vegt, M. (2019). *Cyclic channel-shoal dynamics at the Ameland inlet: the impact on waves, tides, and sediment transport*. Ocean Dynamics (2019) 69:409–425. <https://doi.org/10.1007/s10236-019-01249-3>
- Lodder, Q. (07-11-2022). *Huidig kustverdedigingsbeleid Nerland en Texel*. [Interview]. Coördinerend Adviseur Waterveiligheid, Rijkswaterstaat.
- McLaren, P., Steyaert, F., Powys, R. (1998). *Sediment transport studies in the tidal basins of the Dutch Waddenzee*. Senckenbergiana Maritima 29 (1/6): 53–61.
- Ministerie van Infrastructuur en Milieu. (2015). *Ons Water in Nederland, Nieuw Nationaal Waterplan 2016-2021*. Ministerie van Infrastructuur en Milieu, p. 24.
- Ministerie van Infrastructuur en Waterstaat. (2022). *Inzichten Morfologie - Pilotsuppletie buitendelta Ameland Zeegat*. Monitoring Morfologie pilot AZG. Rijkswaterstaat. Deltares.
- Natura2000. n.d. *Noordzeekustzone*. [map] Retrieved at 14-10-2022 from: <https://www.natura2000.nl/gebieden/friesland/noordzeekustzone/noordzeekustzone-kaart>
- Radermacher, M., De Schipper, M.A., Swinkels, C., MacMahan, J.H., Reniers, A.J.H.M. (2017). *Tidal flow separation at protruding beach nourishments*. Journal Geophysical Research: Oceans. 122, 63–79, doi:10.1002/2016JC011942.
- Ridderinkhof, W., Hoekstra, P., Van der Vegt, M., De Swart, H.E. (2015). *Cyclic behavior of sandy shoals on the ebb-tidal deltas of the Wadden Sea*. Continental Shelf Research 115 (2016) P.14-26. <http://dx.doi.org/10.1016/j.csr.2015.12.014>
- Rijksbegroting. (2013). *Begroting*. [Web page]. Retrieved at 25-05-2023 from: <https://www.rijksfinancien.nl/memorie-van-toelichting/2014/OWB>
- Rijkswaterstaat. (2020). *Kustgenese 2.0: kennis voor een veilige kust*.
- Rijkswaterstaat. (2021). *Uitvoeringsprogramma Kustlijn zorg. Onderbouwing suppletieprogramma 2020-2023*. Ministerie van Infrastructuur en Waterstaat.
- Rijkswaterstaat. (2022). *Vaklodingen_new*. [Data set netCDF]. Retrieved at 21-11-2022 from: <https://opendap.deltares.nl/thredds/catalog/opendap/rijkswaterstaat/catalog.html>

- Rijkswaterstaat. (2022b). *suppleties*. [Data set netcdf]. Retrieved at 21-11-2022 from: <https://opendap.deltares.nl/thredds/catalog/opendap/rijkswaterstaat/catalog.html>
- Rijkswaterstaat. (2023). *Wave period, Wave height, Wave direction, Directional spread*. [Data set CSV] Retrieved at 24-03-2023 from: <https://waterinfo.rws.nl/#!/nav/expert/>
- Van der Moolen, J. (2002). *The influence of tides, wind and waves on the net sand transport in the North Sea*. Continental Shelf Research, Volume 22, Issue 18-19, Pages 2739 - 2762. DOI: 10.1016/S0278-4343(02)00124-3. ISSN: 02784343
- Van Rijn, L. C., Roelvink, J. A., Horst, W. T.. (2000). *Approximation formulae for sand transport by currents and waves and implementation in DELFT-MOR*. Tech. Rep. Z3054.40, WL | Delft Hydraulics, Delft, The Netherlands.

Appendices

A Additional photos SW Texel coastline



Figure A.1: Overview Texelhors and transition area between dune and land.



Figure A.2: Dunes at the southern tip of the island. They are in development stage, and not as developed as the dunes that are within the BKL policy.



Figure A.3: Snapshot of waves coming from the NW. The whitecapping areas show the contours of the ebb tidal channel that is developing on the NUN.



Figure A.4: Cross-shore groyne during low water. It consists mainly of rocks and tar.



Figure A.5: Snapshot of waves arriving at the shoreline. This snapshot is taken during low water, when the cross-shore groyne is emerged. These groynes have a spatial distance of 400m.

B Bathymetry maps from Vaklodingen at SW Texel

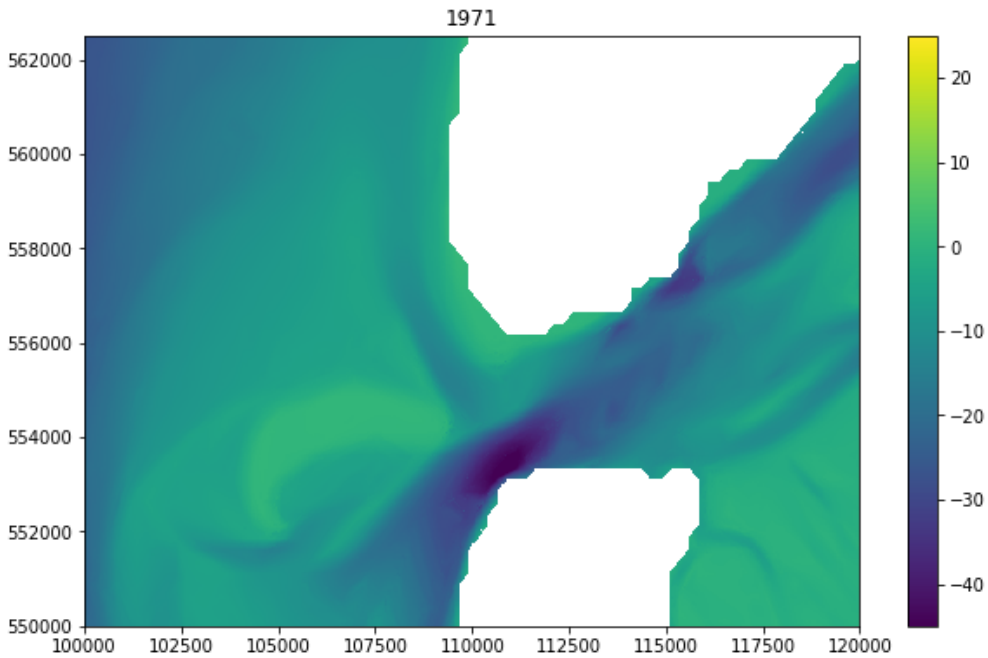


Figure B.1: Vaklodingen data from 1971 at SW Texel. The white area in the north depicts the island of Texel (no bathymetrical data). The white area in the south depicts the tip of Den Helder. The green area in the middle is the shape of the Noorderhaaks in 1971. Color bar indicates m with respect to NAP.

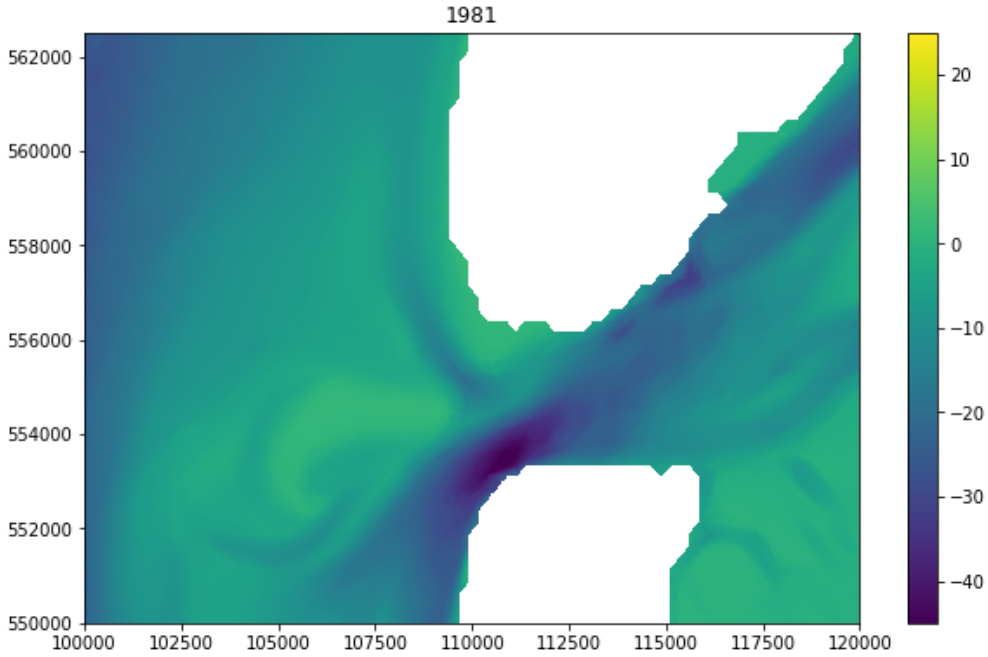


Figure B.2

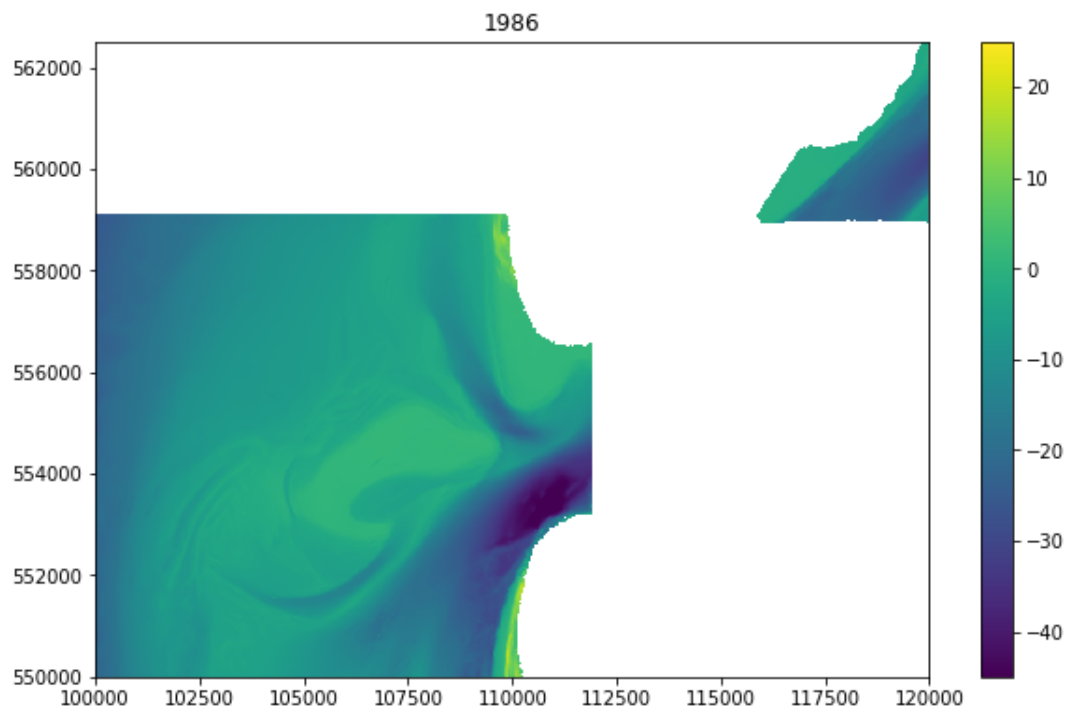


Figure B.3

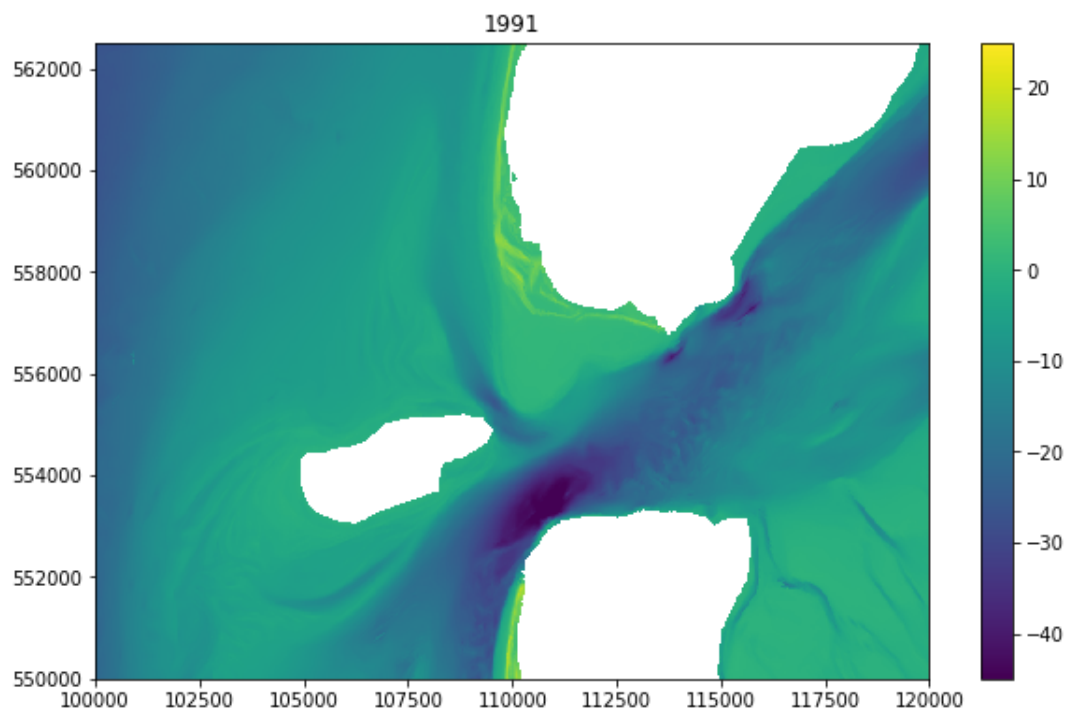


Figure B.4

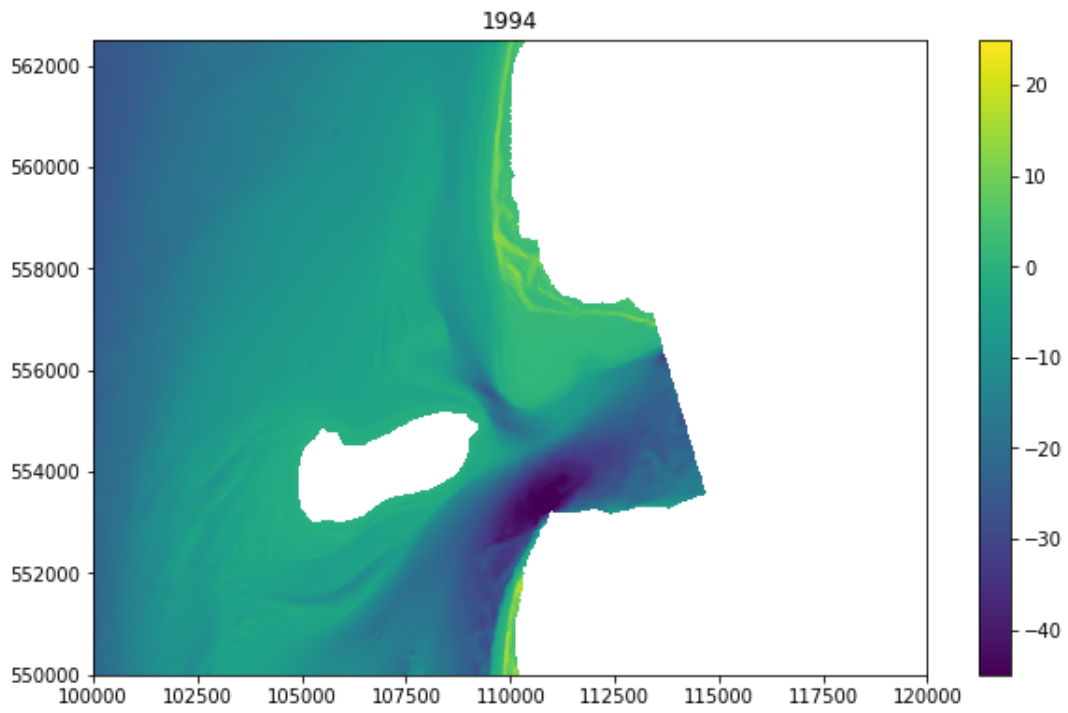


Figure B.5

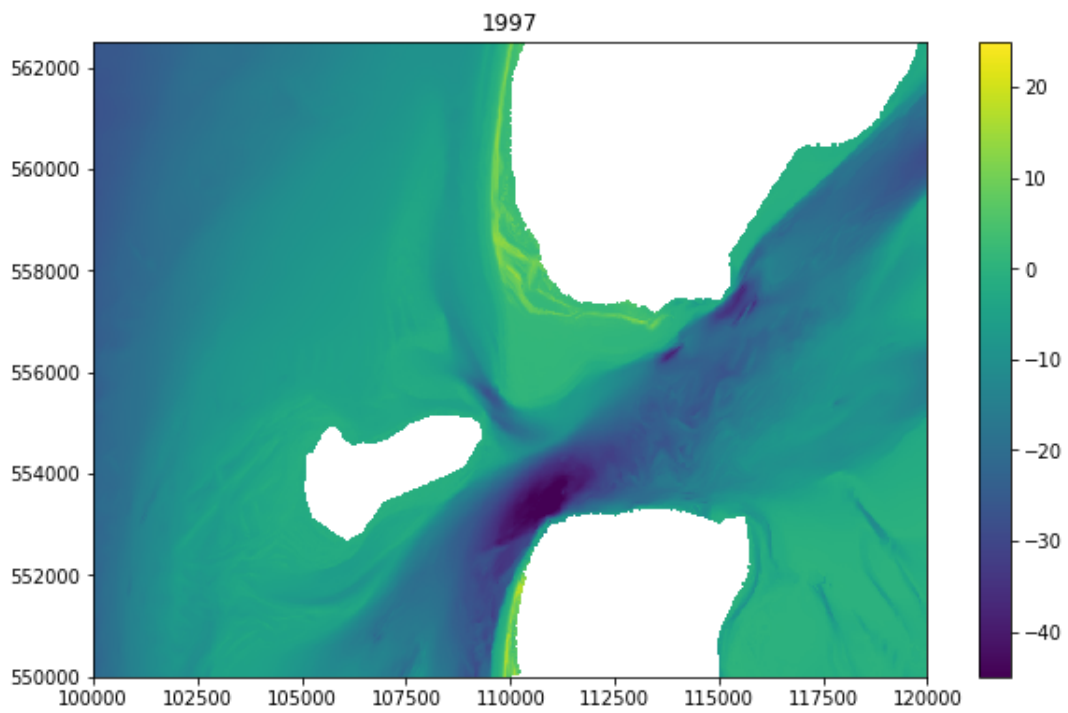


Figure B.6

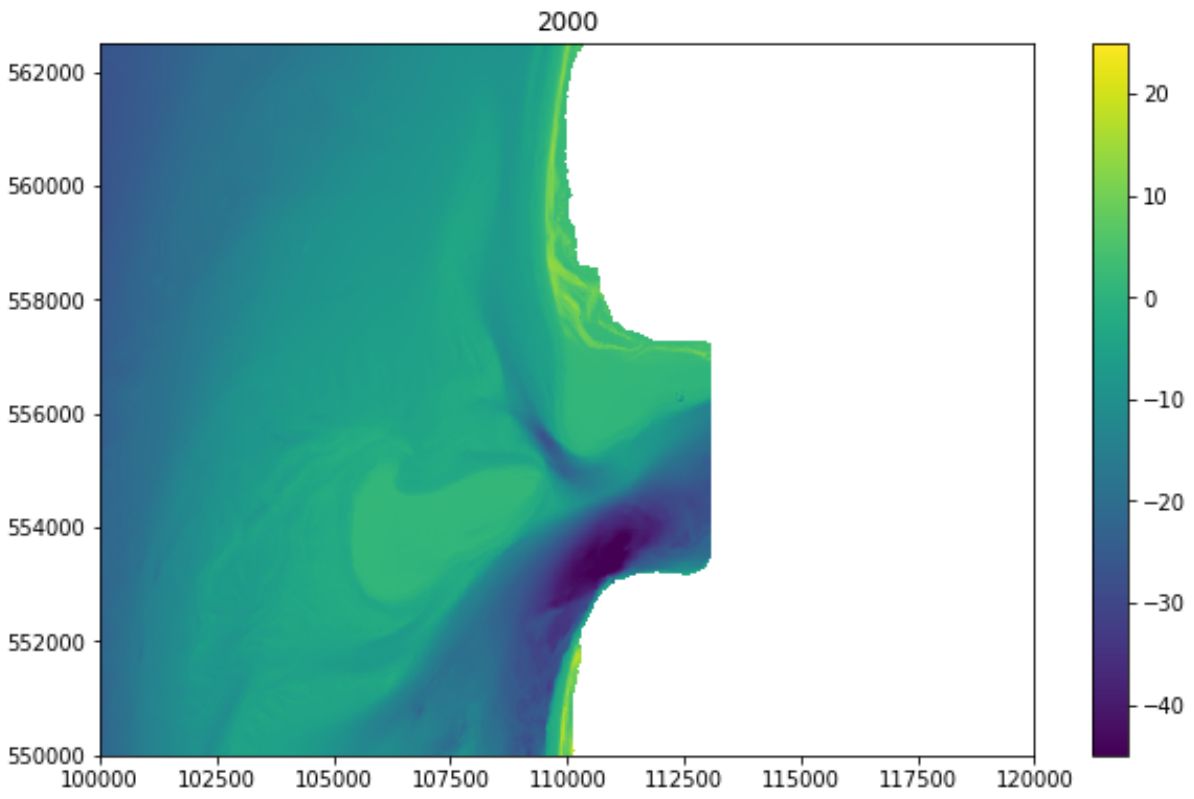


Figure B.7

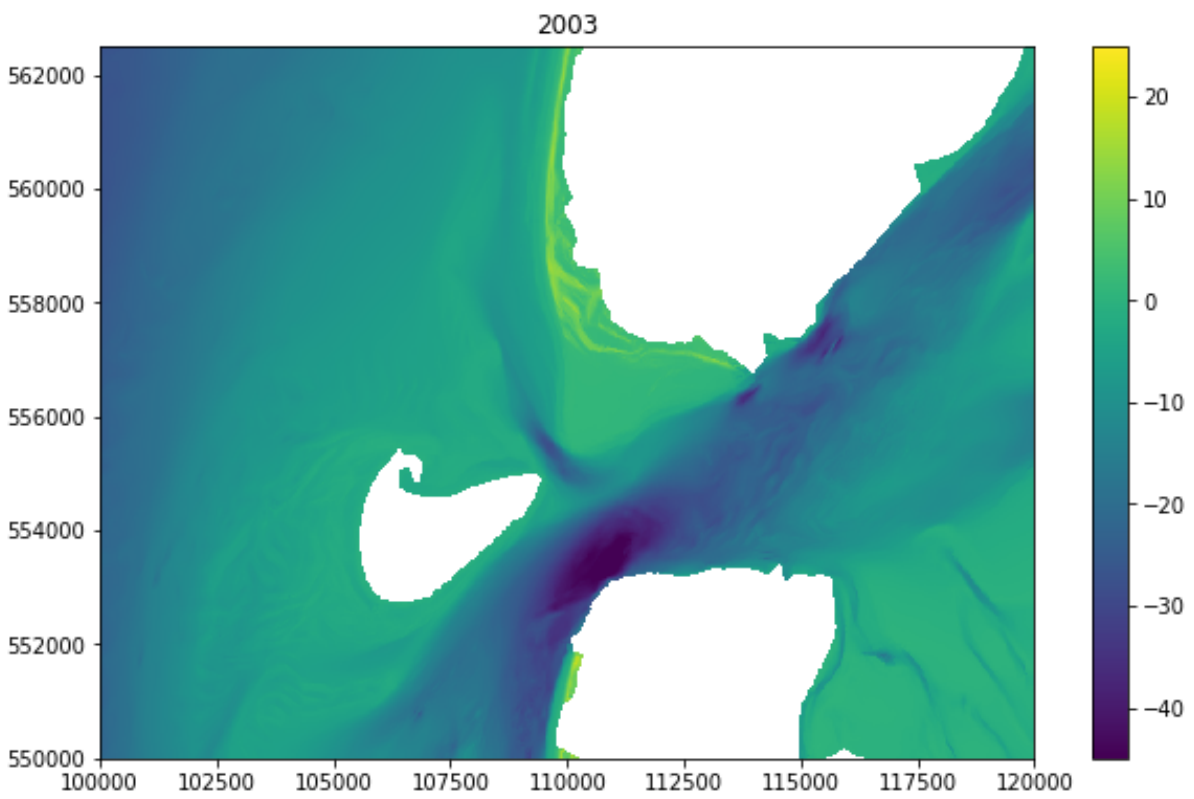


Figure B.8

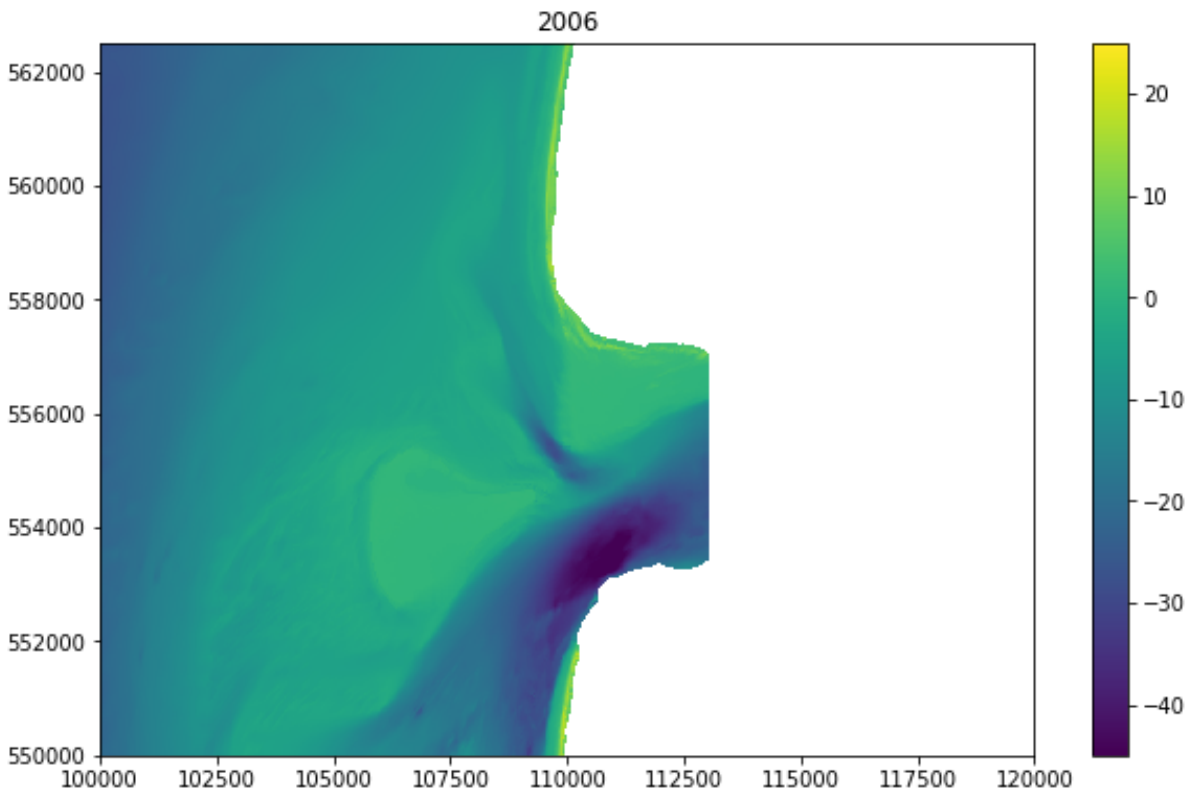


Figure B.9

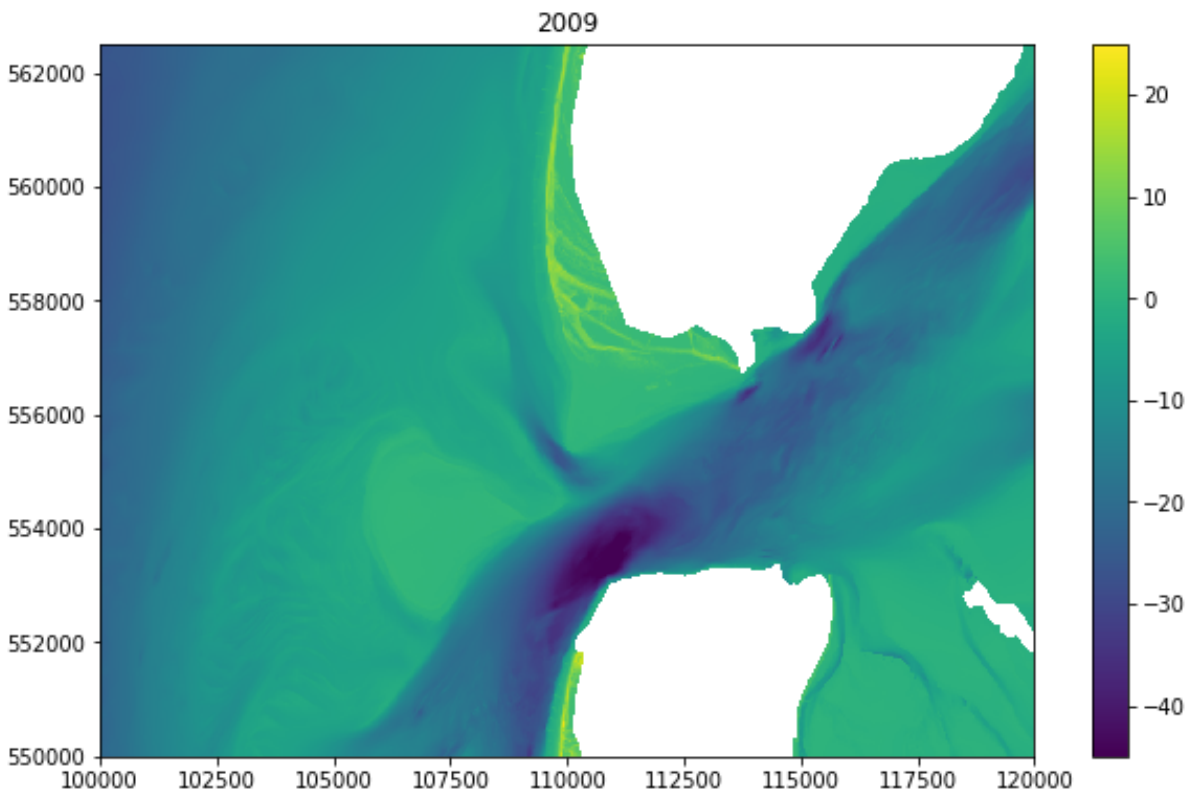


Figure B.10

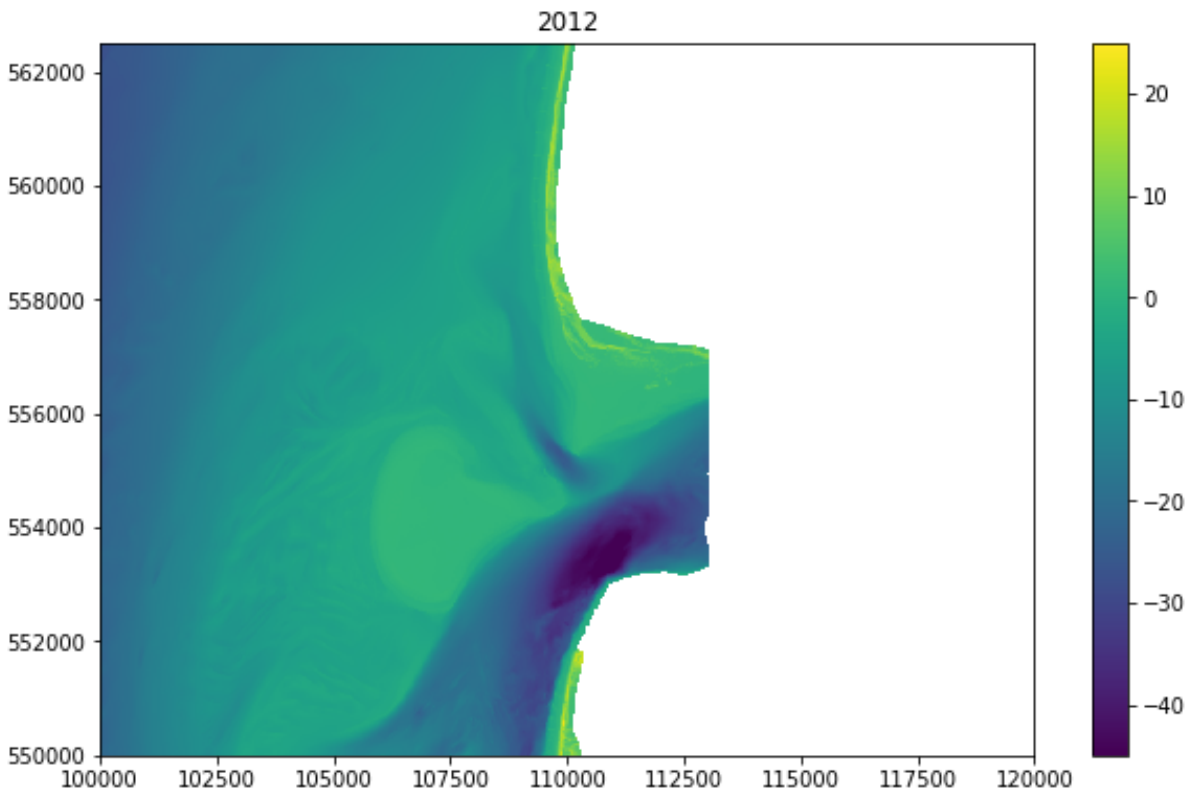


Figure B.11

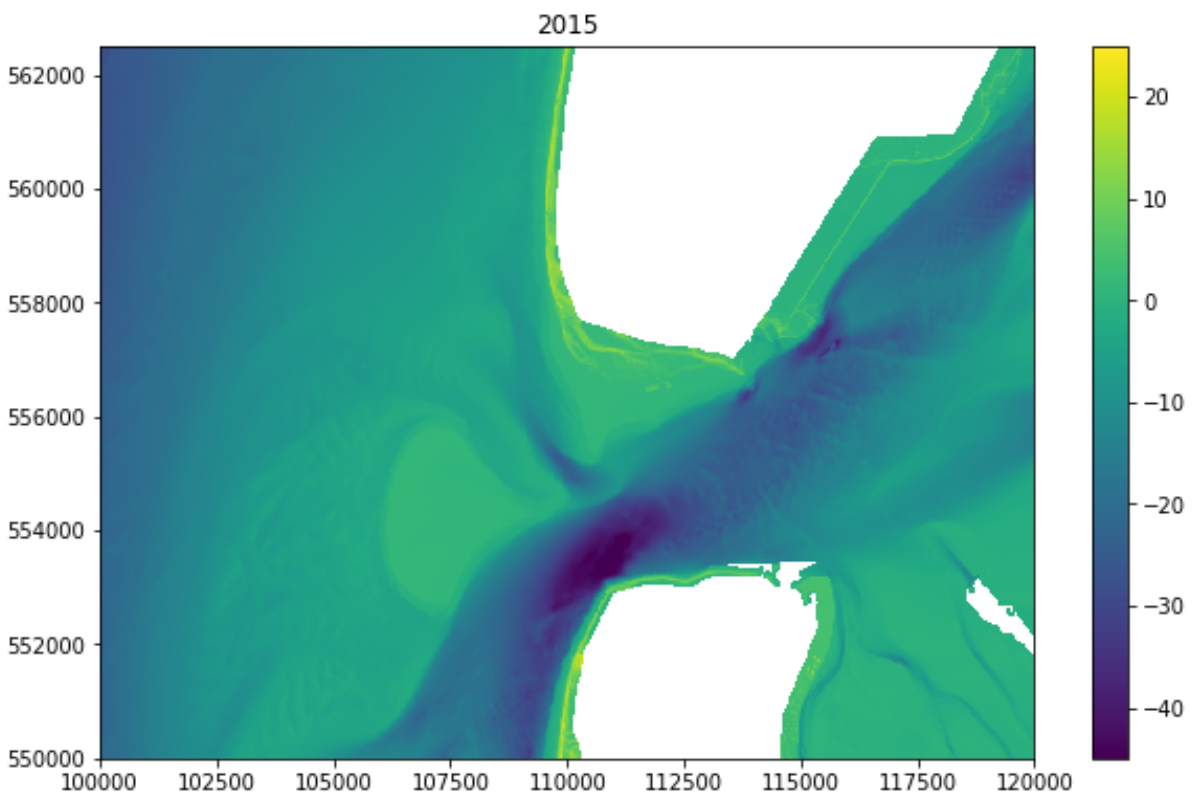


Figure B.12

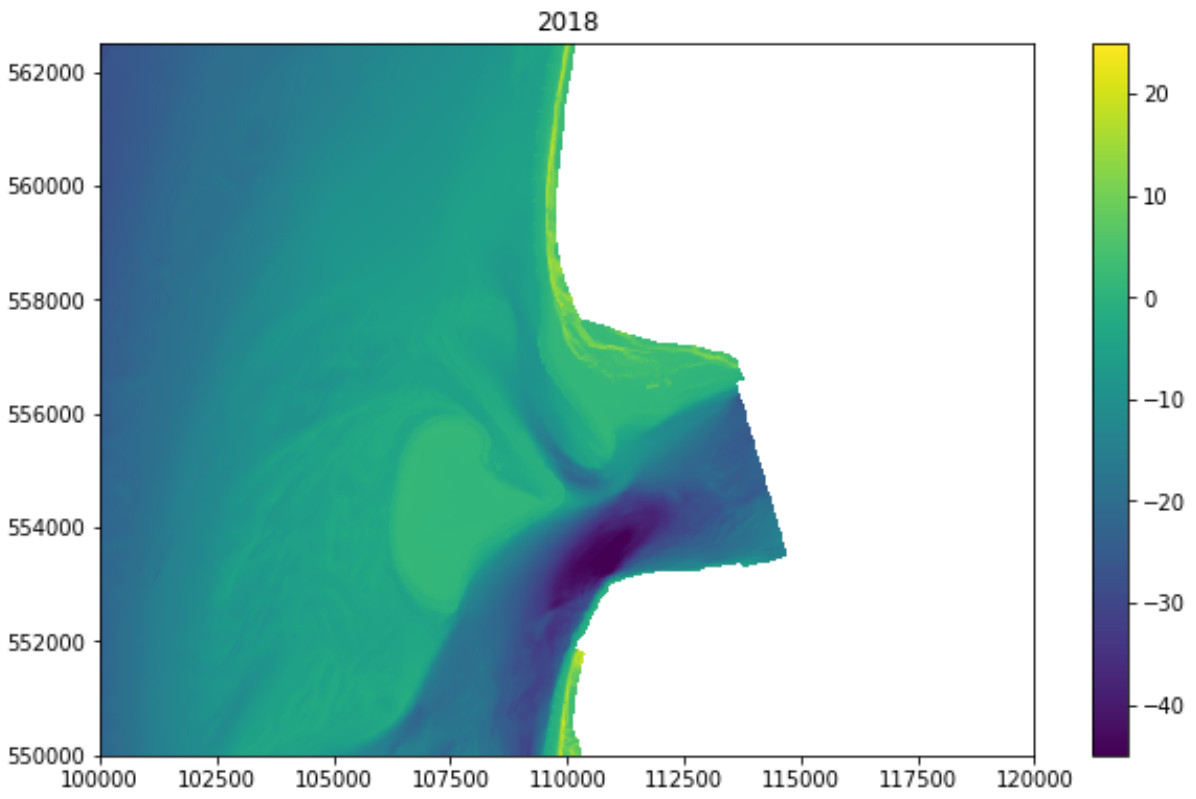


Figure B.13

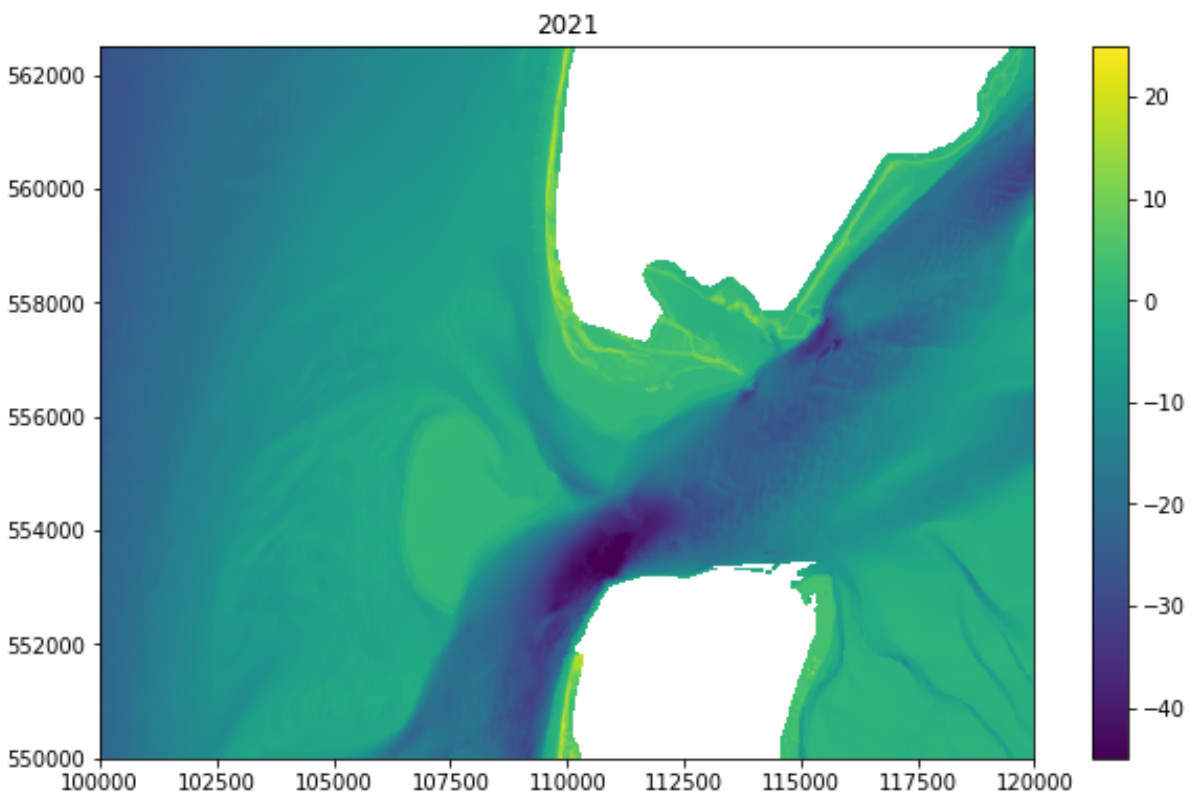


Figure B.14

C Transects of depth profiles along coast (JARKUS)

C.1 Post-1990 transects

Entire JARKUS dataset at all transects that contain post-1990 data. The oldest measurement (1990) is yellow, the most recent (2022) is the dark purple line. The x-values are the distance to the RSP [m], and the y-values the level relative to NAP [m]. The color change indicates progression through time. Figure C.21 and onward shows the transect zoomed on the dune. These are used in Figure 4.15.

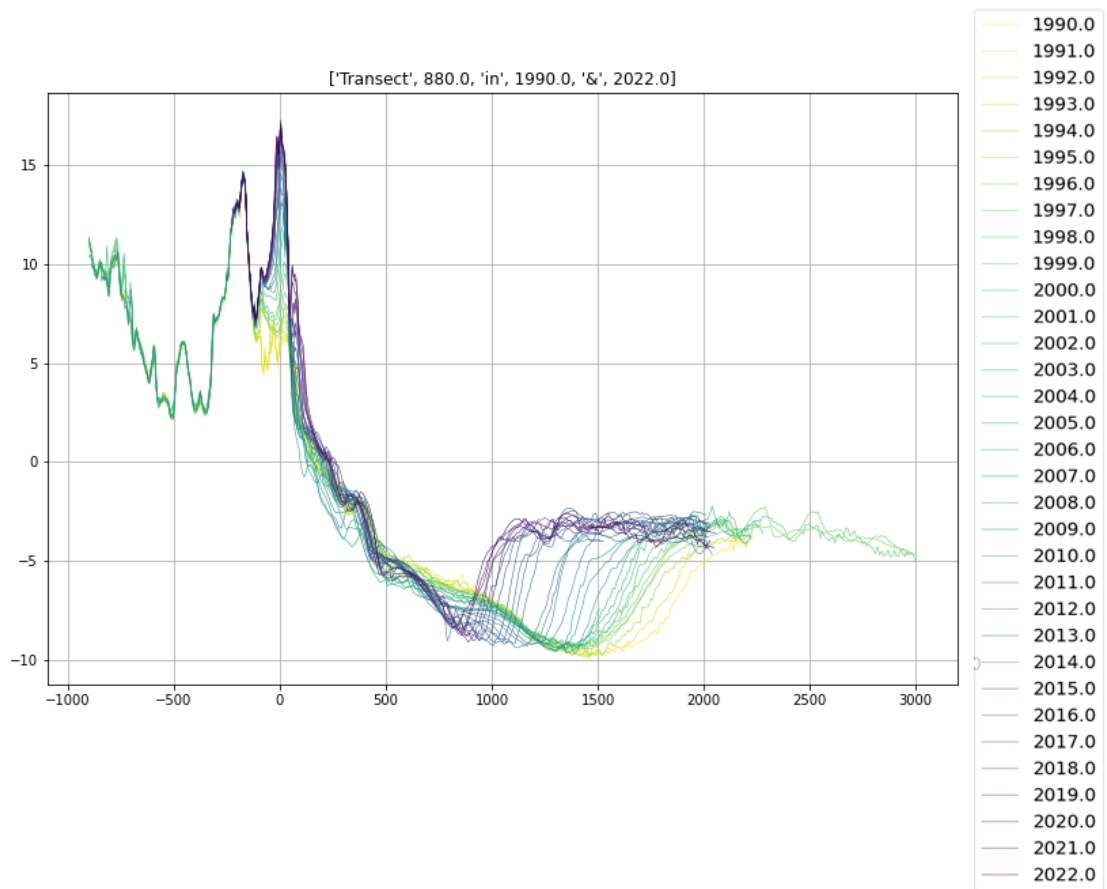


Figure C.1

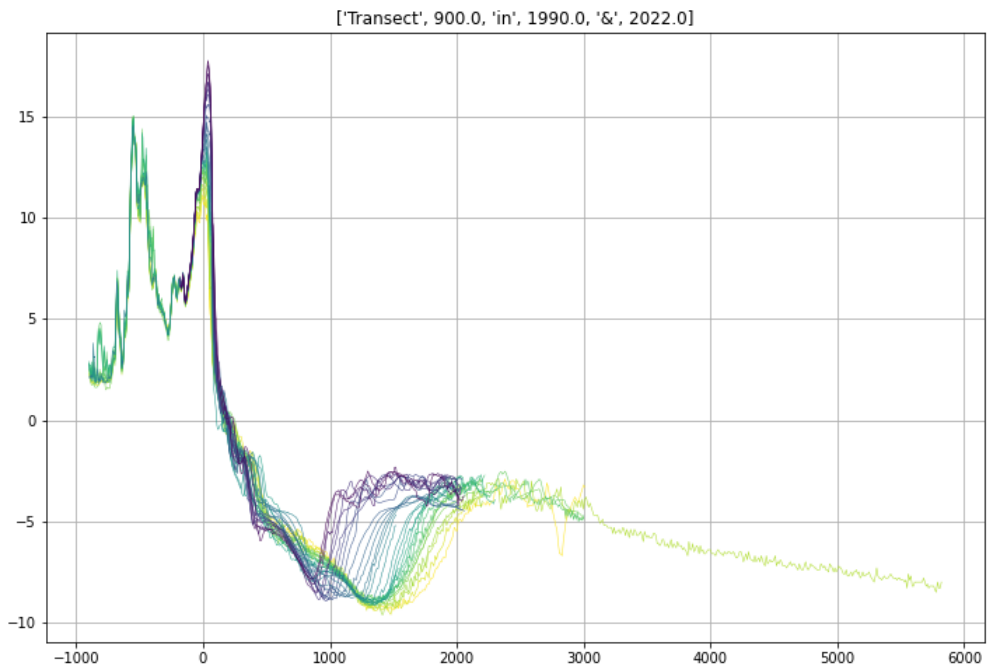


Figure C.2

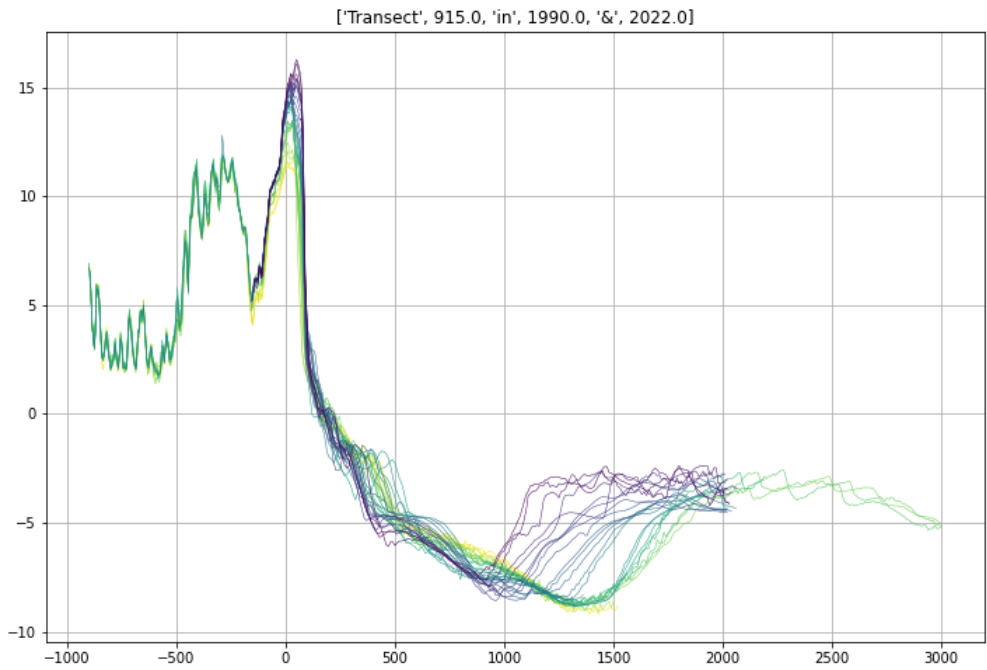


Figure C.3

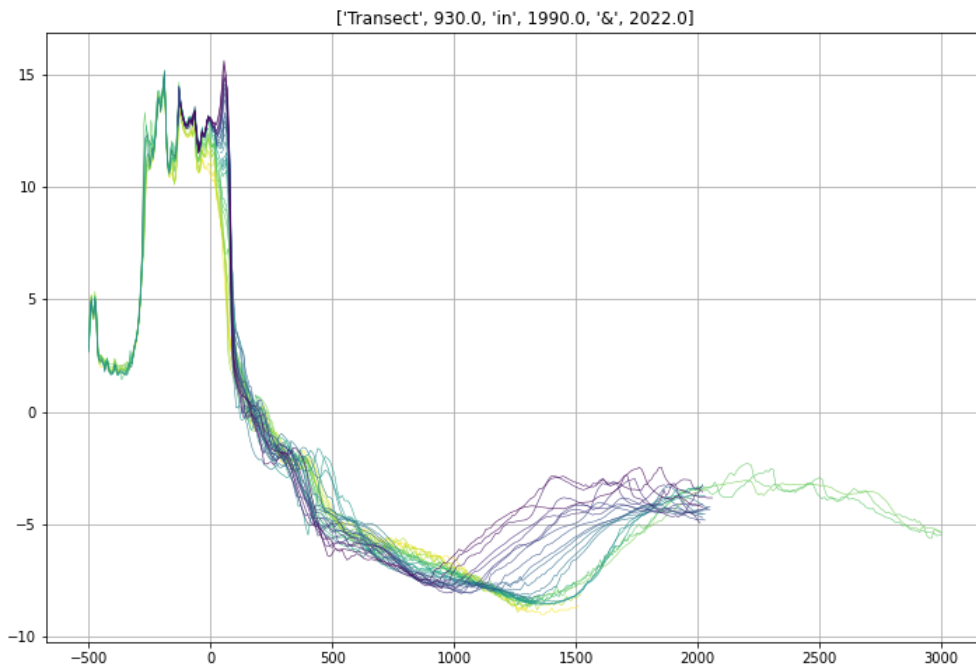


Figure C.4

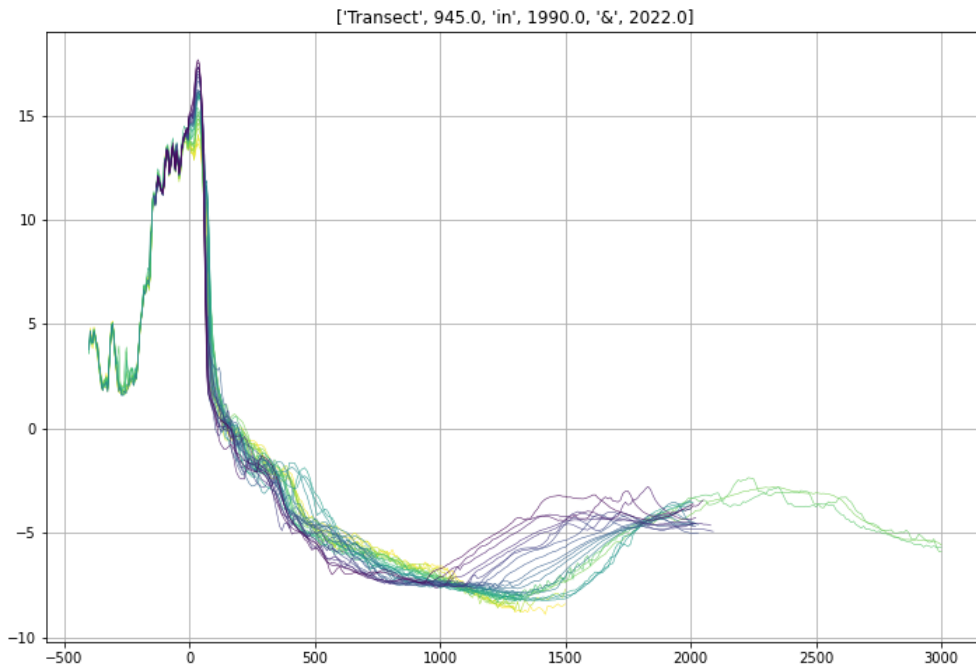


Figure C.5

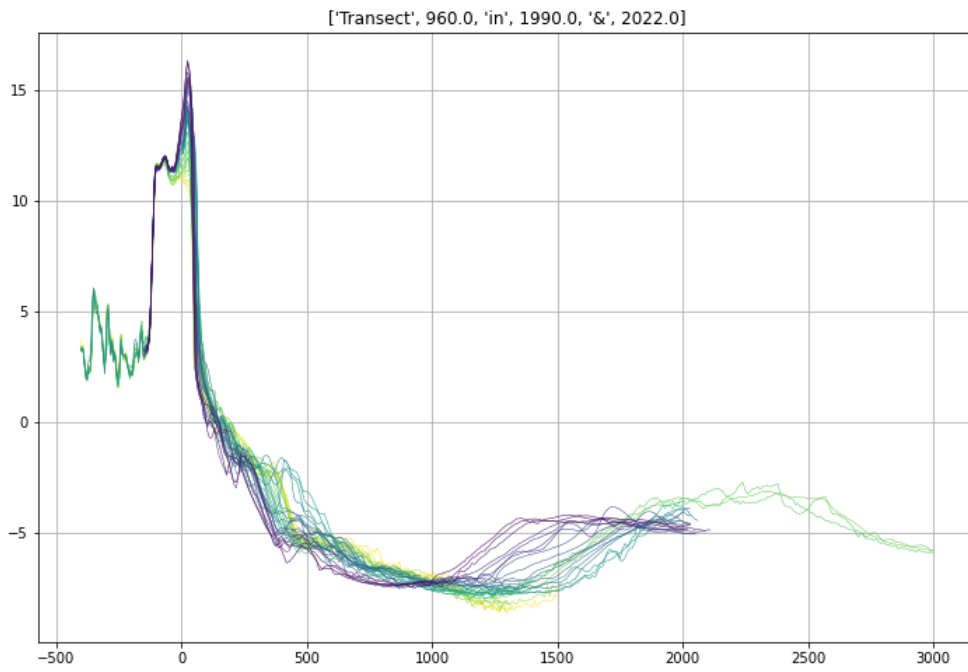


Figure C.6

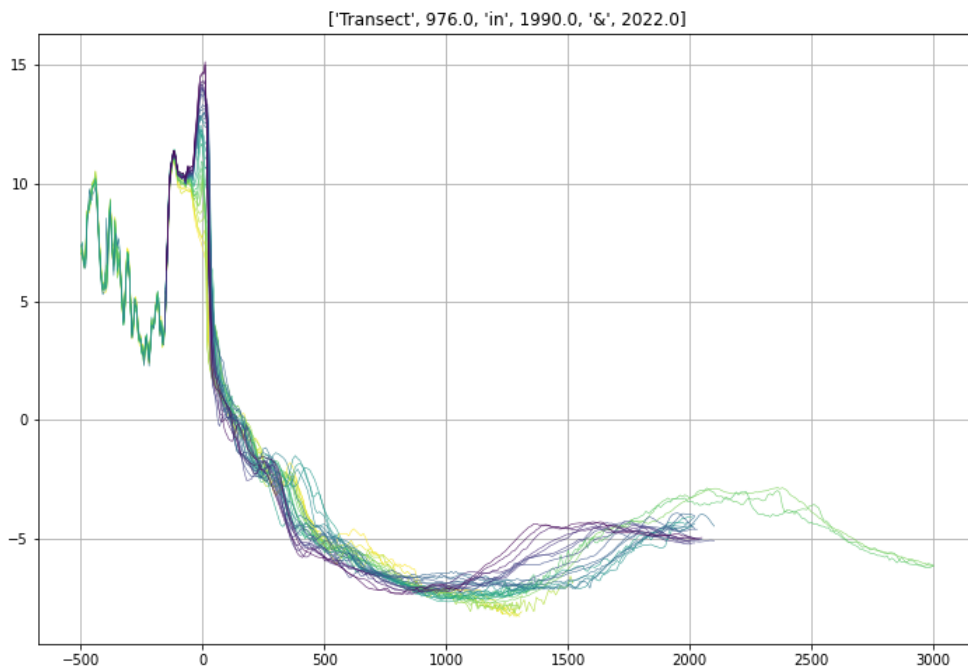


Figure C.7

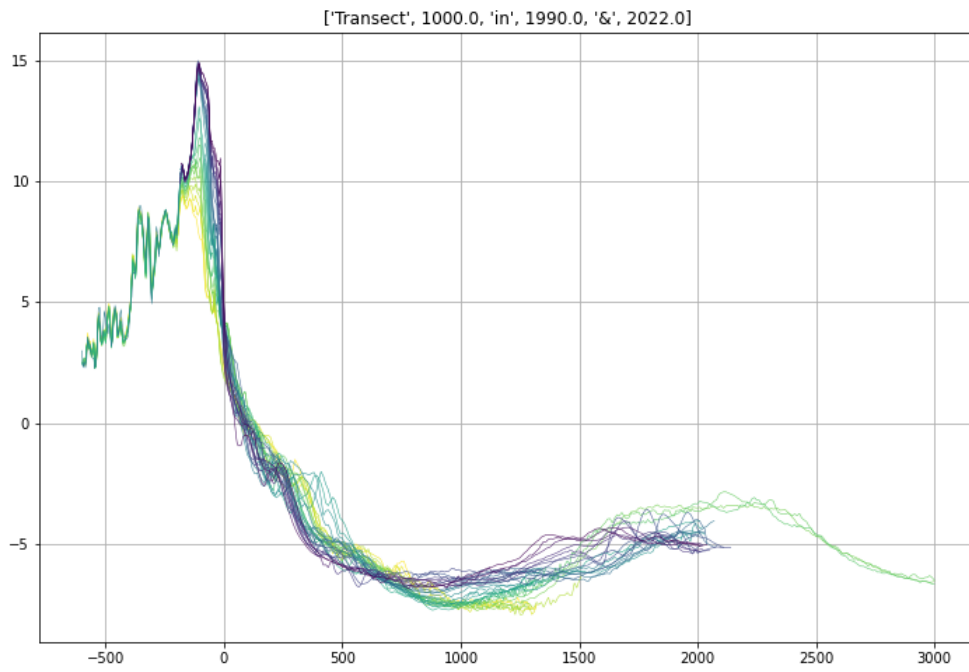


Figure C.8

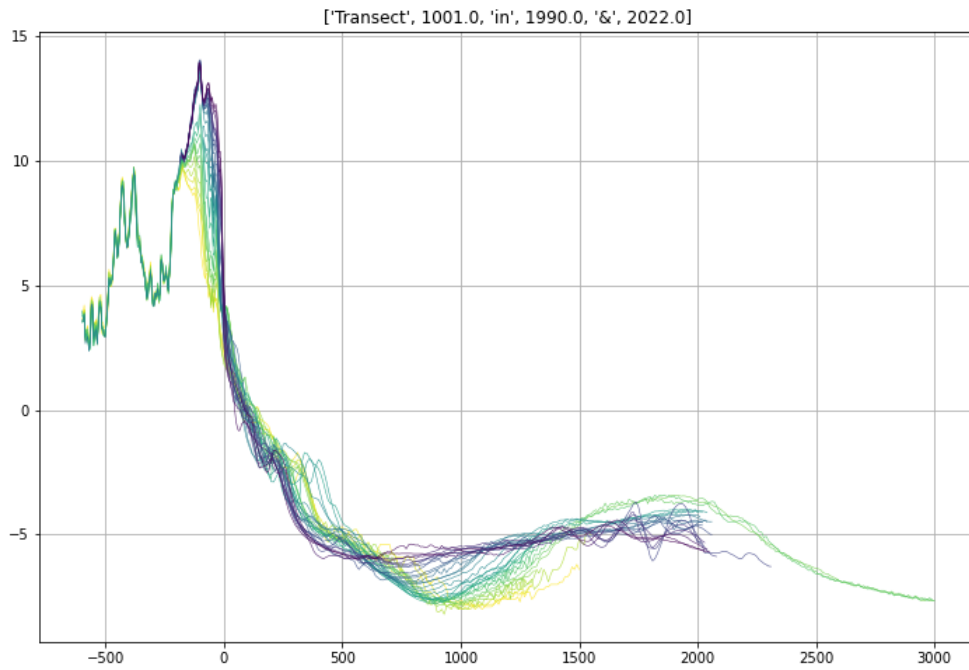


Figure C.9

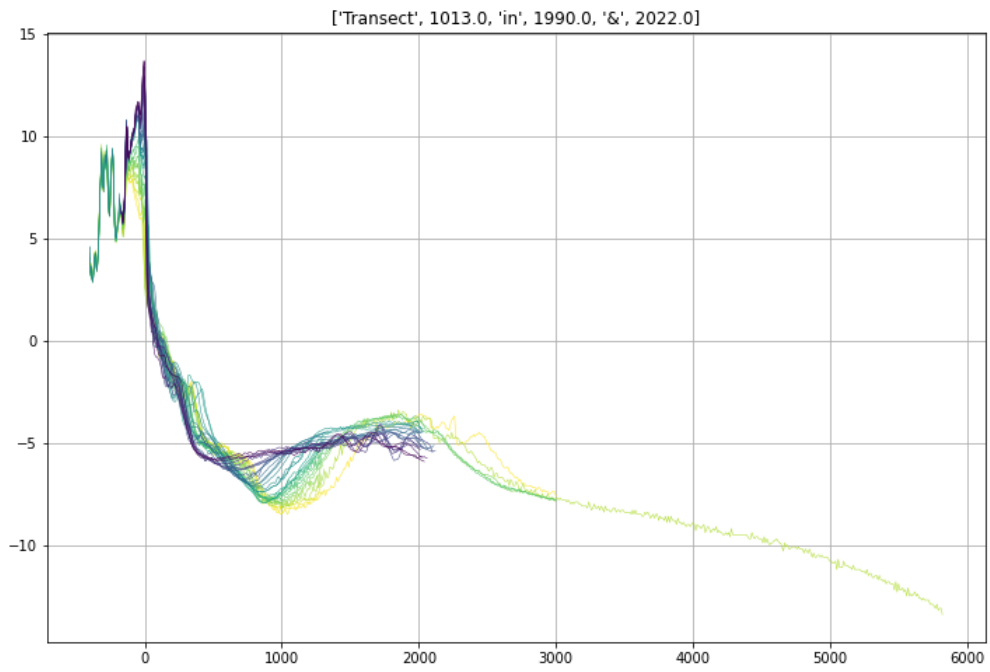


Figure C.10

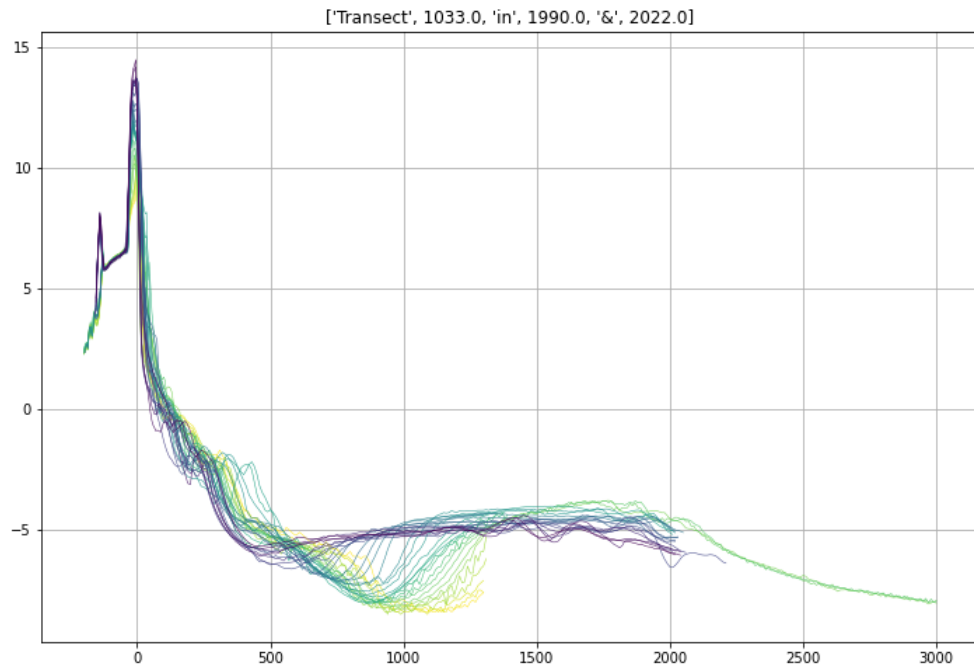


Figure C.11

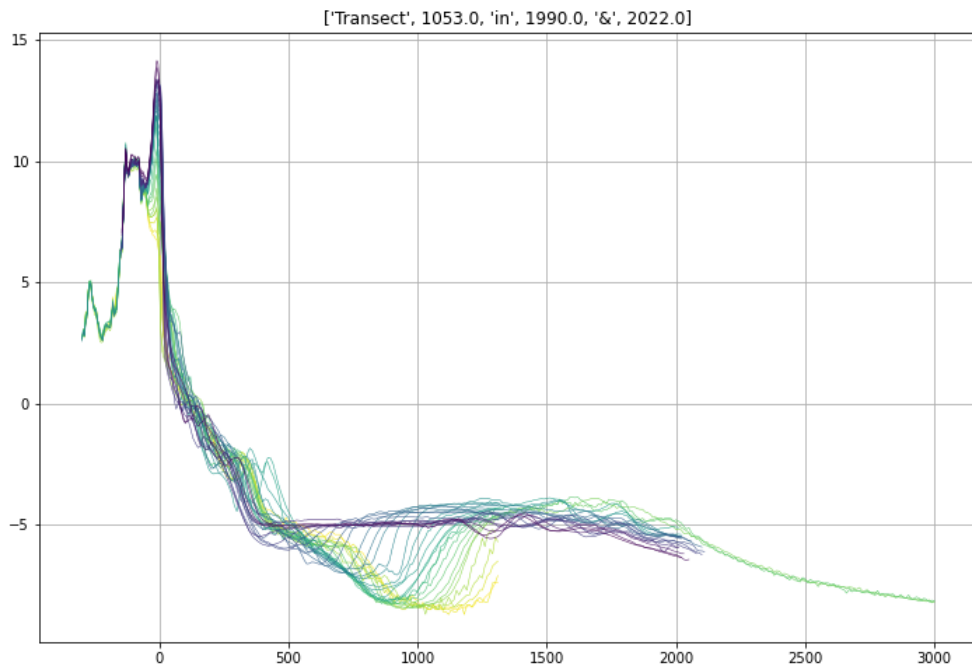


Figure C.12

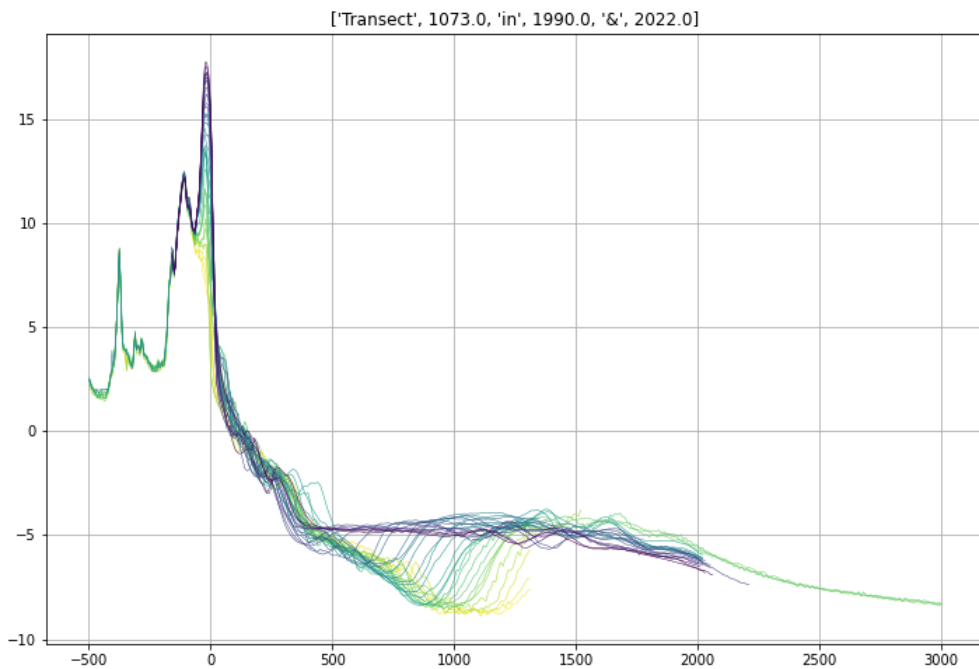


Figure C.13

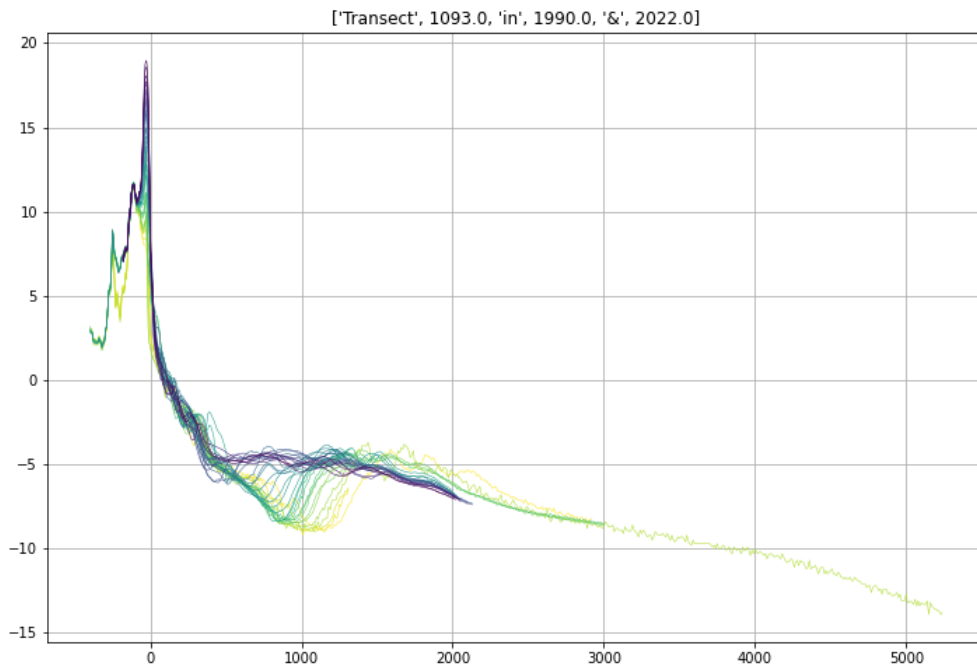


Figure C.14

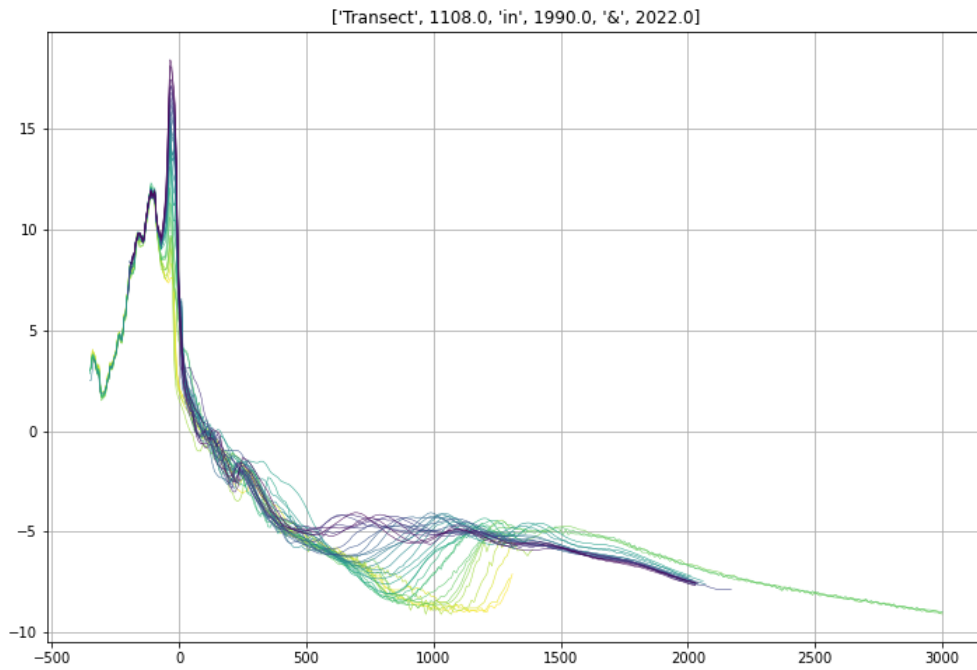


Figure C.15

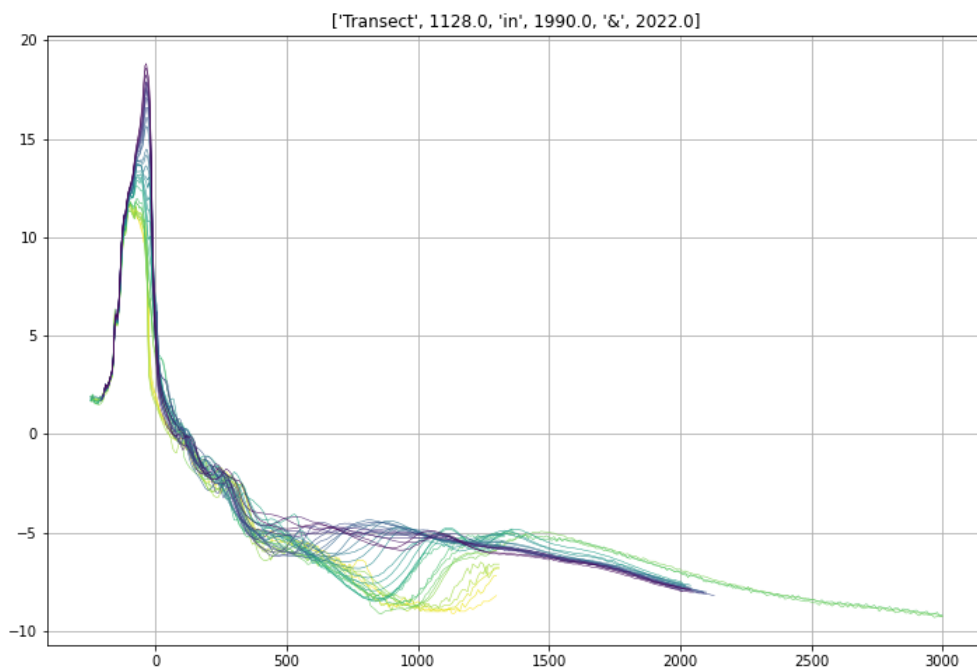


Figure C.16

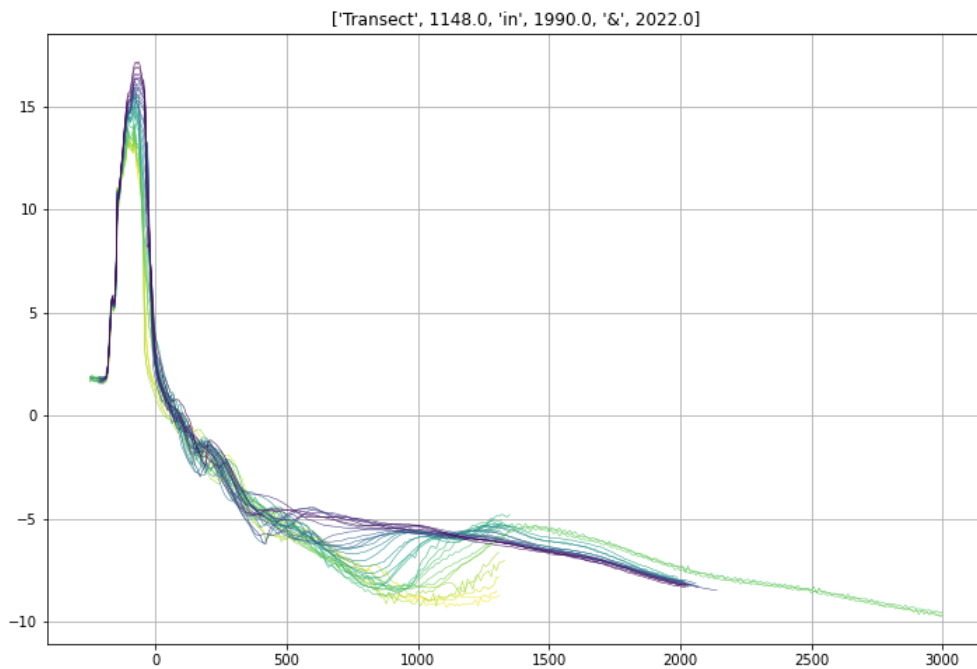


Figure C.17

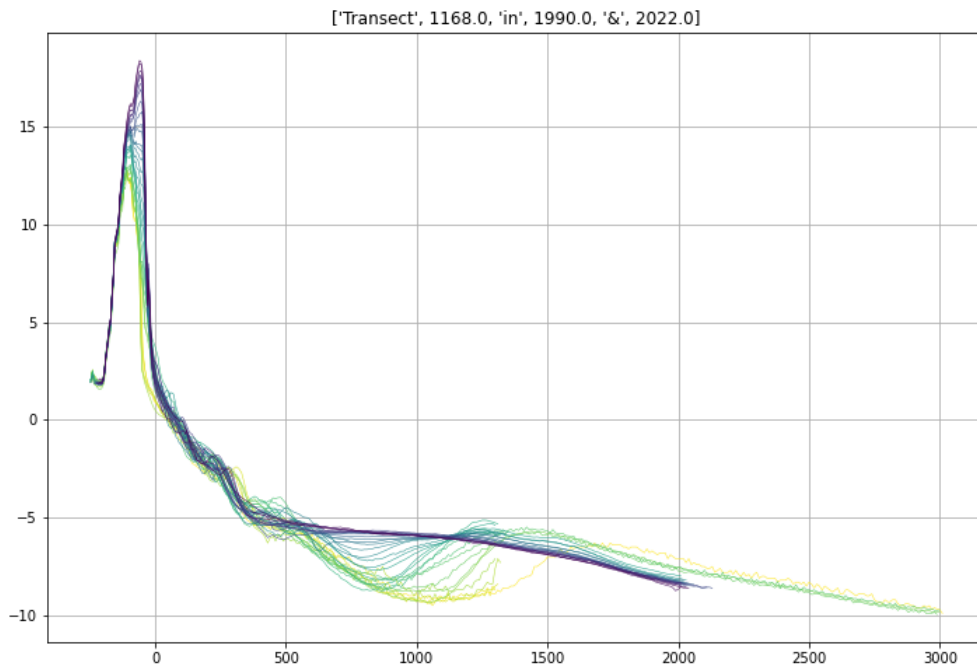


Figure C.18

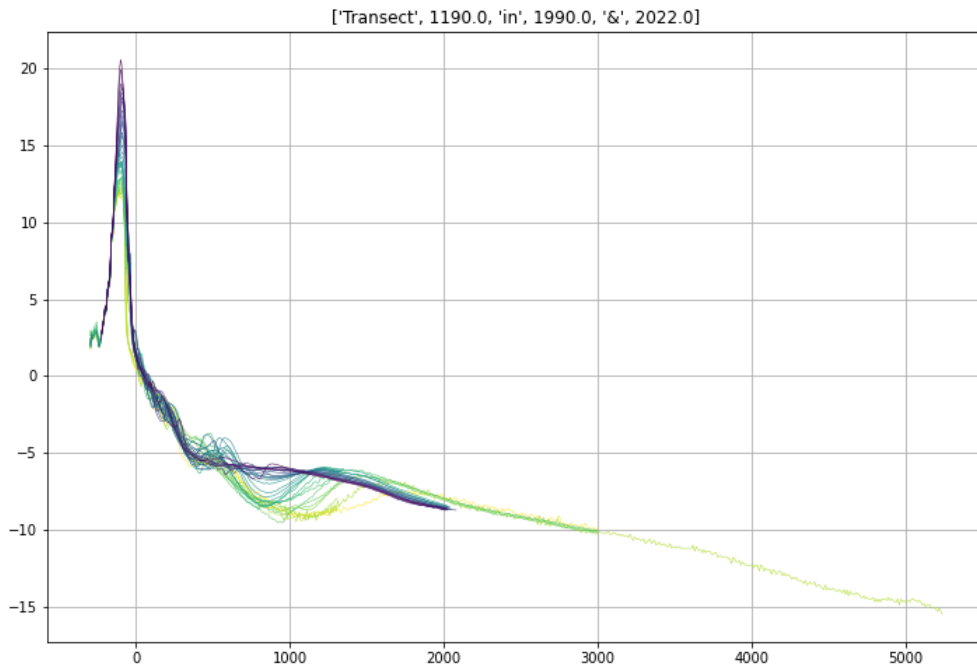


Figure C.19

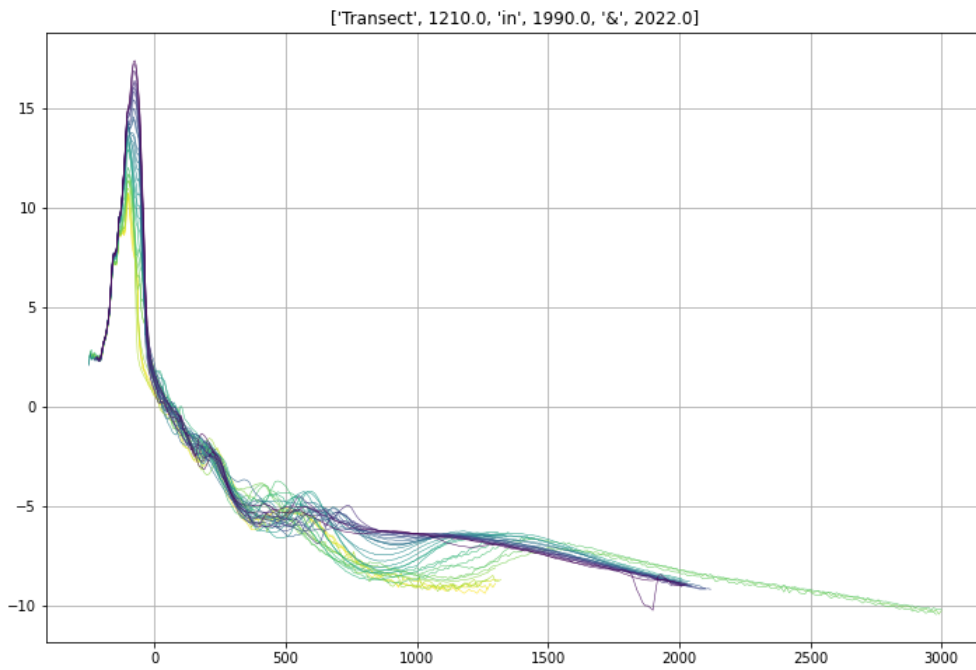


Figure C.20

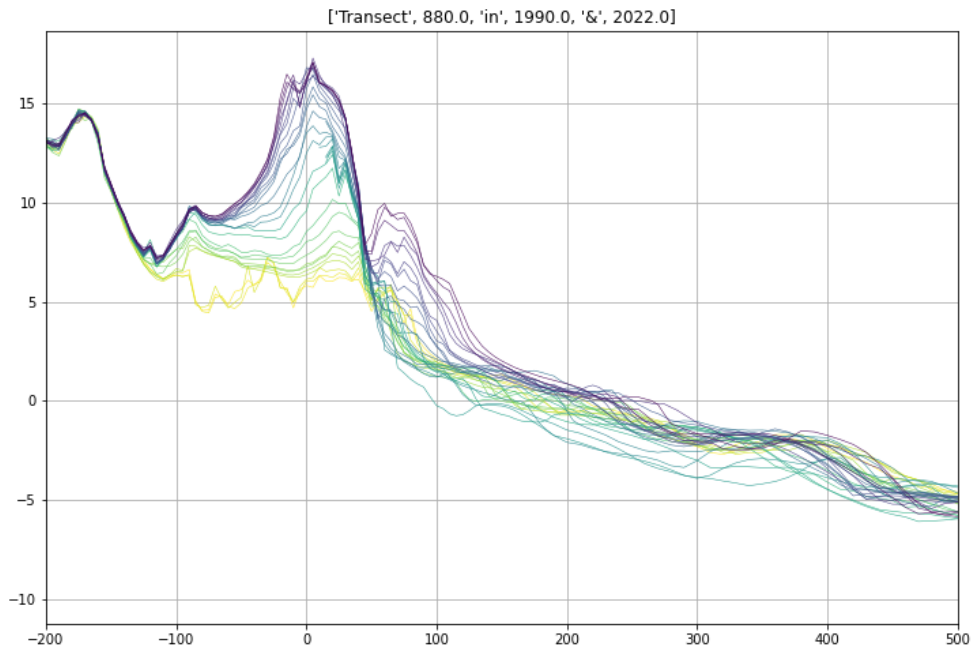


Figure C.21: All JARKUS measurements in transect 880, but zoomed to the dune, beach and the edge of the fore-shore.

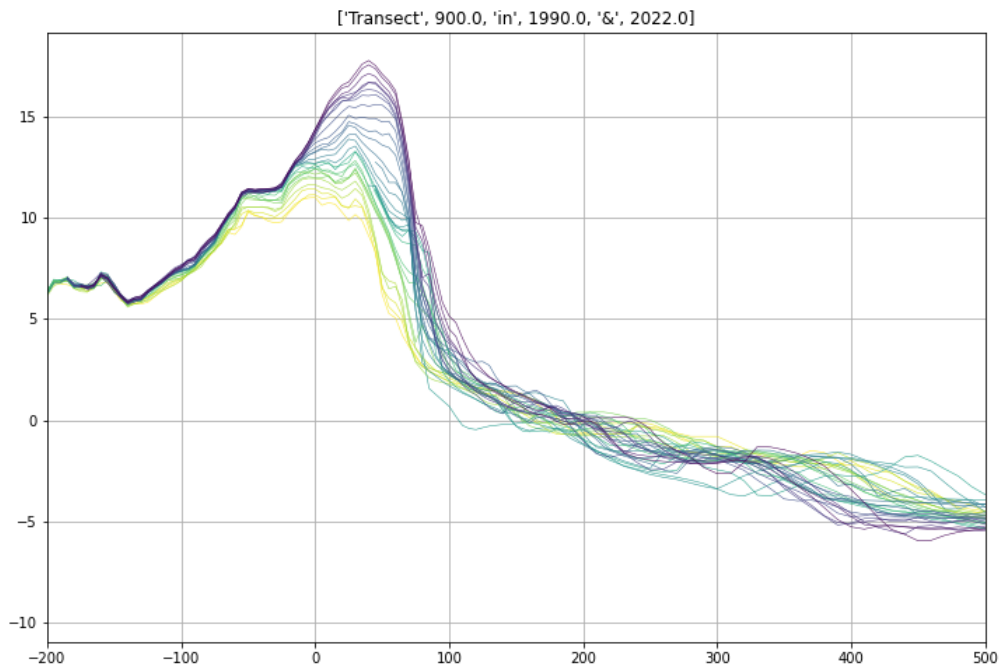


Figure C.22

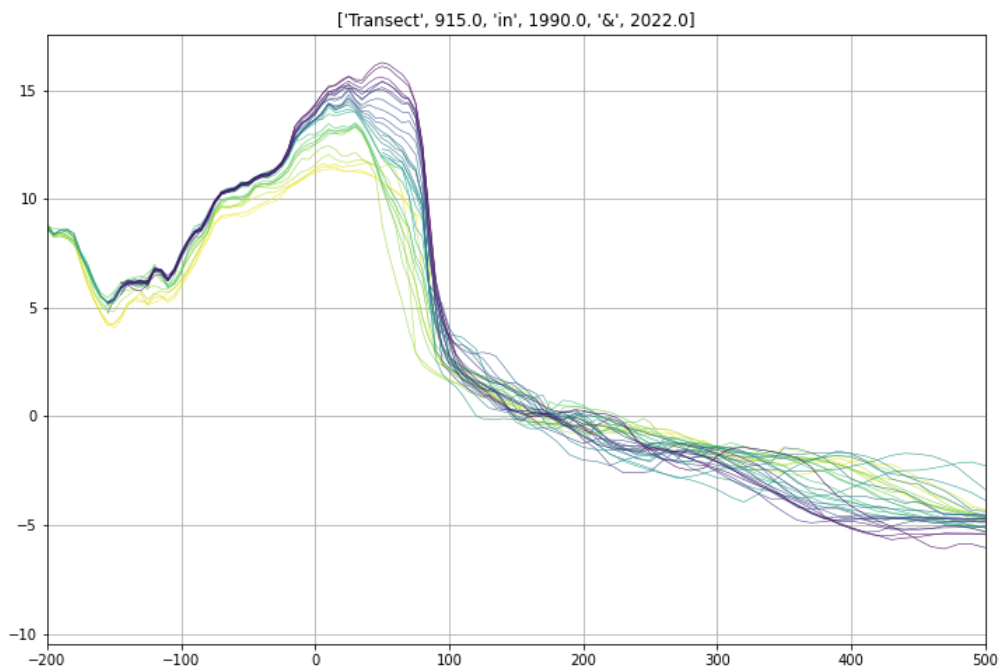


Figure C.23

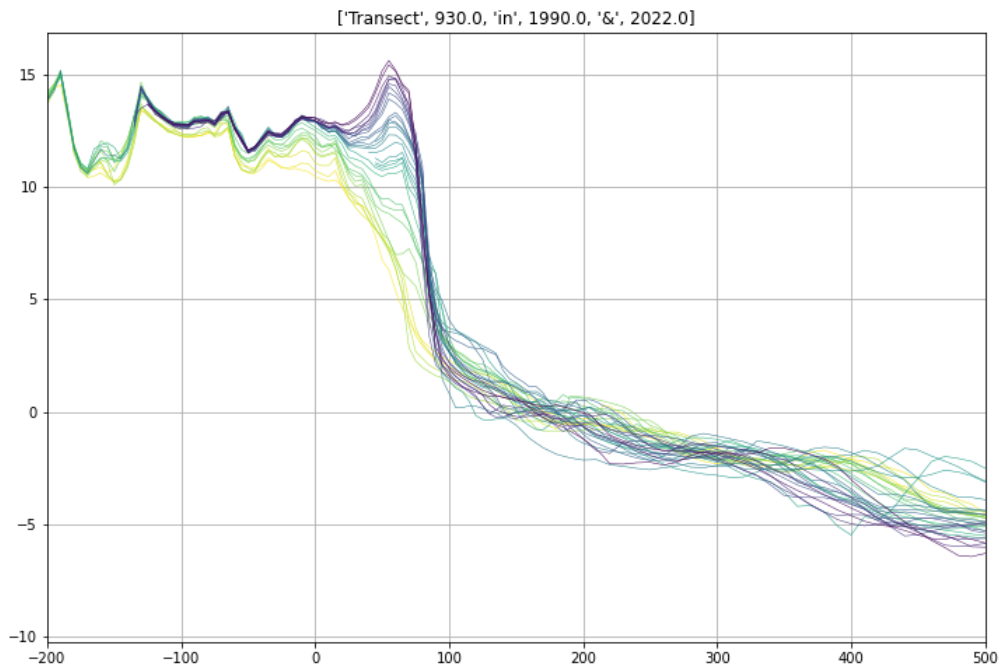


Figure C.24

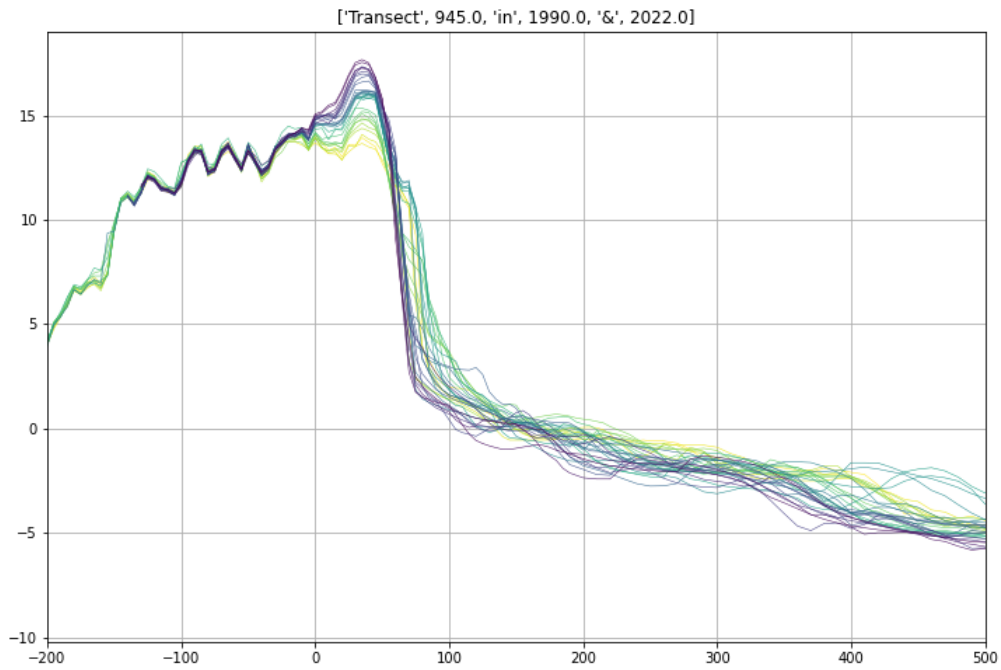


Figure C.25

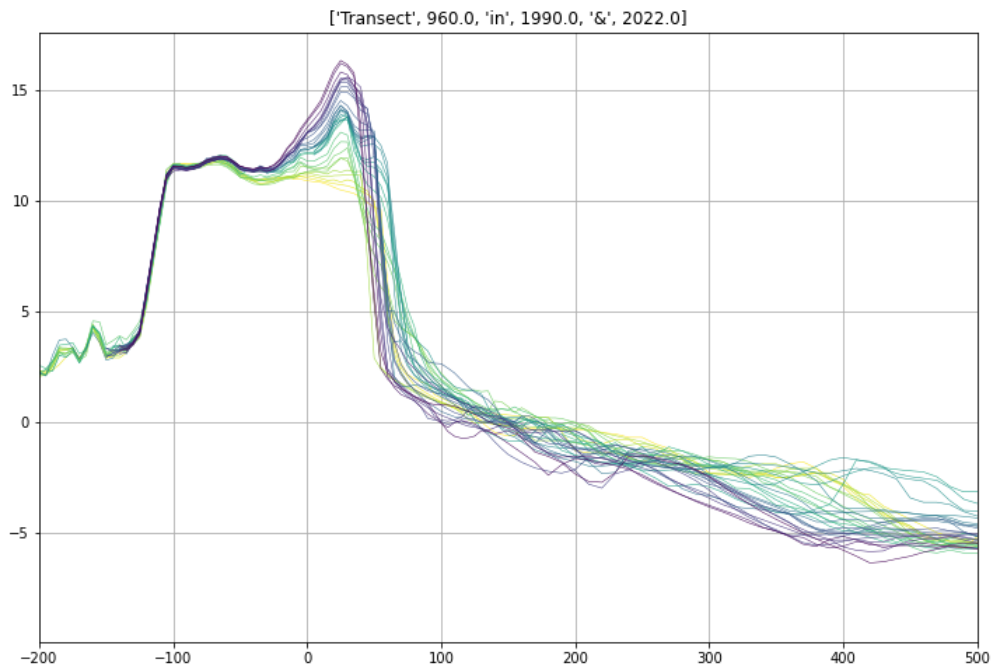


Figure C.26

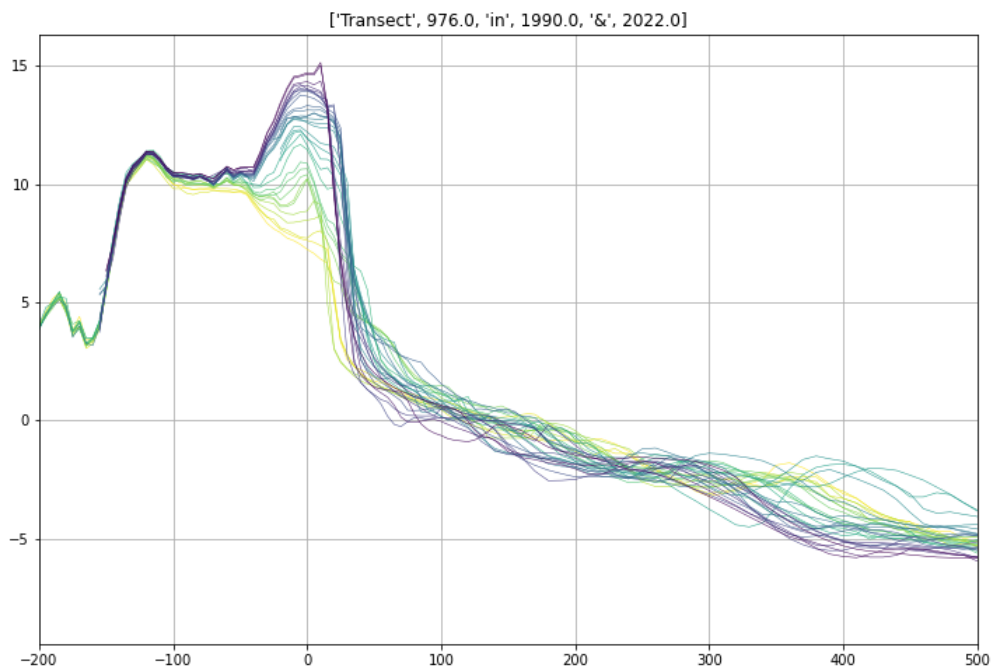


Figure C.27

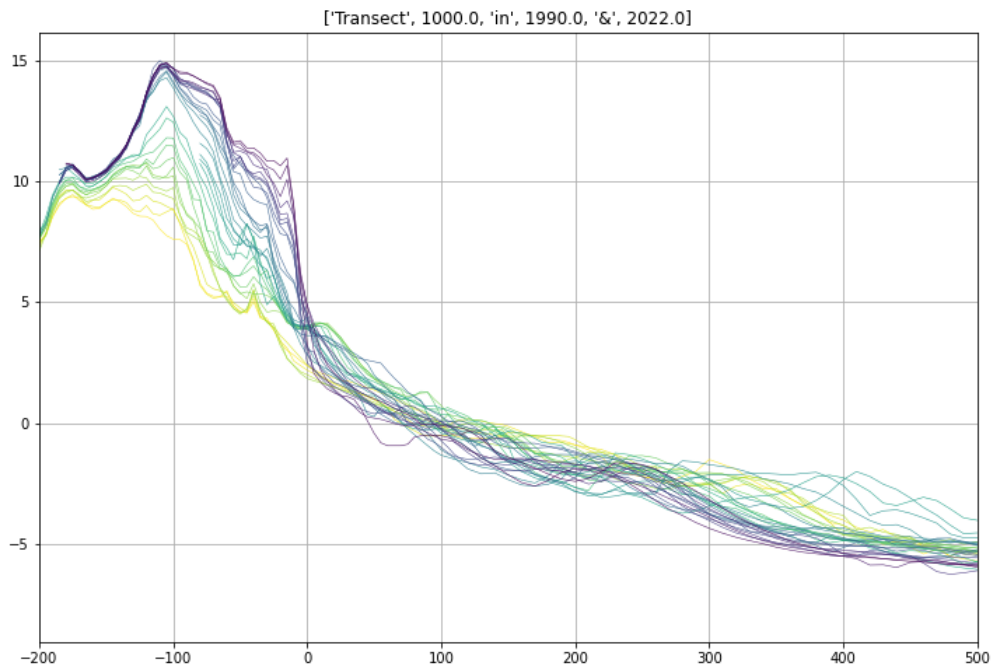


Figure C.28

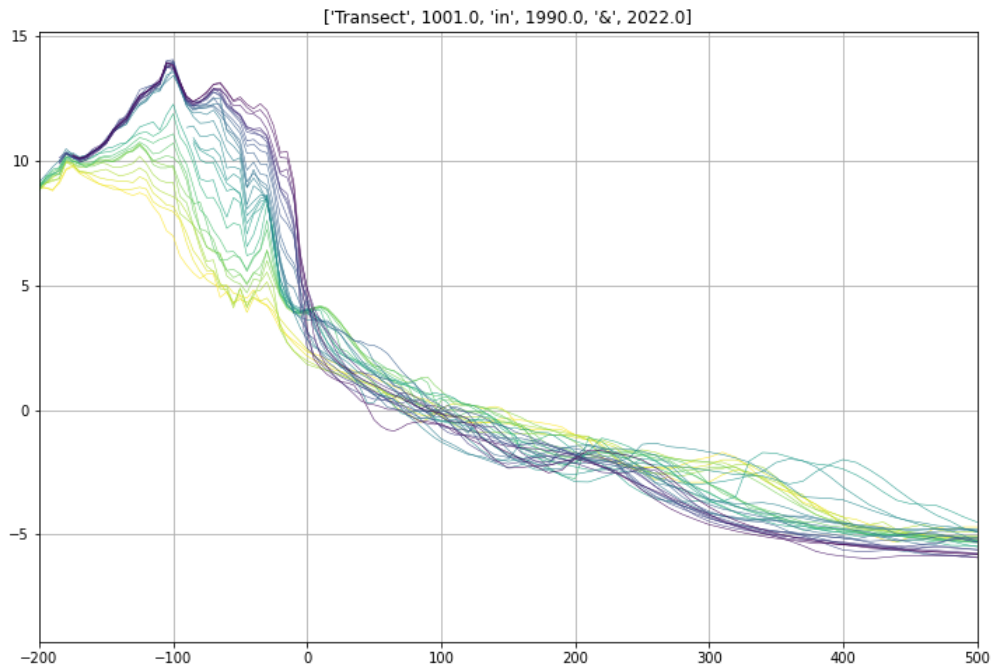


Figure C.29

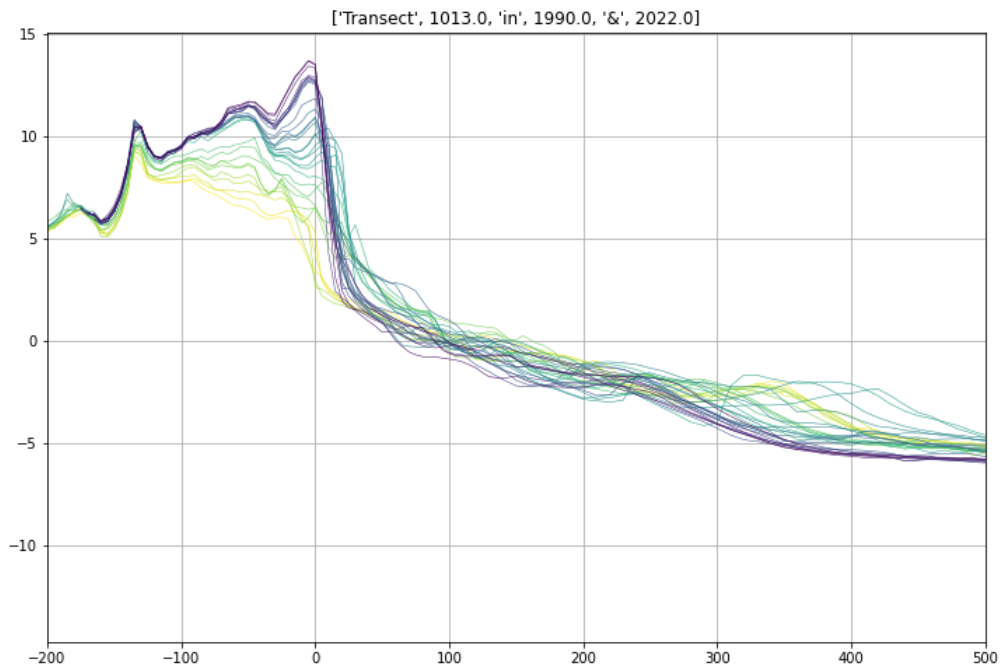


Figure C.30

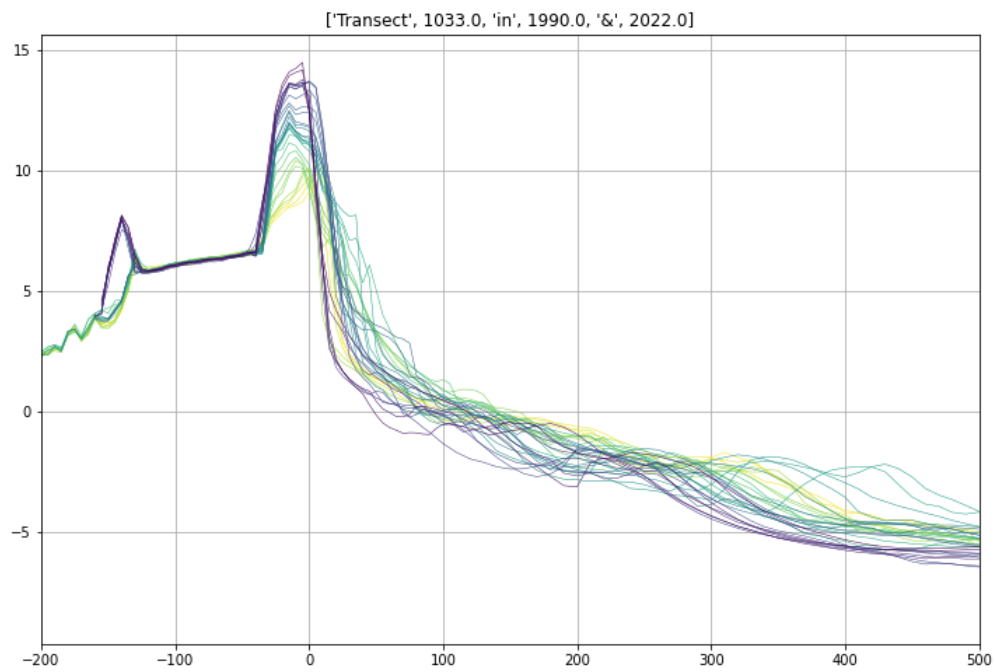


Figure C.31

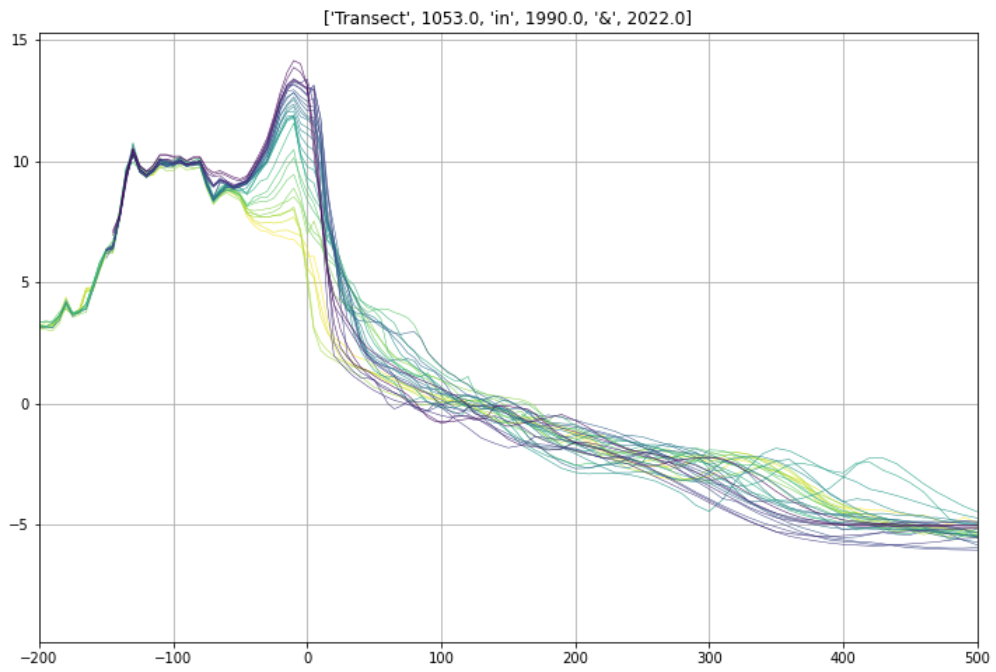


Figure C.32

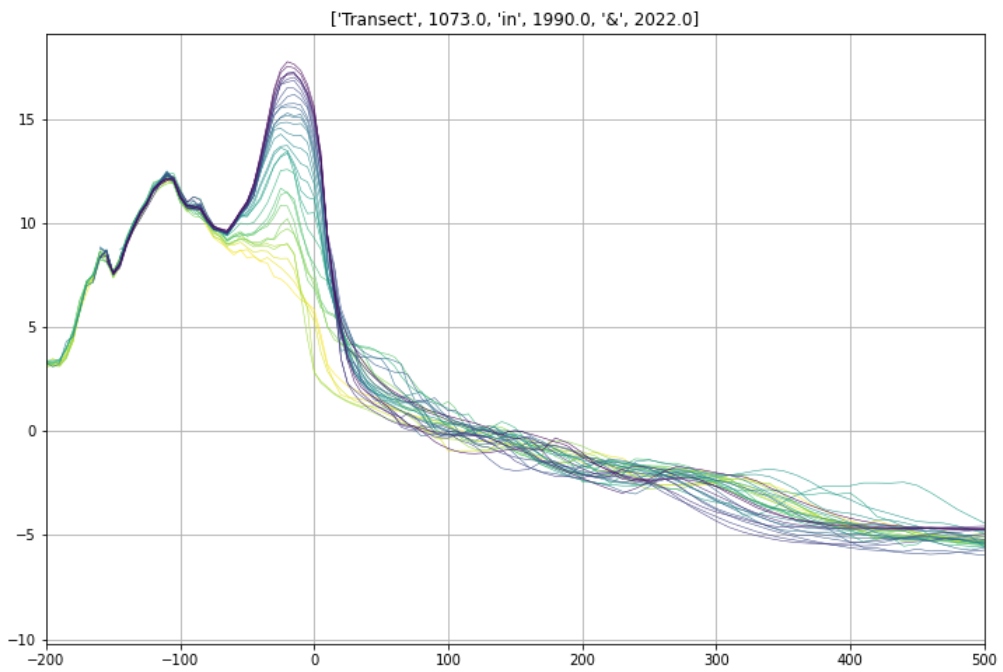


Figure C.33

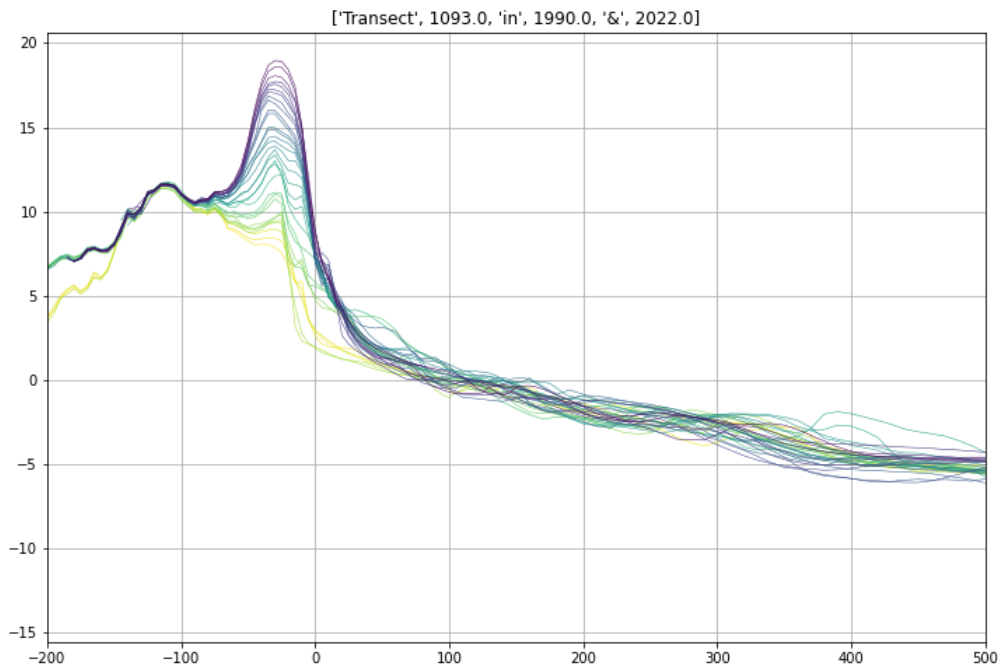


Figure C.34

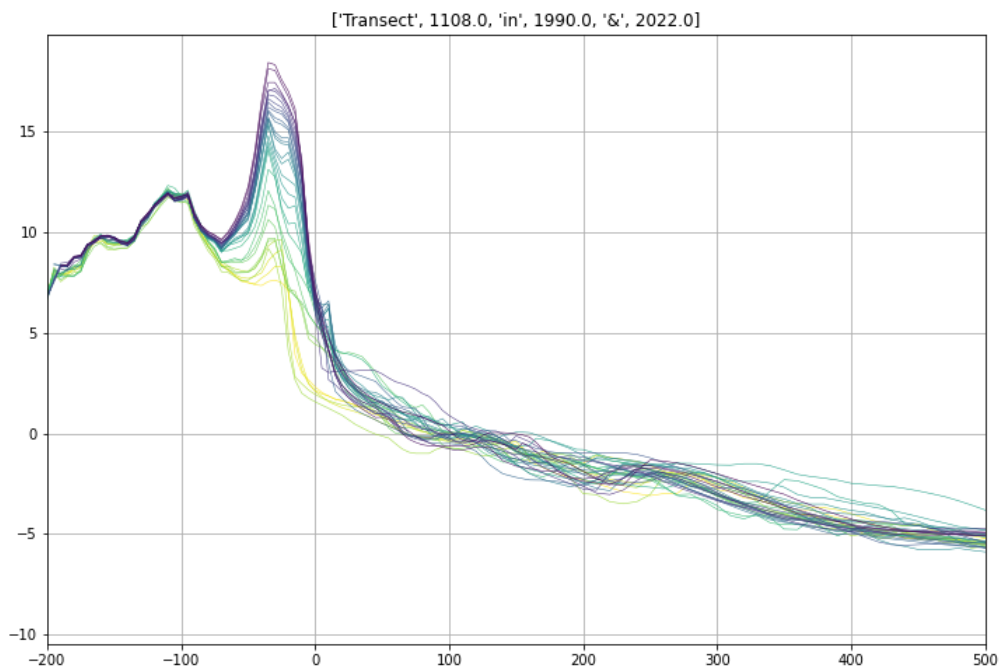


Figure C.35

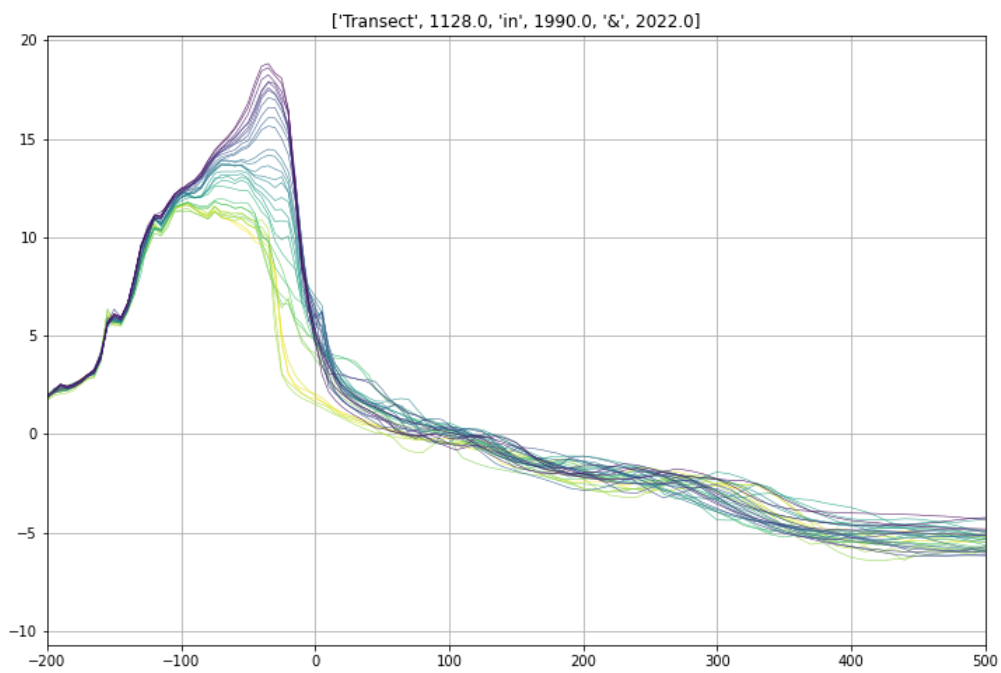


Figure C.36

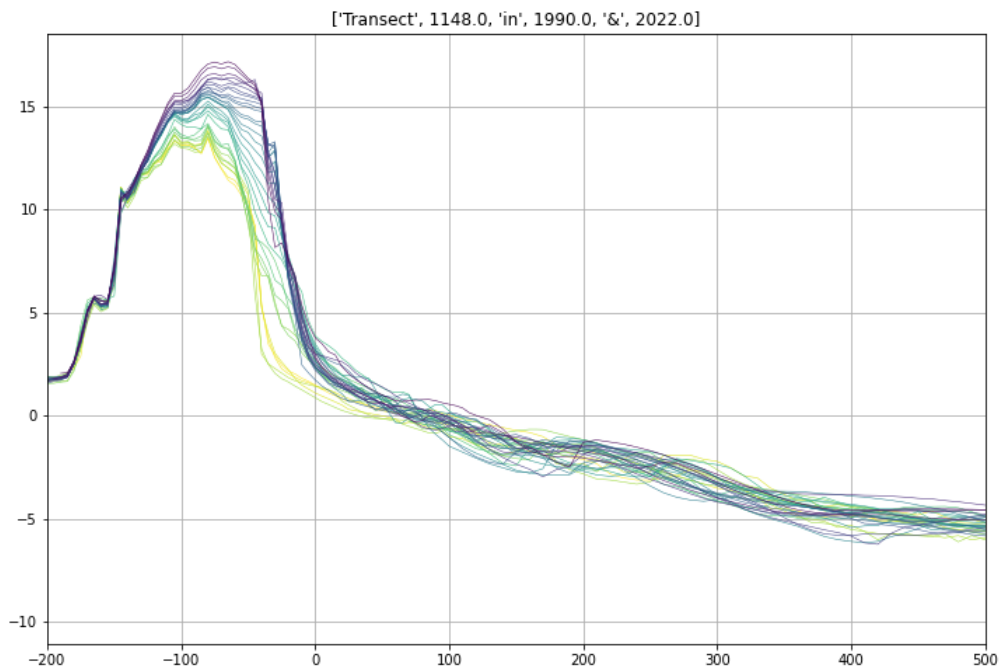


Figure C.37

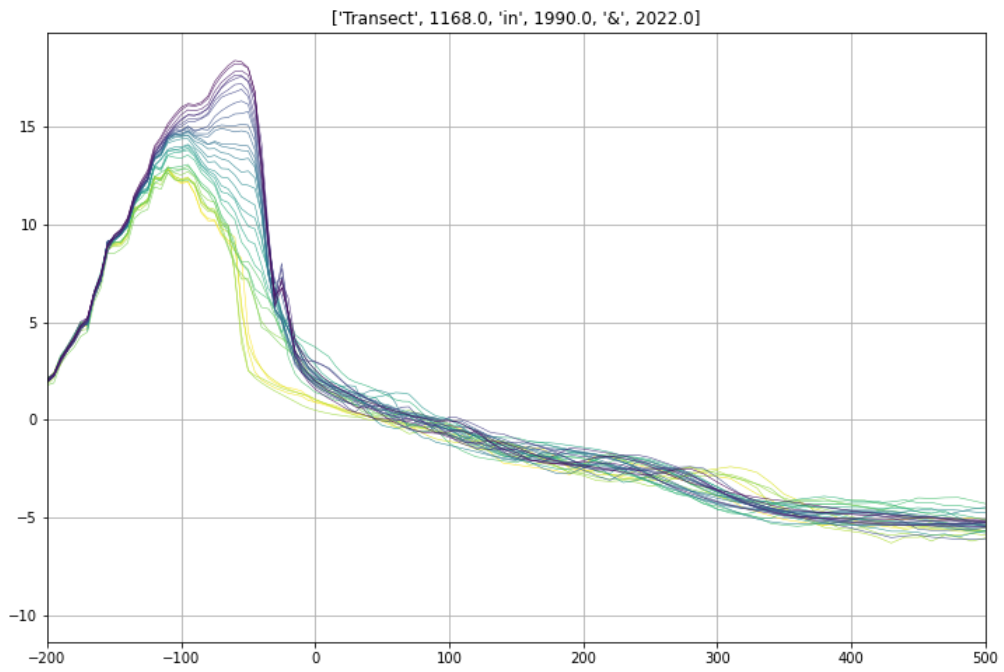


Figure C.38

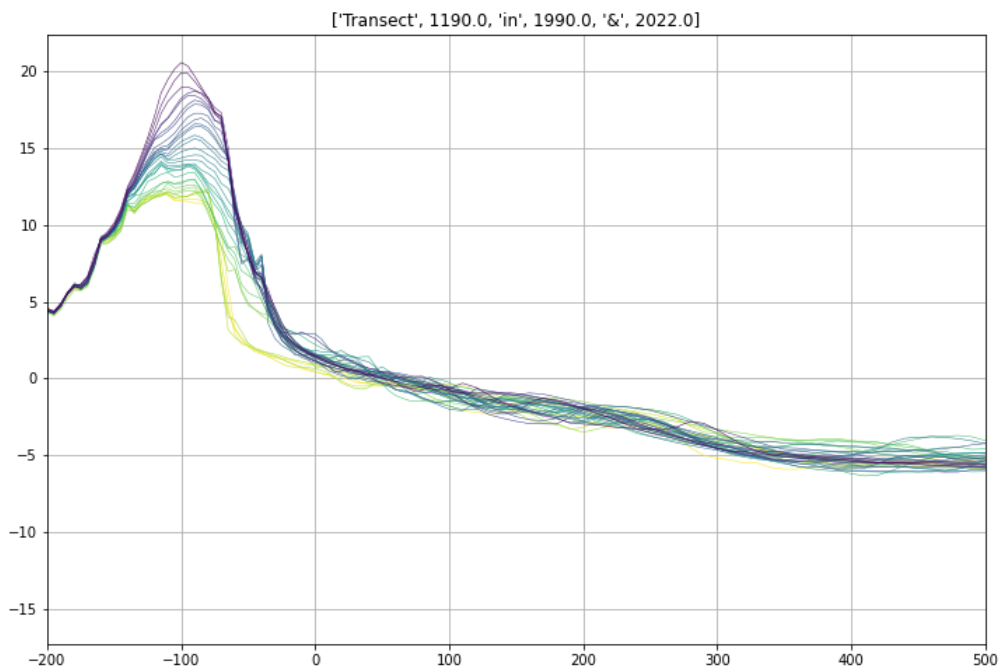


Figure C.39

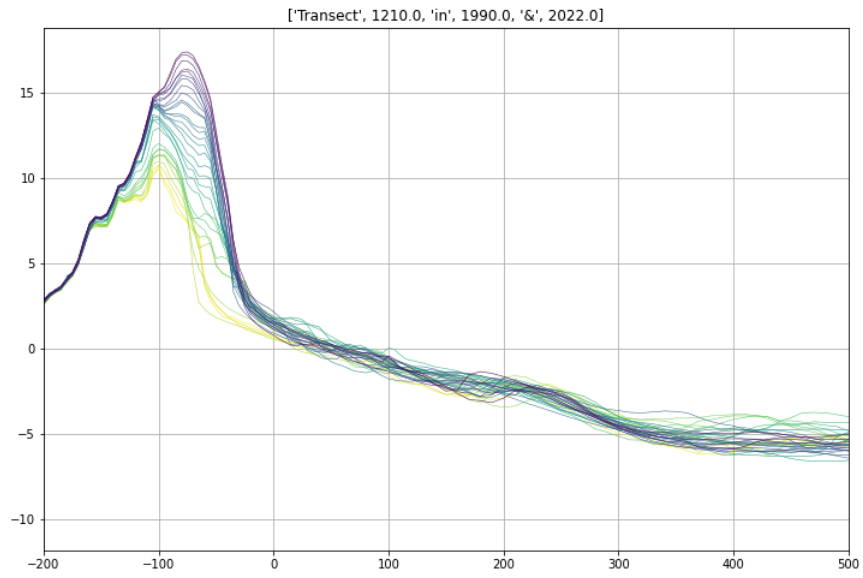


Figure C.40

C.2 Pre-1990 transects

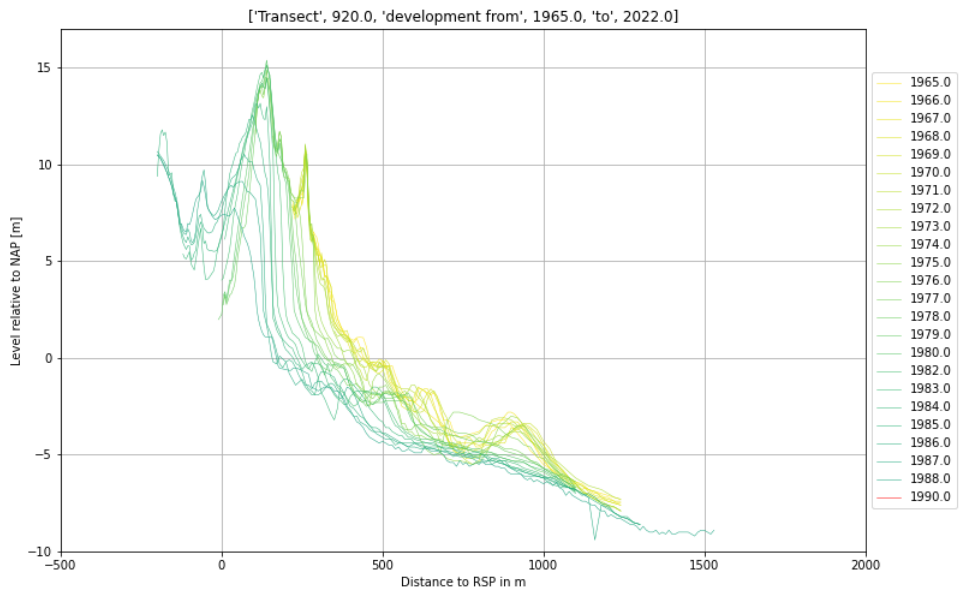


Figure C.41

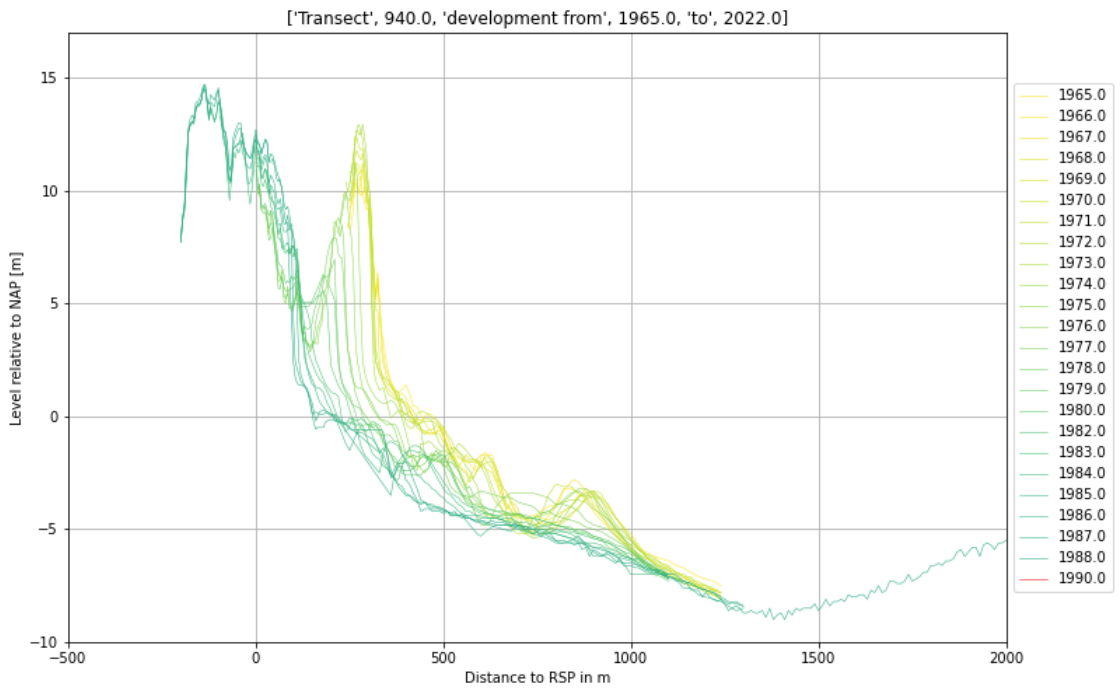


Figure C.42

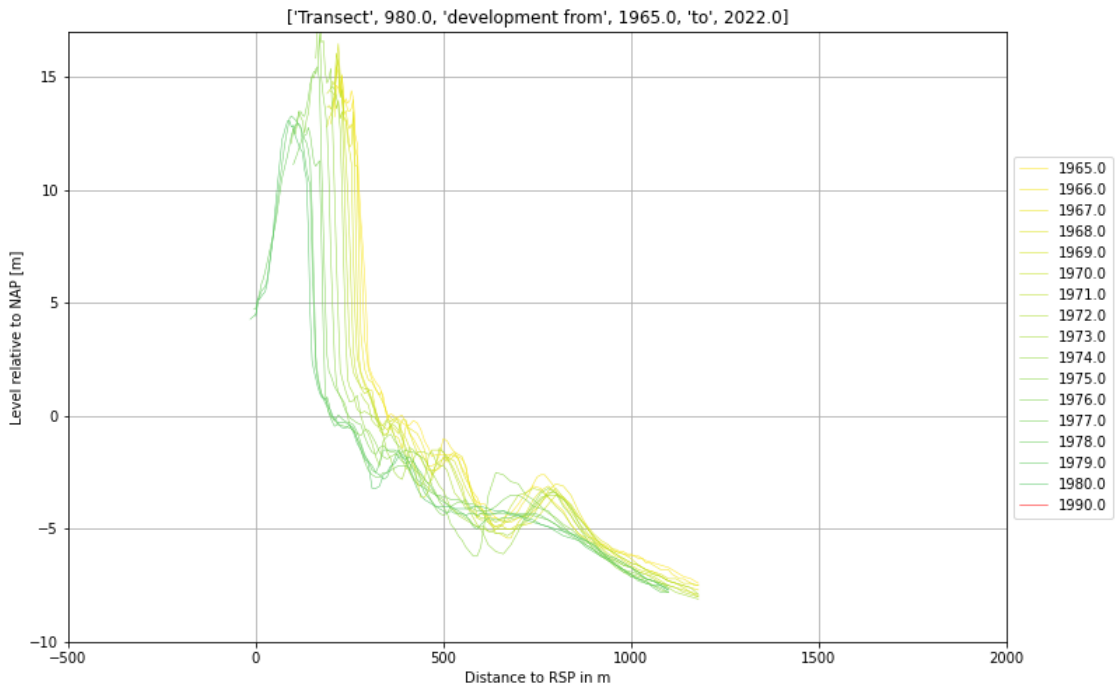


Figure C.43

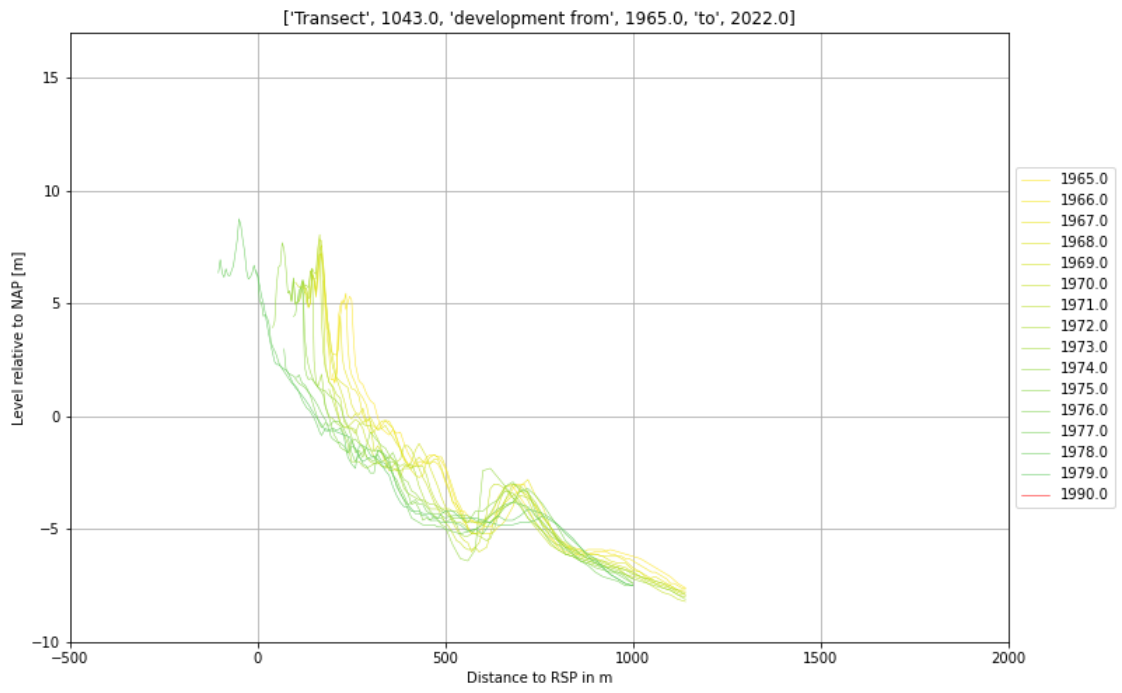


Figure C.44

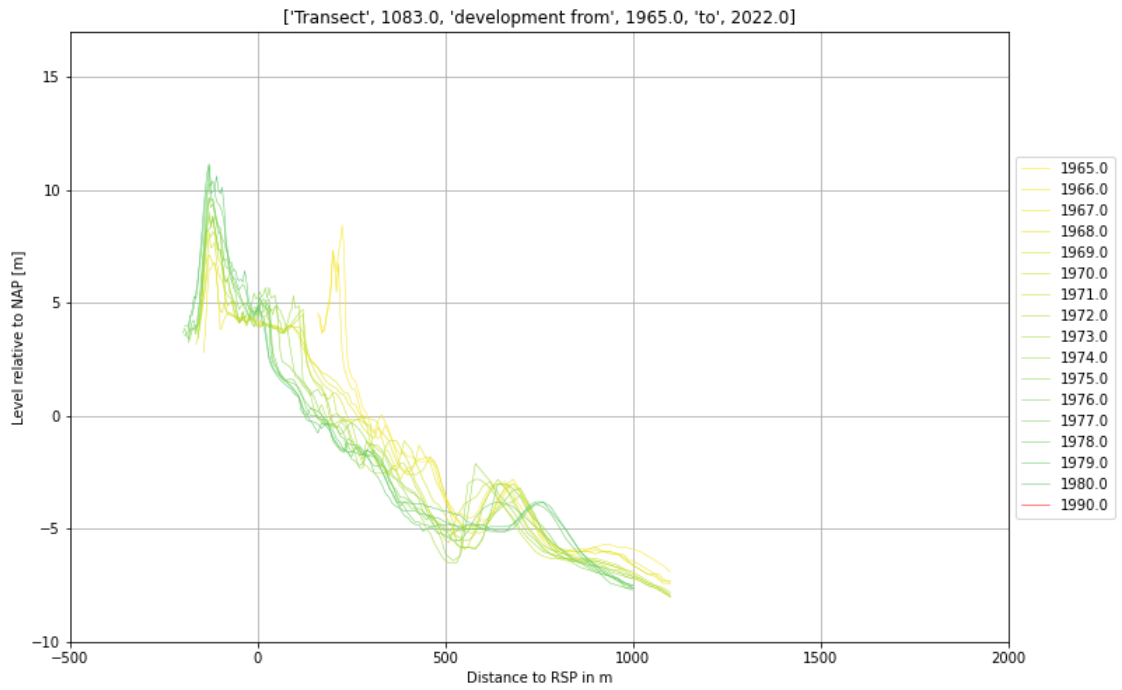


Figure C.45

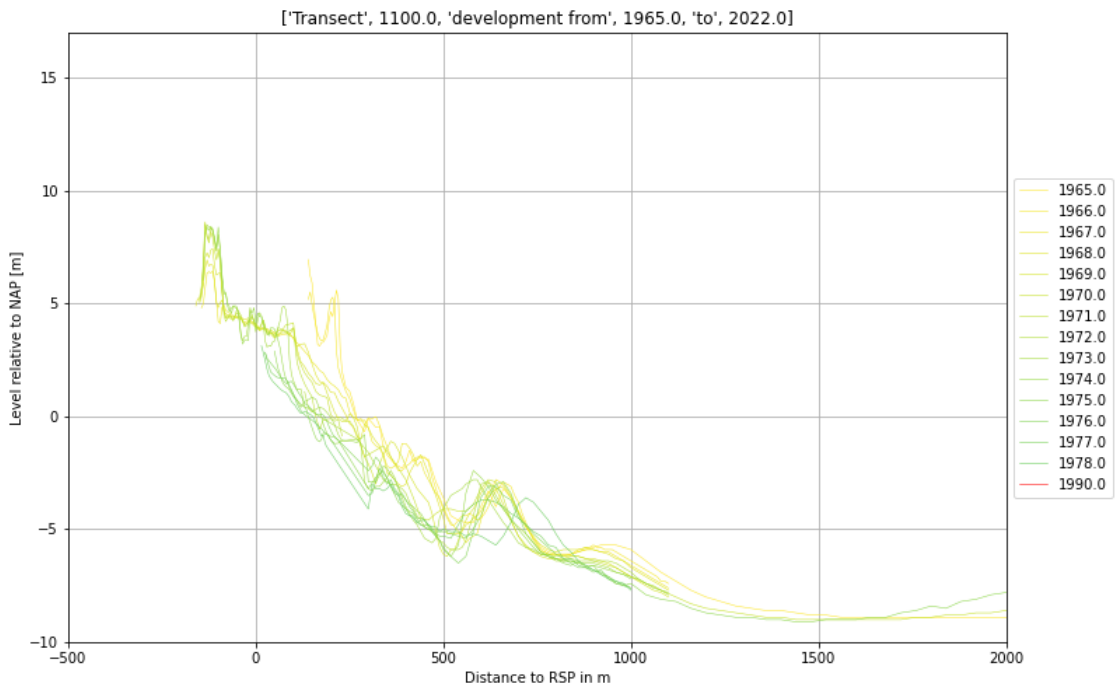


Figure C.46

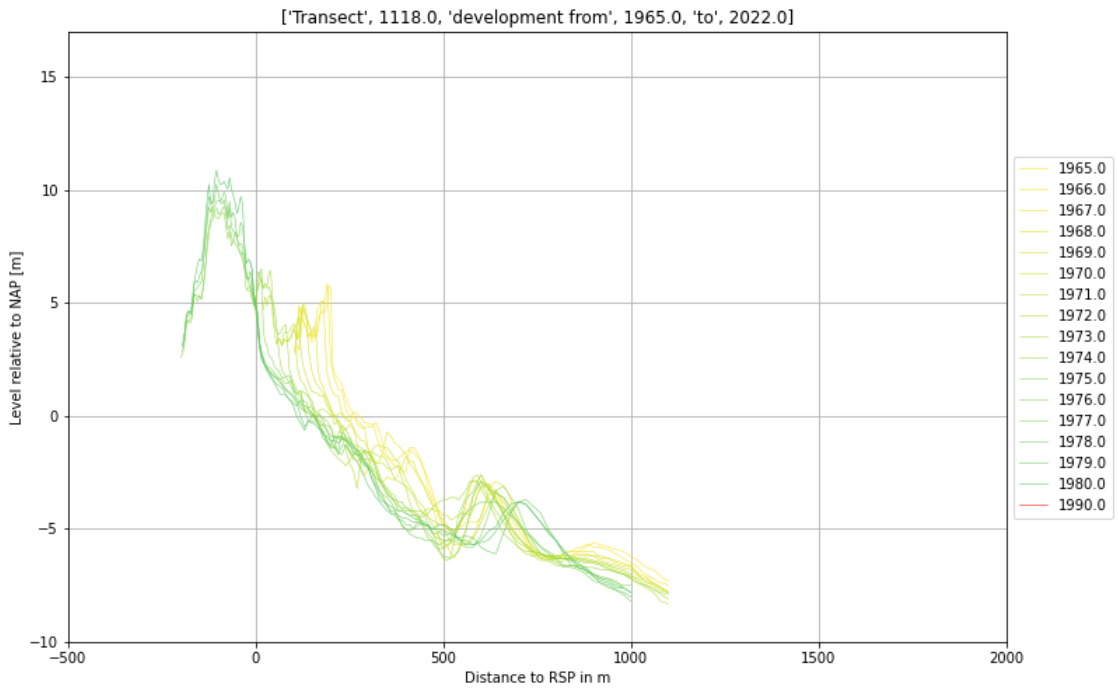


Figure C.47

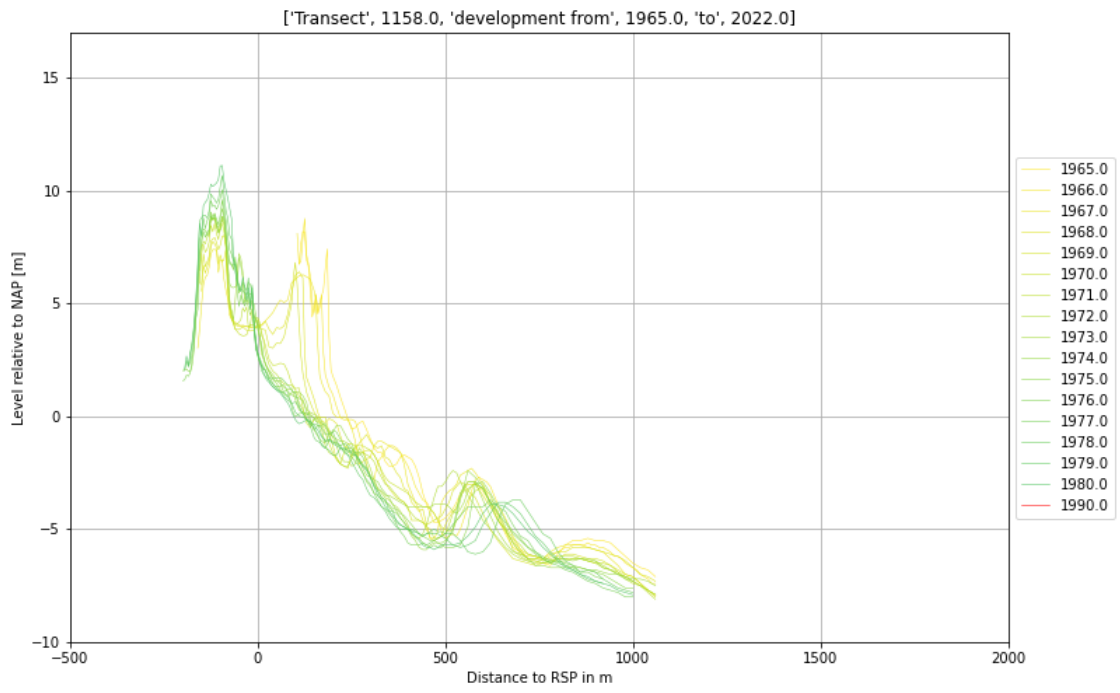


Figure C.48

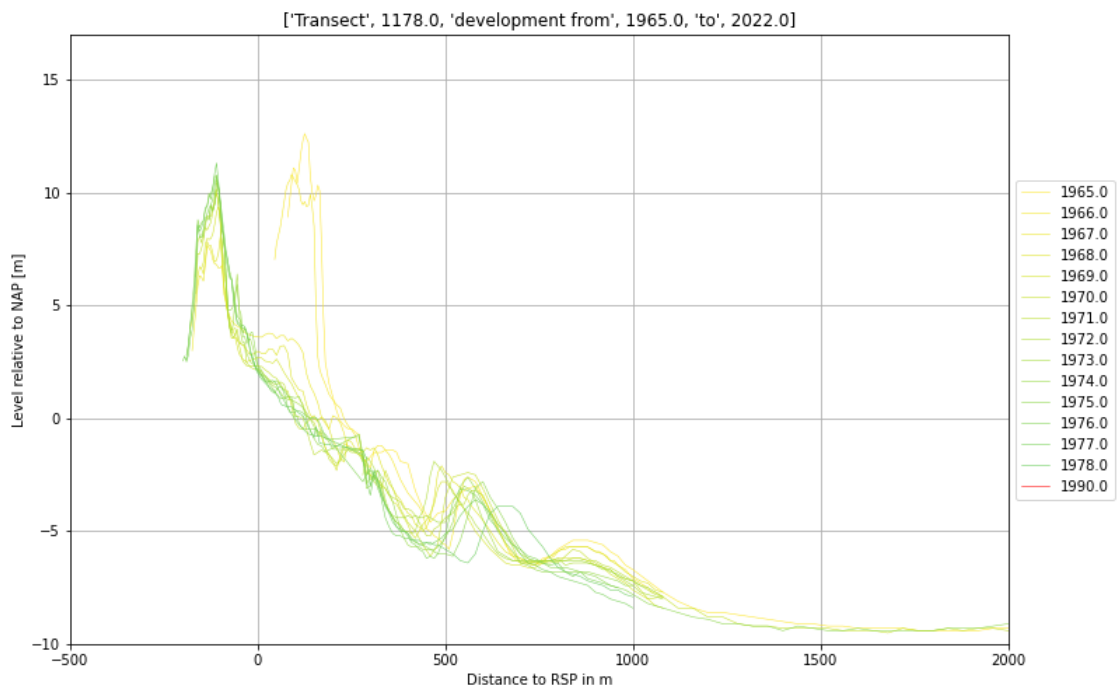


Figure C.49

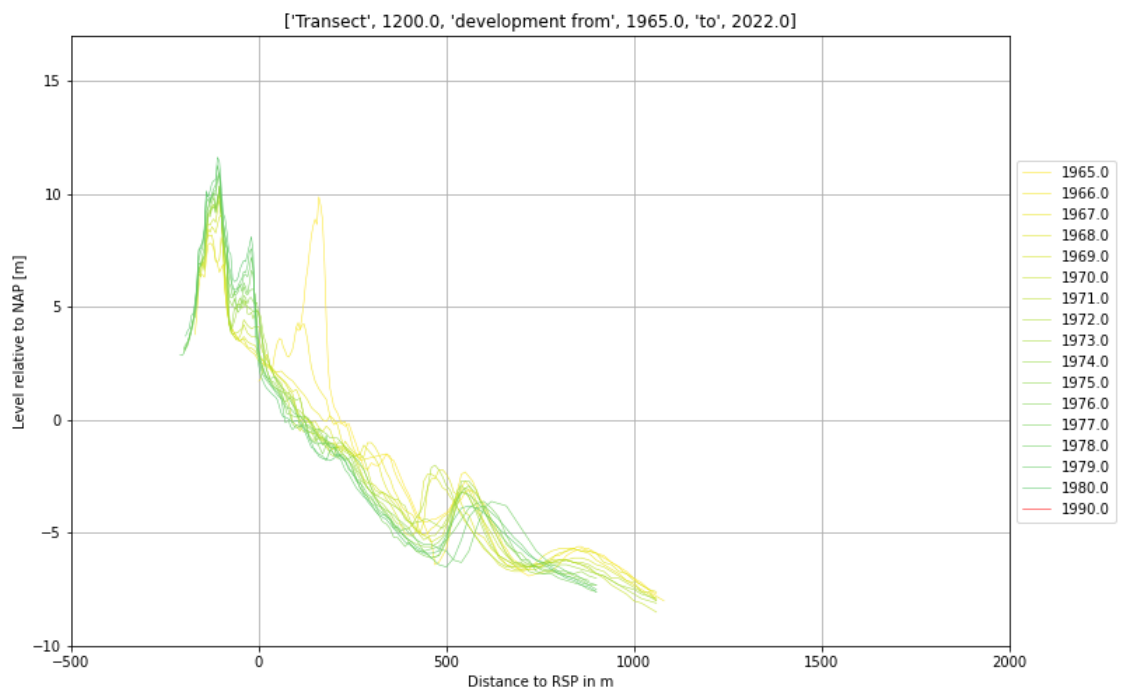


Figure C.50

D List of all nourishments and transect widths at SW Texel

#	Transect Start	Transect End	Year	Volume [Mm ³]	Volume over beach width [m ³ /m]	Type of nourishment
1	880	1063	2005	0.301384	164.6907	Beach
2	900	1148	2003	0.972486	392.1315	Channel wall
3	900	1392	2007	2.00097	406.7012	Shoreface
4	900	1070	2009	0.4	235.2941	Beach
5	900	1210	2012	0.751589	242.4481	Beach
6	900	1190	2017	0.895	308.6207	Beach
7	900	1298	2021* 1	251.2563	251.2563	Beach
8	930	1210	1994	0.761204	271.8586	Beach
9	1001	1190	2000	0.35702	188.8995	Beach
10	1038	1143	1997	0.340038	323.8457	Beach
11	1200	1312	2012	0.5	446.4286	Shoreface

Table D.1: Overview nourishments at SW Texel. *This beach nourishment has not been included in the analysis of Chapter 4, because its impact is not noticeable in the transects of 2021. The nourishment was applied after the measurements were finished.

Transect	880	900	915	930	945	960	976	1000	1001	1013	1033	1053	1073	1093	1108	1128	1148	1168	1190	1210	
$B_{Transect}$	100	175	150	150	150	155	200	125	65	160	200	200	200	175	200	200	200	210	210	210	100

Table D.2: Width of all transects.

E Molengat filling projections transect 703-1210

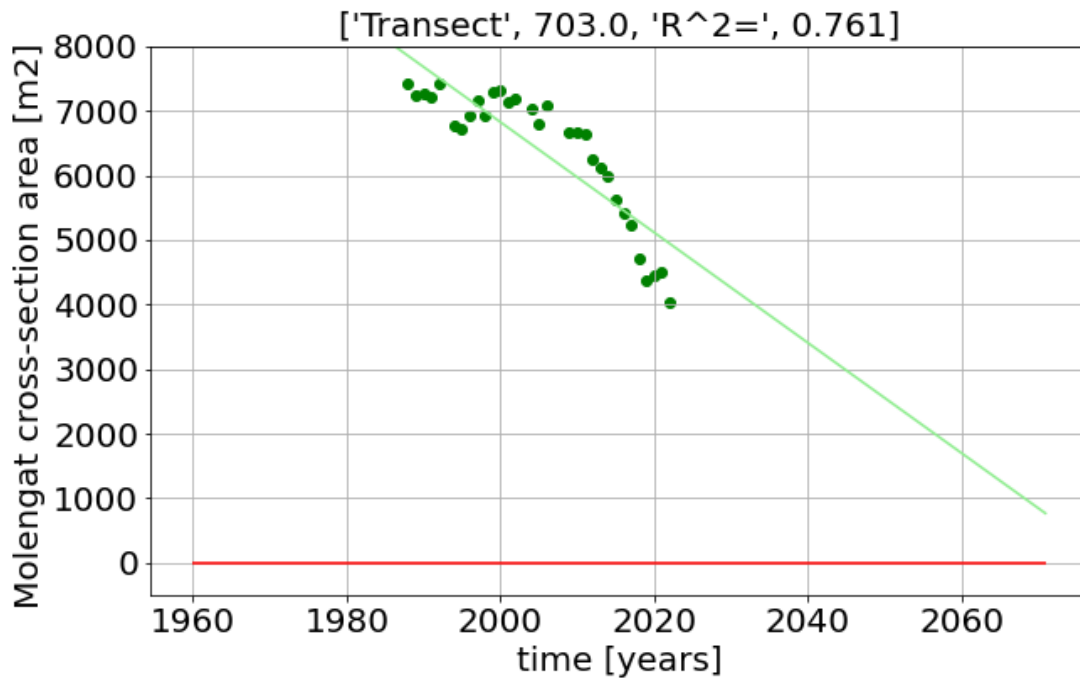


Figure E.1

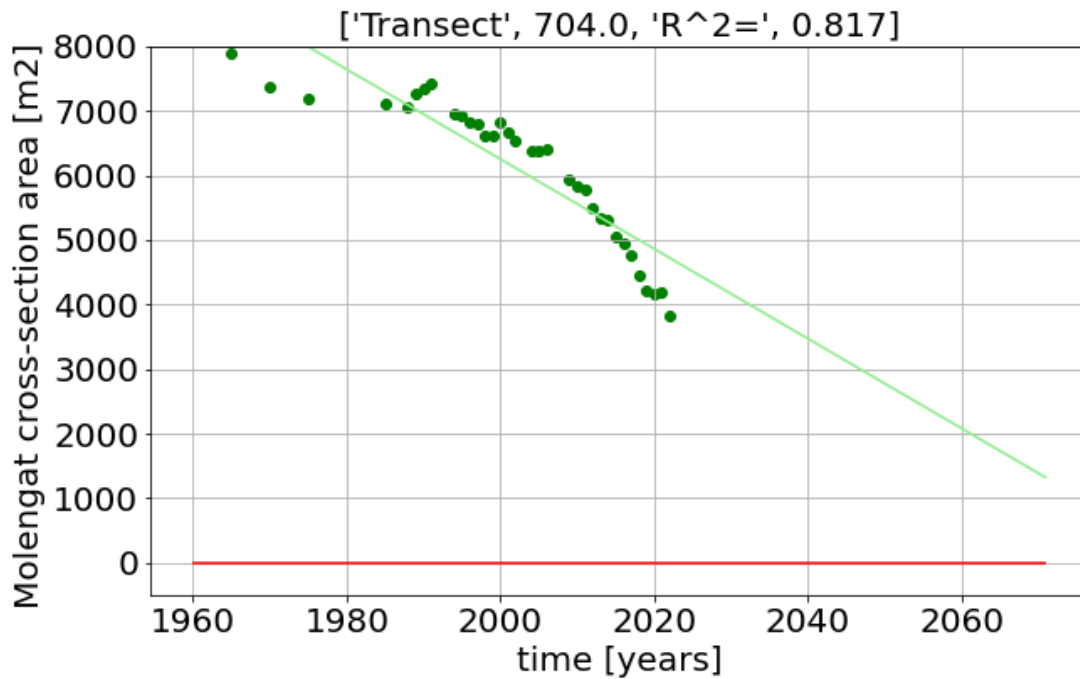


Figure E.2

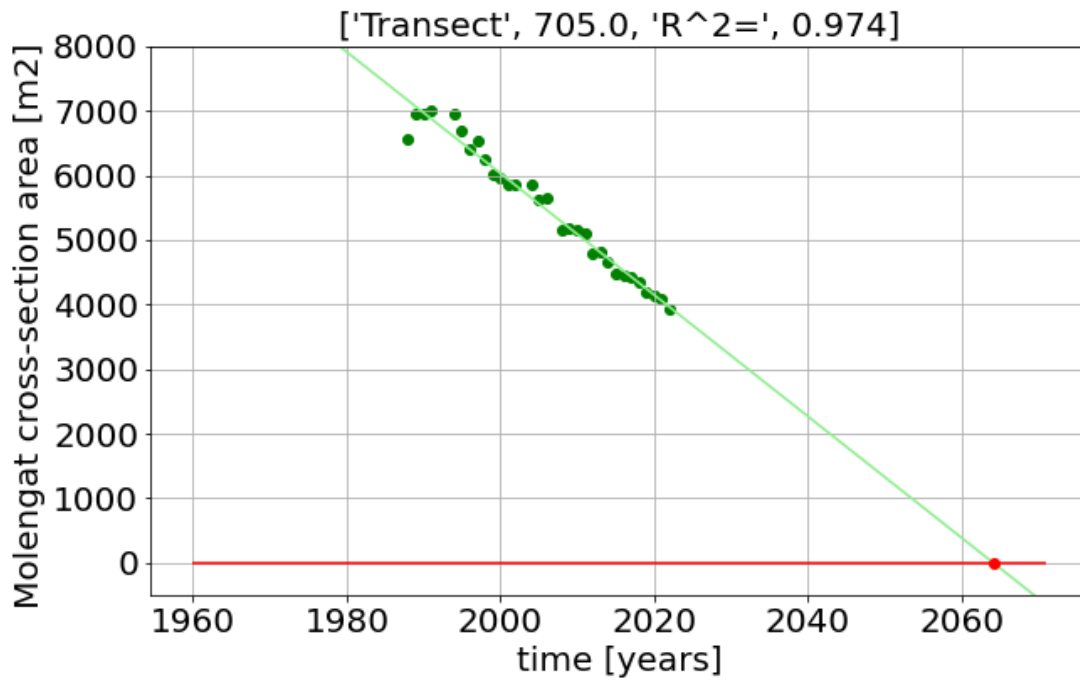


Figure E.3

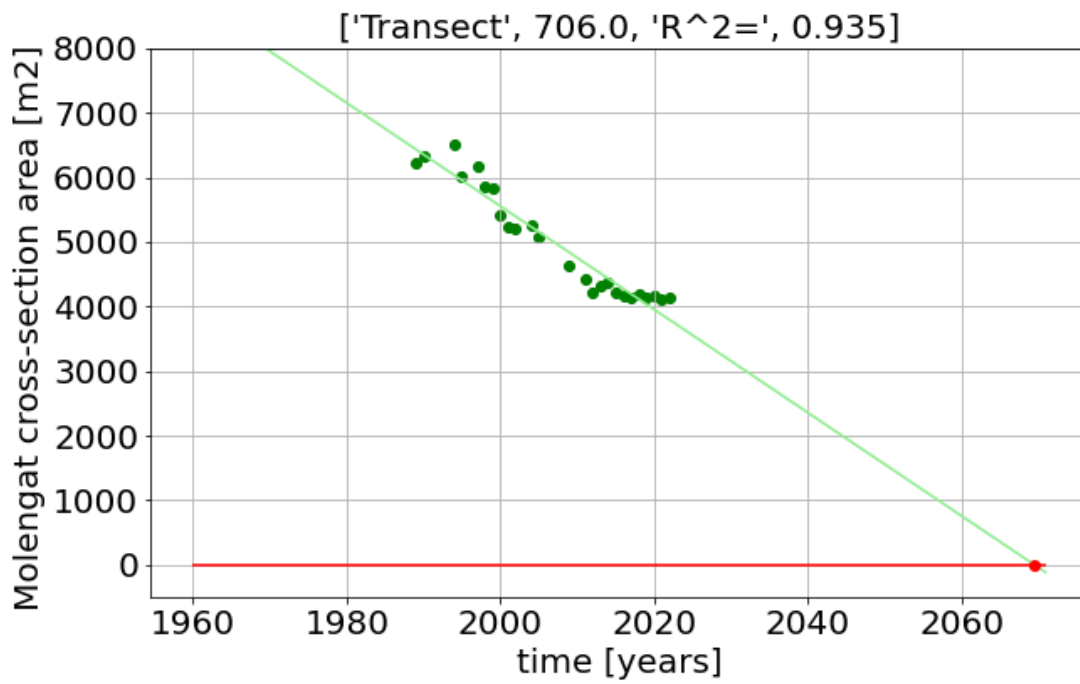


Figure E.4

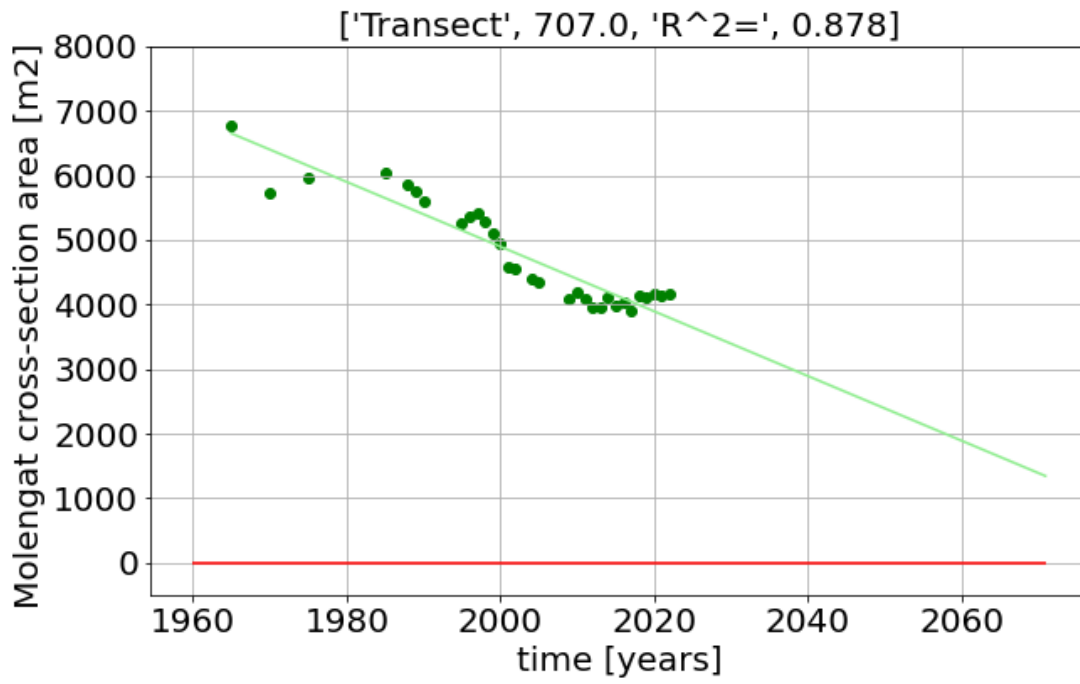


Figure E.5

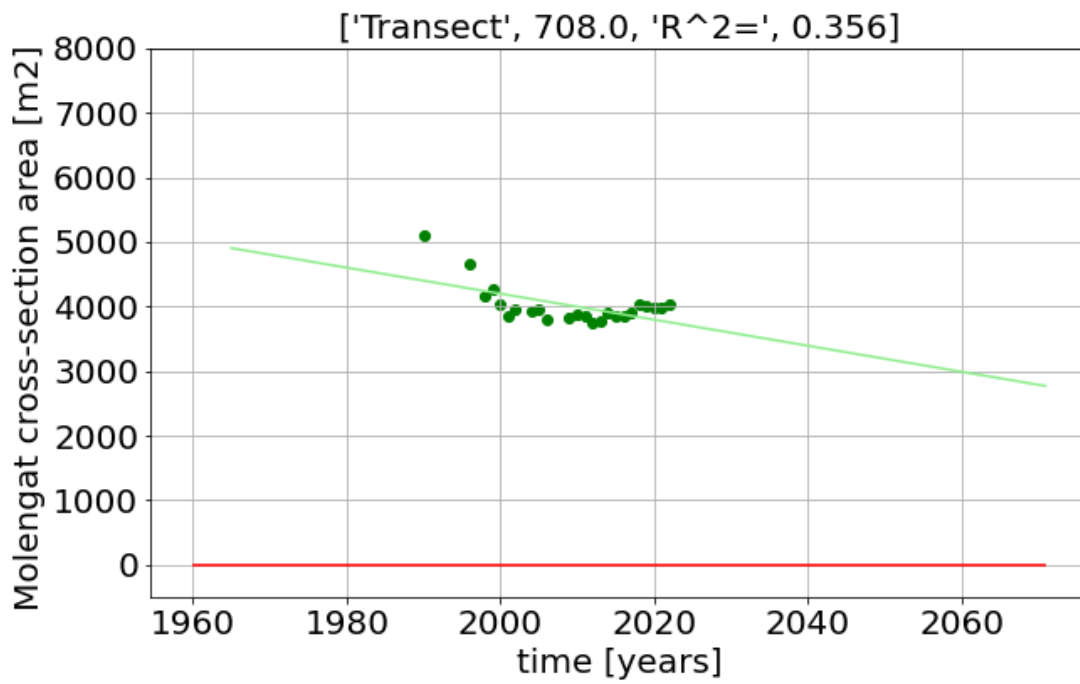


Figure E.6

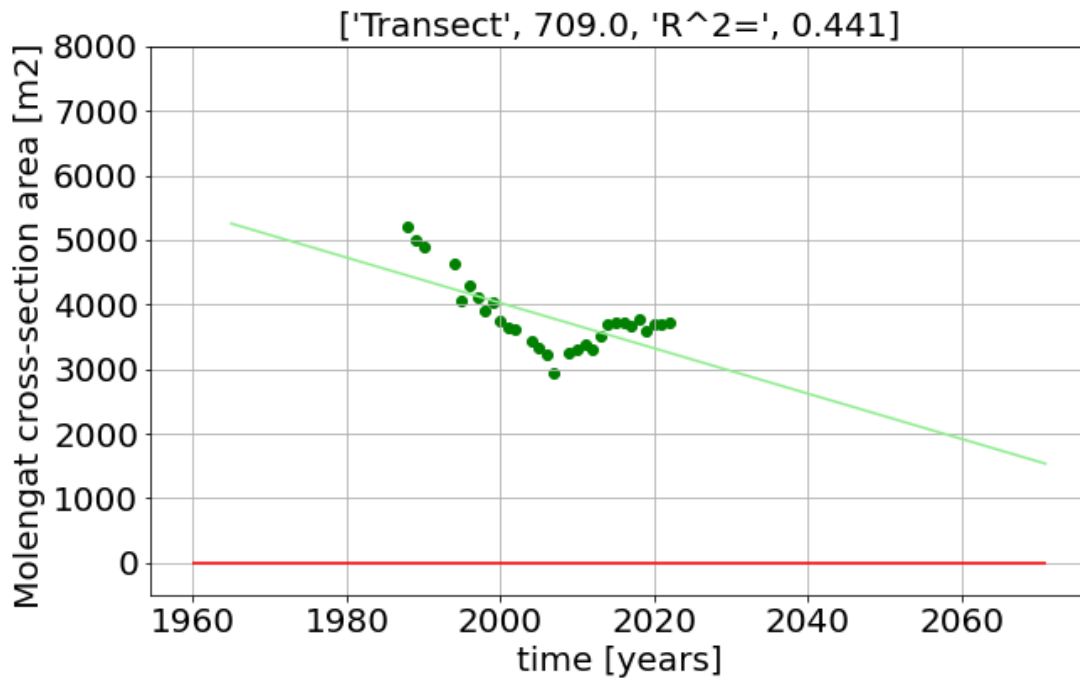


Figure E.7

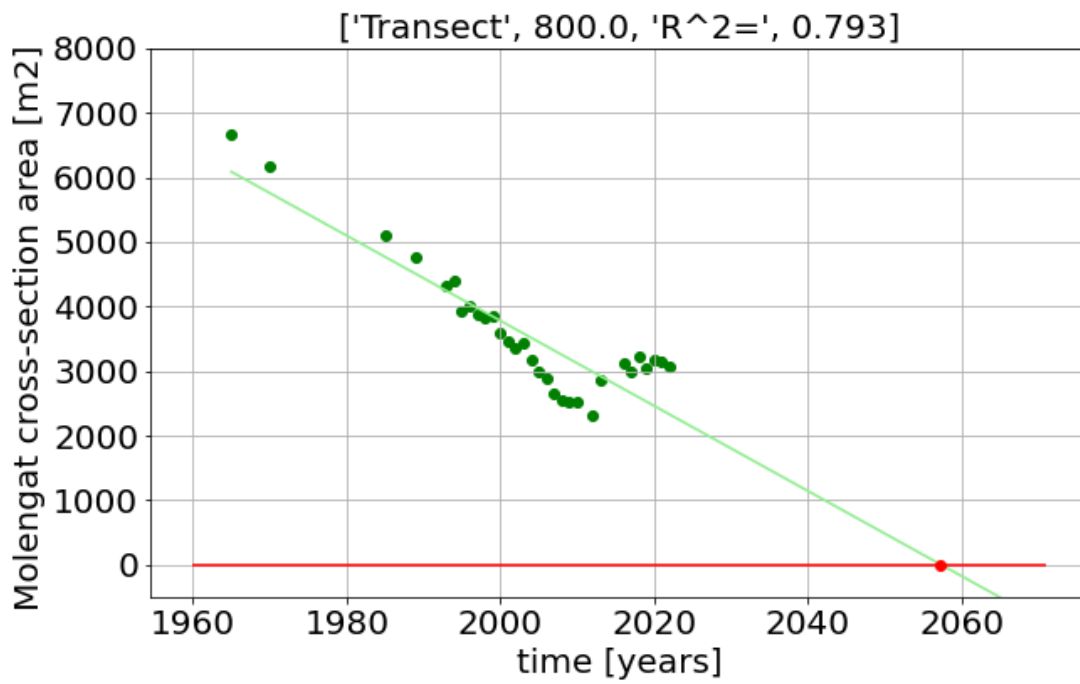


Figure E.8

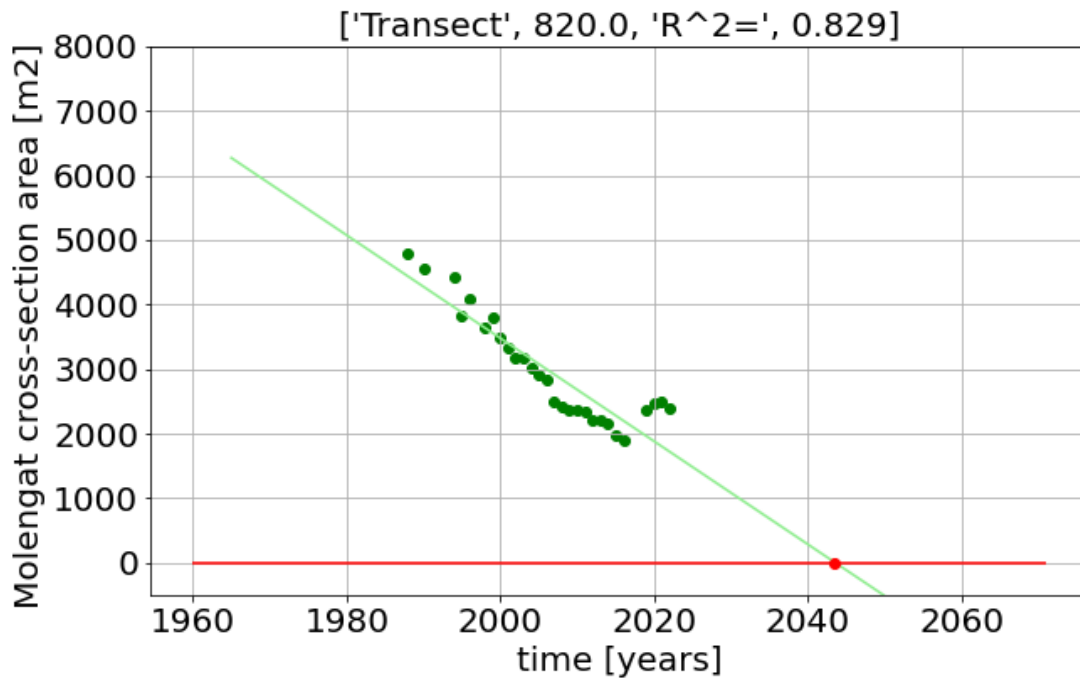


Figure E.9

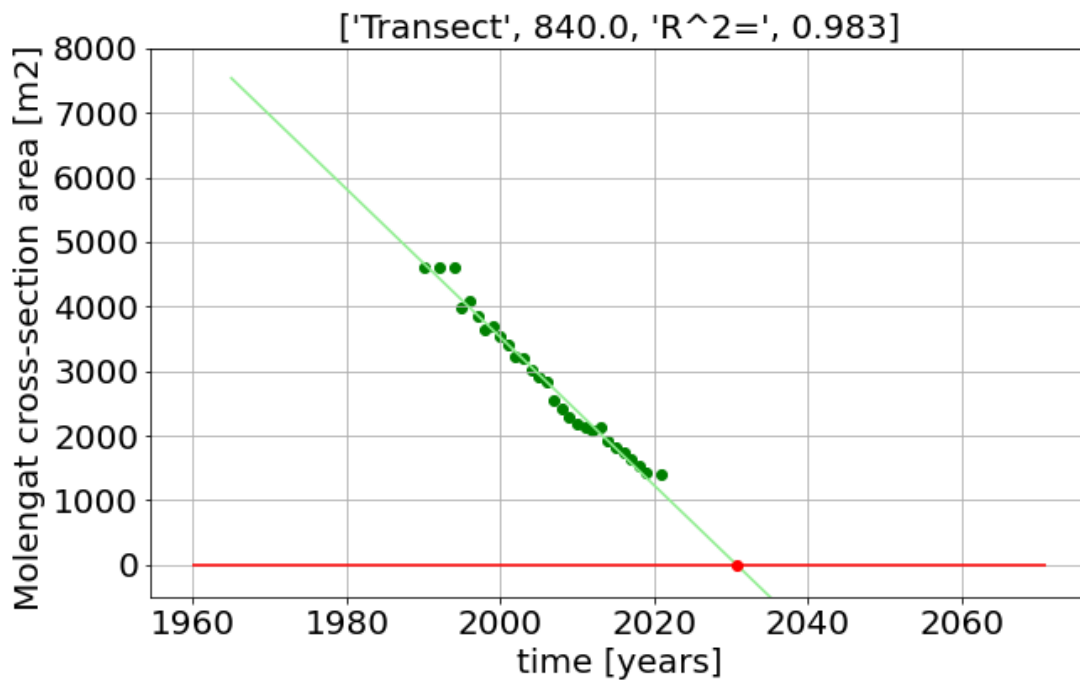


Figure E.10

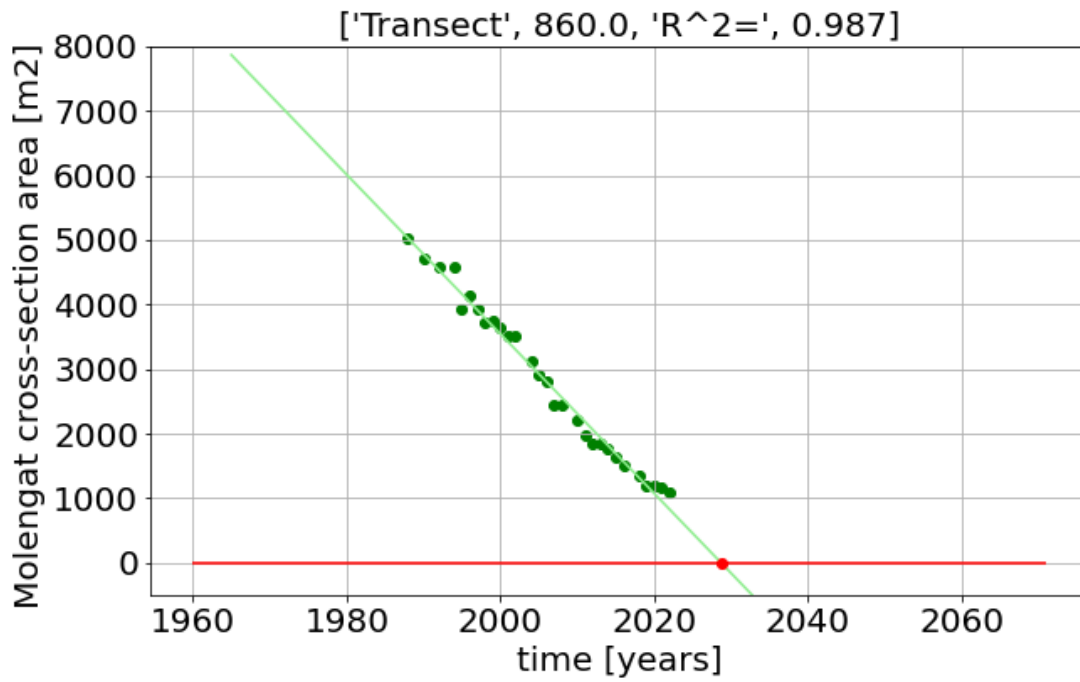


Figure E.11

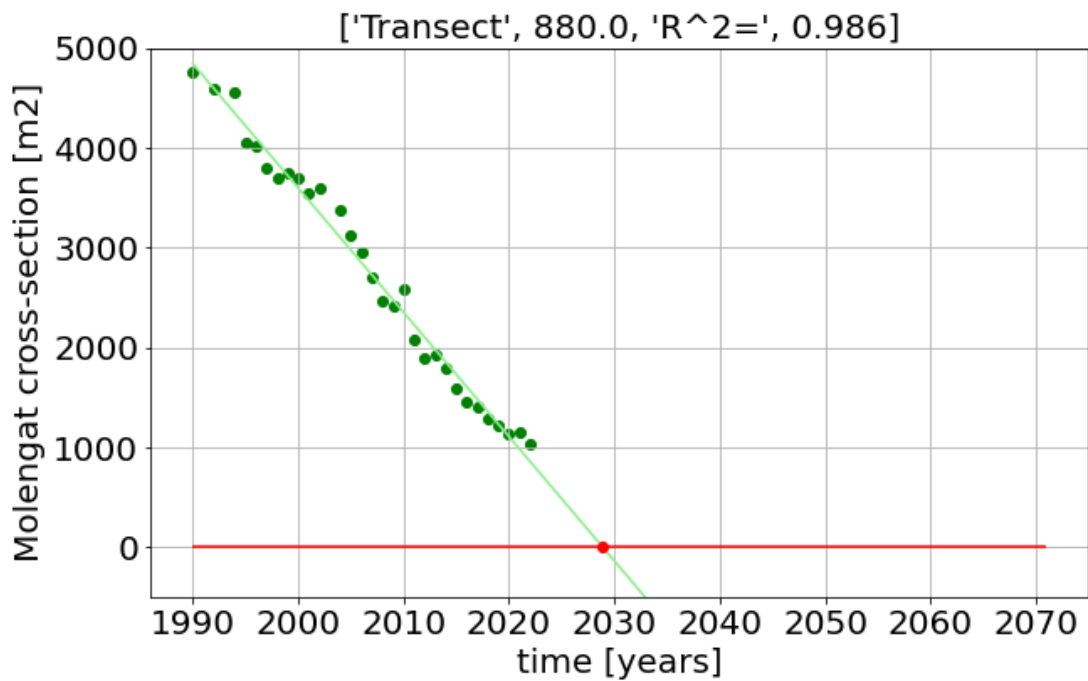


Figure E.12

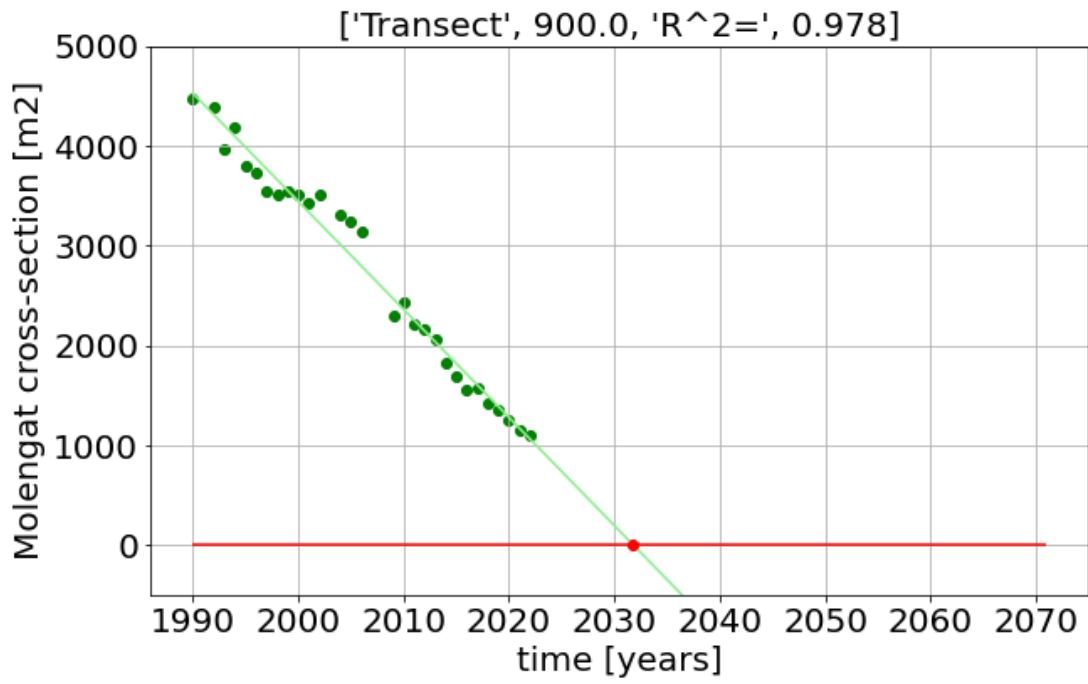


Figure E.13

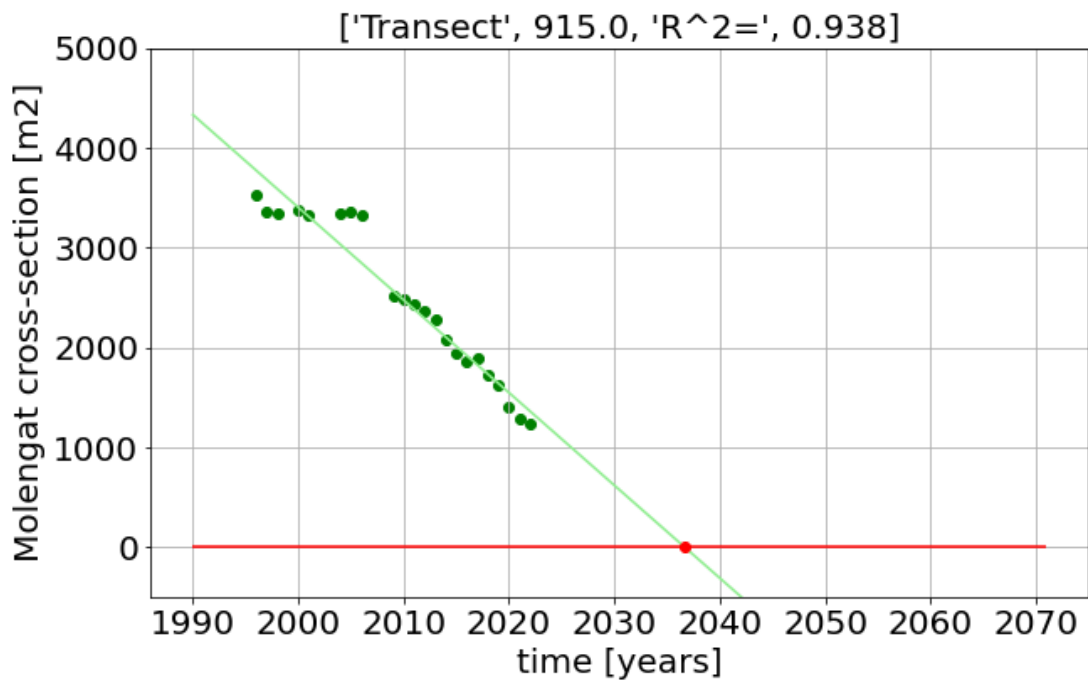


Figure E.14

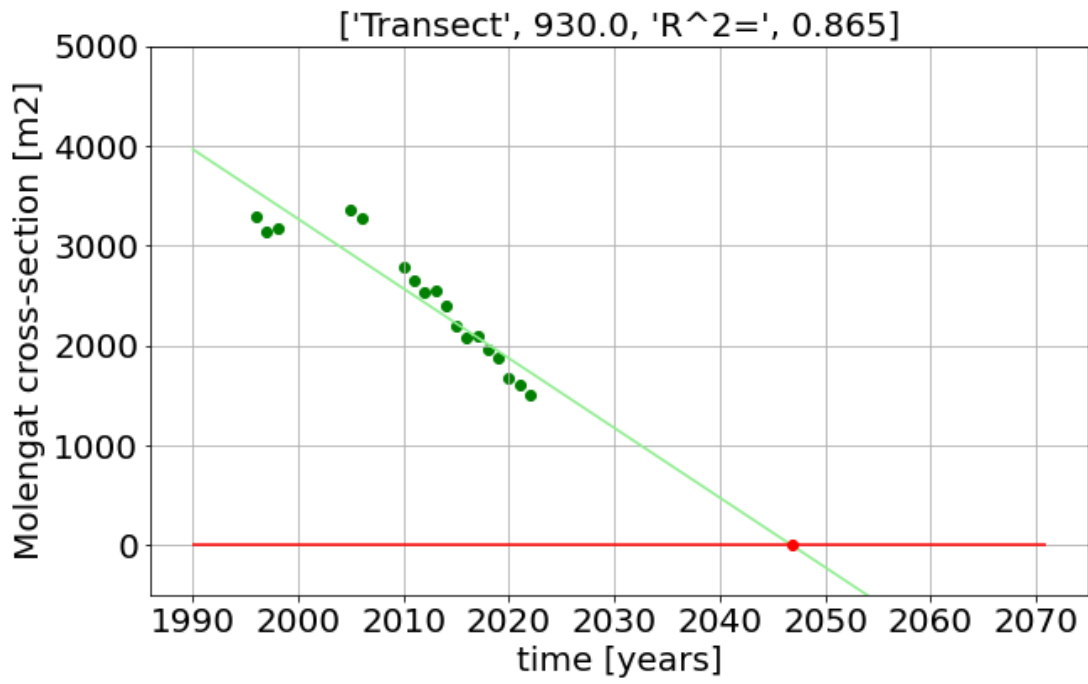


Figure E.15

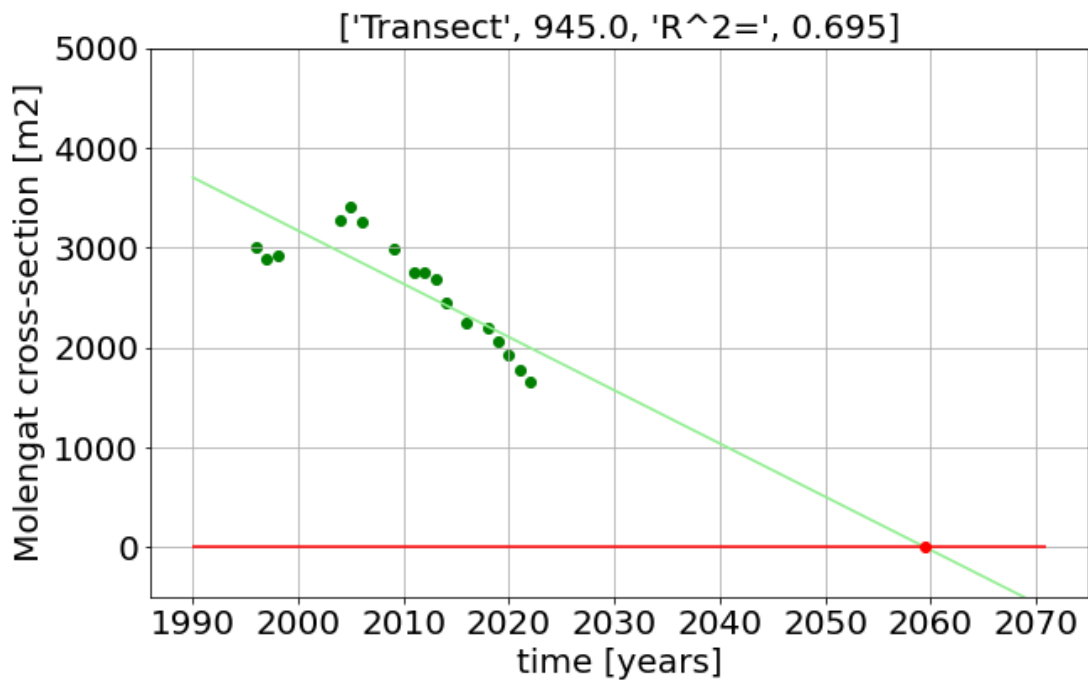


Figure E.16

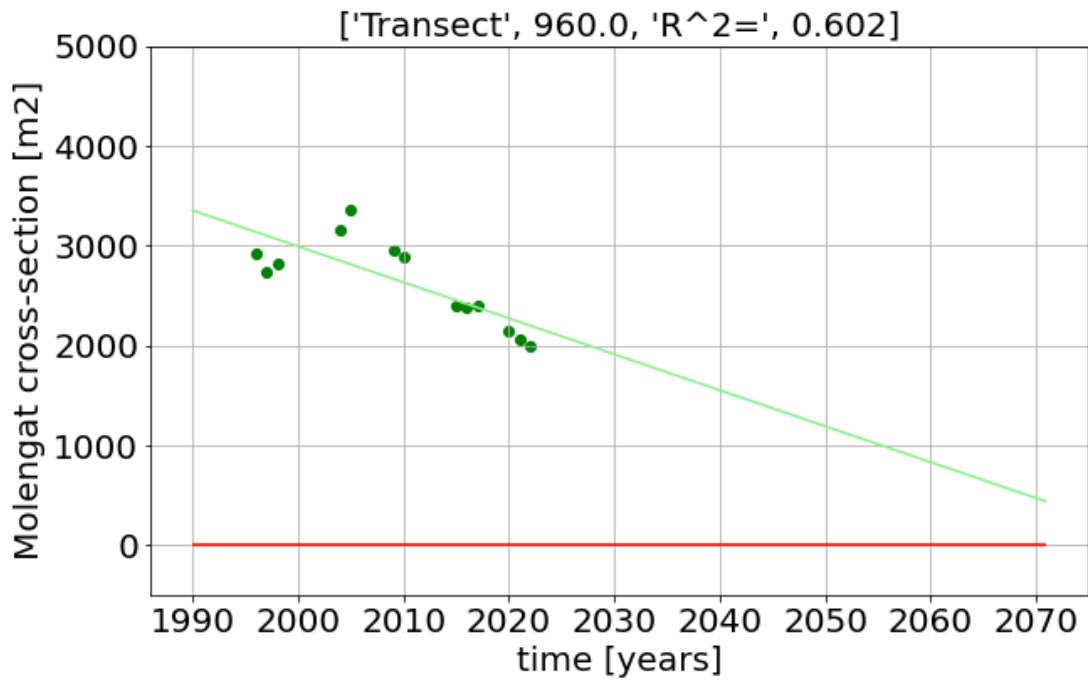


Figure E.17

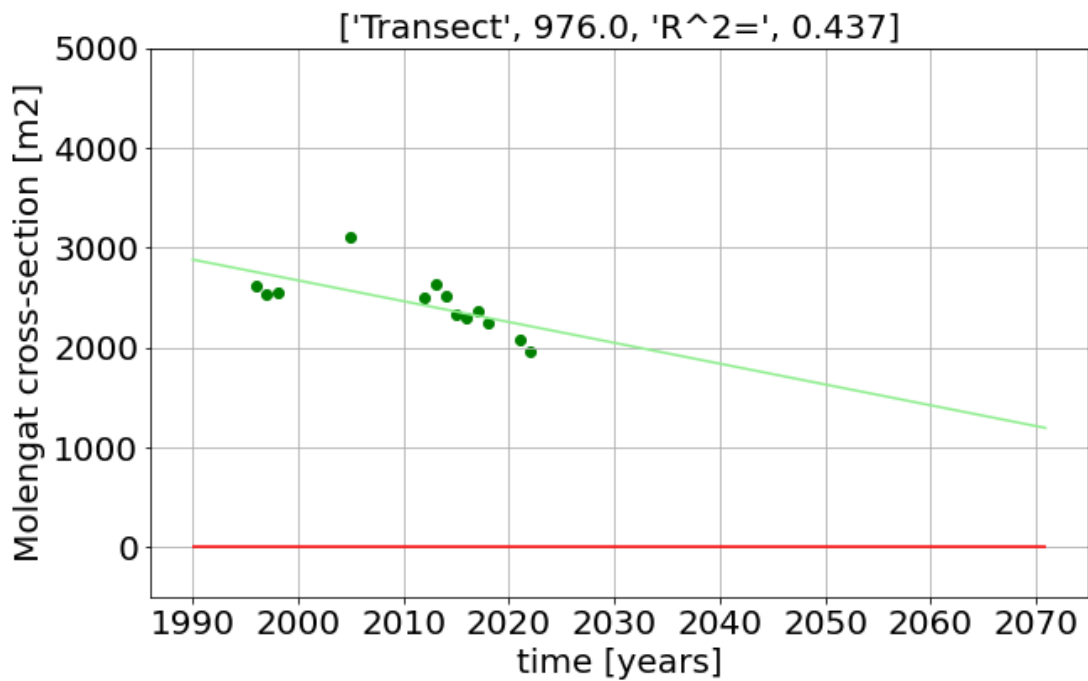


Figure E.18

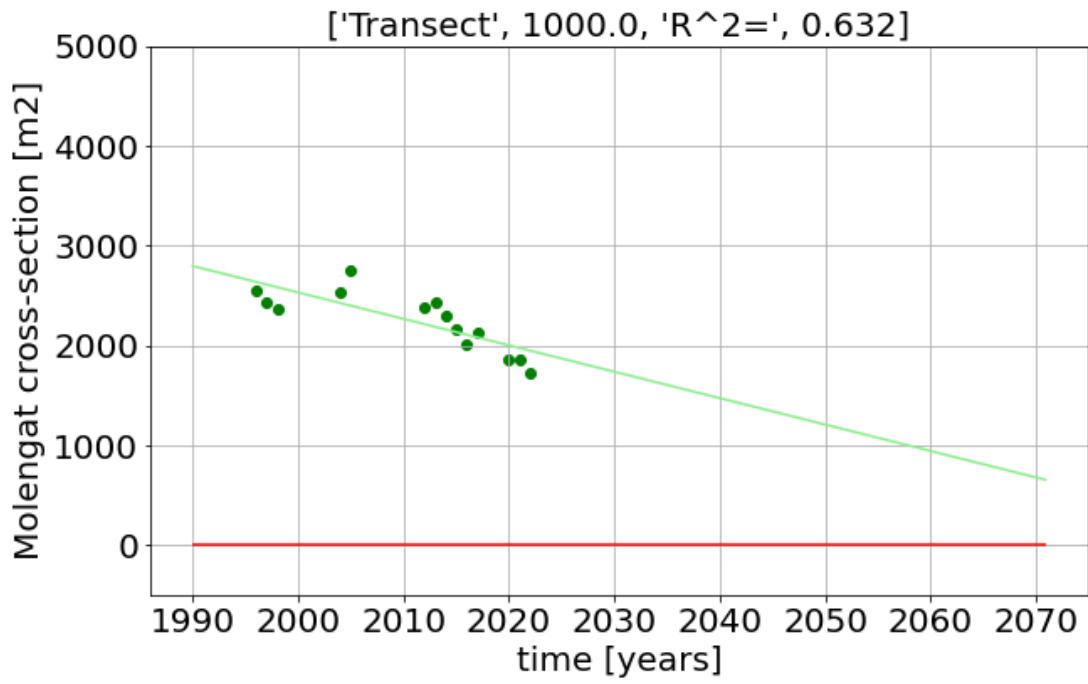


Figure E.19

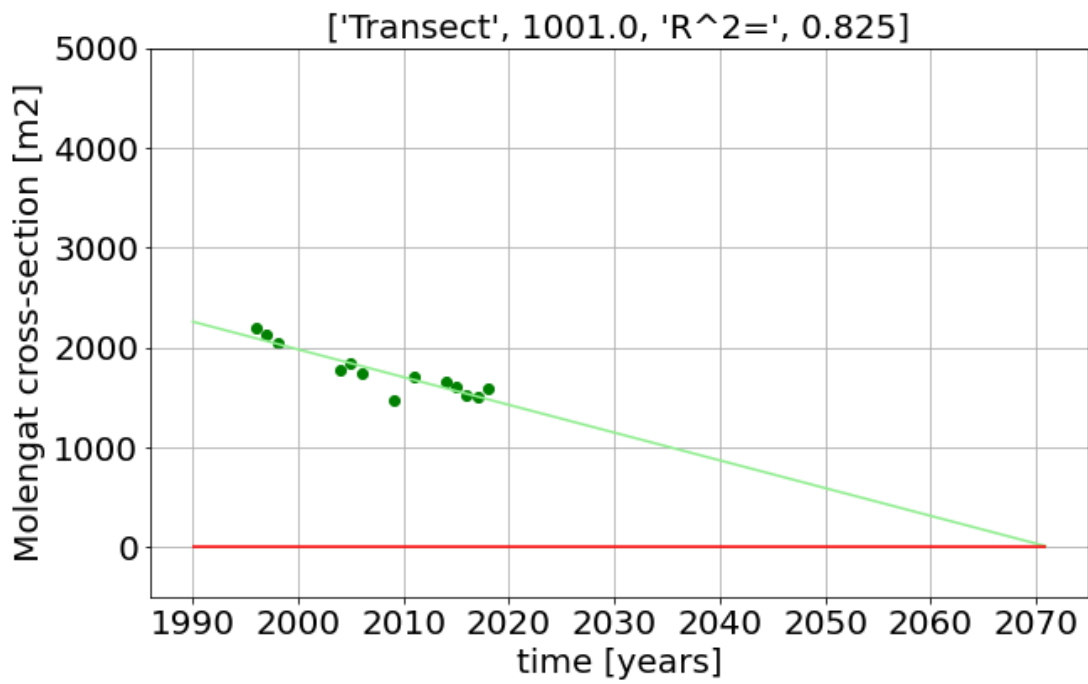


Figure E.20

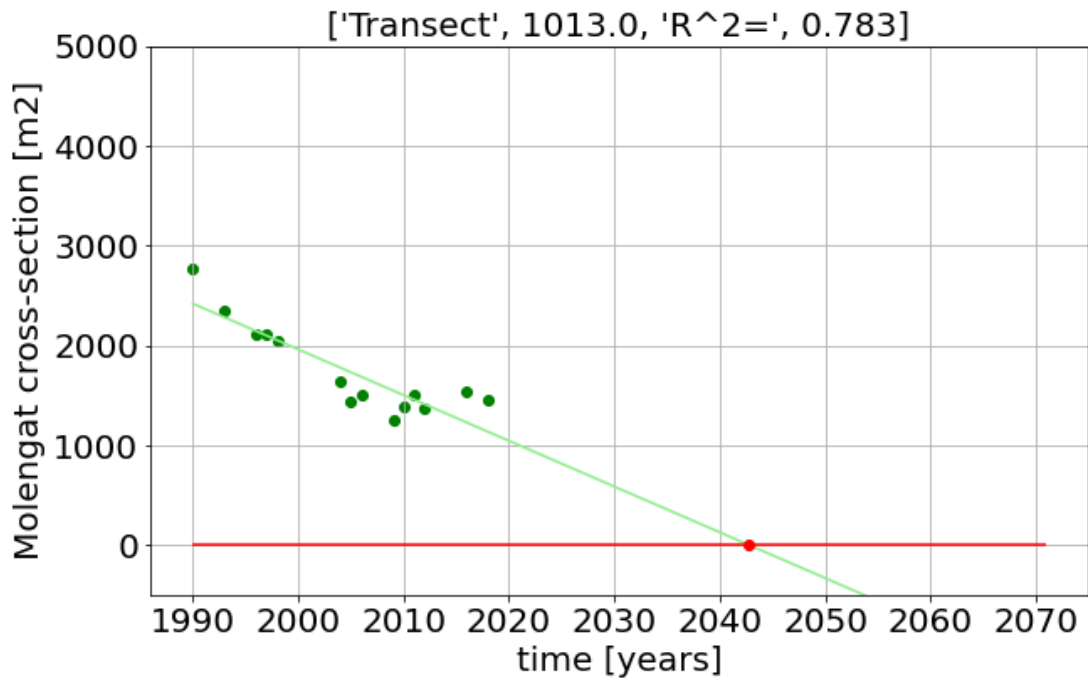


Figure E.21

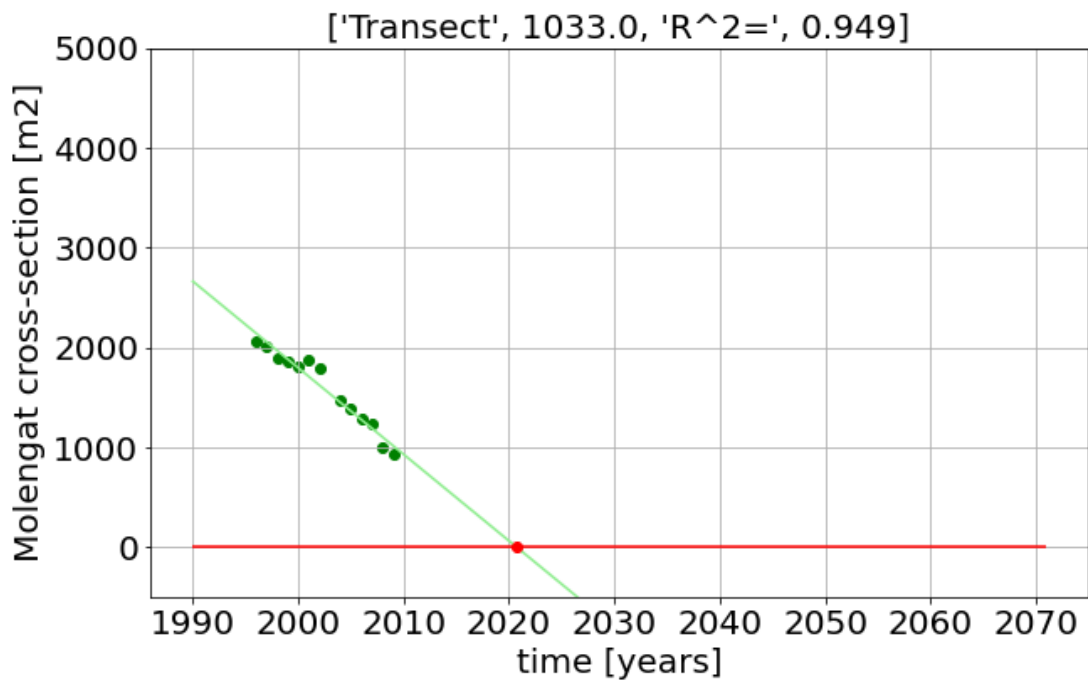


Figure E.22

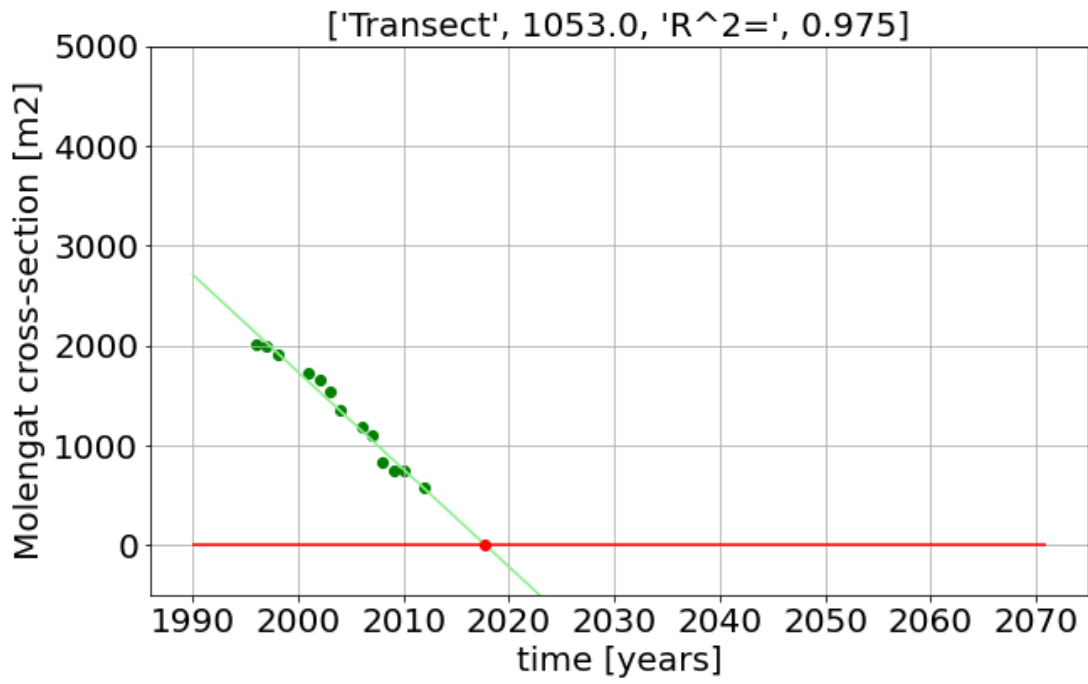


Figure E.23

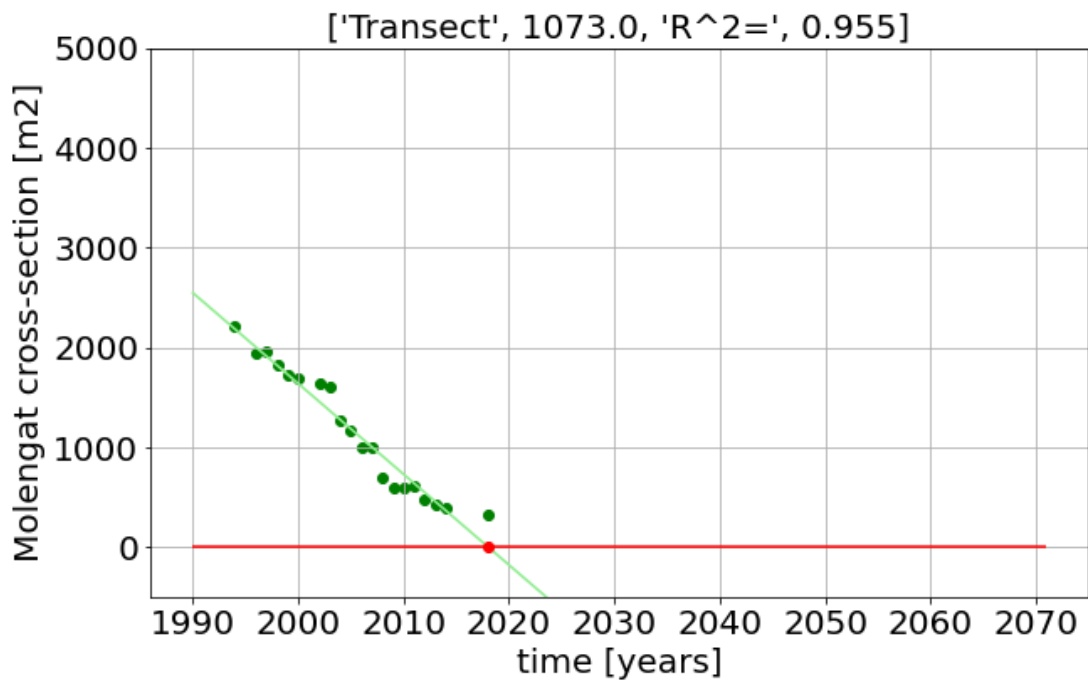


Figure E.24

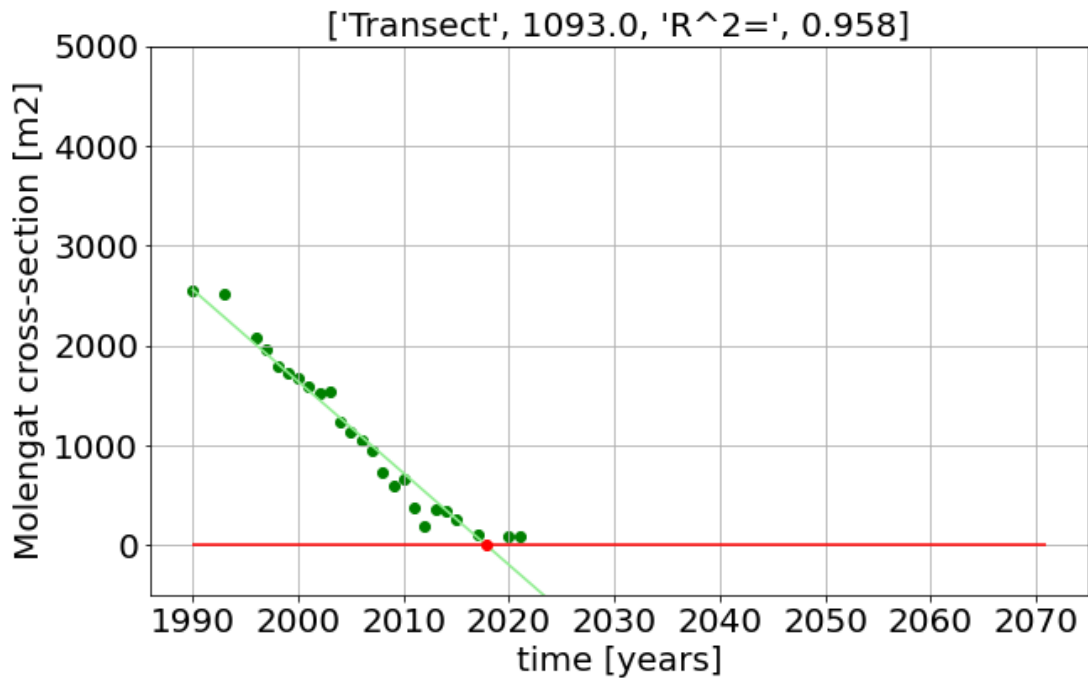


Figure E.25

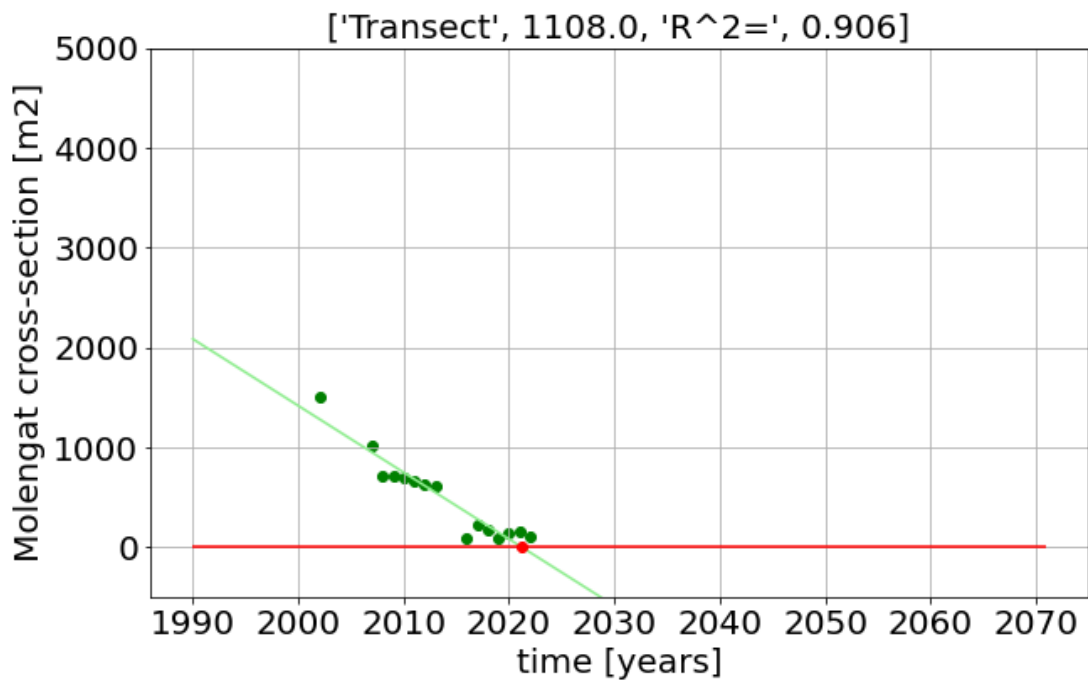


Figure E.26

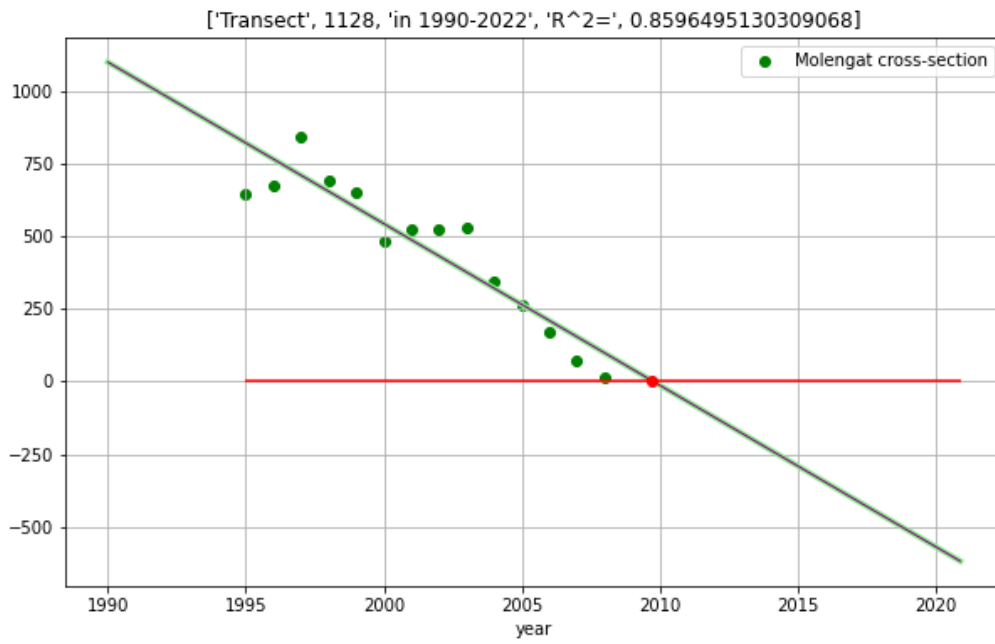


Figure E.27

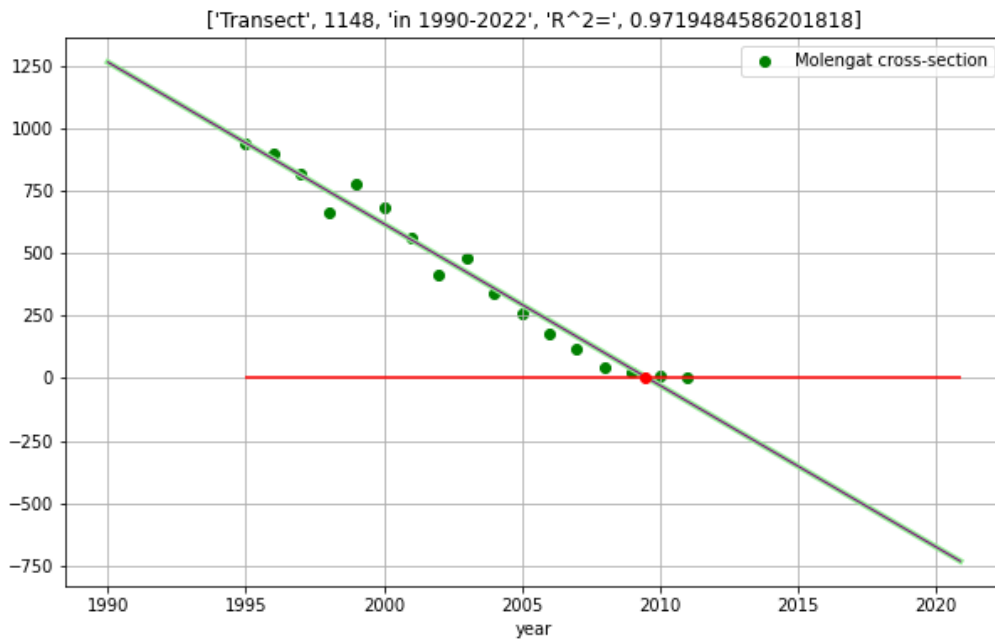


Figure E.28

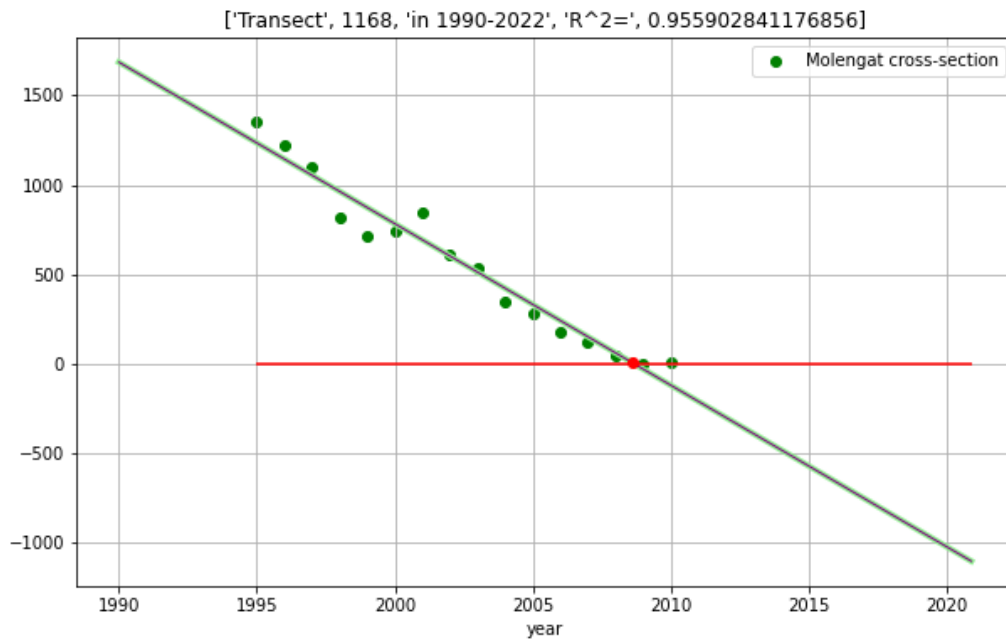


Figure E.29

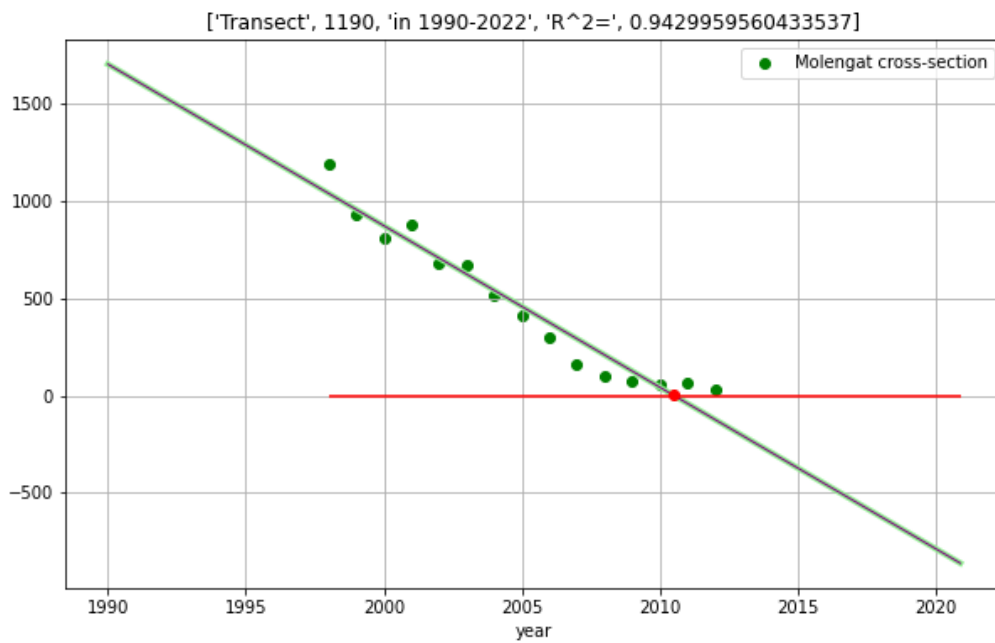


Figure E.30

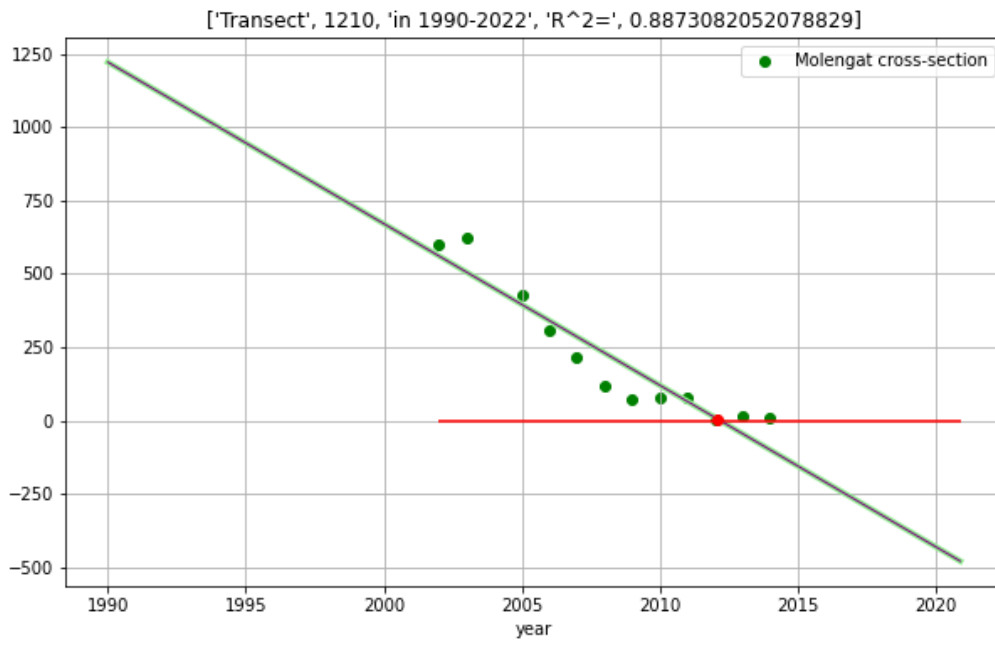


Figure E.31

F Total volume change of transects (Vaklodingen)

These graphs show the total volume change in the transects. The 2 blue lines enclose the area of $V_{shallow}$.

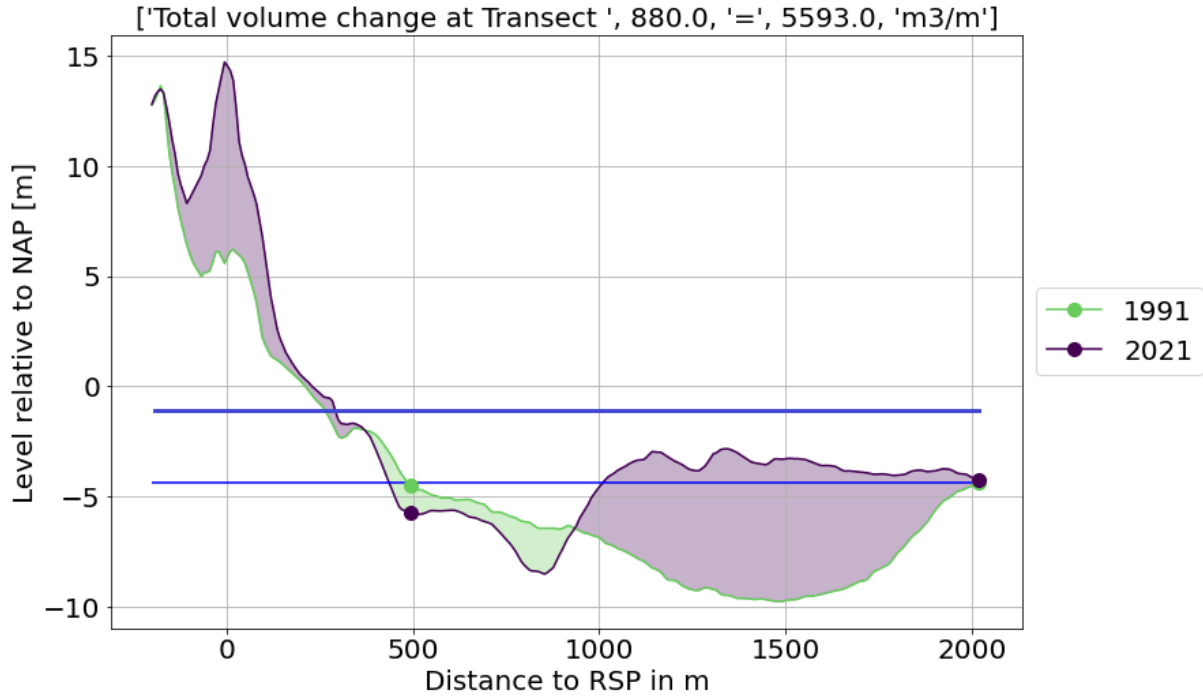


Figure F.1

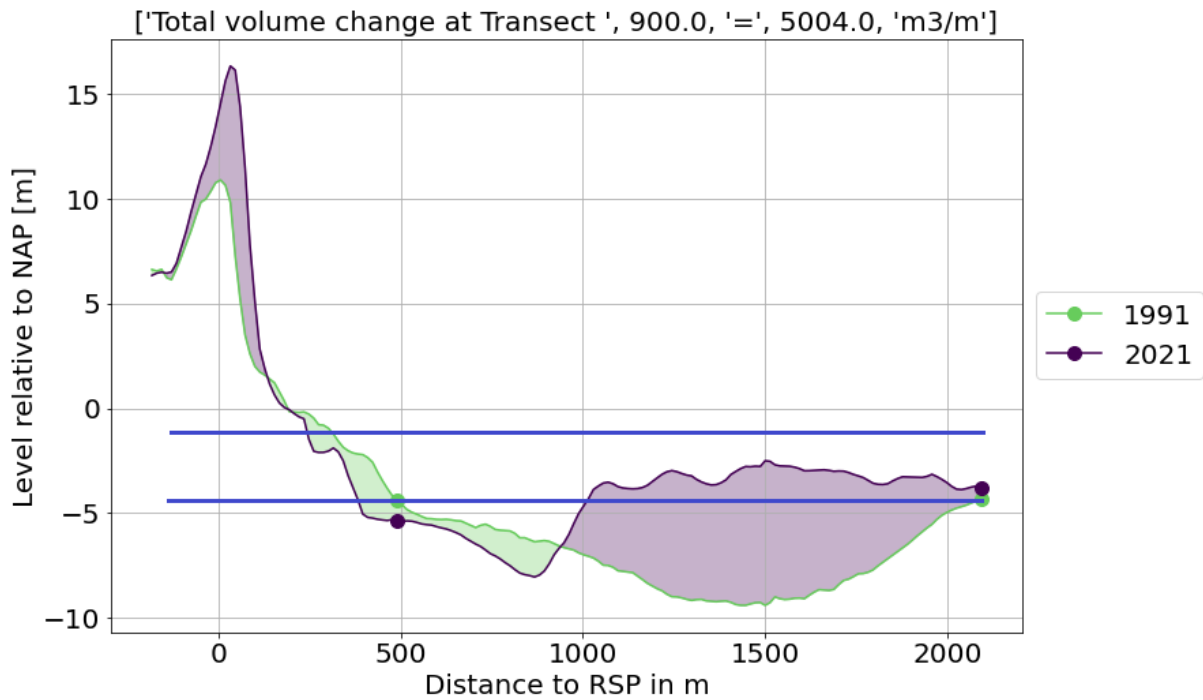


Figure F.2

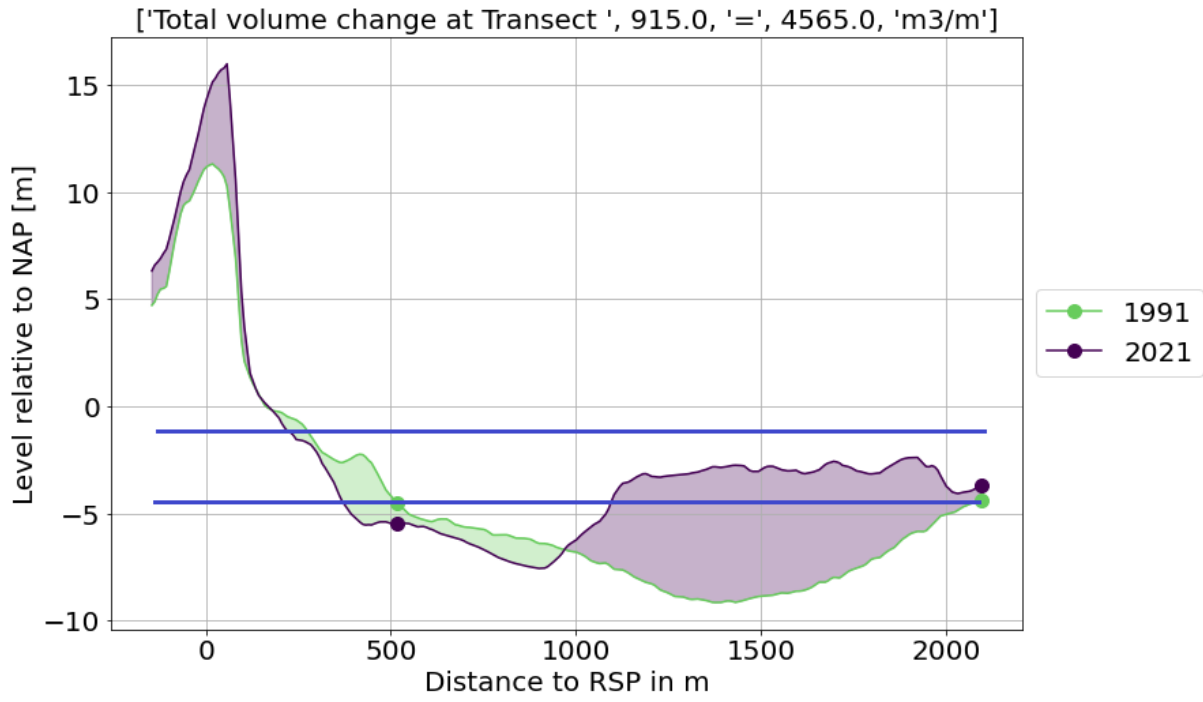


Figure F.3

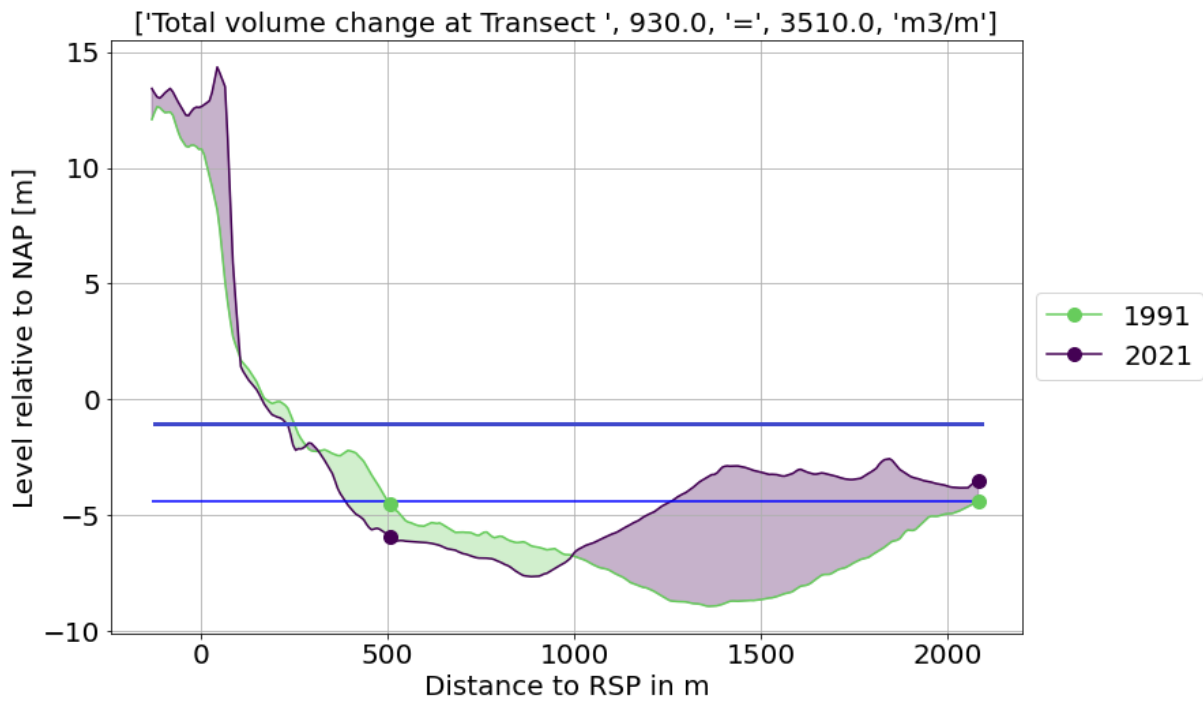


Figure F.4

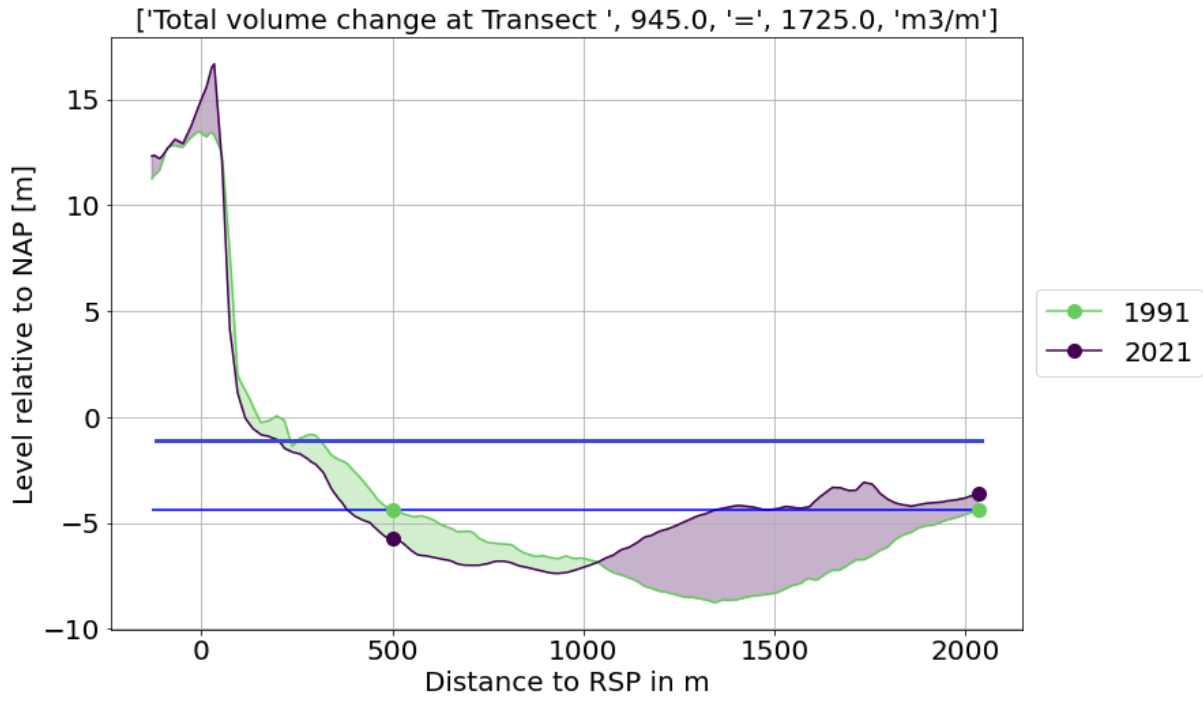


Figure F.5

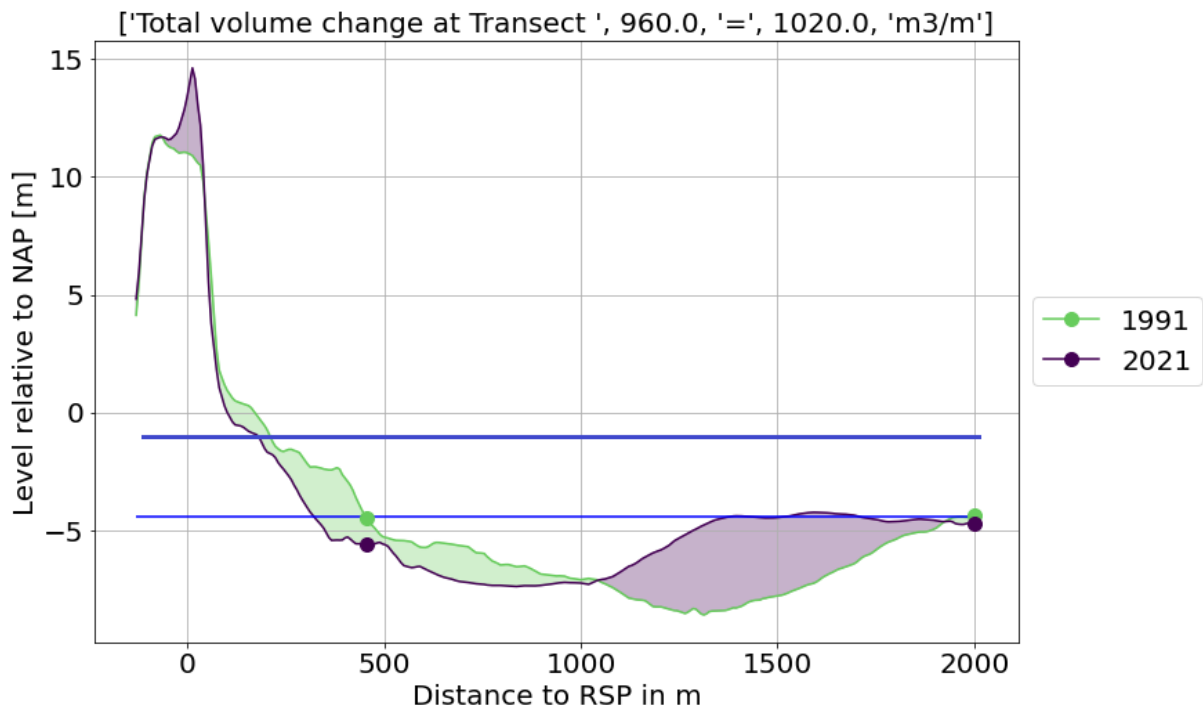


Figure F.6

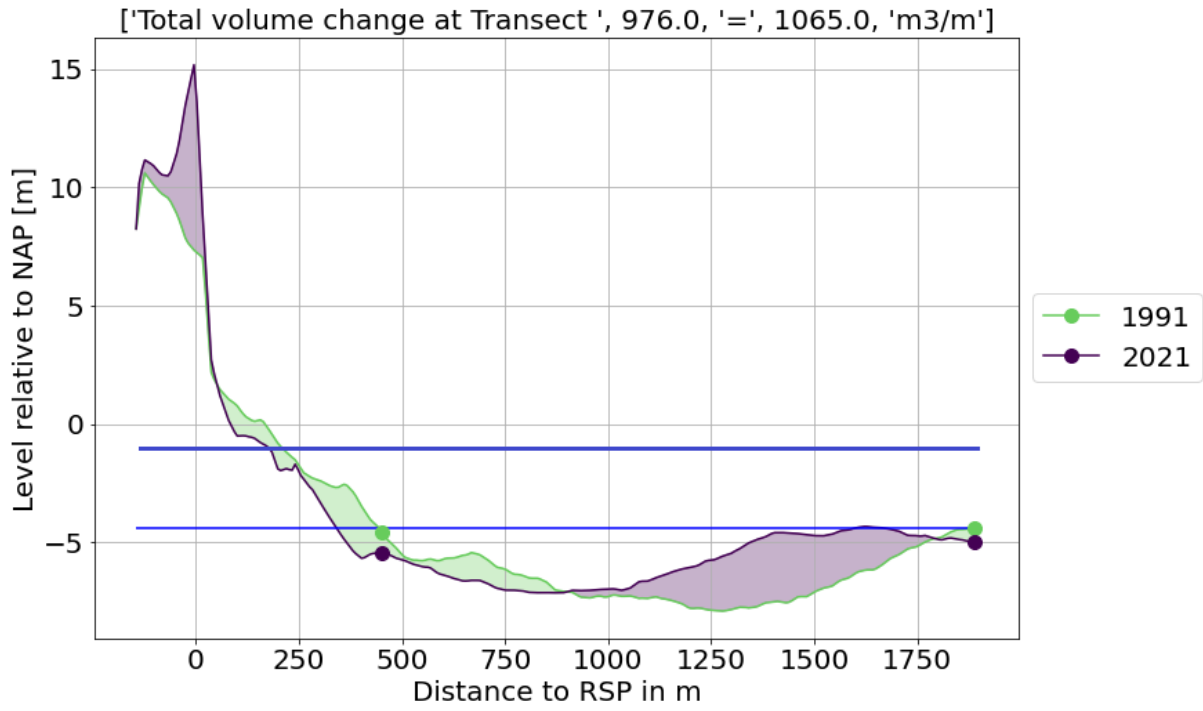


Figure F.7

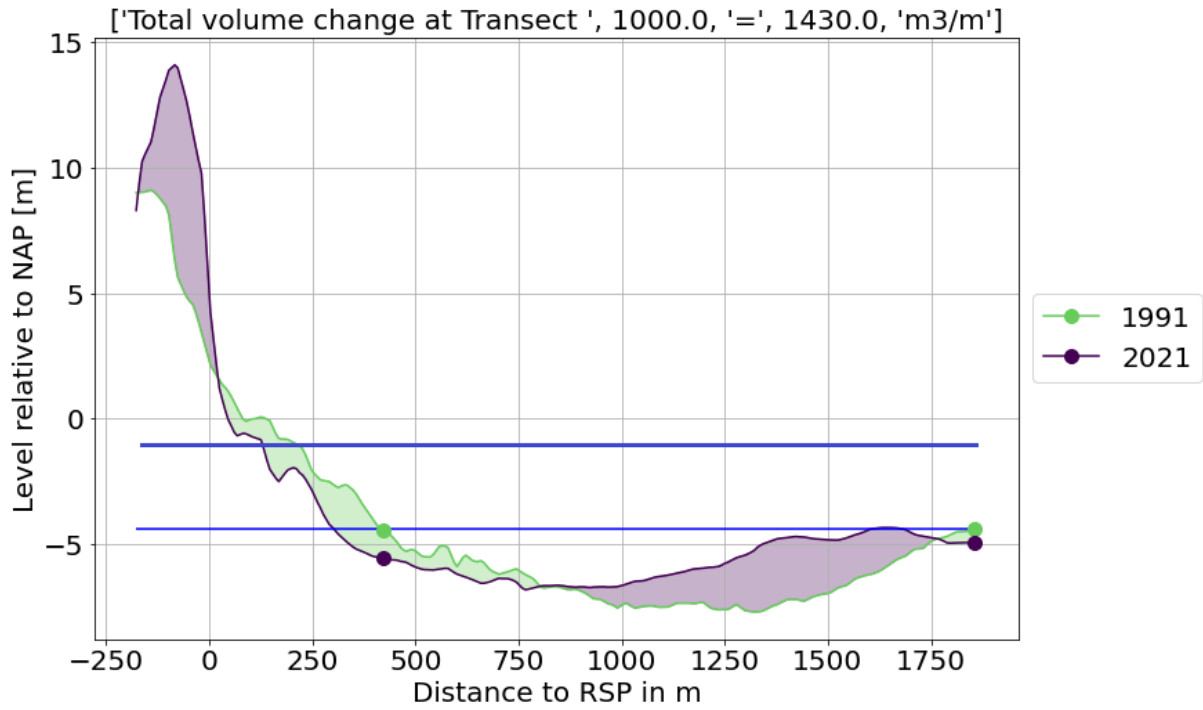


Figure F.8

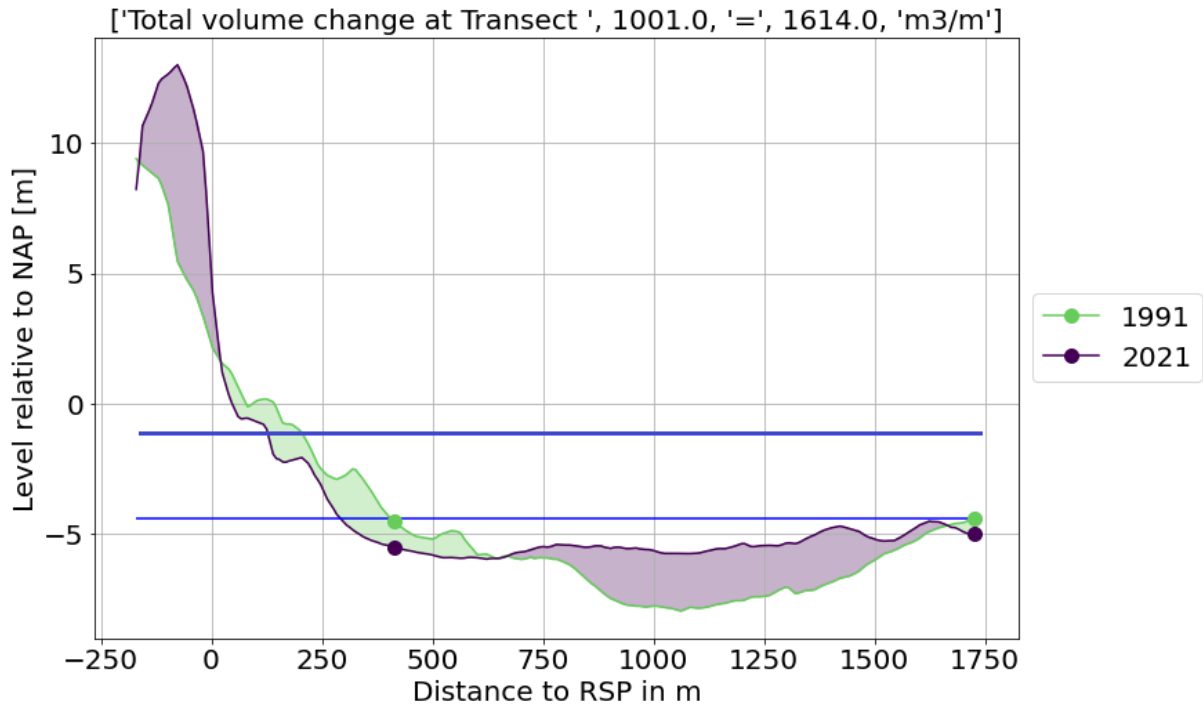


Figure F.9

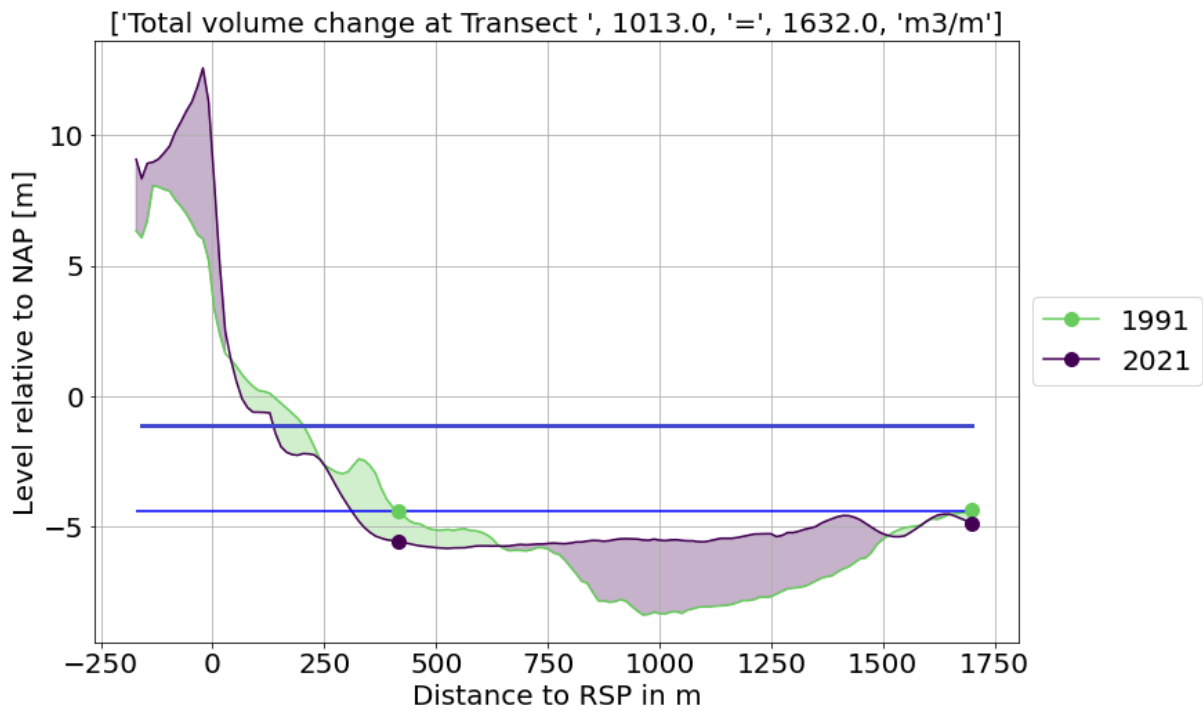


Figure F.10

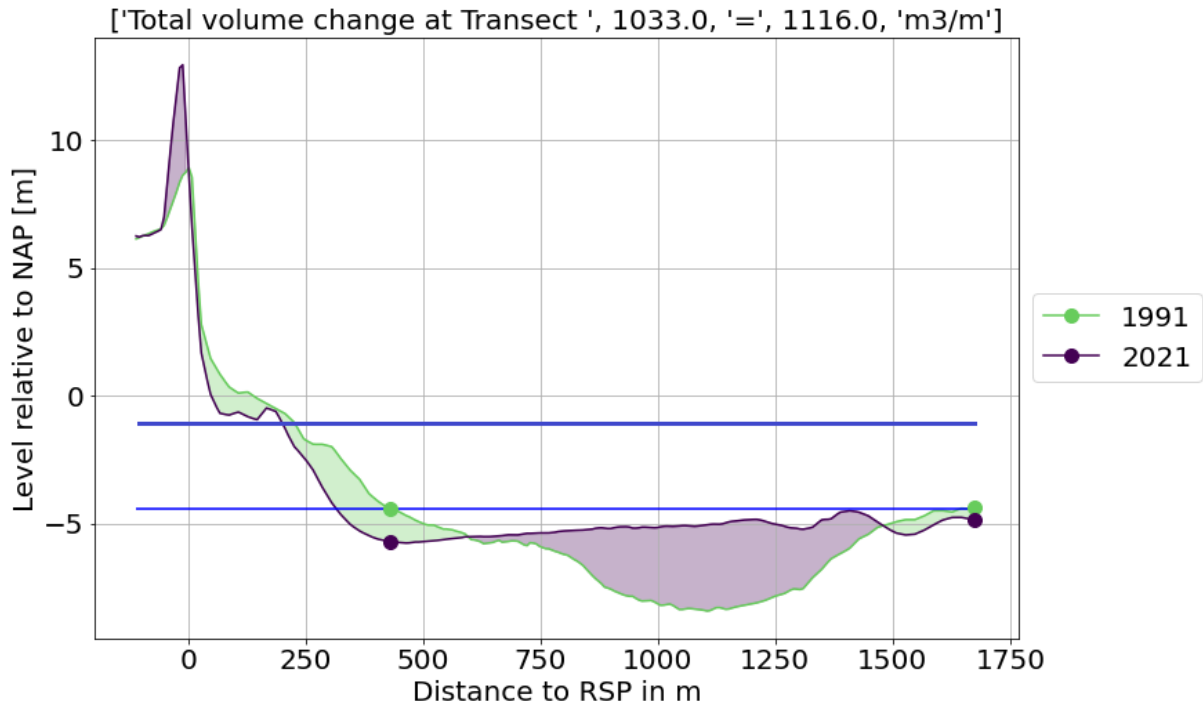


Figure F.11

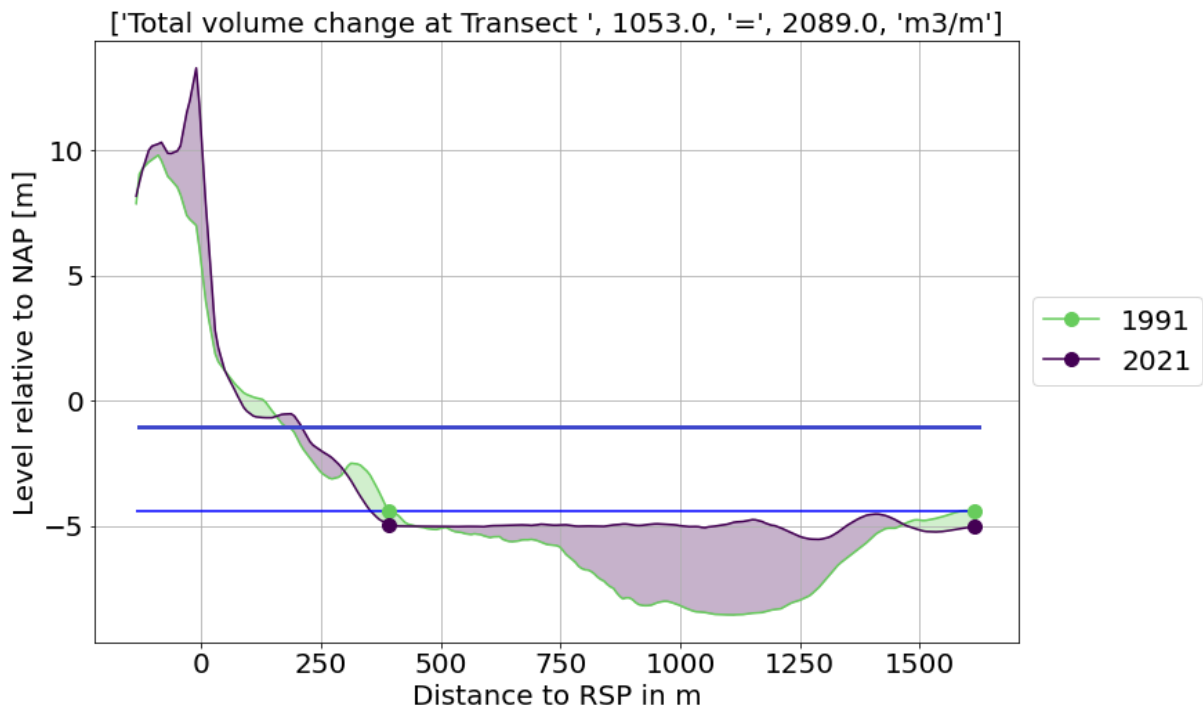


Figure F.12

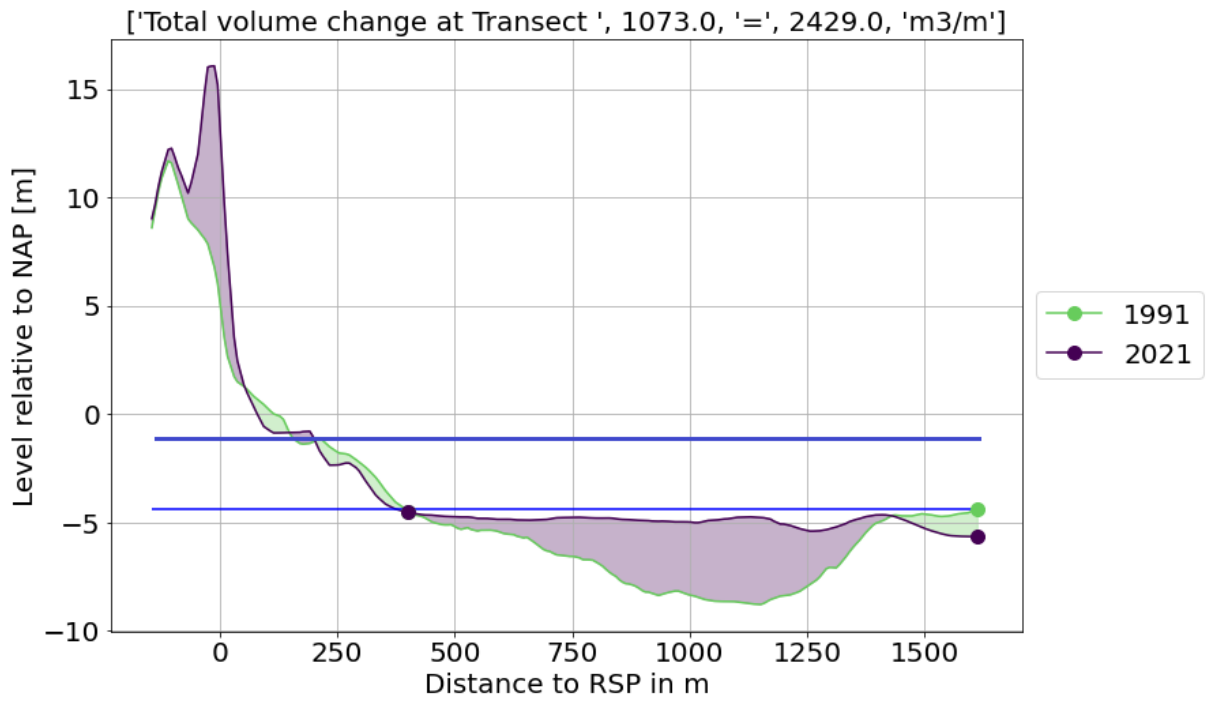


Figure F.13

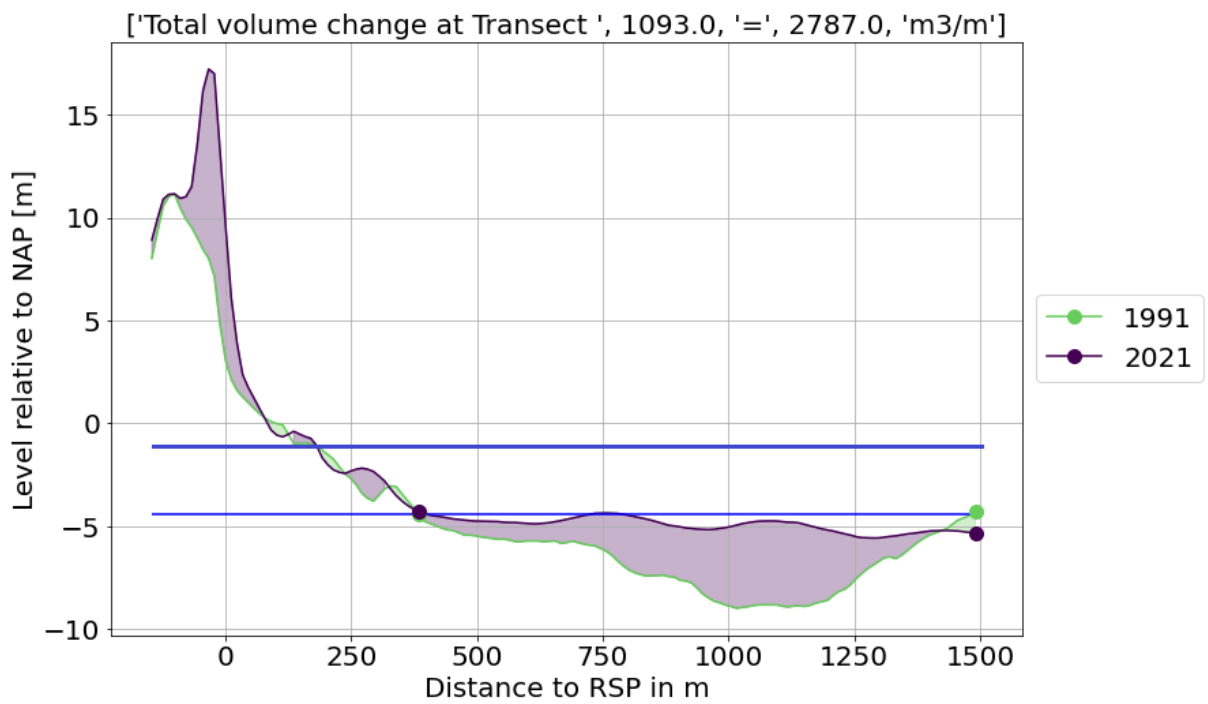


Figure F.14

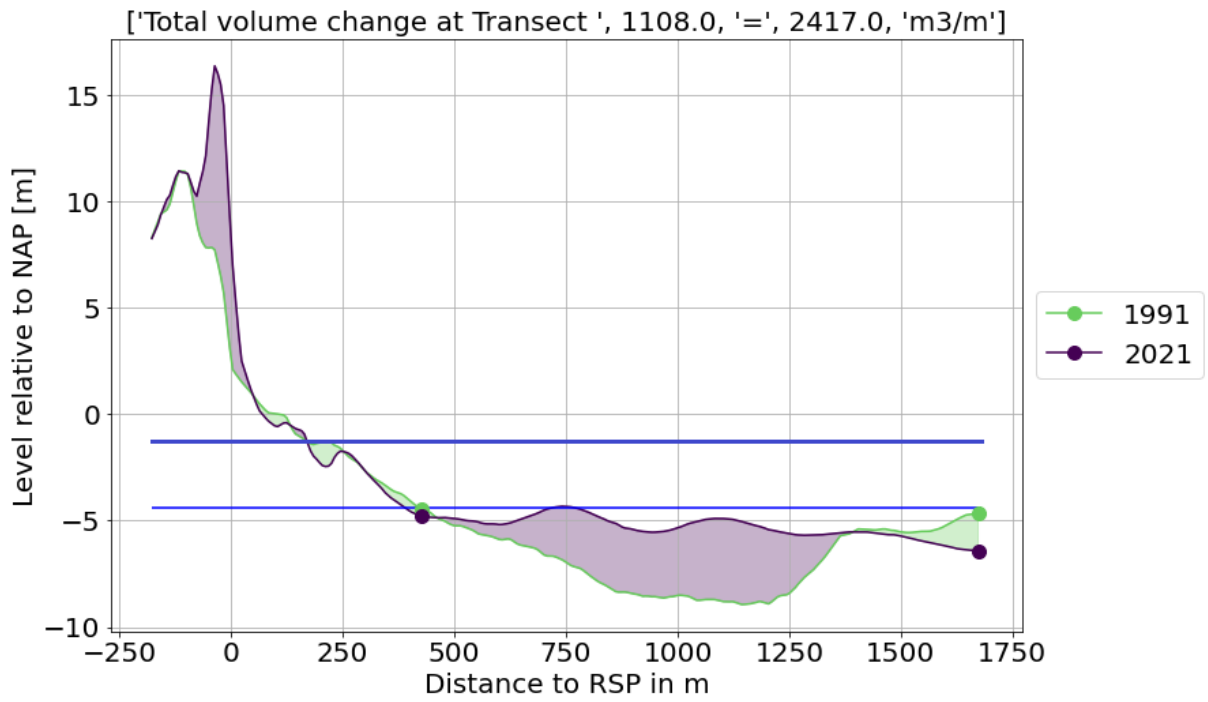


Figure F.15

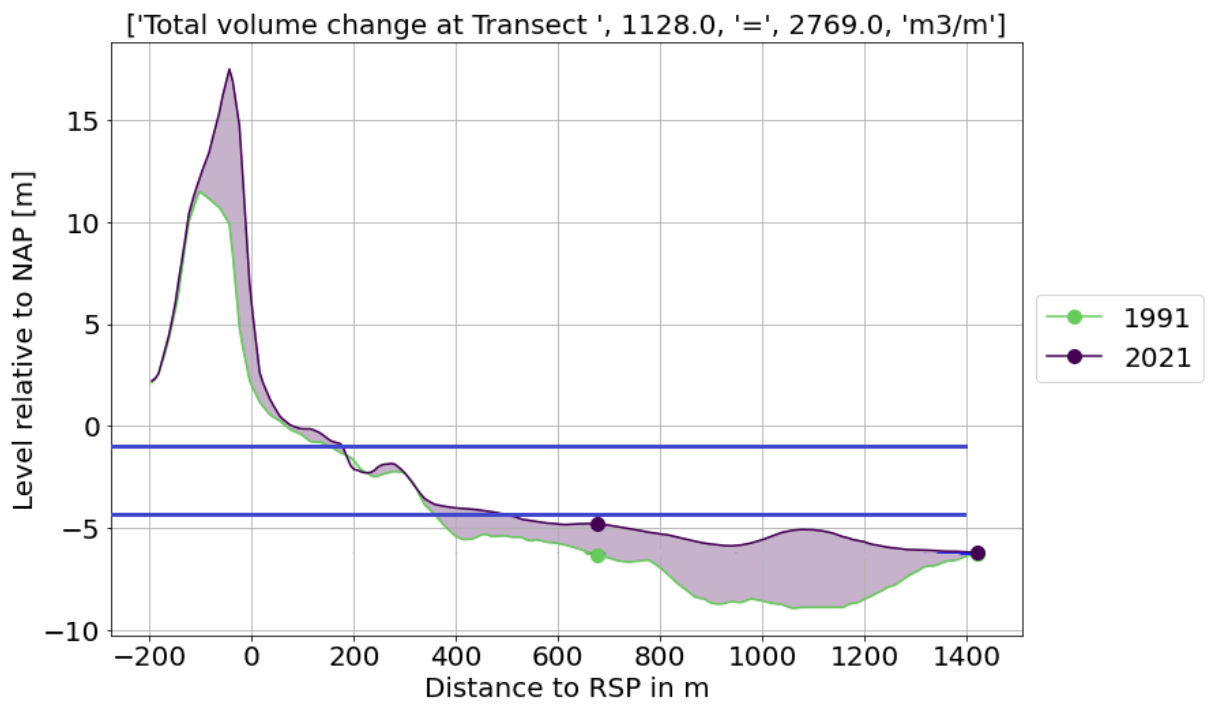


Figure F.16

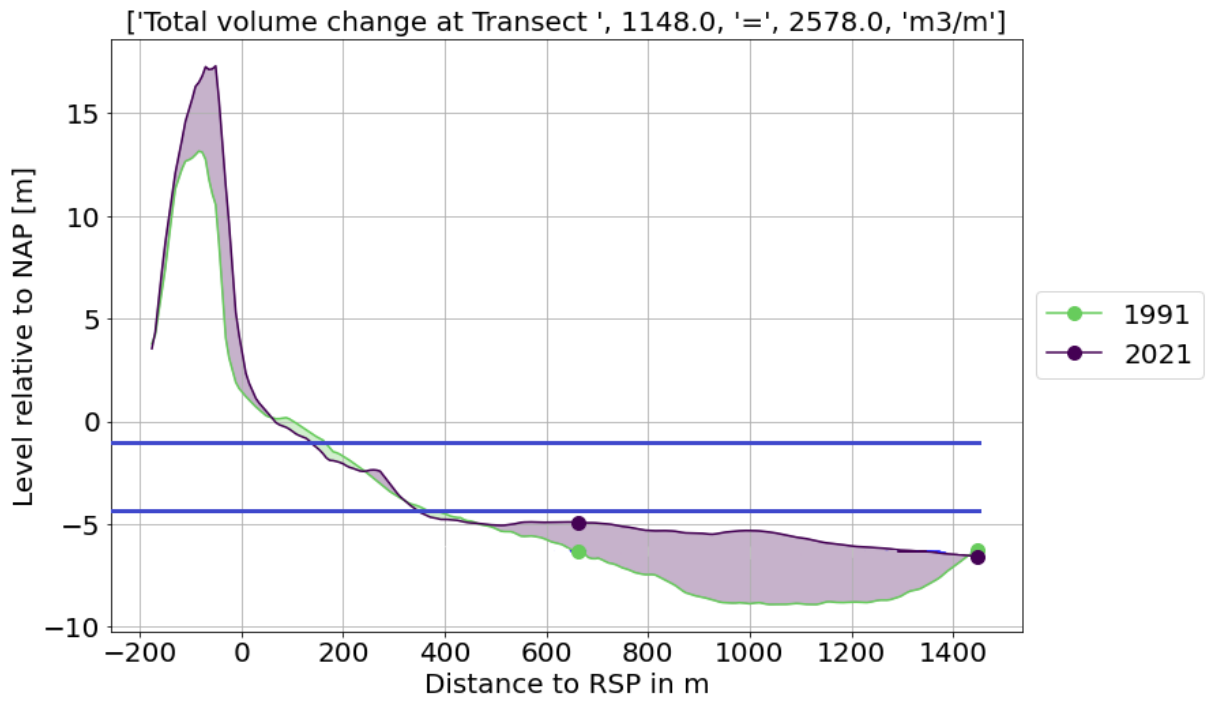


Figure F.17

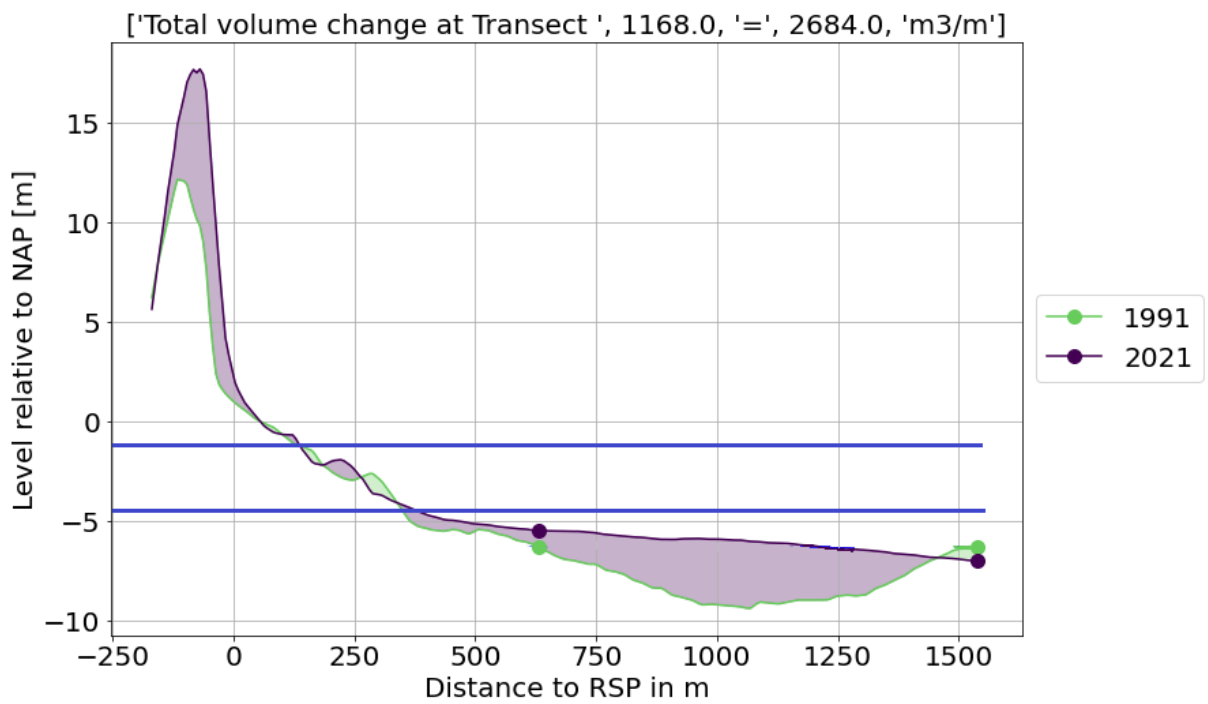


Figure F.18

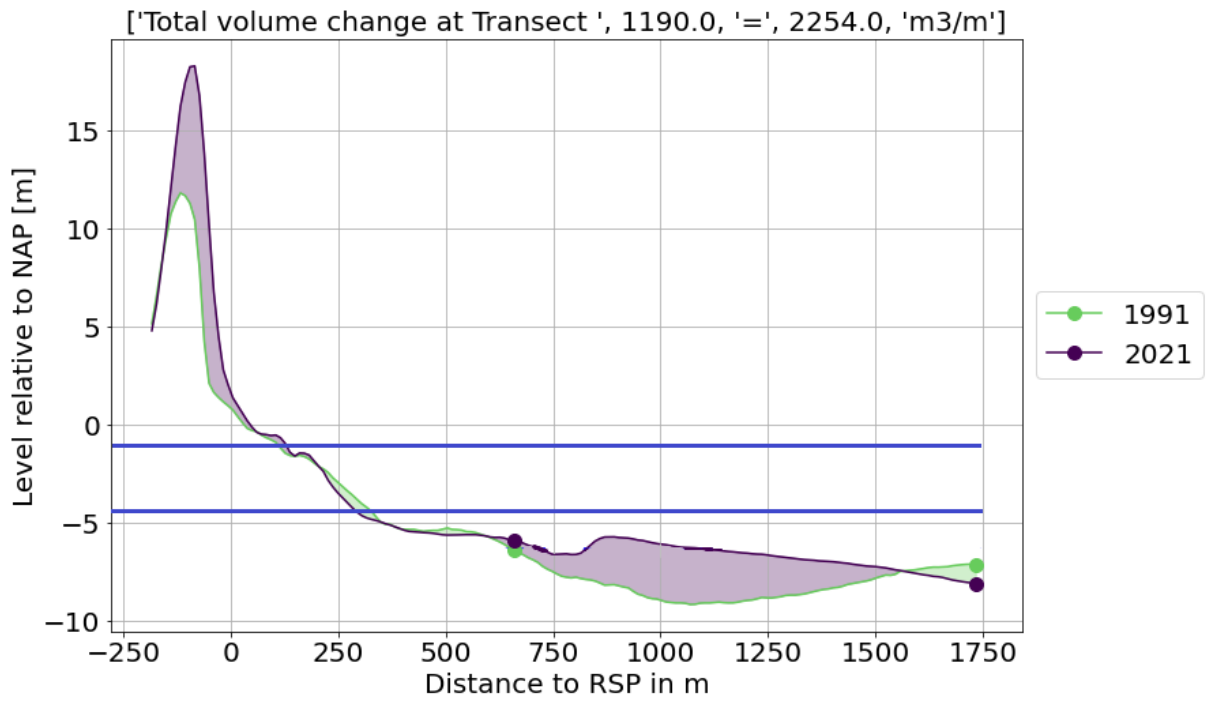


Figure F.19

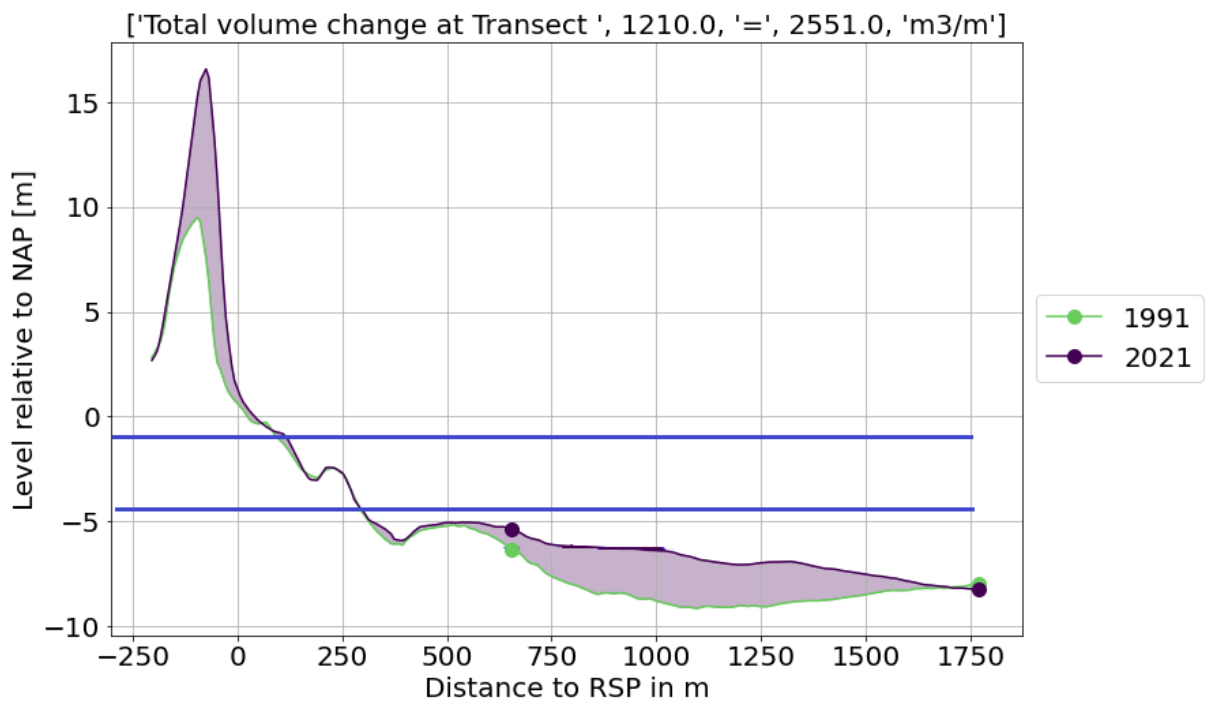


Figure F.20

G Volume tables

Transect	880	900	915	930	945	960	976	1000	1001	1013
$B_{transect}$ [m]	100	175	150	150	155	200	125	65	160	200
$\Delta V_{CM,transect}$ [m ³ /m]	3501	3167	2650	2055	1554	1067	763	961	1227	1320
$\Delta V_{CM,transect} * B_{transect}$ [*1000m ³]	350	554	398	308	233	165	153	120	79.8	211
$\Delta V_{Dune,transect}$ [m ³ /m]	1275	832	641	591	85	161	420	893	895	600
$\Delta V_{Dune,transect} * B_{transect}$ [*1000m ³]	128	146	96.2	88.7	12.8	25.0	84.0	112	58.2	96
$\Delta V_{Beach,transect}$ [m ³ /m]	120	-18.0	-11.3	-61.2	-141	-130	-132	-112	-109	-115
$\Delta V_{Beach,transect} * B_{transect}$ [*1000m ³]	12.0	-3.2	-1.7	-9.2	-21.1	-20.2	-26.4	-13.9	-7.1	-18.4
$\Delta V_{Shallow,transect}$ [m ³ /m]	697	1023	1285	925	226	-78	14	-313	-398	-173
$\Delta V_{Shallow,transect} * B_{transect}$ [*1000m ³]	69.7	179	193	139	34.0	-12.2	2.8	-39.1	-25.9	-27.7
Total $\Delta V_{transect}$ [m ³ /m]	5593	5004	4565	3510	1725	1020	1065	1430	1614	1632
Total $\Delta V_{transect} * B_{transect}$ [*1000m ³]	559	876	685	527	259	158	213	179	105	261

Table G.1: Overview of sub factor values and total volume differences $\Delta V_{transect}$ for transect range 880-1013 in the period 1991-2021. These are the values of Figure 4.18.

Transect	880	900	915	930	945	960	976	1000	1001	1013
$B_{transect}$ [m]	200	200	200	175	175	200	200	210	210	100
$\Delta V_{CM,transect}$ [m ³ /m]	1553	1878	2080	2550	2097	2035	2020	1968	1524	1784
$\Delta V_{CM,transect} * B_{transect}$ [*1000m ³]	311	376	416	446	367	407	404	413	320	178
$\Delta V_{Dune,transect}$ [m ³ /m]	107	333	560	614	532	626	531	693	687	686
$\Delta V_{Dune,transect} * B_{transect}$ [*1000m ³]	21.4	66.6	112	107	93.1	125	106	146	144	68.6
$\Delta V_{Beach,transect}$ [m ³ /m]	-164	-42.9	-37.3	38.9	0.6	94.2	33.1	89.3	53.5	26.9
$\Delta V_{Beach,transect} * B_{transect}$ [*1000m ³]	-32.7	-8.6	-7.5	6.8	0.1	18.8	6.6	18.8	11.2	2.7
$\Delta V_{Shallow,transect}$ [m ³ /m]	-380	-78.7	-174	-416	-213	13.8	-6.1	-66.3	-10.5	54.1
$\Delta V_{Shallow,transect} * B_{transect}$ [*1000m ³]	-76.0	-15.8	-34.7	-72.8	-37.2	2.8	-1.2	-13.9	-2.2	5.4
Total $\Delta V_{transect}$ [m ³ /m]	1116	2089	2429	2787	2417	2769	2578	2684	2254	2551
Total $\Delta V_{transect} * B_{transect}$ [*1000m ³]	223	418	486	488	423	554	516	564	473	255

Table G.2: Overview of sub factor values and total volume differences $\Delta V_{transect}$ for transect range 1013-1210 in the period 1991-2021. These are the values of Figure 4.18.